

ENHANCEMENT OF PEDESTRIAN COMFORT IN THE HOT CLIMATE CITY OF JEDDAH

Presented by:

BADIAH GHASSAN MASOUD

THESIS DIRECTOR: DR. HELENA COCH ROURA

THESIS CO-DIRECTOR: DR. BENOIT BECKERS

PHD PROGRAM: ARCHITECTURE, ENERGY AND ENVIRONMENT

SUPERIOR TECHNICAL SCHOOL OF ARCHITECTURE OF BARCELONA (ETSAB)

POLYTECHNIC UNIVERSITY OF CATALONIA (UPC)

DEPARTMENT OF ARCHITECTURE TECHNOLOGY

THIS THESIS HAS BEEN FUNDED BY THE MINISTRY OF EDUCATION OF THE KINGDOM OF SAUDI ARABIA.

ACKNOWLEDGMENTS

I dedicate this Ph.D. to my Father Ghassan Mohammed Masoud God rest his soul in peace and to my mother, Nadia Yusif Nassif, whom both gave me all their grace and benevolence and for giving me the determination to overcome many tiring moments to pursue my dreams and for making me the woman I am today.

Firstly, I would like to express my sincere gratitude to my advisor Prof. Helena Coch Roura, for the continuous support of my Ph.D. study and related research, for her patience, motivation, and immense knowledge. Her guidance helped me in all the time of research and writing of this thesis. Special appreciations are also dedicated to my Co-advisor Benoit Beckers for his guidance, advice, and support throughout the years of this research.

Besides my advisors, I would like to thank the rest of the professors in the Department of Architecture, Energy, and Environment for the endless support and guidance throughout my Ph.D. thesis and my publications: Prof. Antonio Isalgue, Prof. Isabel Crespo Cabillo, Prof. Carlos Alonso Montolio, Prof. Judit Lopez Besora, and a special thanks to Prof. Jauma Roset for his support especially in helping me in the solar energy analysis.

My sincere thanks and profound gratefulness go to my mother and my siblings (Sahab, Qosai, Waad, Odai, Nomai, and Komai) for the endless love and support, and understanding during the difficult phases of this journey; I honestly cannot thank them enough for all the support I had from them. A special thanks to Waad and Odai, who live with me in Barcelona, for all the support you gave me when I was down and lifting me and the love you gave me.

I want to thank my Ph.D. friends at the Architecture, Energy, and Environment department for their support and for being there for me. I dedicate a huge thanks to all my friends in Barcelona for being there for me and supporting me, especially Perla Zambrano and Sabrina Settinger, for their love and their support.

Finally, I acknowledge with extreme gratitude all my friends back in Saudi Arabia for all the support they send me and the encouragement to hold on in this journey: Kholud, Sara Malouh, Sara Bin Sadik, Haya and Hala Aljifry, Reem Abu Alola, Nayroz Subhi, Ghalia Basyuni, Ghada and Ghufra Alshirbi, Reham, Razan, and Nora. And of course, I dedicate my special thanks to my two best friends and support system Sundos Ashi and Dania Saib, for being there for me from America to Saudi Arabia. Thank you for the long hours you gave me listening to me and the support you always gave me at the work level or mental support.

Table of content

ABSTRACT - RESUMEN.....	8
INTRODUCTION	12
 CHAPTER 1. THE OLD COMPACT CITY IN HOT-DRY CLIMATE	
1.1 INTRODUCTION.....	22
1.2 COMPACT CITIES IN HOT CLIMATES	23
1.3 THE CLIMATE OF THE CITY OF JEDDAH, IN SAUDI ARABIA	27
1.4 SOLAR ACCESS IN THE PUBLIC SPACE, JEDDAH CASE STUDY	33
1.5 ANALYSIS AND RESULTS OF THE CHAPTER	50
 CHAPTER 2. SOLAR RADIATION IN THE EXISTING URBAN GEOMETRY	
2.1 THE URBAN SPRAWL.....	52
2.2 THE URBAN SPRAWL IN HOT CLIMATE CITY OF JEDDAH	55
2.3 SELECTED URBAN LAYOUTS DESCRIPTION	66
2.4 SOLAR ACCESS IN THE URBAN PUBLIC SPACE	72
2.5 SUMMARY OF THE RESULTS	88
 CHAPTER 3. THE PUBLIC TRANSPORTATION AND URBAN FORM	
3.1 TRANSPORTATION AND URBAN FORM	90
3.2 TRANSPORTATION ISSUES ON THE URBAN ENVIRONMENT	93
3.3 PUBLIC TRANSPORTATION AND CITIES.....	95
3.4 JEDDAH PUBLIC TRANSPORTATION PROJECT	96
3.5 ASSESSMENT OF PROPOSED PUBLIC TRANSPORT SYSTEM	99
3.6 JEDDAH FUTURE URBAN DENSITY	102
 CHAPTER 4. THE OASIS EFFAT	
4.1 INTRODUCTION	106
4.2 DEFINITION OF TRANSITIONAL SHADED SPACES.....	107
4.3 OUTDOOR THERMAL COMFORT IN TRANSITIONAL SPACES.....	108

4.4	THE COMPACT CITY: JEDDAH'S DEVELOPMENT CONSOLIDATION AND DENSIFICATION	115
4.5	FOSTER DENSIFICATION AROUND METRO NODES.....	117
4.6	CONCLUSION	119

CHAPTER 5. SOLAR RADIATION IN THE SHADED URBAN GEOMETRY

5.1	THE RAWWASHIN AND THE COVERED STREETS.....	124
5.2	SUN PROTECTION AS A STRATEGY TO PROTECT THE BUILDING AND / OR THE PEDESTRIAN SPACE.....	136
5.3	OVERHANGING FAÇADE SHADING PEDESTRIANS.....	141
5.3.1	Shading view factor in relation to the chosen overhanging facades	144
5.3.2	Results Overhanging Facades Received solar flux in relation to Shading View Factor.....	150
5.3.3	Results of the Overhanging Facade Geometry Influencing the Amount of Solar Flux Received on the Pedestrian Walkway in E_{OVHF} and W_{OVHF}	150
5.3.4	Results of the Overhanging Facade Geometry in Influencing the Amount of Solar Flux Received on the Pedestrian Walkway for N_{OVHF} and S_{OVHF}	154
5.3.5	Effect of Overhanging Facades on the Amount of Solar Flux Received on the Horizontal Surface of E_{OVHF} and W_{OVHF}	158
5.3.6	Effect of Overhanging Facades on the Amount of Solar Flux Received on the Horizontal Surface in N_{OVHF} and S_{OVHF}	160
5.4	EVALUATION OF THE SHADING URBAN GEOMETRY	162

CONCLUSIONS AND FUTURE INVESTIGATION

CONCLUSION.....	173
SUGGESTIONS FOR FUTURE INVESTIGATIONS	176

BIBLIOGRAPHY.....	181
-------------------	-----

LIST OF FIGURES AND TABLES	193
----------------------------------	-----

APPENDICES

APPENDIX 1	207
APPENDIX 2	214
APPENDIX 3	256

ABSTRACT

The ancient cities of hot arid climates, founded and grew linked to pedestrian mobility, followed a preferably compact growth pattern until the beginning of the 20th century. The resulting urban form impacted urban environmental conditions as the configuration of the buildings avoided part of the solar radiation and prevented the arrival of the desert wind.

The appearance of the automobile and its generalized use was favored; from the middle of the 20th century, urban growth models followed dispersed patterns. The city was structured based on the layout of spacious avenues and separate buildings, thanks to the possibility of covering large distances for the daily functional development of the population. The city tended to spread, and solar protection from buildings to others and the urban space was lost. The interiors need air conditioning to maintain acceptable thermal conditions, and the public space becomes little habitable in this type of design, and the need for private transport is further promoted, thus entering a wheel that is difficult to combat. Also, the socio-economic conditions of the societies where these cities are developed do not allow a global urban reform of the already consolidated cities to be proposed to modify their current configuration.

The planning of more recent times is committed to the construction of mass collective transport systems, with the consequent projection of essential infrastructures, in some cases underground, which require large-scale planning, and their construction takes place in the medium and long term. The appearance of these new infrastructures can be an opportunity to reverse the trend of extensive growth over the surrounding territory.

The city's planning design can recover adequate environmental qualities that can be implemented if limited to areas of limited dimensions. The implementation of infrastructure such as the metro can propose regulating the building form around its stations. The subway is an underground transport system for users who move on foot; therefore, the stations along its route become the origin and end of pedestrian mobility, and the design of a comfortable public space becomes a necessity and an opportunity. To apply new approaches, based on the analysis of the urban characteristics of the traditional city, the creation of shaded spaces that protect the user from excess solar radiation, the main factor of discomfort in these climates, is shown as an option.

In this work, we are devoted to designing proposals for the future city based on the analysis of traditional cities. Moreover, put into value solutions typical of traditional urbanism that have been taken up in modern architecture, such as balconies and tribunes on the facades to the street or the porches and setbacks of the ground floors and the formation of covered streets, to form part of the daily journeys of people who move by subway.

All studies and analyses for this work have been done on the city of Jeddah as a case study. The studies of sunlight, sky vision index, and radiation behavior have been done on the old fabric of this city and the project proposals for the modern city have been working on the existing proposals of the same city.

RESUMEN

Las ciudades antiguas de climas áridos, que se fundaron y crecieron vinculadas a una movilidad peatonal, hasta principios del siglo XX seguían un patrón de crecimiento preferentemente compacto. La forma urbana resultante tenía una repercusión en las condiciones ambientales urbanas, puesto que la propia configuración de las construcciones evitaba parte de la radiación solar e impedían la llegada del viento seco del desierto.

La aparición del automóvil y su uso generalizado favoreció, desde mediados del siglo XX, modelos de crecimiento urbano que seguían patrones dispersos. La ciudad se estructuró en base al trazado de grandes avenidas y edificaciones separadas, gracias a la posibilidad de cubrir grandes distancias para el desarrollo funcional cotidiano de la población. La ciudad siguió una tendencia a diseminarse y con ello se pierde la protección solar de unos edificios a otros y de éstos al espacio urbano. Los interiores necesitan aire acondicionado para mantener unas condiciones térmicas aceptables y el espacio público se hace poco habitable en este tipo de tramas y se fomenta todavía más la necesidad de transporte privado con lo que se entra en una rueda difícil de combatir. Además, las condiciones socioeconómicas de las sociedades donde se desarrollan estas ciudades no permiten plantear una reforma urbana global de las ciudades ya consolidadas para que modifiquen su actual configuración.

La planificación de las épocas más recientes apuesta por la construcción de sistemas de transporte colectivo masivo, con la consiguiente proyección de infraestructuras importantes, en algunos casos subterráneas, que necesitan una planificación a gran escala y su construcción se desarrolla a medio y largo plazo. La aparición de estas nuevas infraestructuras puede ser una oportunidad para revertir la tendencia al crecimiento extensivo sobre el territorio circundante.

El diseño programado de la ciudad puede recuperar cualidades ambientales adecuadas que se podrán implementar si se circunscriben a áreas de dimensiones acotadas y la implementación de una infraestructura como el metro puede plantear la regulación de la forma edificatoria entorno a sus estaciones. El metro es un sistema de transporte subterráneo para usuarios que se mueven a pie, por tanto, las estaciones de su recorrido se convierten en origen y final de la movilidad peatonal y el diseño de un espacio público confortable se convierte en una necesidad y en la oportunidad de aplicar nuevos planteamientos. A partir del análisis de las características urbanas de la ciudad tradicional, se demuestra como una opción la creación de espacios en sombra que protegen al usuario del exceso de radiación solar, principal factor de discomfort en estos climas.

En este trabajo se apuesta por propuestas de diseño de la ciudad futura a partir del análisis de ciudades tradicionales y se ponen en valor soluciones propias del urbanismo tradicional que se han retomado en la arquitectura moderna, como son los balcones y tribunas en las fachadas a la calle o los porches y retranqueos de las plantas bajas y la formación de calles cubiertas para formar parte de los trayectos cotidianos de las personas que se mueven en metro.

Todos los estudios y análisis para este trabajo se han hecho sobre la ciudad de Jeddah como caso de estudio. Los estudios de asoleo, de índice de visión de cielo y de comportamiento ante la radiación se han hecho sobre la trama antigua de esta ciudad y los planteamientos de proyecto para la ciudad moderna se han trabajado sobre las propuestas existentes de la misma ciudad.

INTRODUCTION

- I. JUSTIFICATION
- II. HYPOTHESIS STATEMENTS
- III. OBJECTIVES
- IV. METHODOLOGY AND THESIS STRUCTURE

I. JUSTIFICATION

The environmental subject is a challenging topic that cannot be ignored and left for future generations to deal with. Cities affect and at the same time are affected by their environment, including the climate" *Most (if not all) literature on climate and built environment design assumes climate to be central or even the starting point for urban design.*" With these words, Victor Olgyay introduces the theme of the relationship between urban morphology and climate in his famous book "Design with Climate: Bioclimatic approach to architectural regionalism" (Olgyay, 1963), adopting parallelism with physics. So, knowledge of the form leads to the interpretation of forces that have shaped it. Even in the study of urban form and the morphology of the buildings, it is possible to identify the influence of the forces that generated it. Among these, the climate represents an element that has profoundly affected how cities are built throughout history, directly affecting the configuration of the settlement in different geographical contexts. The location of the settlement, streets proportion, public spaces, shape of roofs, and the arrangement of the openings on the facades all reflect the culture and techniques of each place and an adaptation to the local geographical and climatic conditions.

The analysis structure of the historic settlements and the typological characteristic of the built areas shows that a relationship can be identified between urban morphology and climate. Comparable constructive and morphological characteristics can be found in areas in the world that are also quite different in terms of culture and history but share the same climate (Beckers, 2012; Coch & Serra, 1995; Givoni, 1998; Golany, 1996; Olgyay, 1963). Urban microclimate plays a fundamentally active role in thermal comfort in outdoor spaces and building energy consumption. Nowadays, cities need to reduce pollutant emissions, increase energy efficiency, mitigate any evident lack of sustainability, and become more resilient. Urban morphology is one of the urban parameters that affect microclimate in urban settlements.

In various parts of the world, urban development occurs over a long period, allowing urban policymakers time to react to any further changes that could produce adverse impacts on the environment and the well-being of citizens. However, in some countries, urbanization is very rapid and occurs within a comparatively short period, generating a range of environmental and energy challenges. One such country is Saudi Arabia. Saudi Arabia has transformed in the last 80 years into a modern, developing nation due to the massive oil revenues. Within a relatively short period, the country has encountered several significant urban changes that transformed the urban fabric of main cities from the vernacular urban form into a modern one.

The modest efforts in adopting climatic considerations and human dimensions during the design process have increased the severity of the microclimate conditions in such desert regions. These microclimate conditions increase the reliance on an active cooling system in indoor spaces to overcome the decline in the environmental quality of outdoor spaces. The general extreme climate condition in Saudi Arabia and the lack of urban design strategies that take the local climate conditions into account resulted in high energy

consumption (Figure 1), mainly consumed by cooling loads within buildings (Al-Ajlan et al., 2006). 65% of the total generated energy in Saudi Arabia is used for operating urban buildings, and out of this, about 65% is consumed by active cooling systems alone. Recently, the Saudi Arabian Secretary of Energy stated that about 80% of the generated energy was consumed in cooling loads between 12:00 h to 17:00 h (AlArabiyah.net, 2013).

Energy use per person, 2019

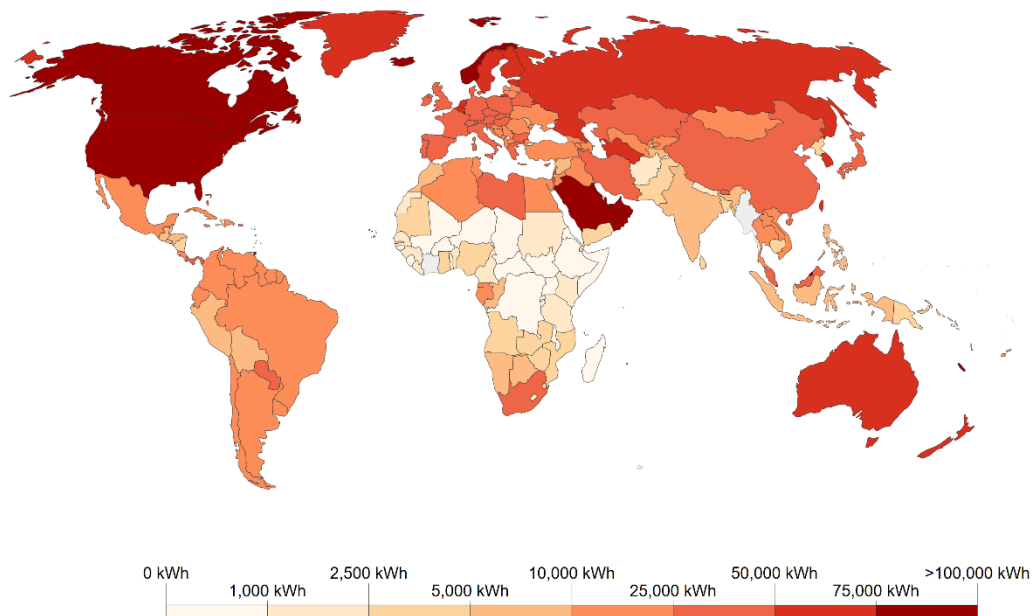


Figure 1. The world map showing the energy use per capita (Source: <https://ourworldindata.org/grapher/per-capita-energy-use>)

The high energy consumption per capita sheds light on the size of the problem in Saudi Arabian cities and indicates the urgent need to adopt a strategy to reduce excessive energy use. Additionally, to these energy numbers, private cars account for the vast majority of all journeys made in Jeddah, with public transportation accounting for less than 2%. This substantial reliance on private transportation also drastically affected the daily business and the livability of the city. Moreover, this reliance on the car is restricting the growth potential of the city. While the population is expected to grow from 3.8 million today to 6.3 million in 2023, it also hosts a substantial annual influx of international visitors in route to Hajj and Umra (pilgrimage). Between two and three million annual visitors, which are ever-growing in numbers, have been received over the last five years for the Hajj pilgrimage alone. According to the new government's 'Vision 2030' released in 2016 by the crown prince Mohammed Bin Salman, the total number of religious visitors is expected to reach over 30 million.

The traveling demand is a derived demand. The need to travel is born due to individual requirements to go to a particular area within the city. This provides a chance for the urban structure to meet this travel demand. On the other hand, the transport supply modifications

entail multiple changes while making choices about the sequence, routes, and mode of travel, i.e., the destinations of the trips. In the long run, the modifications of transport conditions would entail a revision of various activity choices. The urban structure would then itself be modified (Lefèvre, 2009).

Quite simply, Jeddah's existing infrastructure cannot support the city's needs. There is an urgent need for a public transport network to encourage economic development, enhance social well-being, and improve the quality of life. Therefore, Jeddah city will shortly start constructing a public transportation program (JPTP) in response to the city's needs (Figure 1.16). This will radically change the habits of Jeddah's inhabitants.

With the urban sprawl city system, comprising wide streets exposed to the solar radiation and low-rise buildings that permit the solar radiation to penetrate to the streets, the citizens cannot transit from one point to another under this harsh weather without being protected from solar radiation (Figure 2).

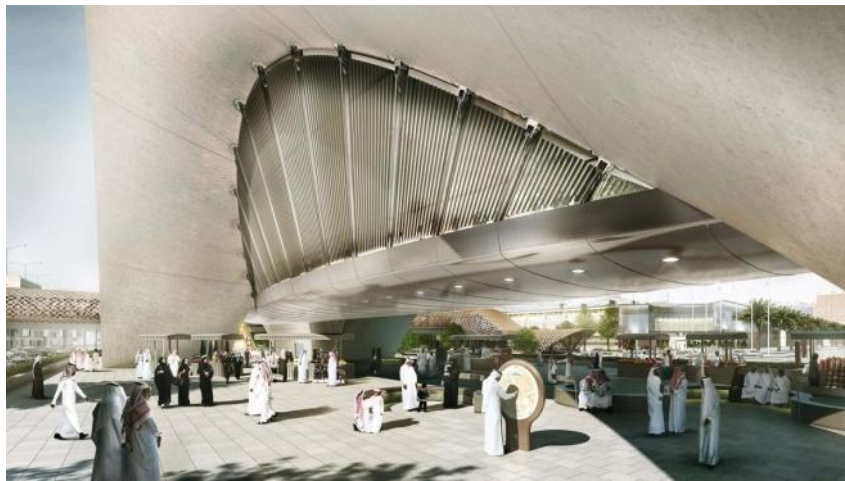


Figure 2. Streets and pedestrian paths highlight where solar radiation penetrates for long hours
(Source: <http://www.metrojeddah.com.sa/>).

Corresponding to the previous statements, the current demand for sustainable-built environments in Jeddah city and Saudi Arabia, in general, is coupled with the need to minimize the effect of the severe solar radiation condition during summer on outdoor pedestrians. The morphology layout of the neighborhoods, quantified by the height to width ratio of streets, the sky view factor, and the street orientations, is utilized in the

present doctoral thesis as a means of bioclimatic urban design to investigate the influence of the morphology of different neighborhood layouts on the direct solar radiation in urban spaces in a hot, arid region. Public transportation would solve the problem at hand and modifying the urban morphology would allow pedestrians to avoid this harmful solar radiation.

II. HYPOTHESIS STATEMENTS

This thesis focuses on the direct solar radiation condition of compact and dispersed urban morphologies in hot climate cities. The four hypotheses for the incident of the solar radiation on the street surface are the following:

- In hot-climate cities, compact morphology reduces the solar radiation potential more than the dispersed urban morphologies, which would moderate these cities' climate.
- In this climate, it is always crucial to create shade to protect from direct solar radiation.
- Reduction of the incident solar radiation potential at street level through adjusting the morphology is not the only way to enhance pedestrian comfort in hot-climate cities.
- Assessing, analyzing the urban morphology parameters, H/W ratio, sky view factor (SVF), and street orientations of a city on different existing urban layouts will provide urban designers and decision-makers with applicable design guidelines and information enhance pedestrian thermal comfort.

III. OBJECTIVE OF THIS STUDY

The doctoral research attempts to expand the understanding of the physical and environmental phenomena in built environments. More specifically the thesis investigates the relationship between the characteristics of the urban environment and the direct solar radiation focusing on the compact and sprawl urban morphology in hot climate cities. The overall long-term goal is to enhance the capacity of urban settlements for providing high-quality spatial environments.

This research intends to extract concepts from the old compact area of Jeddah city and the modern (sprawl system) layouts to develop an outstanding future, strategic, and compact morphology to facilitate a dynamic development of the city and enhance pedestrians' comfort avoiding the harsh solar radiation.

The main objective is to analyze the direct solar radiation behavior on the horizontal surface (streets) of the different chosen urban morphologies. To assess the intensity and the time interval on the street level.

To achieve the general goal of the thesis, the following secondary objectives are defined:

- Analyzing the urban morphology and the streets' placements and orientations of Jeddah city.
- Assess the influence of the **direct solar radiation** of urban surfaces on the thermal environment of the street within compact and sprawling built geometries.
- Assess the incident solar radiation and the **sky view factor** on different urban morphologies of Jeddah city of the urban surfaces.
- Assess the effects of **shading** on an urban scale as a modifier of the street's thermal environment.
- Assessing the possible influence of the numerous parameters; this includes the street orientation and the building height-to-width ratio, and the sky view factor.
- Proposing and evaluating hypothetical urban geometries on the existing urban geometries represented by modifying the pedestrian walkways with a **horizontal shading system** to enhance shading in the built environment.

IV. METHODOLOGY AND THESIS STRUCTURE

The urban scientific field needs to reinforce and merge the link between theoretical research and practical actions in existing and future urban settlements. This type of approach cannot be done without direct and profound knowledge of the old urban realities and the constrictions and peculiarities that inevitably affect and characterize it. Therefore, to carry out the present investigation relating it directly to existing urban cases, and not with ideal archetypes.

A good choice of research method must be based on careful consideration of the nature of the problem under study. Given that the present doctoral thesis is multidisciplinary, it was necessary to combine various methods to answer the research questions. Therefore, numerical modeling will be carried out. Before that, a comprehensive review of available knowledge is performed to shed light on the size of the problems under investigation in the global context and within the local built environment in Jeddah City.

The numerical models generated used the urban design and building regulations followed in Jeddah city regarding local street width, building height, and the available cadastral information. Assessment simulations evaluated the incident solar radiation in the urban layouts at street level and building facades using the software "Heliodon2" (Beckers, 2006) (direct shortwave, Sky View Factor) and for the hypothetical study "Heliodon plus" (Nahon, 2016) (climatic data) at street level. Solar potential simulations evaluated the existing and possible scenarios.

The thesis is divided into five main topics; they are correlated, leading to solving the main problem, and the chapters are divided accordingly. The thesis will start with analyzing the **old compact cities** in hot arid climates (Chapter 1), an analysis of Jeddah climate, continued with the assessment and evaluation of the direct solar radiation on the old area of Jeddah urban morphology. Next, Chapter 2 is composed of an analysis of the **sprawling system** and how this type of urban development affected the microclimate in this type of climate, with an assessment and evaluation of the direct solar radiation of the new urban layouts of Jeddah city (mid-rise buildings and low rise-buildings. After, an overview of the relationship between urban form and public transportation, showing planning of recent times, how they are committed to constructing mass collective transport infrastructure, taking the underground as an example, and demonstrating the new metro station plan Jeddah city (Chapter 3). Following that, Chapter 4 will discourse how the appearance of these new infrastructures may be an opportunity to improve the environmental conditions of the pedestrian public space around the stations and nodal links by presenting the **Oasis Effect concept** and the design of the future city of Jeddah is proposed based on the analysis of traditional cities. Subsequent, Chapter 5 will propose an analysis and evaluation of **the horizontal design geometry elements** in different urban morphologies (the compact layout of Jeddah and the mid-rise buildings) that will lead to enhancing shaded public spaces; this proposal will support the Oasis effect concept to enhance pedestrian comfort in hot climate cities.

Chapter 1: Provides an overview with a broad background discussing the formation and structure of compact Islamic cities in the hot arid climate and their historical way of formation. Following that, a brief description of the geographical characteristics and climatic features. Including a clear explanation of the structure of Jeddah's old City (AlBalad). Then the direct solar radiation simulation of (AlBalad) streets and facades; and assessing the morphological parameters (aspect ratio, street orientation, sky view factor) gave results to extract concepts from the old compact area. The evaluation and analysis utilize Heliodon2, simulation software, which provides possible data about the cumulative distribution of solar energy from the streets and the building envelopes (facades) on the 21st of June and the 21st of December. Heliodon2 is a program that simulates the sun's path at a specific geographic site and provides graphical and numerical information about the evolution and the distribution of solar radiation, considering the shadows cast by neighboring obstructions and not considering any materials. To carry out the simulation creation of a 3D digital mock-up model using the cadastral information with an adequate level of detail for this analysis in the city of Jeddah (LoD 1: the buildings lack windows or doors and have flat roofs).

Chapter 2: Presents the significant events that marked the change of vernacular urban design transformation. Then, more details are given about Jeddah city within the urban context, including the urban development that Jeddah city went through, the urban sprawl; the process and development are explained, showing the significant events that marked the transformation of the vernacular Islamic urban design in a hot climate city to the now climatic and energy-vulnerable contemporary city. Then, supporting the information with two existing case studies from the new urban development of Jeddah city. Analyzing and studying the map of Jeddah, displaying the urban structure, observing the orientation of the layouts and streets, this all will provide an overall understanding of the issue. Also, the two existing neighborhood layouts in Jeddah are explained in detail, assessing, and evaluating the direct solar radiation, Sky View Factor using Heliodon 2 for the simulation. The average intensity of the incident solar radiation is investigated for the solstice days of summer and winter. A relationship is analyzed between the morphology parameters and direct solar radiation intensity performance of the urban layouts, focusing on the urban morphology implications. Describing the quantitative distribution of incident radiation which enables us to identify specific aspects.

Chapter 3: Presents how the evolution of transportation led to changes in urban form. Next, it will give a brief explanation of the transportation issues in the built environment. Following that, a clarification of how public transportation affected the urban form of different cities worldwide. Then, elucidating Jeddah public transportation project and assessing the proposed public transport system showing how it will affect Jeddah's future urban density.

Chapter 4: This chapter gives the definition of transitional shaded spaces. Then, it presents the literature review of outdoor thermal comfort that is focused on urban solar control by transitional shading elements. Further, this chapter will discuss Jeddah's future metro plan that advocates for a TOD policy to be introduced around major interchanges

and metro stations. Ultimately it will address the Oasis effect concept applied in Jeddah city by densifying the urban fabric around metro nodes through reinforcing the idea by presenting the Foster project proposal.

Chapter 5: This chapter will test geometry design solutions in streets. Assessing different horizontal shading systems provided a clear scientific idea of the proportion needed to avoid and protect from solar radiation. We will then discuss and explain a newly proposed parameter in urban morphology that will help improve the investigation on shaded spaces and pedestrian comfort in hot climate cities, the Shading View Factor. Moreover, it discusses the proposed study applied to the chosen existing urban layouts. The outcome of the numerical simulation is analyzed and evaluated.

Conclusions: The main findings and conclusions are drawn in Chapter 6, recommendations and further works are outlined, based on the achieved results.

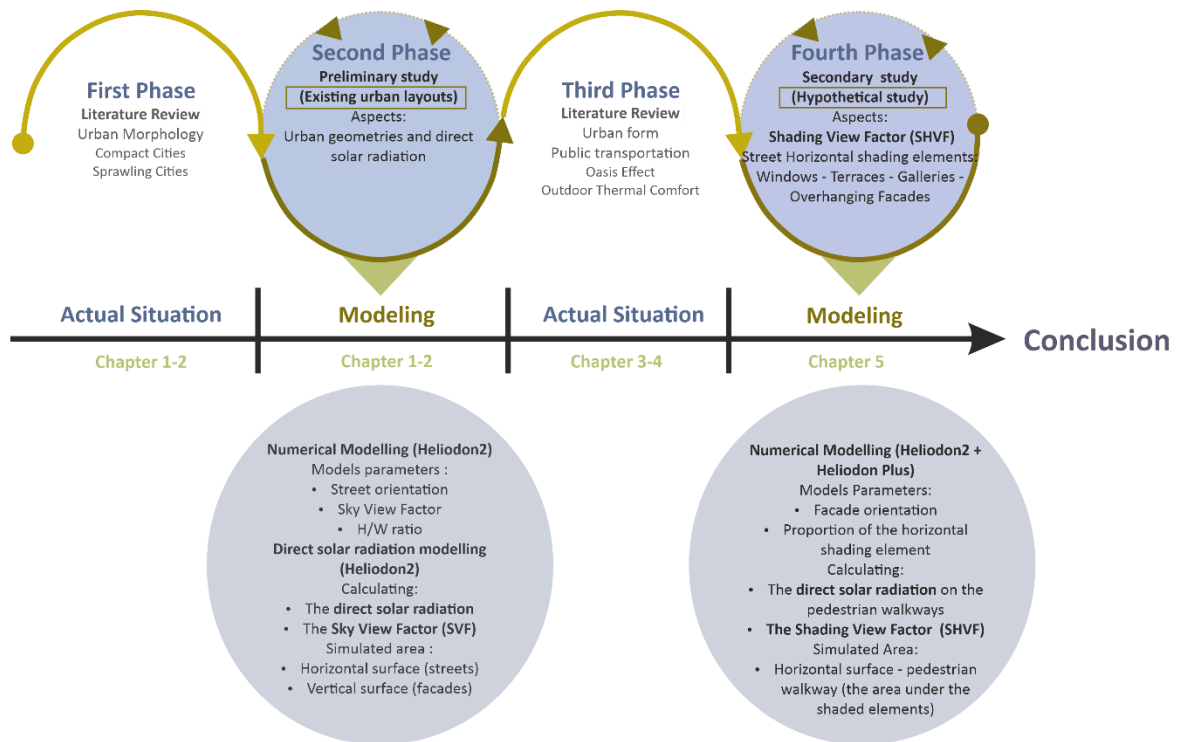


Figure 3. Investigation Methodology.

CHAPTER 1

THE OLD COMPACT CITY IN HOT-DRY CLIMATE

“It is a recognized fact that the forces of nature have a direct effect on the formation of objects. As sometimes in physics, the knowledge of forms leads to the interpretation of forces that molded it, at other times the knowledge of the forces at work guides a better insight into the form itself.”

Victor Olgyay

1.1 INTRODUCTION

1.2 COMPACT CITIES IN HOT CLIMATES

1.3 THE CLIMATE OF THE CITY OF JEDDAH, IN SAUDI ARABIA

1.4 SOLAR ACCESS IN THE PUBLIC SPACE, JEDDAH CASE STUDY

1.5 ANALYSIS AND RESULTS OF THE CHAPTER

1.1 INTRODUCTION

Understanding the morphology of a city and its historic urban form is essential to analyze its energy performance and its relation to the climate. This chapter discusses the formation and structure of Arab Islamic cities in the hot desert region. Explains the main components and how they come together into an urban fabric. Arab-Islamic city features had a climatical, cultural, social, political, and economic logic in terms of physical fabric and provided a lesson for modern planning and design practices. An essential feature of the severe hot climate cities is the compact urban fabric in order to improve the microclimate conditions reducing the sun's severity.



Figure 1.1. Old compact urban form in the city of Tunis. (Source: <https://arab-aa.com/2011/07/06/traditional-urban-fabric-in-the-arab-world-pic/>)

1.2 COMPACT CITIES IN HOT CLIMATES

Historically, cities in regions with very extreme climates, especially in hot-dry climates, grew as compact settlements to respond to the climate (Golany, 1996)

City-making is a process whereby social, economic, political, and physical urban components interact. Urban forms are more or less a result of urban experiences, which are the key to human settlements, culture, and society. The material organization of urban space is decisive in producing and reproducing social and economic arrangements and divisions. Therefore, any city results from a complicated relationship between its socioeconomic, spatiotemporal, and environmental processes and practices" (Lynch and Rodwin, 1958).

Analyzing the historic settlement's structure and the built areas' typological characteristics there is no doubt that a relationship can be identified between building typology, urban morphology, and climate.

Many factors influence cities' design in the large belt of hot and arid zones reaching from North Africa to India. These areas were marked by a rich nomadic hinterland and prevailing tribal structure. The natural living conditions encouraged specific environmental, urban, and architectural responses (Elkabir, 1983).

Generally, the city in Islamic territories is considered as a collection of similar homogenous and integrated neighborhoods (Figure 1.2). Over the centuries, there have been tremendous changes in traditional society. Integrated neighborhoods were bound together by ties of climate, culture, customs, beliefs, and art. While historical Islamic cities show a variety of origins and growth patterns, they were nonetheless established by a standard set of social, geographic, and religious factors that led to similar morphological principles, developing the urban fabric (Ben-Hamouche, 1999; Bianca, 2000; Lapidus, 1973; Saqqaf, 1987).

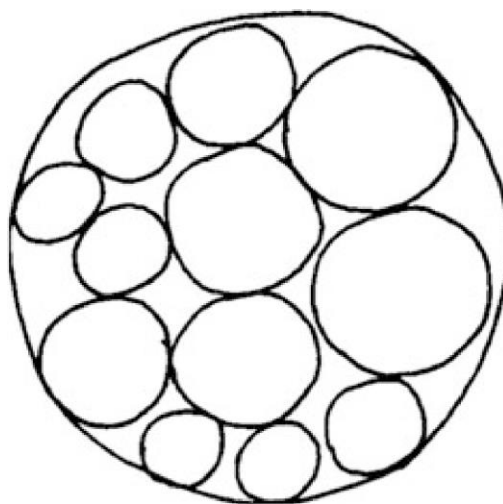


Figure 1.2. The Muslim city as a collection of homogenous areas (Source: Rapoport, 1977).

Moreover, Islamic cities are grouped based on their origin and divided into three types: the first: urban settlements of organic growth (exemplified by Erbil, ancient Arbela) (Figure 1.3). And the second type is, the cities of Graeco-Roman planned origins which were taken over by the Muslims as their empire expanded (for instance, Aleppo or Damascus) (Figure 1.4); and third, new cities founded in conquered lands by the Muslims armies (for example, Baghdad or Tunis) (Morris,1972).



Figure 1.3. Old city of Erbil (ancient Arbela), example of the existing urban settlement types (Source: Morris, 1994).

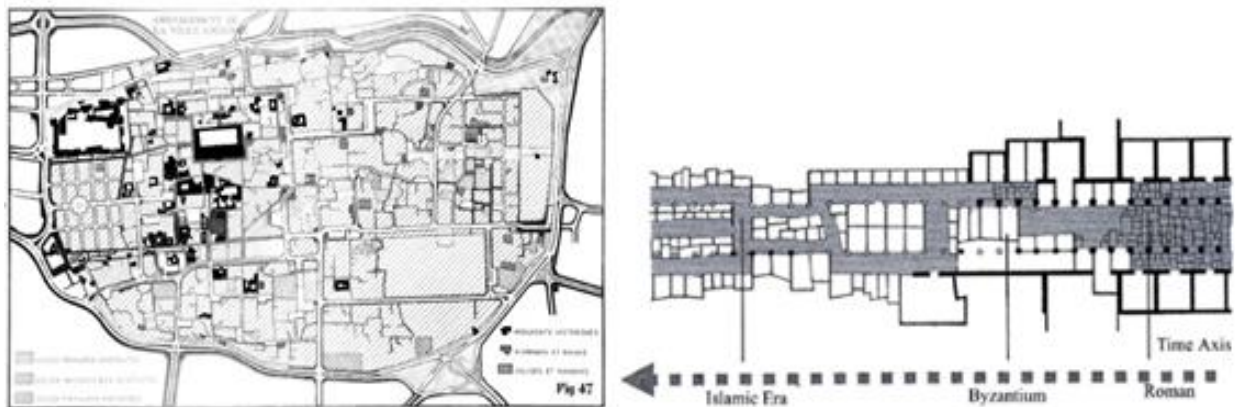


Figure 1.4. The old city of Damascus. City example of the Greek and Roman planned origin types (left) (Source: https://archnet.org/authorities/3603/media_contents/96452). The street transformation process from the Roman colonnaded avenue to the later Islamic suqs (right) (Source: Bianca 2000, p.127, original Schoenauer, 1981).

A basic feature of Arab Muslim cities is a strong centrality in urban organization and a marked separation between a multi- functional public urban core, and the private zones of residence. The city center encompasses different layers of interconnected souks (permeable space open to the

“other”, usually organized around a covered market and the principal mosque, which could have at the same time been a university (Von and Jaber 2013).

The defensive system of an Islamic city included a relatively simple wall, strengthened by towers, with defensive additions at the gates. With few exceptions, the Kasbah (the citadel of the ruling elite) was positioned against or astride the city wall, a characteristic seemingly inherited from ancient Mesopotamia, that was in direct contrast to Western European form where the citadel was in the center (Morris, 1972)

The intricate street system, determined by the aggregation of residential buildings, was mainly composed of two types of streets: the thoroughfares, with a width of (3.23–3.50 m), allowing passage of two laden camels; and the culs-de-sac, with a width of about (1.84 m - 2.00 m), allowing passage for one laden camel (Figure 1.5). In this system of extremely narrow streets, the presence of a square, facing a mosque or comprising a market, would be an exceptional public space element. Also, there are three-four hierarchical levels and the principle which usually prevailed was the branching out of a planned route from a matrix route (the centripetal main streets that converged at the center from a city gate), a possible further Y-shaped branching out of a secondary planned route from the main one, and a further subdivision in a layout of a lesser order, but rarely finding connecting routes among these streets (Figure 1.6) (Von and Jaber 2013).



Figure 1.5. Collector streets helping in breaking the way from the public areas to the residential quarters in Fez (left) (source: Bianca, 2000, p. 83). Saudi Arabia, AlQasim narrow streets, covered alleyways (right) (Source: Hakim, 1986).

Therefore, the internal narrow roads did not have provisions for vehicular movement and hence preferable mode of movement was walking with complete segregation of private and public spaces leading to purely residential land use. Each neighborhood cluster has its own set of tradition and culture which further integrated into a united urban form (Bianca, 2000; Hakim, 1986).

Housing districts were composed of several housing clusters, clusters were in turn composed of enclosed units around a central courtyard, wrapping around internal dead-end alleyways (Figure 1.6). The courtyard house became the favored typology of most Arab Muslim cities, its enclosed and introverted private space perfectly served the requirements of the Islamic social order centered on the holiness of family life but equally optimal for the climate. (Von and Jaber 2013). Plots of Islamic cities were very irregular both in terms of form and size. Except for a courtyard, building coverage was extremely high and each house would occupy the whole plot. (Schoenauer 1981).

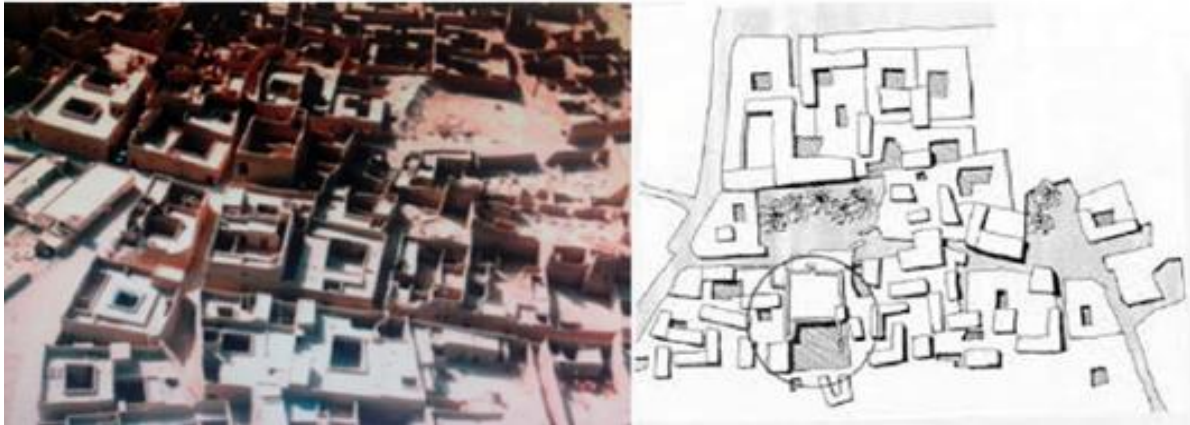


Figure 1.6. Old urban fabric of Riyadh city (Source: (left) Aina, et al. 2013 & (right) Al-Hemaidi, 2001)

Also, the hot and arid climate along with the need for segregation of private spaces from semi-private and public spaces led to introverted urban plans. The old settlements possessed a high degree of ethnic and religious homogeneity, where outside intruders were not allowed into private spaces of inhabitants. The openings opened inside the central courtyard rather than the main streets to ensure high-level privacy, especially for its women (Kiet, 2011).

Consequently, housing in this type of climate arranged in compact patterns, one close to the other, leaving minimal separation in the form of alleys or patios, thereby reducing the areas exposed to the sun and blocks the hot wind (Figure 1.7) (Coch, 1998; Foruzanmehr, 2017).



Figure 1.7. Ghadames City, Libya (Source: Eltrapolsi and Altan 2017)

One of the essential lessons learned from historic vernacular settlements is the compact form. Between the urban design strategies suitable for the hot-dry climate city, Golany (1980) mentions: "Urban experience in the arid zones shows that compact forms are effectively adjusted to climatic stress."

This type of pattern became universally adopted by the people of the region. Anybody experiencing the severe climate of the desert naturally seeks shade that is incorporated into the cities by the orientation and by narrowing the streets (Fathy, 1986). This street structure helps avoid the hot solar radiation and winds from the desert. This is achieved by making the streets winding in shape with closed vistas. Fathy (1973) states: "*At first sight, the plan of an Arab city, with its irregularities, might appear to have developed haphazardly. However, from further analysis, we shall see its functional and logical reasons.*"

1.3 THE CLIMATE OF THE CITY OF JEDDAH, IN SAUDI ARABIA

In this thesis the city of Jeddah has been selected as a case study. Jeddah lies in the Western regions with coastal cities that overlook the East coast of the Red Sea. With 3.9 million inhabitants, Jeddah is considered the second-largest city in Saudi Arabia in terms of population after Riyadh, the capital city. With a land area of approximately 1600 km², Jeddah is the most important seaport in Saudi Arabia. The city lies at the latitude 21° 32' North and longitude 39° 10' East at approximately 12 m above the sea level (Figure 1.8).

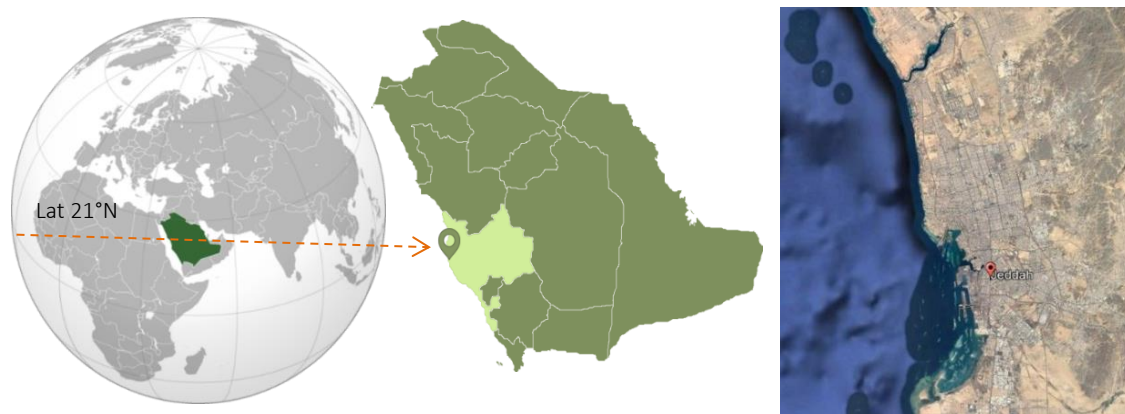


Figure 1.8. Location of Jeddah on the Saudi Arabian map showing the latitude.

The Kingdom of Saudi Arabia (KSA) lies between latitudes 32°N and 17.5°N and longitudes 50°E and 36.6°E (Figure 1.9). The land elevation varies between 0 and 2600 m above sea level. Complex terrain is found in the Southwest region of the Kingdom. The East and the West coasts of the Kingdom are located on the Arabian Gulf and the Red Sea (Figure 3.4).

The country occupies an area of approximately 2,149,690 km². Thus, Saudi Arabia comprises about 80% of the Arabian Peninsula and shares borders with several countries including Jordan and Iraq to the North; Kuwait, Bahrain, Qatar, and the United Arab Emirates to the East; and Oman and Yemen to the South (Rehman, Bader, & Al-Moallem, 2007).

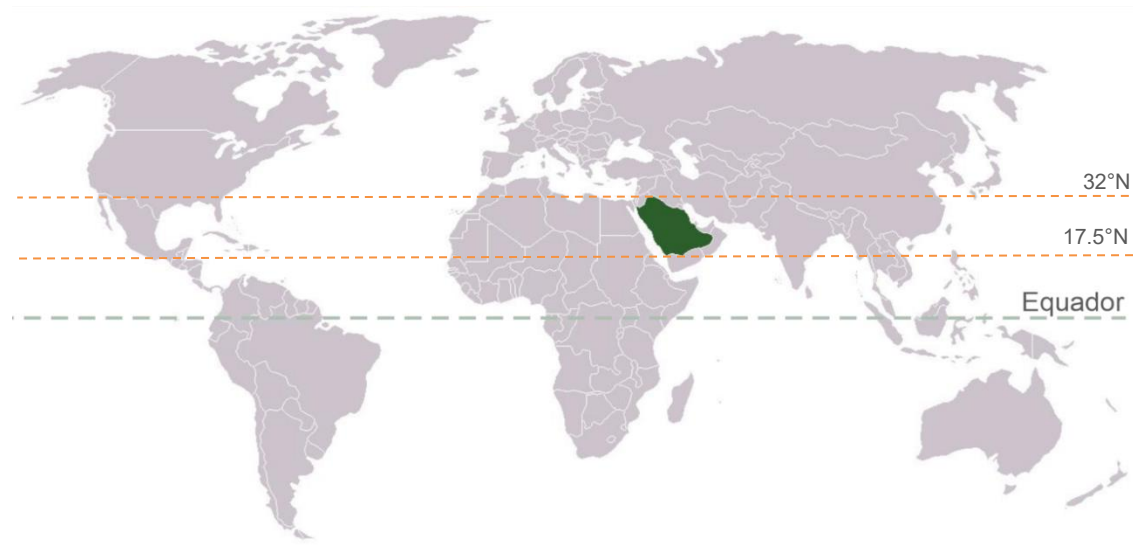


Figure 1.9. Saudi Arabia on the world map highlighted in green.

Saudi Arabia has a population of approximately 34.1 million inhabitants, according to the last statistics of the census (GAS, 2018). Indeed, over 23 million, or equal to 82.29% of the population, are living today in urban areas as reported by the World Bank (World Bank, 2014).

According to Köppen's climate classifications (Peel, 2007), the climate in Saudi Arabia in general is classified as BWh which is a hot-arid climate region (Figure 1.10). Countries located within this BWh climate zone have a desert climate with an extremely high temperature, extreme diurnal temperature differences, low humidity, high evaporation, and scarce precipitation. However, various climate conditions can be observed in the countries that are characterized by hot-arid depending on the land's topography and distance from water bodies.

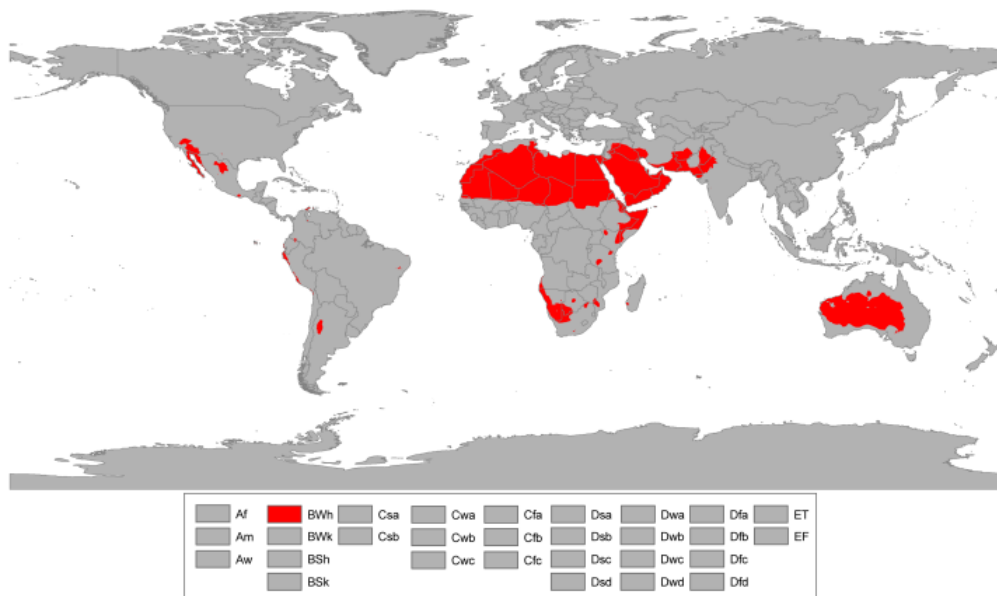


Figure 1.10. Classification of the BWh climate region (in red) (Source: Beck, 2018)

Jeddah lies very close to the Tropic of Cancer; the climate of Jeddah city is directly affected by its geographical location. The Red Sea moderates the high temperatures, and being a coastal city, the humidity is moderate. This affected to a large extent the urban structure of the old part of the city as well as the traditional houses before cars appeared. Generally, it has a hot climate with an average low/high temperature varying between 18°C and 39°C, rarely going below 16°C or above 41°C. The relative humidity varies between 48% to 72%. Rainfall in Jeddah is generally sparse and usually occurs in small amounts in November and December (Figure 1.11).

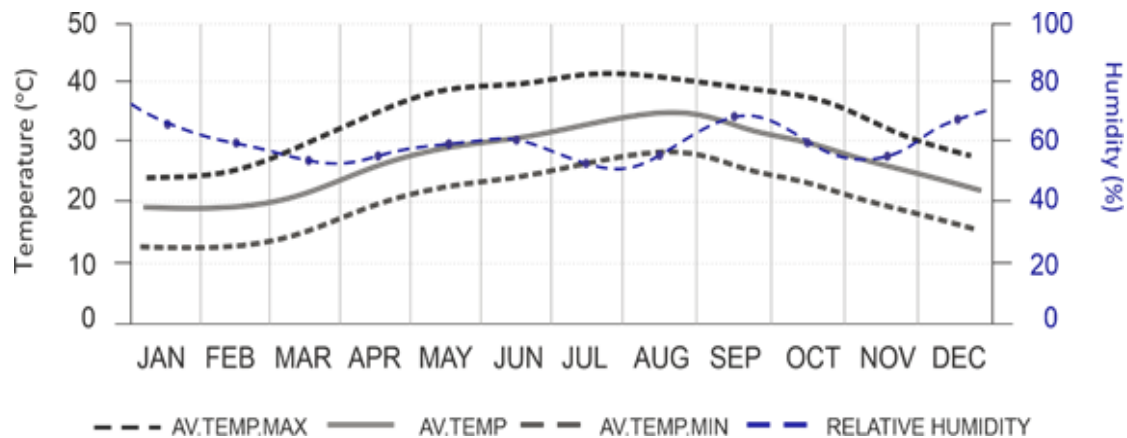


Figure 1.11. Temperature (Average maximum, Average and Average minimum), and average relative humidity of Jeddah city.

In cities with a hot-dry climate and located in mid-latitudes, solar radiation is the most important climatic factor (Coch & Serra, 1995); therefore, this thesis articulates this climatic factor. As a desert city at a medium latitude, Jeddah's sky is almost always clear the entire year-round.

In cities with a hot-dry climate and located in mid-latitudes, solar radiation is the most important climatic factor (Coch & Serra, 1995); therefore, this thesis articulates this climatic factor.

In the graph in Figure 1.12, the values of global solar radiation from King Abdulaziz Airport Station's meteorological data are compared with direct solar radiation obtained through Heliodon2. The airport station presents values between 3.5 kWh / m² per day in December to 8 kWh / m² per day in April, with an annual average of 5.9 kWh / m² per day. The simulation values vary between 2.6 kWh / m² per day in December to 7.2 kWh / m² per day in June, with an annual average of 5.2 kWh / m² per day.

The total annual horizontal irradiation value is between 2,267 - 2,400 kWh / m² (World Bank, Global solar atlas 2018). The city receives an average annual solar radiation of 5.9 - 7 kWh / m² per day on the horizontal plane.

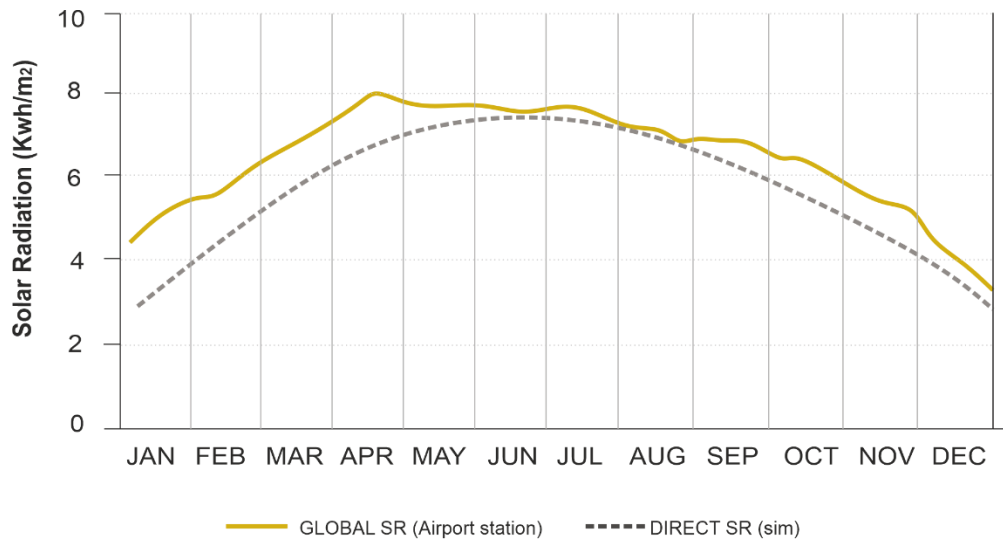


Figure 1.12. Comparison of the global solar radiation (Global-SR) (Airport station) (Source: <http://www.meteonorm.com>), with the simulated direct solar radiation (Direct-SR) (Heliodon2)

As a desert city at a medium latitude, Jeddah's sky is almost always clear the entire year-round. The intensity of the blue sky (The low coverage of clouds) in mid-latitudes is related to high short-wave radiation (direct radiation), it influences the amount of solar radiation received on the surface, and at the same time, with a high radiative cooling capacity (Figure 1.13) (Torres-Quezada, 2018).

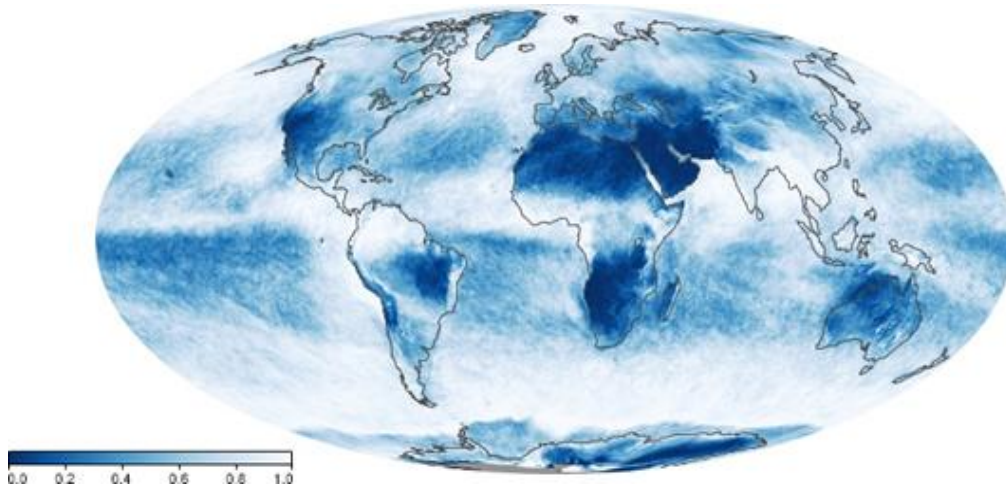


Figure 1.13. Cloud coverage map satellite images Jun 2018 NASA (Source: https://earthobservatory.nasa.gov/global-maps/MODAL2_M_CLD_FR)

To determine clouds' presence in Jeddah city, a hypothetical analysis was done to correct Heliodon's theoretical energy data. They are compared with the local meteorological station's real data, and a correction factor is established using Heliodon Plus (Nahon 2016). Observing the difference between the theoretical and measured values of direct radiation, we establish a correction factor with the following formula:

$$\text{Correction factor} = \frac{\text{Solar radiation calculated from the measured value.}}{\text{Solar radiation calculated by Heliodon.}}$$

To obtain the values, the attribute table displays the clouds correction factor calculated all year round with the software Heliodon Plus. using Jeddah city's meteorological data from Meteonorm. Also, In the following tables, 1.1 and 1.2 display the lower the value, the more clouds are in that month. Months (highlighted blue) have the higher cloud coverage and could be considered the lowest favorable months to emit heat from the earth's surface in hot climate cities to cool the surface. Moreover, the months (highlighted red) have low cloud coverage.

Table 1.1 (Latitude 21.32' N) Jeddah correction Factor Heliodon

Months	Jan	Feb	Mar	Apr	May	Jun	July	Aug	Sep	Oct	Nov	Dec
Correction	0.59	0.78	0.84	0.82	0.72	0.57	0.53	0.53	0.69	0.82	0.74	0.66

Table 1.2 Jeddah meteorological cloud data from Meteonorm (an okta is a unit of measurement of cloud)

Months	Jan	Feb	Mar	Apr	May	Jun	July	Aug	Sep	Oct	Nov	Dec
OKTA	4	2	2	2	0	2	2	1	1	2	3	4

Figure 1.14 shows that July and August have the most presence of clouds (53% correction on the theoretical calculation of direct solar radiation according to the presence of clouds in Jeddah) where the temperature is the highest in those two months and the humidity is low as shown in the highlighted figure. While March has the least cloud coverage with an 84%, and the annual mean cloud presence would then be 69%.

We must highlight here that the minimum and maximum correction factor we obtained does not match the minimum and maximum cloud fraction from metronorm. The cloud cover fraction traduces the fraction of the sky covered by clouds and does not consider the 'thickness' of the clouds (thick dark clouds that block any direct radiation or semi-transparent thin white clouds).

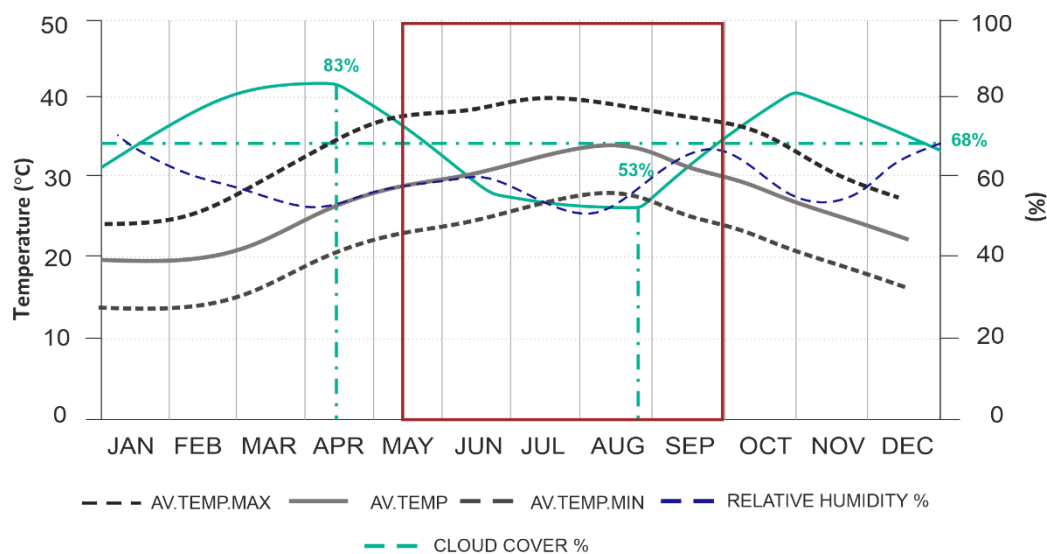


Figure 1.14. Monthly mean cloud cover (cloud cover %) (Heliodon plus cloud correction), compared with the temperature (Average maximum, Average and Average minimum), and average relative humidity of Jeddah city

Furthermore, as shown in Table 1.3, the sun almost reaches the zenith at the summer solstice, reaching 45° at the winter solstice. The difference in day length between the two solstices is two hours and forty minutes. As shown on the isochronal projection in Figure 1.15 (Beckers, 2006), solar height is up to 40° between 10:30 and 13:30 during the entire year, and the direct radiation is then up to 800 kW/m² during sunny hours, reaching 1000 kW/m² in the summertime (Heliodon software).

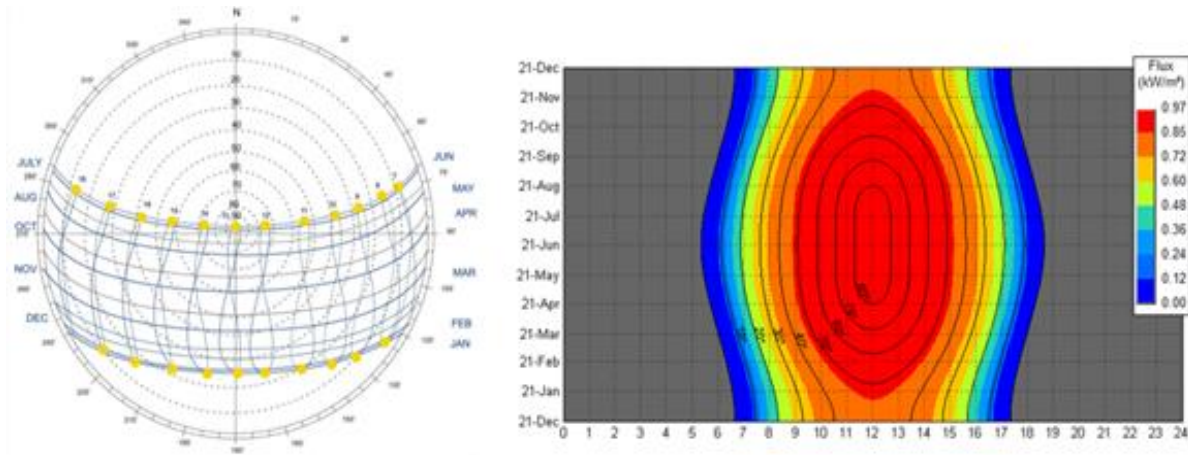


Figure 1.15. Stereographic (left) (Source: Masoud 2013) and isochronal solar figures for Jeddah (right) (Source: Heliodon software).

Table 1.3 Sunrise, Sunset, and solar height at noon for 21st June and 21st December.

	Sunrise	Sunset	Solar height at noon
21 st June	05:20	18:40	88°
21 st December	06:40	17:20	45°

The climatic factor of solar radiation, as seen in this section, plays an important role in a city like Jeddah. Therefore, to carry out the study, more detailed analysis would be required on the incidence of solar radiation at the urban level.

1.4 SOLAR ACCESS IN THE PUBLIC SPACE, JEDDAH CASE STUDY.

The history of ancient Jeddah is a long one, Throughout the history, Jeddah was founded as a fishing hamlet in 522 BC by the Yemeni Quda'a tribe (بنو قضاة). The city of Jeddah acted as the main gate to the Holy cities (Mecca and Medina); it first achieved prominence around AD 647 when third Muslim Caliph Othman Bin Affan ordered the town to be a port to welcome pilgrims coming for the Holy Pilgrimage. The historical town of Jeddah covered an area of 3 km² (Figure 1.16) and comprised of four original quarters, bounded by the city wall. The population then was estimated to be stagnating between 10,000 and 25,000. The main economic base was revenues from commerce and services offered to pilgrims (Al-Naim, 2008).



Figure 1.16. Orthophoto of Jeddah at different scales in 2021. (Source: Own elaboration based on Google Earth Pro)

The high-density houses were connected by shaded, narrow alleyways. These alleyways started growing from semi-public spaces [*cul-de-sac*] until reaching the main public space close to the main mosque. The old town known as (AlBalad) comprised *four* main quarters: *Sham, Madhlum, Bahar, and Yemen*¹ (Figure 1.17) (Khan, Sergeldin, & El- Sadek, 1982).

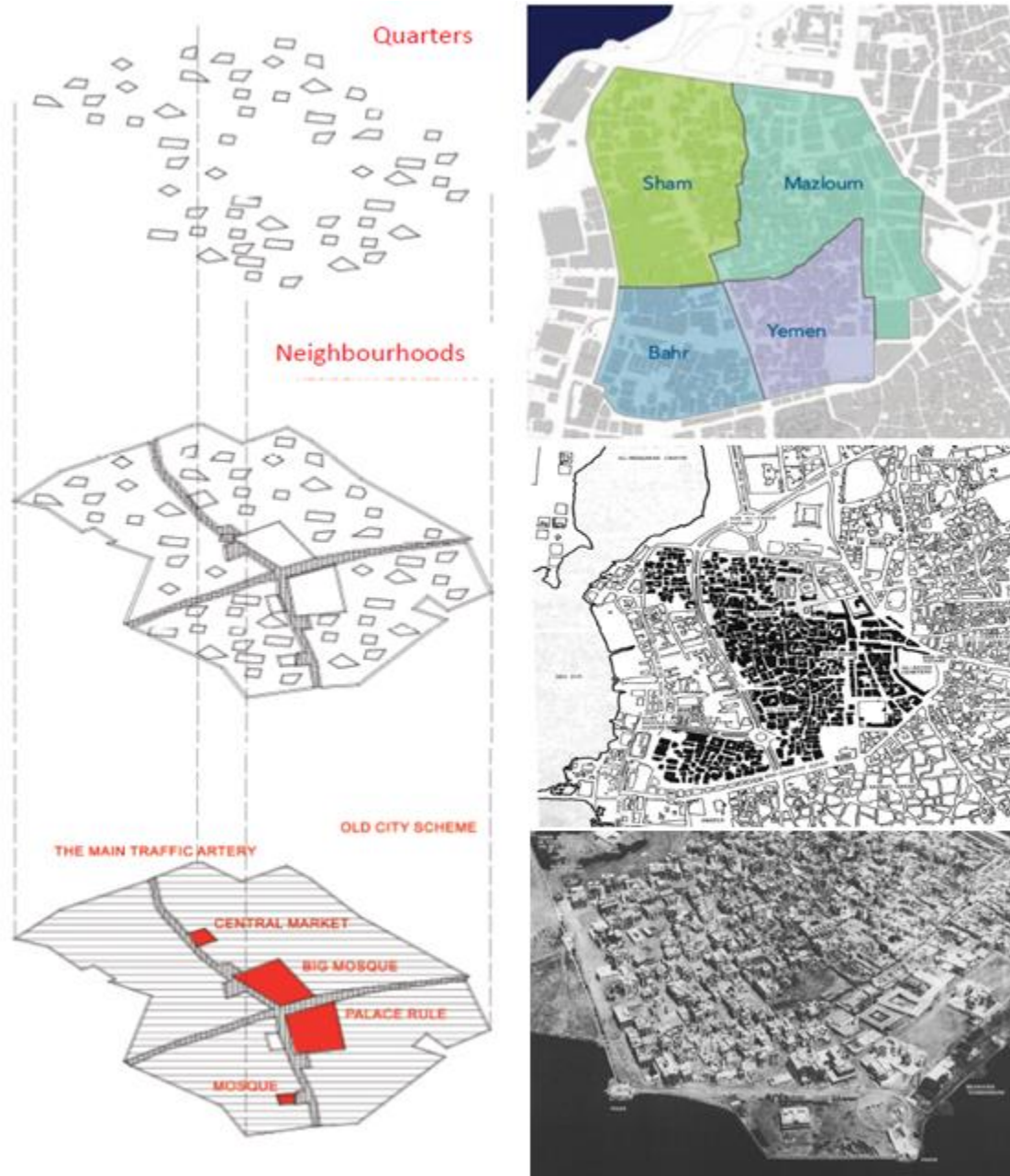


Figure 1.17. (A) The profile of the main commercial axis at the traditional district (Source: Osra, 2018) (B) the four main quarters. (C) Jeddah old urban maps on the and (Source: Historic Jeddah Municipality, Saudi Arabia, 2013, p. 241). And (D) 1938 aerial view of the Old City of Jeddah. (Source: Wikipedia. Retrieved May 2019)

The urban fabric of the Red Sea coastal cities was extremely compact. Housing blocks were typically surrounded by streets from each side and established a direct visual relationship with the semi-public and public spaces by using an architectural element at the front of the house around the main entrance called a *roshan* [window] (Figure 1.18). The *roshan* ensured a safe visual connection with the surrounding by alleviating any concerns related to the privacy of the women dwelling inside the house. The architectural style in Jeddah has been described as an introverted style (Baik and Boehm, 2017).



Figure 1.18. Examples of Jeddah's old buildings showing the wooden extruded windows on the facades with different colors (from different Sources).

The street pattern in the old town obviously did not conform to any rigid geometric pattern. It developed naturally and in stages according to specific needs (Khan et al., 1982). The width of the streets varied according to function and location. The narrower cool and shaded alleys (Figure 1.19) mostly located within the residential quarters were called *Aziggah* (sing., *zugag*) and were sometimes as narrow as 2 meters. The wider streets, sometimes as wide as fourteen meters, were generally called *Shwar'* (Shari') - streets (Al-Hathloul and Mughal, 2004). These streets were the major links between the town gates and the central part of the town. Most of the commercial activities were concentrated on these streets. Diversity of functions and major movements created there an intense activity (Figure 1.20). The basic spatial character is strongly related to the vertical organization of the house facades (Abu-Ghazze, 1994, Alharbi, 1989).



Figure 1.19. The narrow street of old Jeddah city (AlBalad)

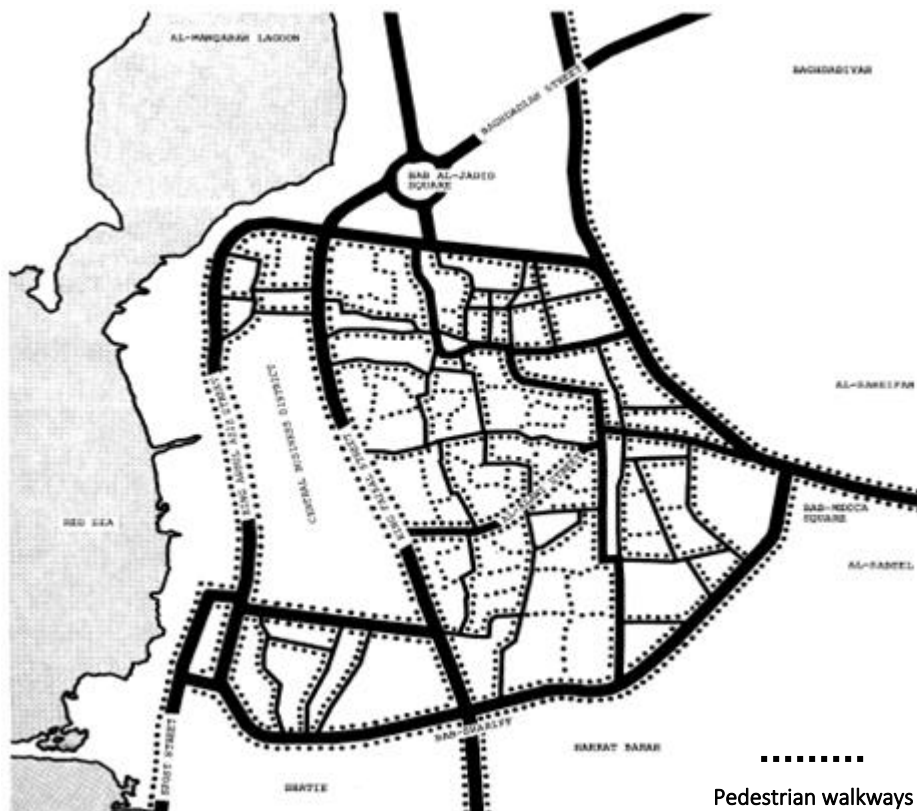


Figure 1.20. Jeddah old area map (AlBalad). The dotted lines show the pedestrians paths (Source: Faden, 1977).

Another unique feature to the street pattern of the old town is the common area. The narrow alleys of the residential quarters usually lead to a series of semi-private tiny squares or plazas. Most often the common area is a simple widening of the alley as it turns a corner, sometimes no more than a setback in the alley, or the junction of two alleys (Figure 1.21). Thus, the narrow alleys and common areas blended with the feeling of sociability, creating an interplay of spatial tension and release and, for climatic reasons, protecting from the sun and to direct the wind (Al-Hathloul and Mughal, 2004).



Figure 1.21. Examples of plazas highlighted in red lines on the left. On the right, the dotted lines demonstrate the path pattern of the pedestrian's walkways within the old area (Source: Alharbi, 1989).

Figure 1.22 shows the examined and analyzed portion of the old fabric (AlBalad), considering that new buildings and new streets were applied. Nevertheless, the examined old portion was the old morphology's central area. The following figures will demonstrate the street ordinations and building heights in the studied area.

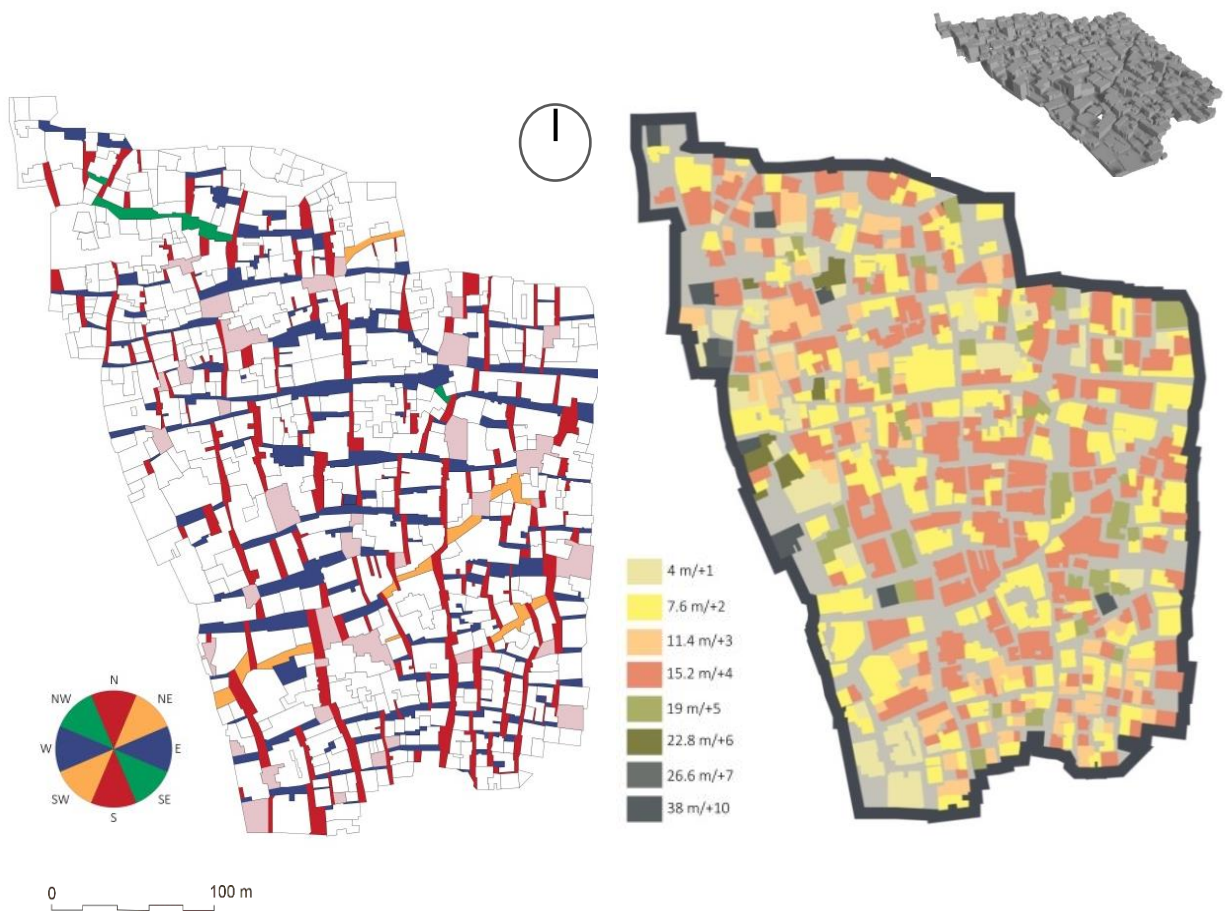


Figure 1.22. Street orientation in AlBalad (left). Building heights in AlBalad (right)

The map on the left in Figure 1.22 demonstrates some of the street orientations in Jeddah's old layout. It also shows the irregularity of the streets. The red lines represent the North-South streets-orientation axes, the blue lines represent the East-West streets orientation axes, the green is the Northwest-Southeast, and the orange is the Northeast-Southwest orientation axes. The most dominant street orientations are the Red and blue lines (North-South and East-West) Axes.

The urban portion of Jeddah, AlBalad, is characterized by narrow streets as mentioned previously; Figure 1.23 demonstrates a sample section of the buildings showing a sample of the existing height to width ratio that elucidates the narrowness of the streets. The building heights range between two to ten levels.

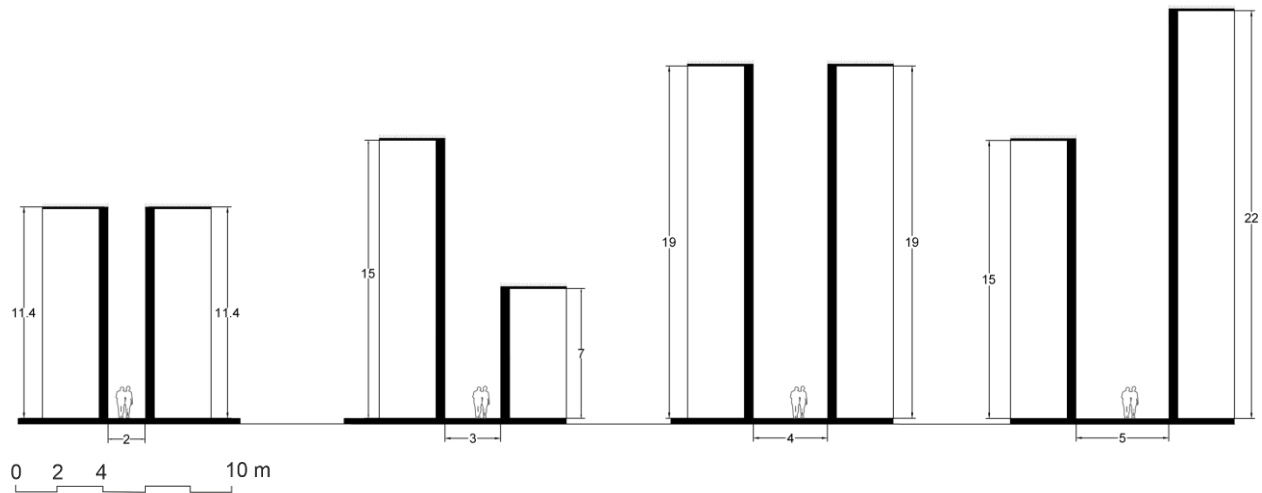


Figure 1.23. Section samples of streets in the AlBalad layout without the projected windows (Rawashin).

After studying and reviewing the formation of old cities in the hot- desert climate, one of the essential conclusions regarding its compact urban morphology to create a better microclimate and outdoor thermal comfort was **shading**. Shading is one of the counteracting measures to thermal stress in hot climate cities since it reduces the solar radiation that is received on the surfaces; it also reduces direct shortwave radiation reaching buildings and ground surfaces and humans (Spronken-Smith and Oke, 1999). The street orientation and canyon geometry generally determine the direct solar radiation amount and shading effect in terms of sky view factor and height-to-width (H/W) ratio (Johansson and Emmanuel, 2006, Oliveira *et al.*, 2011, Shashua-Bar *et al.*, 2012).

The incident solar flux expresses the behavior of the streets and canyons of an urban fabric regarding its immediate radiation intensity. It is calculated as a theoretical energy gain and the exposure surface of the horizontal surface (streets and canyons). The solar radiation simulation considers the influence of the shadows thrown by the surrounding buildings to which reference can be made.

Solar flux results on the given layout and the direct solar radiation changes through chosen days during the summer and winter seasons. In this sense, morphological relationships are shown through a graphical representation of the outcomes that identify the essential morphological parameters concerning direct solar radiation performance. The main geometrical variables

assessing the effect of incoming radiation are the street orientation and sky view factor and height-to-width (H/W) ratio (Johansson and Emmanuel, 2006, Ali-Toudert and Mayer, 2006, Abreu-Harbich et al., 2014, Oliveira et al., 2011, Shashua-Bar et al., 2012).

The outcome derived from the results enables an assessment of the incident solar radiation on the AlBalad urban layout on the horizontal (streets) and the vertical surface and evaluating the amount of solar flux on both surfaces.

The urban layout system's overall parameters for solar assessment are specified to be adapted to different selected components of the urban morphology and the various aspects of their solar behavior. Table 1.4 shows a complete list of solar radiation indicators that will be used throughout the discussion.

Table 1.4 List of solar radiation indicators.

Solar indices	Units
Incident solar flux $Q=$	kWh/m ² /day or kWh/m ² per day
Sky view factor (SVF) $\Psi =$	%
Solar time interval =	h

1.4.1 The SVF Influence on the Compact Urban Morphology (AlBalad)

Theoretically, “the sky view factor (SVF) is a geometrical concept that describes the fraction of the overlying hemisphere occupied by the sky” and is a dimensionless parameterization of the quantity of visible sky at a given point (Oke, 1981). It is a graded value between zero and one and in percentage is from 0% to 100%. It represents the sky's openness to radiated transport, for open spaces where the sky is entirely unobstructed, allowing all outgoing radiation to cast freely into the atmosphere (Brown et al., 2001)

The simulated layout clearly shows the street orientations different behaviors regarding the SVF (Figure 1.25). The distribution of the average SVF differs from one street orientation to the other. The proportion of the urban street H/W ratio directly impacts the SVF value and solar radiation incidence on the horizontal surface (street). Oke (1987). Also, it is assumed that a more vertical development, urban canyon resembles a progressively smaller visible portion of the sky and that this performance development exhibits itself both in the streets, Plazas, and in the street's intersections.

The color map in Figure 1.25 is composed of colors ranging from dark gray (lowest value) to white (highest values), with the lighter gray-scale color representing average values. The simulation showed (Figure 1.25) in the old compact layout (AlBalad) the average SVF for the entire streets' layout generally of 28% and a maximum average SVF of 81.5 %. Plazas (public open spaces) are the spaces that receive the highest value of SVF among all streets, with an average of 40% to 80%. Due to the plazas' function in this urban setting, they are more exposed resulting in a higher value.

Due to the narrow street construction, the old urban layout's streets have an aspect ratio ranging between 3 and 10. The simulation shows that the average SVF value for streets orienting N-S ranges from 10% to 25%. Whereas the E-W streets range from 30% to 40%, the NE-SW streets between 20% to 50%, and the NW-SE streets between 30% and 50%. The plazas range from 50% to 90%. Therefore, the N-S-oriented streets are more shaded than the E-W and NE-SW.

It is observed from the simulated layout that the orientation North-south canyon has the lowest average SVF value of all orientations, even if it has low obstructions. Among the rest of the orientations (East-West, Northeast-southwest, Northwest- Southeast), the East-West orientation generally provides a greater degree of vision towards the celestial vault concerning the street orientations, average SVF value, and that corresponds to the solar access.

The horizontal surfaces (Streets) have a more unfavorable condition concerning facades with respect to the solid sky angle. How is this behavior explained? Vertical surfaces (Facades) have a more unfavorable starting condition with respect to the streets in terms of solid sky angle. Nevertheless, the average SVF of both surfaces are quite similar (Figure 1.24). Moreover, the influence of obstructions is considerable in the minimum level of the urban canyon. Therefore, the urban street obtains greater visibility of the celestial vault due to the solar angles.

In the subsequent discussions, the effect of the value related to solar radiation intensity and the correlation between the solar period and SVF will be examined to identify which parameters are more useful for creating geometrical rules that will reduce the intensity of the incident solar radiation.

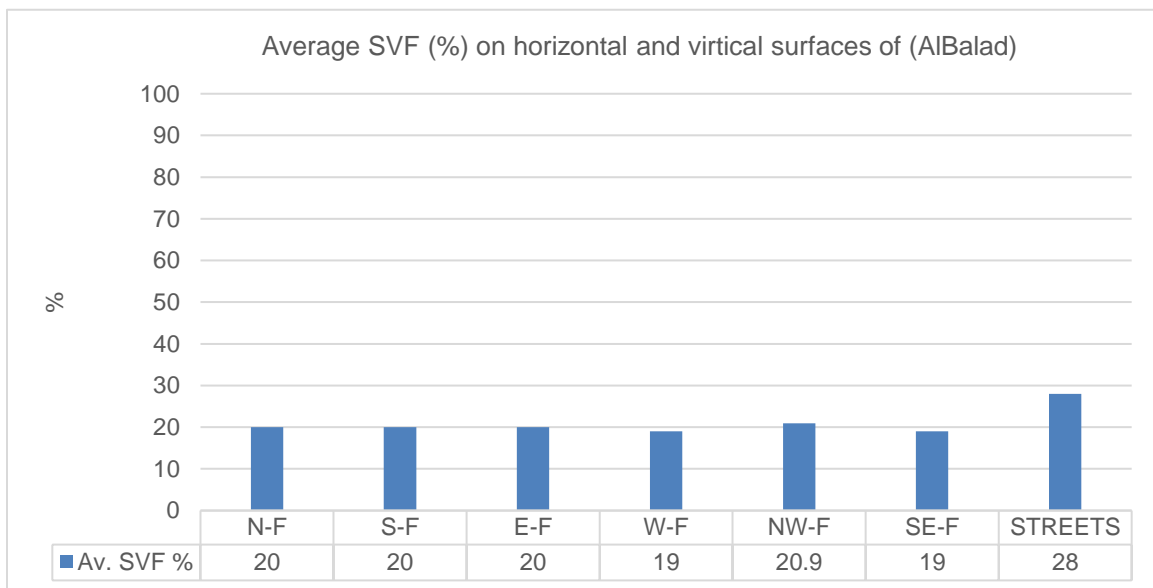


Figure 1.24. The average Sky View Factor of the Streets and the different-oriented facades in the old compact layout (AlBalad).

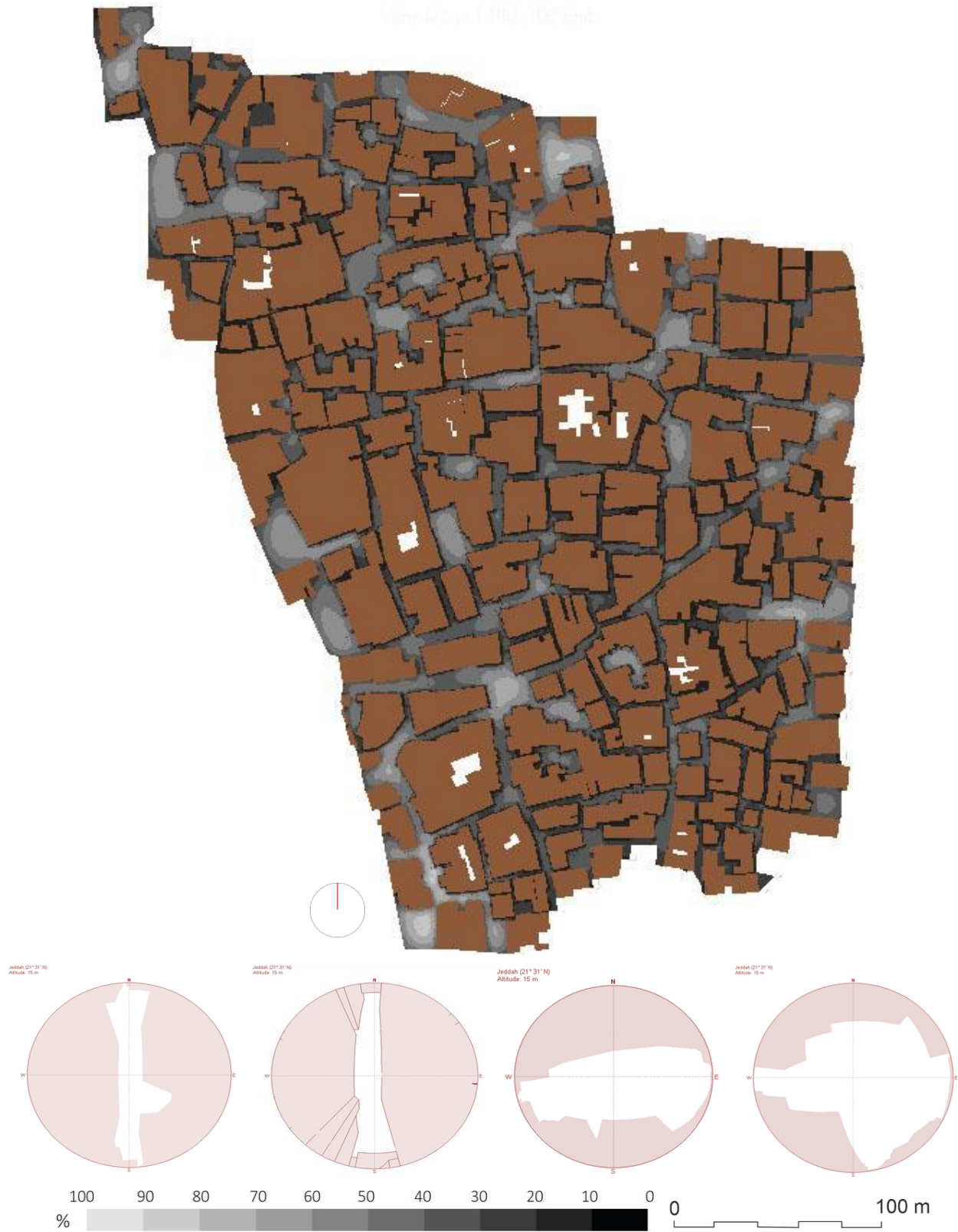


Figure 1.25. AlBalad (the old layout) Sky View Factor (top) Sky View Factor orthograph projections some of the streets and plazas (bottom). (Source: Heliodon software).

1.4.2 Solar Radiation evolution and Time Interval on the Horizontal Surface (streets) of AlBalad -Summer and Winter Solstice

The solar angle during summer and winter impacts the direct solar radiation on the street surface. Thus, simulations were performed on the whole layout rather than from a specific point. This means that the morphology evaluation is conducted to examine how far the urban geometry affects the incident solar radiation intensity, considering all the obstructions and the parameters that affect each street rather than investigating one street. The simulation revealed that the average solar flux of the old compact layout AlBalad on the street level is 3.27 kWh/m²/day, and in winter, 0.58 kWh/m²/day.

Figure 1.26 shows the solar radiation evolution in the layout on the horizontal surface of the roads, and it reveals the hour with the most elevated solar radiation in the layout. There is also a difference in day length between the two solstices to be considered. The simulation revealed that AlBalad streets starts receiving incident solar radiation in summer at 7:00 o'clock, and this continues until 17:00 o'clock, with a total of 10 hours. Nevertheless, the intensity is different from one time to the other, influenced by the morphological parameters. As expected, the role of compactness was decisive. As shown in Figure 1.26, the streets receive between 20 – 740 Wh/m² peaking between 11:00 o'clock to 13:00 o'clock with 600- 740 Wh/m². Due to the building heights and the street width, the obstructed buildings prevent direct solar radiation from penetrating easily.

The irradiance starts to reduce before and after noontime as the solar angle moves during the day. On the other hand, the layout receives in winter direct solar radiation between 8:00 o'clock and 15:30 o'clock, which is 7½ hours of direct solar radiation, ranging from less than 50 Wh/m² to 180 Wh/m². The peak hour of winter direct solar radiation in the streets is between 10:30 o'clock and 13:00 o'clock when they receive between 100 Wh/m² and 180 Wh/m². The highest time incident solar radiation received is at noon with 180 Wh/m². Almost all streets are largely protected from the sun in the morning as well as in the afternoon. Nevertheless, results indicates that streets experience more heat stress over a longer time at noon in both seasons, summer and winter.

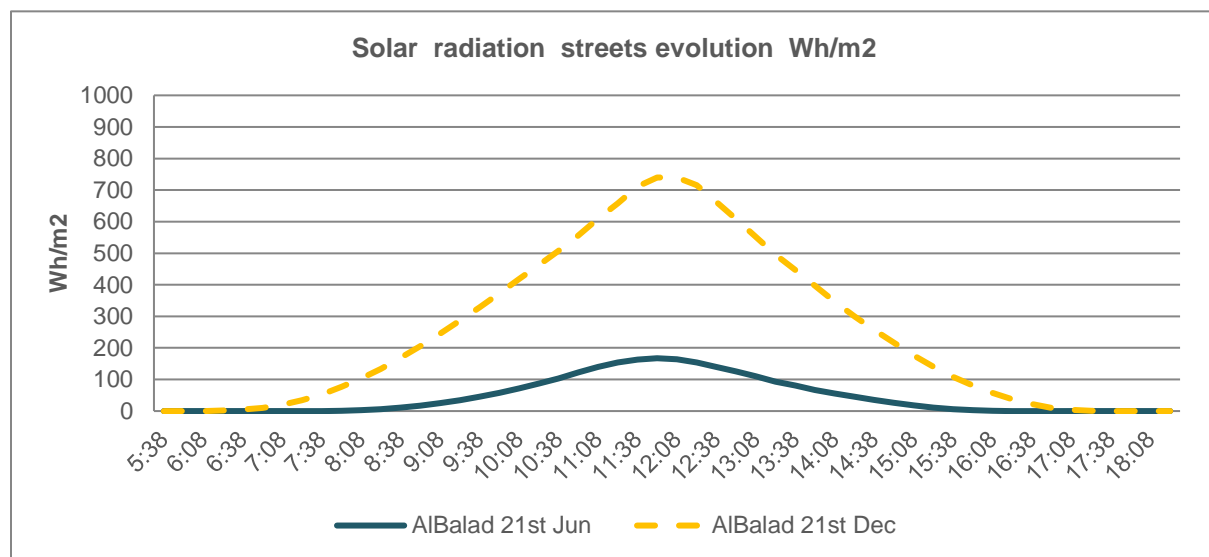


Figure 1.26. Solar flux evolution of the horizontal surface (streets) for the old layout (AlBalad) with a maximum and a minimum in summer 21st June and winter 21st. December

The solar access time interval shows the capability of streets receiving sunlight through property lines with or without obstructions. The solar time interval impacts the solar heat of the streets. By reducing the solar period through the urban morphology, heat penetration is reduced accordingly.

The solar time interval in AlBalad is analyzed according to the obstructions that are redefined through the urban morphology parameters H/W ratio and SVF together with the street orientation, they determine the radiation performance. Figure 1.27 and the Heliodon maps in Figure 1.28 for summer and Figure 1.29 for winter indicate the resulting levels of solar access time visualized by color scales. The colors in the map range from blue (lowest value) to red (highest value) via green, yellow, and orange (which are average values).

Figure 1.27 shows the sun-time interval between N-S, E-W, and NS-SW streets. The differences are high due to Jeddah's location, notably its latitude. The asymmetrical streets, the height of buildings, and the irregularities of the streets all have an impact on the results on the surfaces. In AlBalad, the N-S orientations have a low sun period due to the deep streets in relation to the street orientation and the solar angle during summer. In summer, the N-S streets receive an average of 2 h to 2½ h of solar radiation and in winter an average of ½ h to 1 h. This is explained by the difference in solar angle between winter and summer and the high built-up density of the urban layout that obstructs solar radiation from penetrating.

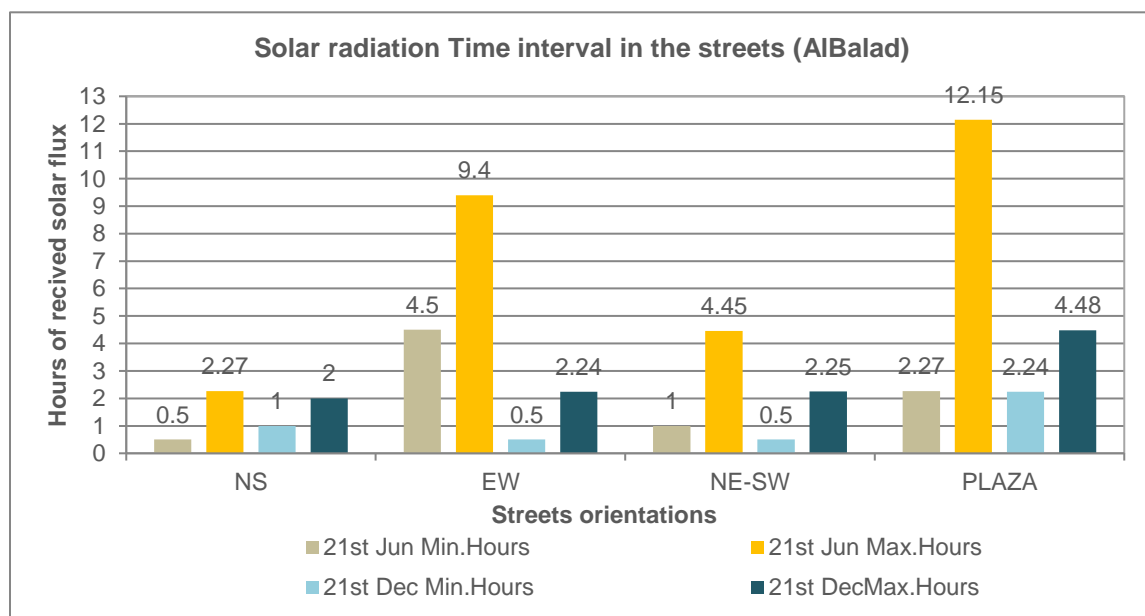


Figure 1.27. AlBalad (the old layout) Solar radiation time interval on all street orientations.

Moreover, during summer, the streets in E-W orientation receive an average of 5 h to 9 h of solar radiation, sometimes as long as 10 hours (Figure 1.28). In winter, they range between 0 h to 2h 24 minutes of solar radiation (Figure 1.29). The almost 0 h is due to the perpendicular axis in relation to the solar angle in summer and winter. In contrast, the intermediate orientation NS-SW canyons receive on average 1 h to 4 h of sun during summer, at times almost 5 h. For plazas, solar radiation ranges from 2 h 27 minutes to 12 h due to a higher SVF. Basically, N-S canyons receive the least sun hours compared with other canyon orientations and E-W canyons have the

longest sun period. This relationship between the canyon orientation in relation to the different aspect ratios and SVF shows the difference in the sun temporal period which displays the effect of the built obstructions.

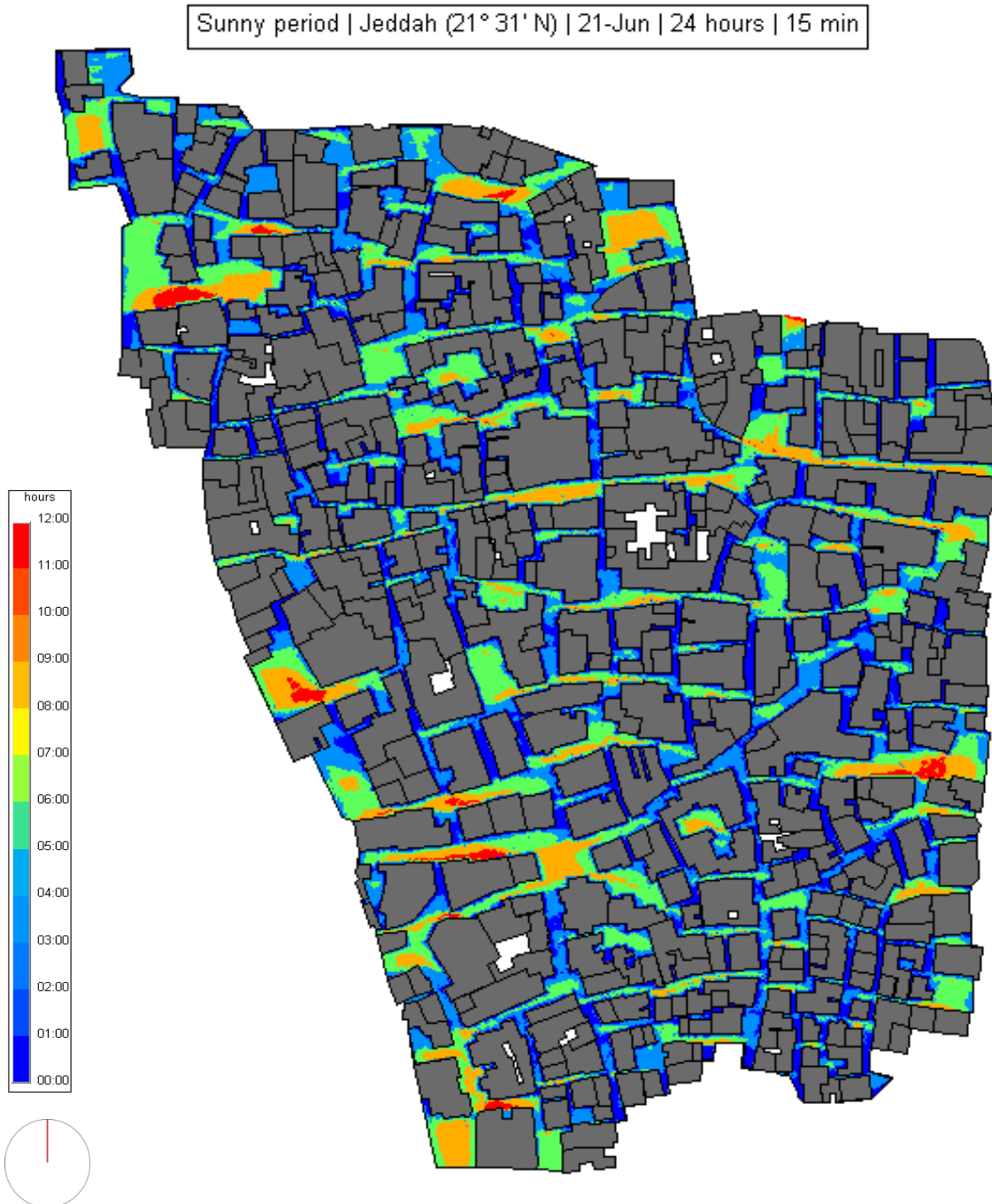


Figure 1.28. AlBalad (the old layout) summer, 21st of June, solar radiation time interval (sun period). Source: Heliodon software.

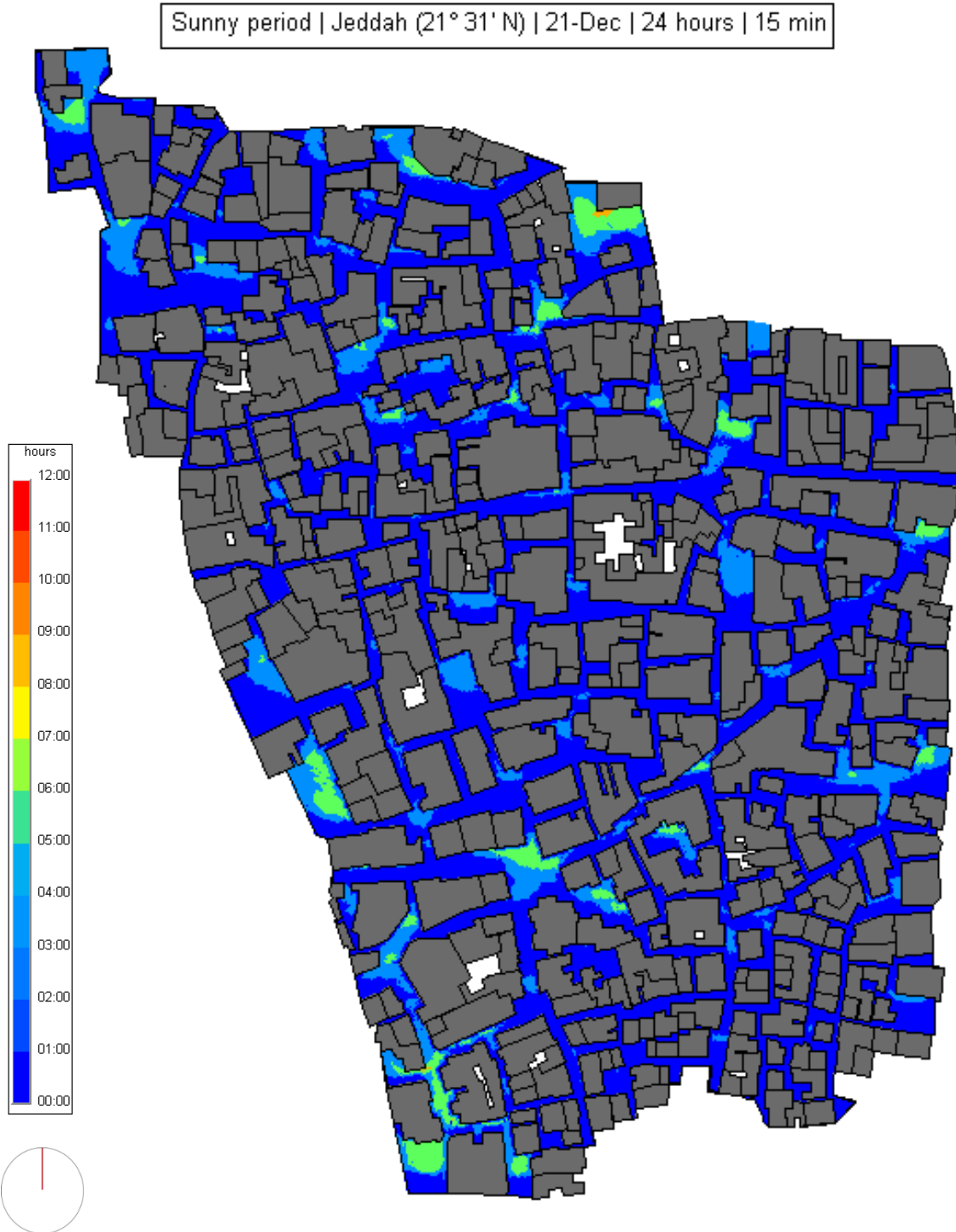


Figure 1.29. AlBalad (the old layout) winter, 21st of December, solar radiation time interval (sun period). Source: Heliodon software.

1.4.3 Solar Flux in Relation to the Compact Urban Morphology in AIBalad

The amount of direct solar radiation on the streets, including the discomfort that it produces in the human body, was determined by analyzing and assessing the solar flux received on the streets- using the sunshine duration and Sky View Factor. This was done by dividing the total amount received on a horizontal surface and the area including streets, facades, and plazas as shown below in the graph (Figure 1.30).

As mentioned earlier the simulation reveals that the average solar flux received on a horizontal surface (streets) in summer is 3 kWh/m² per day and in winter, 0.58 kWh/m² per day. As for the vertical surfaces (Facades) has an average Solar Flux of 1.8 kWh/m² per day and in winter 0.90 kWh/m² per day. Given that narrow streets characterize the old layout, building blocks are obstructing the solar radiation from penetrating to the streets and facades.

Figure 1.30 below shows the streets-oriented N-S with H/W ratio 3 to 10 and an average SVF ranging between a minimum of 20% and a maximum of 40%. This orientation amounts to an average solar flux of 1 to 2.5 kWh/m² per day during summer, while in winter, 1 kWh/m² per day it is due to the high H/W ratio and the low average SVF including the low solar angle.

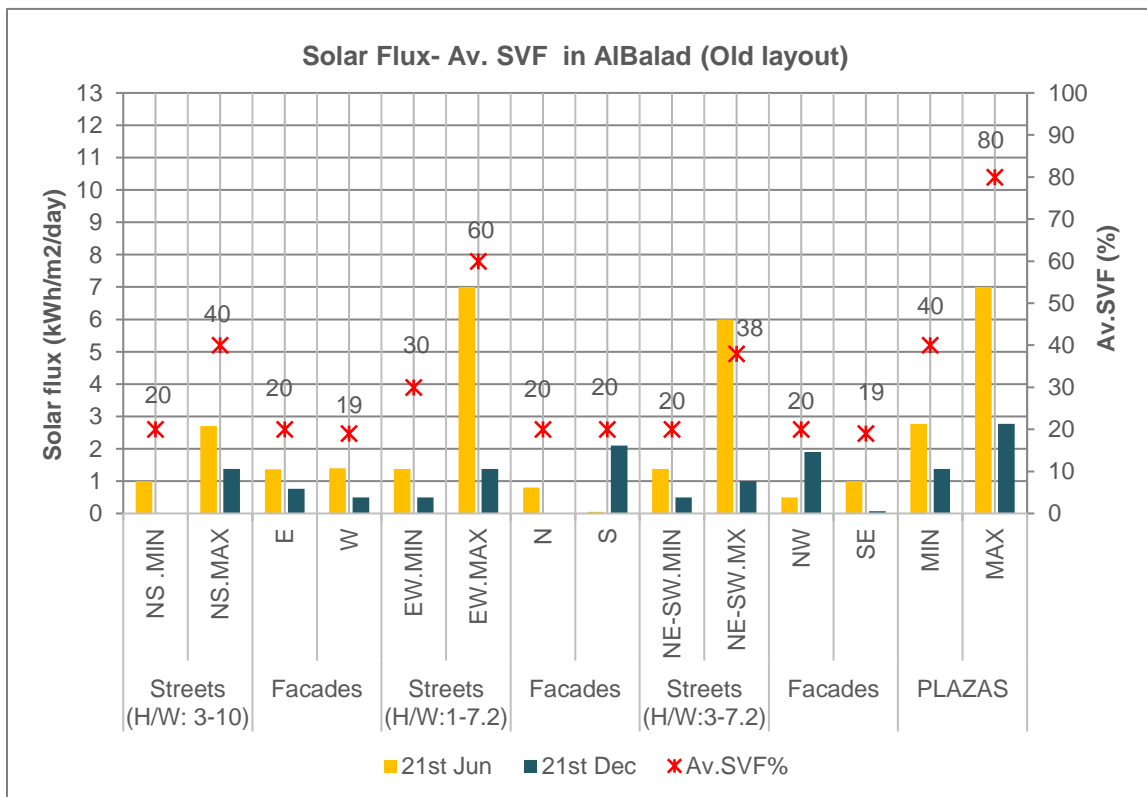


Figure 1.30. Summer and winter solar flux and the average sky view factor of streets and facades in the old compact layout (AIBalad).

Furthermore, Figure 1.30 and 1.31 shows for summer that the E-W orientations have an H/W ratio ranging from 1 to 7.2, an average SVF ranging between a minimum 30% and a maximum 60% receiving an average solar flux of 1.5 to 7 kWh/m² per day. In winter (Figure 1.30 and 32), ranges between 0.5 to 1.5 kWh/m² per day. In addition, the intermediate NW-SE orientation with an H/W ratio of 3 to 7.2 records an average SVF between a minimum 20% and a maximum 38%. In summer, the average solar flux is between 1.3 to 6 kWh/m²/day and in winter between 0.5 to 1 kWh/m² per day. On the other hand, plazas have an average SVF ranging from a minimum 40% and a maximum 80% with an average solar flux of 3 to 7 kWh/m² per day in winter and 1.3 to 3 kWh/m² per day in summer. Here, it should be noted that while the E-W canyon orientations are characterized by a lower average SVF than described for plazas, they still receive the same amount of solar flux due to a street-orientation alliance in relation to the solar movement.



Figure 1.31. AlBalad (the old layout) summer, 21st of June, solar flux. Source: Heliodon software.

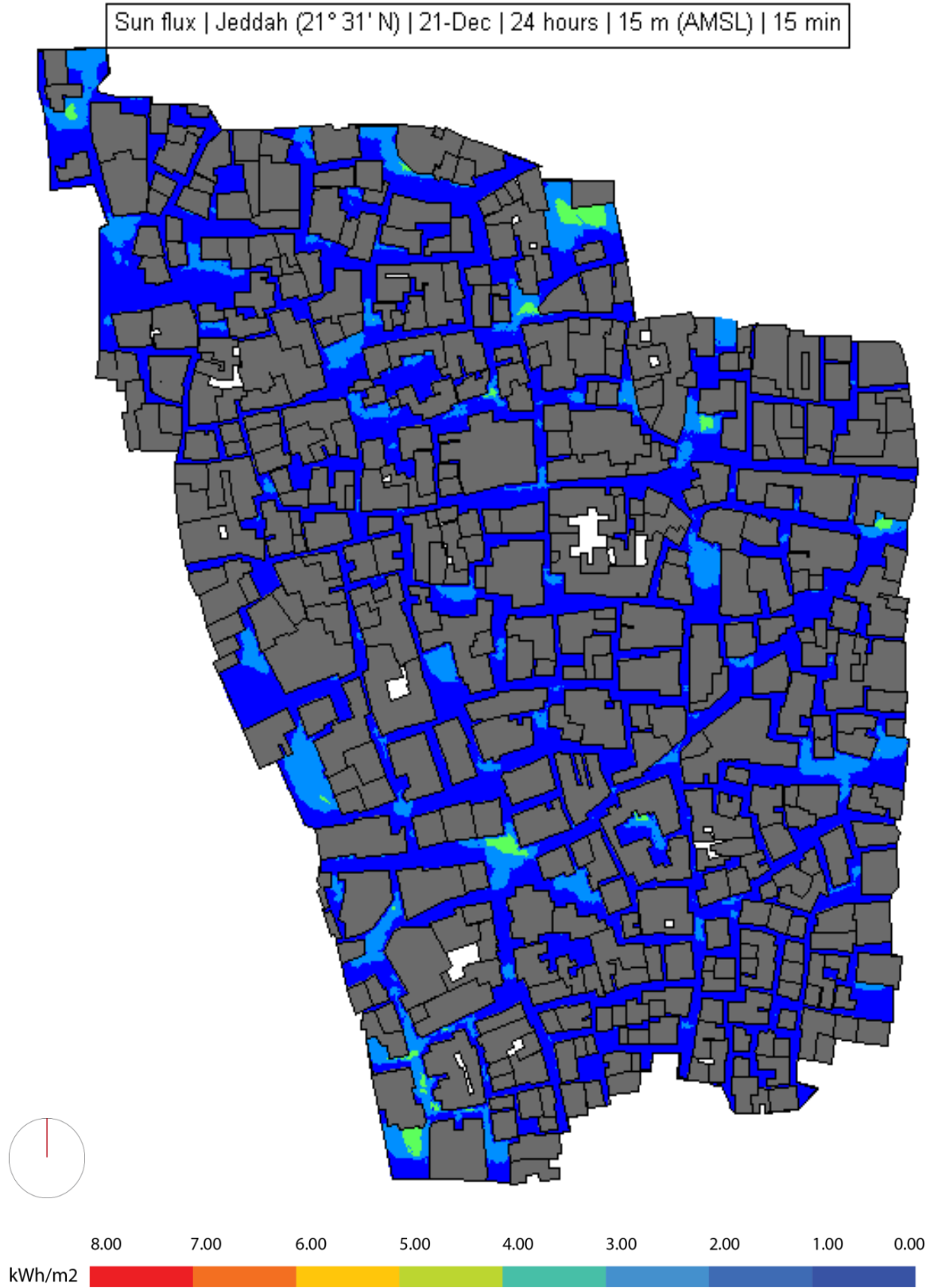


Figure 1.32. AlBalad (the old layout) winter 21st of December, solar flux. Source: Heliodon software.

The overall results in old Jeddah selected urban layout, the vertical surfaces (Facades) receive less incident solar radiation than the horizontal ones (streets) as shown in (Figure 1.33). Additionally, vertical surfaces receive fluctuated solar radiation depending on the façade orientation and the solar angle. Accordingly, on the 21st of June, the façade that obtains the most solar flux value is the East & West facades, receiving 1.40 kWh/m² per day with an average SVF of 20 % and the lowest is the north façade, which receives 0.05 kWh/m² per day with an average SVF of 21%. Also, the Southeast façade receives 1 kWh/m² per day.

On the 21st of December, the South and Northwest façade obtains the highest amount of solar flux value, receiving on the South façade 2.1 kWh/m² per day, and the Northwest façade receives 1.90 kWh/m² per day. Furthermore, the North façades receive zero-incident solar energy on the winter solstice day due to the solar angle on the summer solstice is higher than it is on the winter solstice. Additionally, due to the high built-up density and compactness of the old urban layout, the average Sky View Factor is constant in all vertical surfaces (facades).

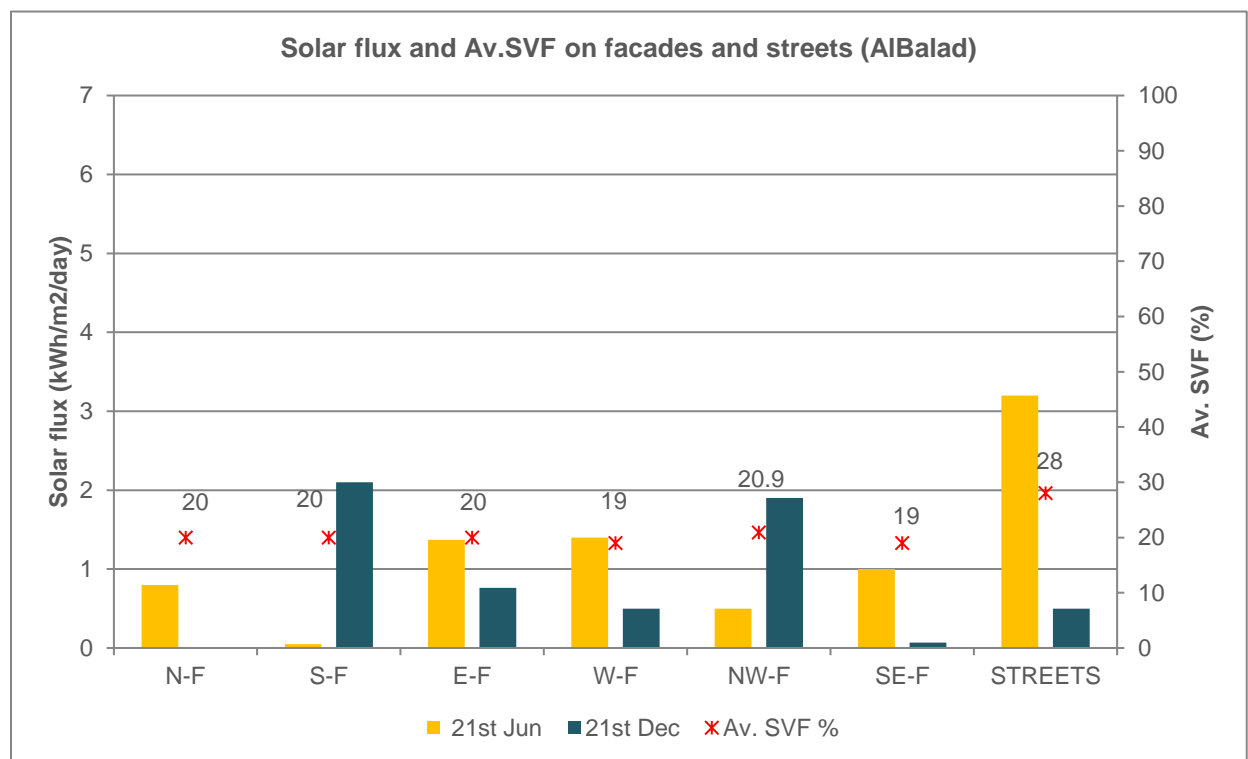


Figure 1.33. Summer and winter solar flux and the average SVF of the streets and the different-oriented facades (AlBalad).

1.5 ANALYSIS OF THE RESULTS

From the analysis presented in the case study, it can be stated that SVF values in urban fabrics of the old city do not exceed 60%, and the average is around 28%.

It has been observed that this value is not decisive to establish the exposure to solar radiation in cities with desert climates since orientation is also essential. Streets with a layout parallel to the North-South orientation have less radiation than those with East-West orientation, although their SVF is the same. With a 25% of SVF, the East-West having 7 to 9 hours of solar radiation time-interval, receiving an average direct solar radiation of 7 kWh/m². And the North-South with the same Av.SVF has 4 hours of solar radiation, receiving direct solar radiation of 2 kWh/m².

Consequently, the results, in this case, show that the correlation between Solar Radiation and the SVF depends strongly on the orientation. Vernacular urban structures in hot desert climates are very compact to avoid solar radiation excess in the urban space.

CHAPTER 2

SOLAR RADIATION IN THE EXISTING URBAN SPACE

“Streets moderate the form and structure and comfort of urban communities.”

Allan B. Jacobs

2.1 THE URBAN SPRAWL

2.2.THE URBAN SPRAWL IN HOT CLIMATE CITY OF JEDDAH

2.3 SELECTED LAYOUTS DISCRPTION

2.4 SOLAR ACSSES IN THE URBAN PUBLIC SPACE

2.5 SUMMARY OF THE RESULTS

2.1 THE URBAN SPRAWL

The arrival of the industrial revolution gave way to industrial capitalism in England, spreading throughout the rest of the world during the second half of the 19th century and the first decades of the 20th century (W. Caves, 2005).

The industrial revolution marks a turning point of the historical precedent by startling technological, social, and economic changes of epochal importance that have profoundly changed how we conceive, build, and live-in cities. It has produced an impressive rise in global consumption, focusing on the latest urban services. Therefore, this led to a rise in the urban population, an increase in transport systems, development of new hygiene and sanitation measures (networks supplying clean drinking water and sewerage systems) and, finally, a notable increase in citizens' living standards (Lapidus, 1973).

The industrial revolution had a delayed impact on Muslim cities and societies. Some of the Muslim cities and societies were affected by European colonial expansion and development. By 1920, the European influence, reinforced by that of the USA, covered a significant part of the world (Bianca, 2000; Lapidus, 1973). Besides, the Middle East urban growth was determined by the financial resources of each country. Countries like Saudi Arabia, Iran, and the Gulf States generated their urban developments from oil revenues. In fact, oil revenues accounted for the rapid industrialization of predominantly rural Asia, the Middle East, and North Africa (Antoniou, 1981).

The introduction of transportation systems brought a complete separation between energy sources and urban center locations. The transportation industry's subsequent expansion allowed for new urban structures, morphologies, and typologies to access energy. It produces a profound modification of the urban organization. (Burchell et al., 1998). Cities worldwide and in the Middle East began a transformation process with horizontal and expanded urban growth leading to the rise of the "housing dispersion" (**or urban sprawl**) (Bianca, 2000) (Figure 2.2). The transport networks brought low-density structures without any public space and social centers. (Burchell et al., 1998).

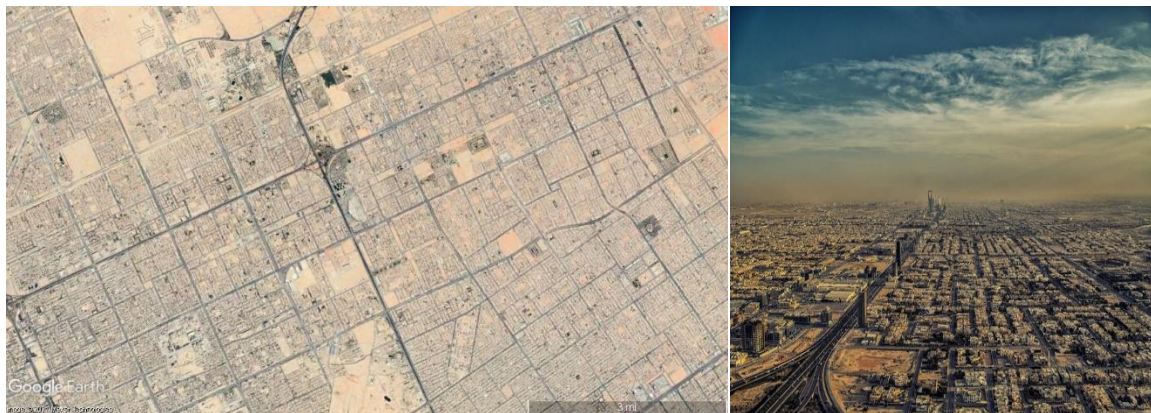


Figure 2.1. Riyadh, Saudi Arabia urban Sprawl (right) (Source:

<http://www.thereviewanddebatesatnyu.com/all/2016/4/27/18isp66tz74in1sym27v4fc8ilup5g>) Riyadh Satellite map (left) (Source:_Google earth)

Four land use characteristics often define sprawl: low density, scattered development (decentralized sprawl), commercial strip development, and leapfrog development (Ewing, 2008). The last three are spatial-structure-based phenomena of sprawl, as opposed to density-based sprawl. Commercial strip and leapfrog developments often occur in parts of a metropolitan area, such that the degree of derived sprawl of a whole metropolitan area depends on such factors as the size and degree of discontinuity of these local sprawl conditions (Tsai 2005)

This type of urban growth determines changes in both urban patterns (settlement morphology and urban form) and processes (spatial distribution of economic functions, socio-spatial differences, political and cultural factors consolidating the role of peri-urban areas) (Figure 2.2). Urban Sprawl physical elements related to space have been extensively evaluated to analyze how sprawl has manifested and taken place in metropolitan regions (Burchell et al., 1998, Tsai, 2005; Kazepov, 2005; Couch et al., 2007).



Figure 2.2. Urban Sprawl of American cities as an example of Cape Coral in Florida. (Source: <https://www.theguardian.com/cities/2017/apr/19/where-world-most-sprawling-city-los-angeles>)

Scientists have argued that sprawling urban and suburban development patterns create negative impacts, including habitat fragmentation, water, air pollution, increased infrastructure costs, inequality, and social homogeneity (Ewing 1997, Squires 2002). This urban morphology influenced the city structure from a social view and had significant consequences for the environment (Burchell et al., 1998; Galster et al., 2001; Frenkel and Ashkenazi, 2008). The leading grounds of sprawl can be considered in:

1. A complex system of interacting factors at the base of the dispersed expansion of cities and metropolitan regions (Gargiulo Morelli and Salvati, 2010)
2. Lack of efficient planning systems at the regional scale and, more frequently, at the urban scale (Gibelli and Salzano, 2006)
3. A land-use pattern presents low levels in some combination of dimensions: density, continuity, concentration, clustering, centrality, unclarity, mixed uses, and proximity (Figure 2.4) (Galster et al., 2001)
4. A generalized misuse of non-urban land determined by policies regulating cities' growth and the development of peri-urban regions (Giannakourou, 2005)
5. Generation of waste and loss of land, it generates social problems such as inequality, racial and economic segregation, and high energy consumption (Batty et al., 2003)
6. Not acceptable for pedestrians with repetitive zones of a mono-functional nature, which isolates its inhabitants (Gehl, 2011)

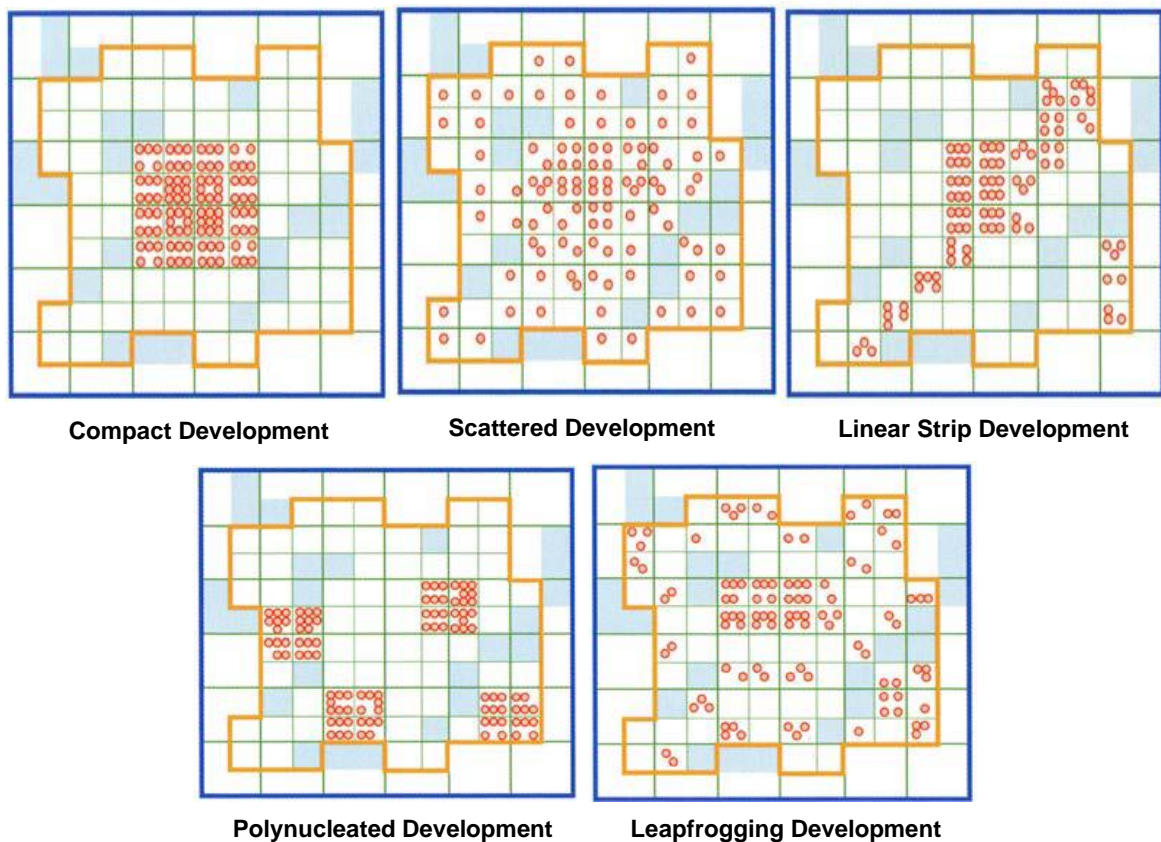


Figure 2.3. Physical Patterns Defining Sprawl (Source: Galster et al., 2001)

Since sprawl is based on several interacting factors, it is difficult to understand how urban distribution is structured over time and scale, making it difficult to implement appropriate strategies of urban containment and sustainable land-use management policies (Bruegmann, 2005, Couch et al., 2007). From these premises, sprawl appears to be a vital issue for contemporary cities (Costa et al., 1991).

2.2 URBAN SPRAWL IN HOT CLIMATE CITY OF JEDDAH

As a result of the high attention in development plans given to the city by the government, Jeddah city has transformed from a small walled coral town with an area of 1 km² into a port of a modern country with an area of about 1600 km² (Figure 2.4).

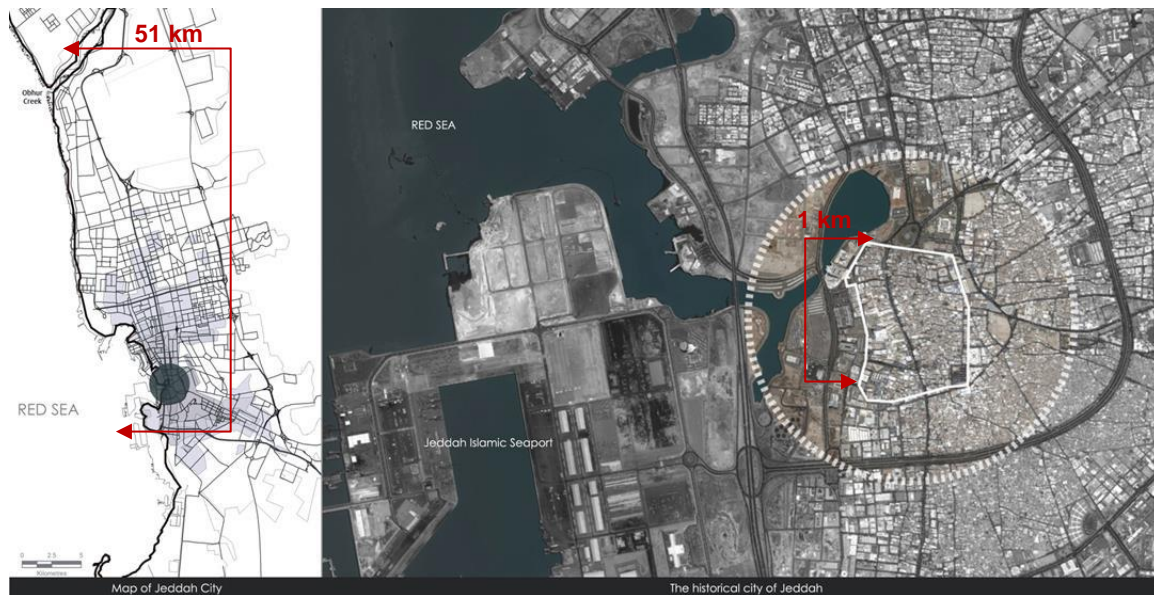


Figure 2.4. Map showing the location of the historical city of Jeddah (Source: Jeddah Municipality, 2013, Jeddah Strategic Plan, Introduction, 16. Google Earth 2013. Jeddah)

The urban development path of Jeddah grows along the line of the Kingdom of Saudi Arabia's economic development. The city's urban growth has rapidly increased since the oil boom in 1938, with up to 90% of Jeddah's urban planning being implemented during the late 1940s (Al-Hathloul and Mughal, 2004,).

This continuous expansion resulted in changing local forms, structures, patterns of city planning, building, residents' lifestyles, and the Islamic identity of the city (Bokhari, 1979). However, the key factor that significantly contributed to changing the city's urban fabric was the introduction of the automobile in the city landscape. 1964 and 2007, Jeddah city witnessed rapid population growth, spatial expansion, land-use change, and transport infrastructure expansion with rates of changes ranging from 0% to over 100%, indicating a wide variability across space, as depicted in Figure 3.11. Two types of urban growth can be distinguished in Jeddah: an outward expansion and a **sprawling** development (Figure 2.5) (Aljoufie et al., 2013).

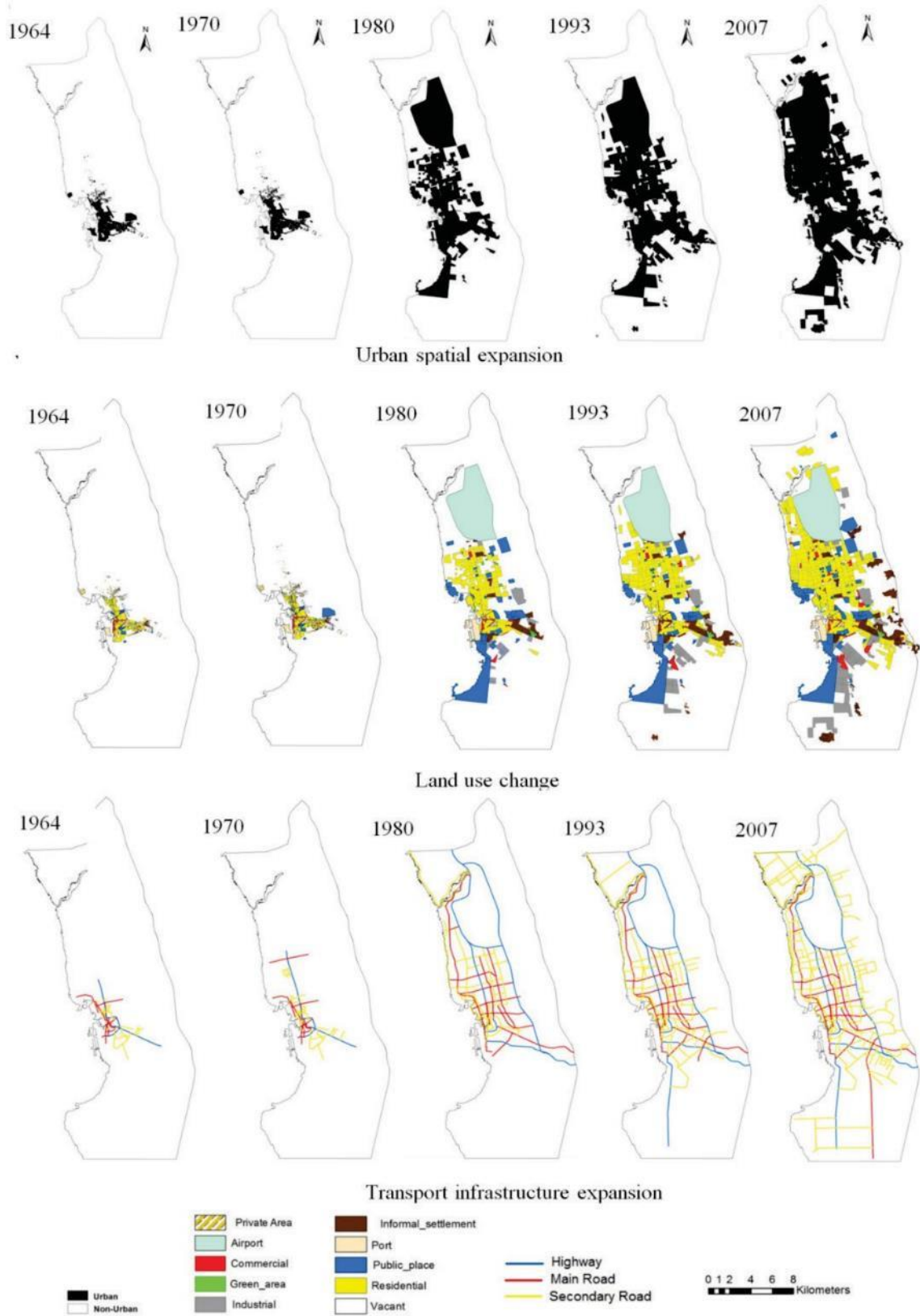


Figure 2.5. Jeddah spatial-temporal changes (Source: Aljoufie et al., 2013)

A transitional district appeared between 1950-1960 (Figure 2.6); during this period, the government allocated a portion of the resulting national income to modernize important cities to accommodate the increasing shift towards a modern lifestyle. The introduction of cars and shortage of adequate public transportation systems replaced the narrow alleyways with wide streets. Despite these efforts, these roads were still not wide enough. Also, there was only a limited number of car owners in the area. Furthermore, the traditional district's forms and structures remained embedded in the local psyche, resulting in the newly developed streets being used to continue the same socio-cultural activities even after the introduction of cars.

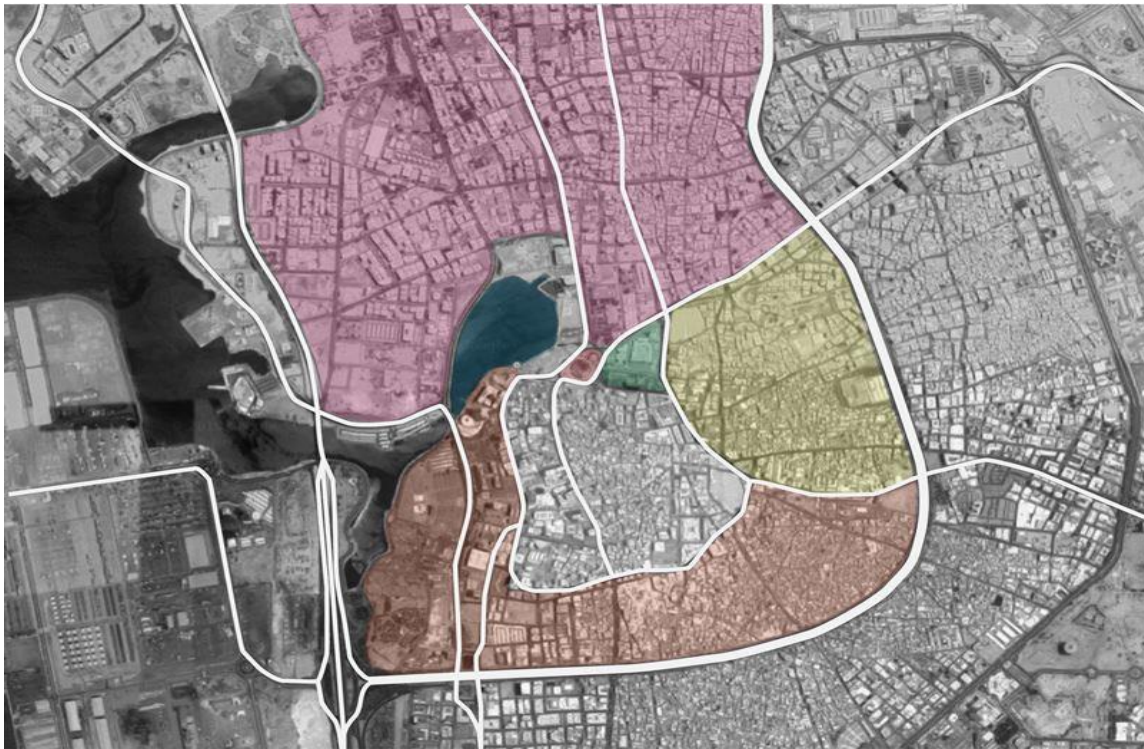


Figure 2.6. Transitional urban development of Jeddah city.

In the transitional area, a new phenomenon has been introduced, in that the ground floors of most of the developed areas, particularly that along the major roads, are given to commercial and light industrial use.

Most of the transitional parts of the city's neighborhoods share many characteristics of the urban form of the old town of Jeddah and other Islamic neighborhoods. These include the compact urban form, the narrow winding streets, the variety of open spaces. The historic growth of the transitional area is clearly expressed in the urban fabric, such as introducing the gridiron pattern in a few areas along the city's two major roads, Makkah Road towards the Southeast Al-Meddinah road towards the North of the city.

The narrow and winding alleys are disappearing at a greater rate in the areas developed from the mid-1950s onwards, particularly in those that can be described as middle or upper-middle class, such as 'Al Sharaffiah' and 'Al Kandarrah' (Figure 2.7).



Figure 2.7. Transitional urban layout samples of Jeddah city (Source: Alharbi, 1987)

The transitional neighborhood's organic plan, which provided intimate spaces and irregular areas, enhanced the urban interaction. Most of the streets in the transitional area of the city are irregular. They are shaded from the glaring sun by the buildings. In the most transitional neighborhood, there is a hierarchical order in the streets' formation, where the wide streets are usually found at the boundary of the neighborhood and the narrower ones towards the center.

The hierarchy mentioned above of streets seems to have been implemented while the automobiles were still limited. However, due to the increasing number of automobiles, the hierarchy of streets has broken down. In some areas, especially those at the periphery and the transitional part of the city, the streets became wide and relatively straight, and sometimes they were in a gridiron pattern (Figure 2.8). The latter was found in areas that were planned by the municipality and occupied by higher-income people. In these areas, the car appeared as the primary mode of transportation. The transitional urban morphology has an organic form: streets are wider to serve cars. Nevertheless, it served cars and pedestrians simultaneously, creating a situation of conflict between the pedestrian and the vehicular traffic (Figure 2.9) (Faden, 1977; Alharbi, 1989).

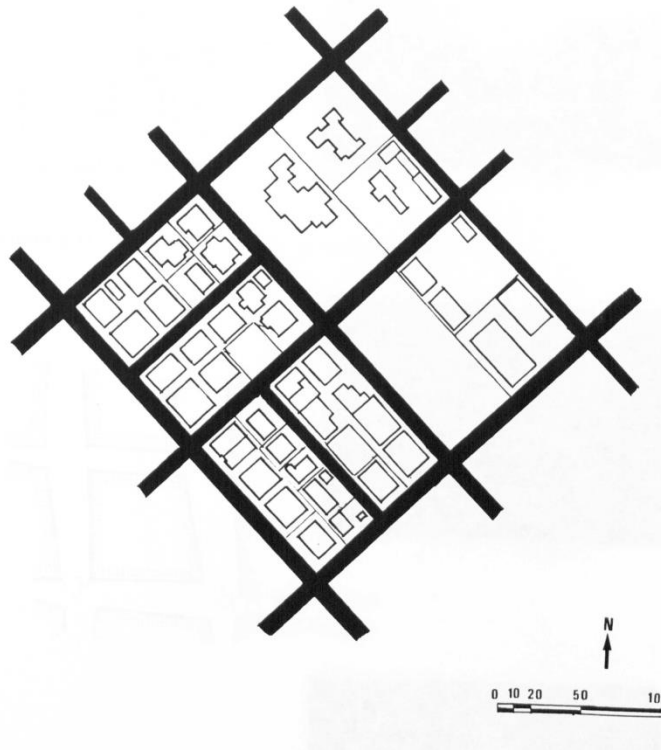


Figure 2.8. Transitional gridiron pattern of Al Nuslah and Al Sharqiah. (Source: Alharbi, 1987).

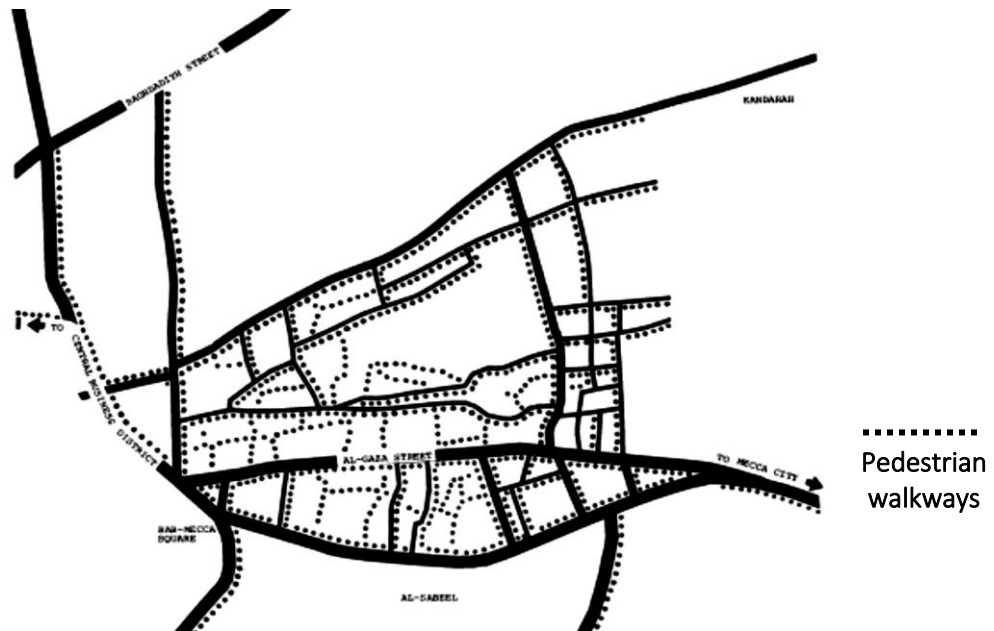


Figure 2.9. Jeddah transitional urban morphology. The dotted lines show the pedestrians paths (Source: Faden, 1977).

The revolution in the economy of the country, which began in 1973 and continued until 1985, affected the socio-physical characteristics of Jeddah. The city witnessed a massive building boom and a rapid development in economic sectors, especially in distribution and public services, which transformed Jeddah from a small city to a metropolitan area.

The modern district appeared in the early 1970s following the approval of new planning policies and building regulations by the government (Al-Hathloul and Mughal, 2004). These policies and regulations widely changed the urban morphology of cities in Saudi Arabia. During this period, the streets were divided into several levels, such as highways, major, and service roads. The gridiron pattern dominated the planning of Jeddah (Figure 2.10) (Abdulaal, 2012).

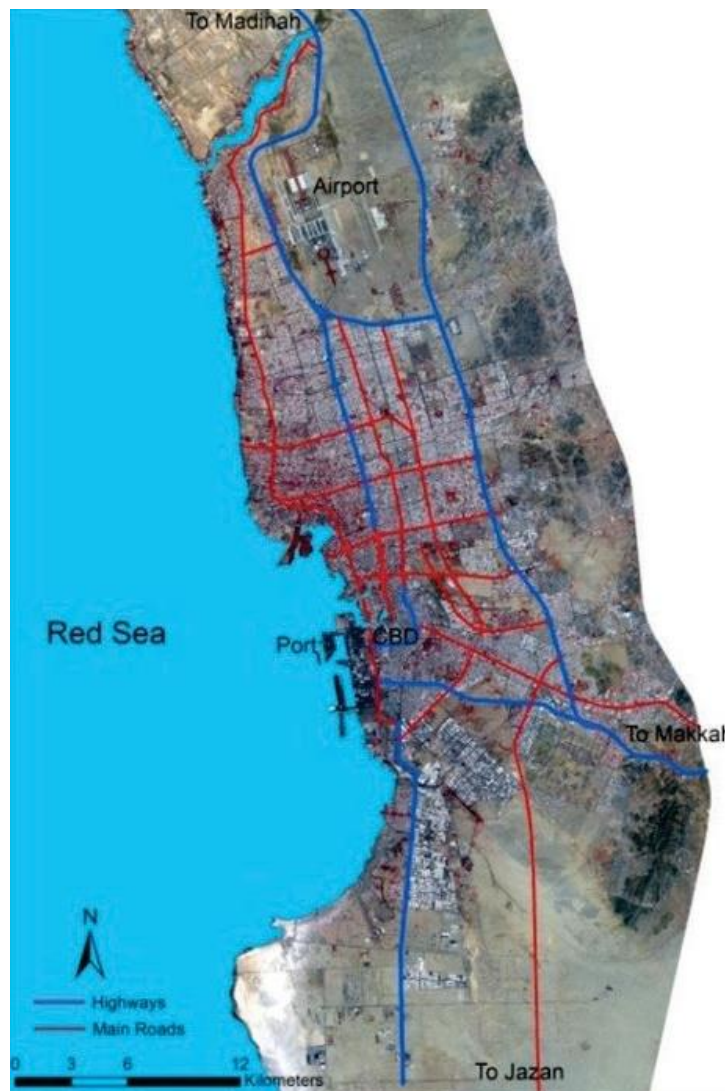


Figure 2.10. Jeddah city map showing in blue the Highways and the main roads in red. (Source: Aljoufie, 2012)

The gridiron pattern at the neighborhood level enhanced the new housing pattern with larger individual plots that produce lower densities. There is a significant increase in the proportion of the public areas of land assigned to streets and open spaces. The plan creates a new physical environment differing from the traditional one in scale, density, and pattern (Figure 2.11). The basic urban structure of the newly planned areas is alike. The gridiron street pattern, buildings standing in the middle of the plots, the square and rectangular shapes of flat-roofed buildings all combined give the modern areas a distinctive urban form that contrasts with traditional areas (Alharbi, 1989). For details regarding the processes of selection of consultants and the planning process itself, see Mathew (RMJMP, 1972), Duncan (1987), and Salagoor (1990).

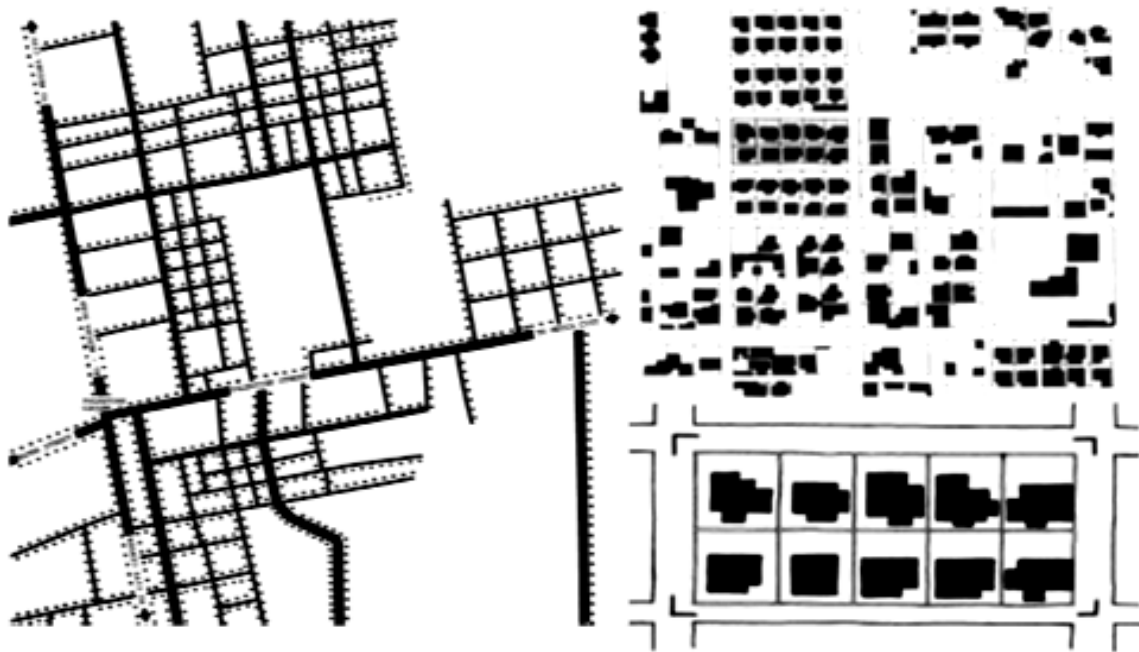


Figure 2.11. Modern urban layout morphology showing different street levels. The dotted lines show the pedestrians paths (left). The gridiron pattern of Jeddah (right) (Source: Faden, 1977).

Moreover, Jeddah's urban pattern has lost its unique features, which functionally contribute to solving environmental and socio-cultural matters. Wide roads, intersections, and highways have replaced traditional walkable historic narrow alleyways, while most public spaces have been transformed into parking areas and local grocery shops to supermarkets. (Alharbi, 1989).

Due to this rapid urban transformation, the hot city of Jeddah has witnessed dramatic changes in its physical environment, which led concurrently to a lack of quality spaces, a gradual change in the residents' indigenous socio-cultural values, and a car-dependent city with no walkable areas.

The 'energy revolutions' have profoundly changed the characteristics of the urban settlements' traditional morphology as seen.

Jeddah hosts a permanent population of 4,082,184, on a built-up area that covers 84,675 hectares. The city in its entirety extending from the core area of AlBalad to the neighborhoods recently built on the Northern extents of the city, has a population density of 48.21 p/ha (Figure 2.12).

The density within the built-up area varies from 1 to 427 p/ha in Jeddah. More than 15% of the population live in a density of more than 300 p/ha. These very high-density areas are largely located at the urban core and cover an area of 1680 hectares. Successively, a population of more than 20% of the city's population, live in densities between 150 to 300 p/ha over an area of roughly 4600 hectares.

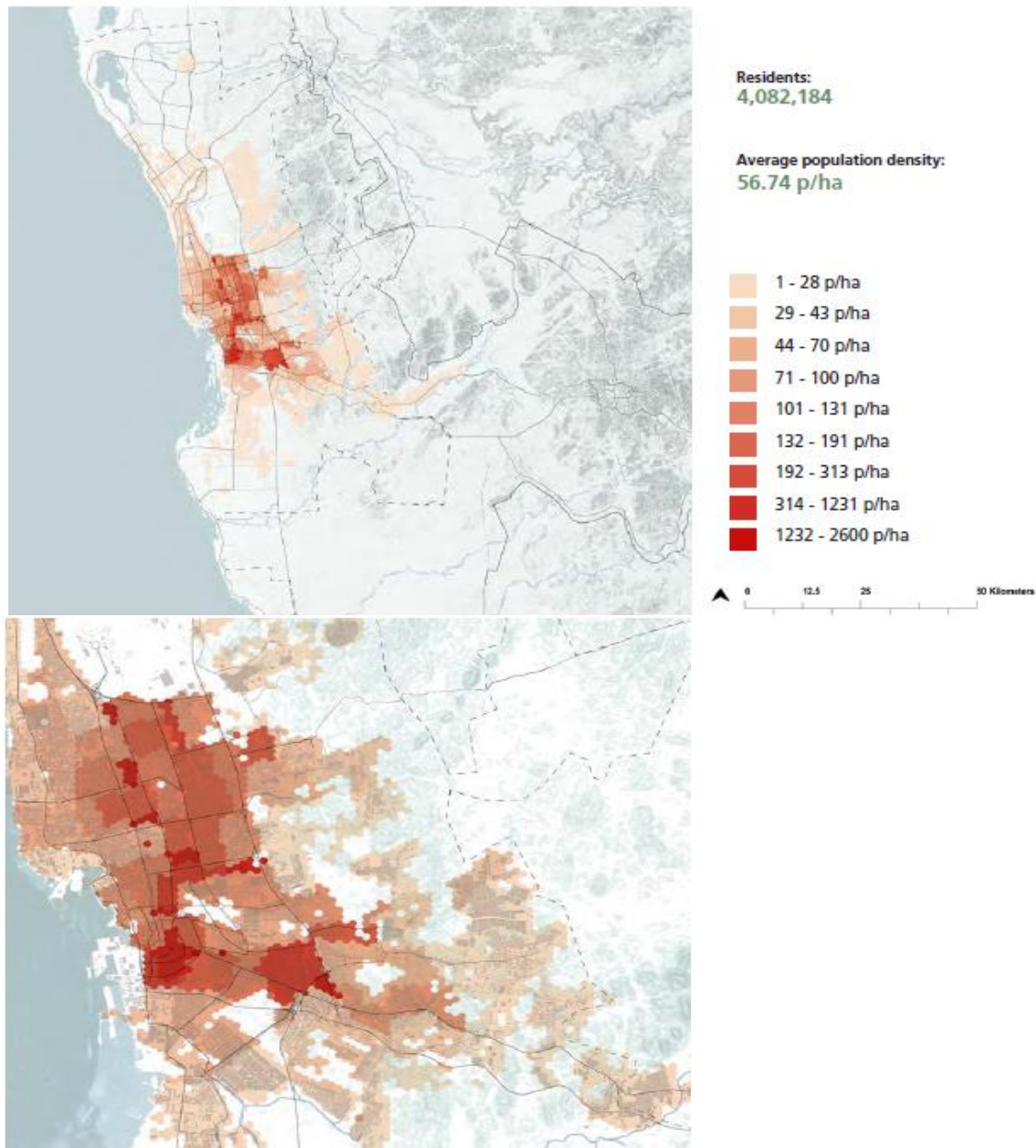


Figure 2.12. distribution of population density in Jeddah City (Source: Ministry of Municipal and Rural Affairs King Fahd National Library, UNHabitat, 2019)

Conversely, vast amounts of the population live in medium to low density areas. Almost 18,930 hectares of land occupied by 1,681,000 inhabitants, reflects 42% of the total population in the city, with a medium to low density of 50-150 p/ha. More than 857,000 inhabitants, more than 21% of the population lives in 53,120 hectares of very low-density areas, with less than 50 p/ha. For example, Jeddah's waterfront - currently known as the villa's neighborhood - has a density of 25-30 p/ha and is mostly occupied by family villas with gardens (Figure 2.12)

Since 1970, the Jeddah urban area has grown by more than 400% while, in the same period, its population has grown by more than 1000%. This demonstrates that density has been increasing in Jeddah. Despite this increment, the average density is still far from the preferred level. The urban built-up area can still be densified to move closer to 150 p/ha, as recommended by UN-Habitat.

According to the last Saudi Arabian census (2010), Jeddah is experiencing a population growth at a rate of 3.2% per annum, and its population is projected to reach more than 5,200,000 by 2033.

The urban morphology layouts say a lot about its relation to solar radiation. One of the mentioned steps that were taken to understand the morphology is to differentiate and analyze the different morphologies within a city. Consequently, I started with a general map analysis of the urban patterns and layouts of the whole city and how they are oriented, demonstrating the unplanned urban pattern and gridiron patterns and layouts.

Two different urban morphologies currently dominant and exist in the city of Jeddah (21 'N) (Figure 2.13). The city of Jeddah shows the eligibility of an urban pattern and the consistency of the city's spatial organization. Furthermore, on the map in Figure 00, each layout type is represented by a corresponding color, depending on its type. A large area of a low-rise building, with low- density isolated buildings each building surrounded with a fence (wall separating the building from the public space), and the other type we find the new urban center, consists of a mid-rise; mixed-used buildings, considered as a medium-density building. This analysis was done using the city council's maps in AutoCAD format, then applying the map in illustrator design and performing the analysis using different colors

The physical characteristics of the selected urban segments, i.e., building heights and outlines, were illustrated according to the satellite vector map obtained from Jeddah development authority, which provides information about the existing urban components in the adopted urban areas, including building heights and outlines, building types, and the outlines and width of the local streets.

This urban environment is of particular interest in the thesis field since it constitutes a representative example of a sprawl fabric typical of the later industrial city and appears in Saudi Arabia, as mentioned previously after the oil boom and the car's introduction.

The basis of the work was simulating the received direct solar radiation of these layouts on the streets (horizontal surface and facades (vertical surface)). The simulation was carried out with Heliodon the same as the simulation used in chapter 1 for the old area (AlBalad), analyzing the layouts using the same parameters. The selection of the studied layouts responded to the above reasons.

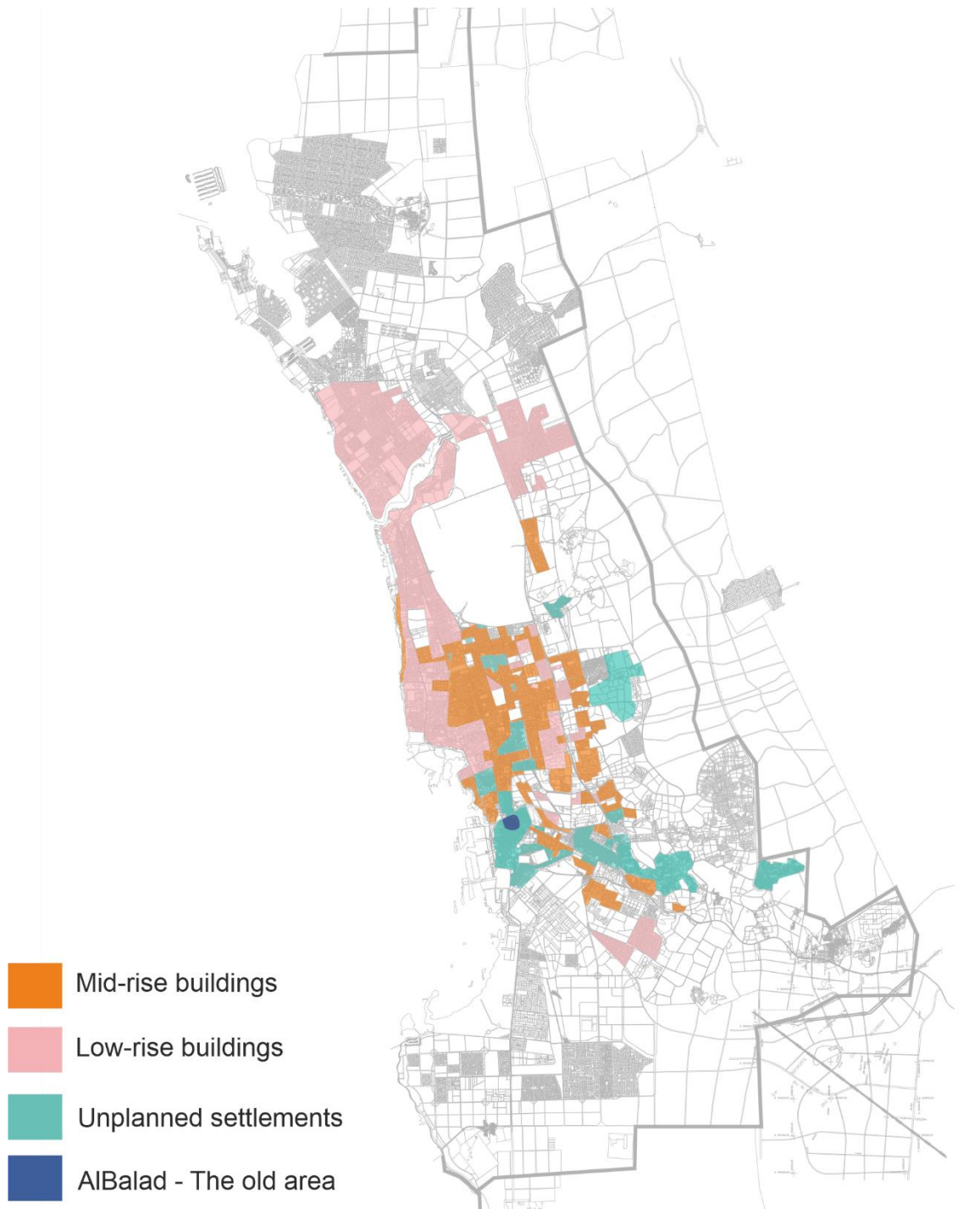


Figure 2.13. Types of urban morphologies that exist in Jeddah City.

Moreover, after highlighting and demonstrating the different types of urban morphologies on the Jeddah map, I looked more closely at the streets' orientation. As shown in the map in Figure 2.11, I decided to show some of the street orientations in Jeddah city, which gave a clear vision and image of the streets' orientations and connectivity it helps for a primary understanding to their relation to the solar radiation access, as street orientations are important urban morphology parameters that affect the solar access to streets and buildings. This method's application was similar to the previous map taking the AutoCAD Jeddah map and analyzing its streets.

In Figure 2.14, the red lines represent the North-South street-orientation axis, the blue lines the East-West street-orientation axis, green the Northwest-Southeast, and orange the Northeast-Southwest orientation axis. The most dominant street orientations are the red and blue lines (North-South and East-West).



Figure 2.14. Jeddah map showing the different streets orientations. Red lines: North-South street-orientation axis, blue lines: East-West, green lines: Northwest-Southeast, and orange: Northeast-Southwest.

2.3 SELECTED LAYOUTS DESCRIPTION

Two existing layouts of Jeddah city were chosen for the incident solar radiation analysis in the modern morphology. Both areas are in the Northern part of Jeddah, representing the modern urban layout of the city with either a mid-rise building (AlSalamah district-Case A) or a low-rise building (Obhur AlShamalya district Case B) (Figure 2.15).

To evaluate the urban fabric, the analysis must be limited by reducing the number of variables to formal parameters for example, choosing cases with the same floor coverage ratio and different building intensities in a 500m x 500m layout. This characteristic was evaluated using the floor area ratio and floor space index (GSI &FSI) (Pont et al., 2010) check appendix 2 (section 2.2), which quantifies the amount of floor space concerning the gross land area. The same approach was used in the (Compagnon, 2004) study of solar and daylight availability in Fribourg's urban area (Switzerland). The floor area ratio constant was preserved, and the performance of different hypothetical configurations was checked. Using the same strategy, this study identified two urban layouts: (AlSalamah) from the modern area in Jeddah that has a medium-density and is characterized by high rise buildings, and another layout (Obhur AlShmalya) from the contemporary area of Jeddah that has a low density and is characterized by low rise buildings. The creation a 3D digital mock-up, using the cadastral information available, as shown in (Figure 2.17 and 2.20).

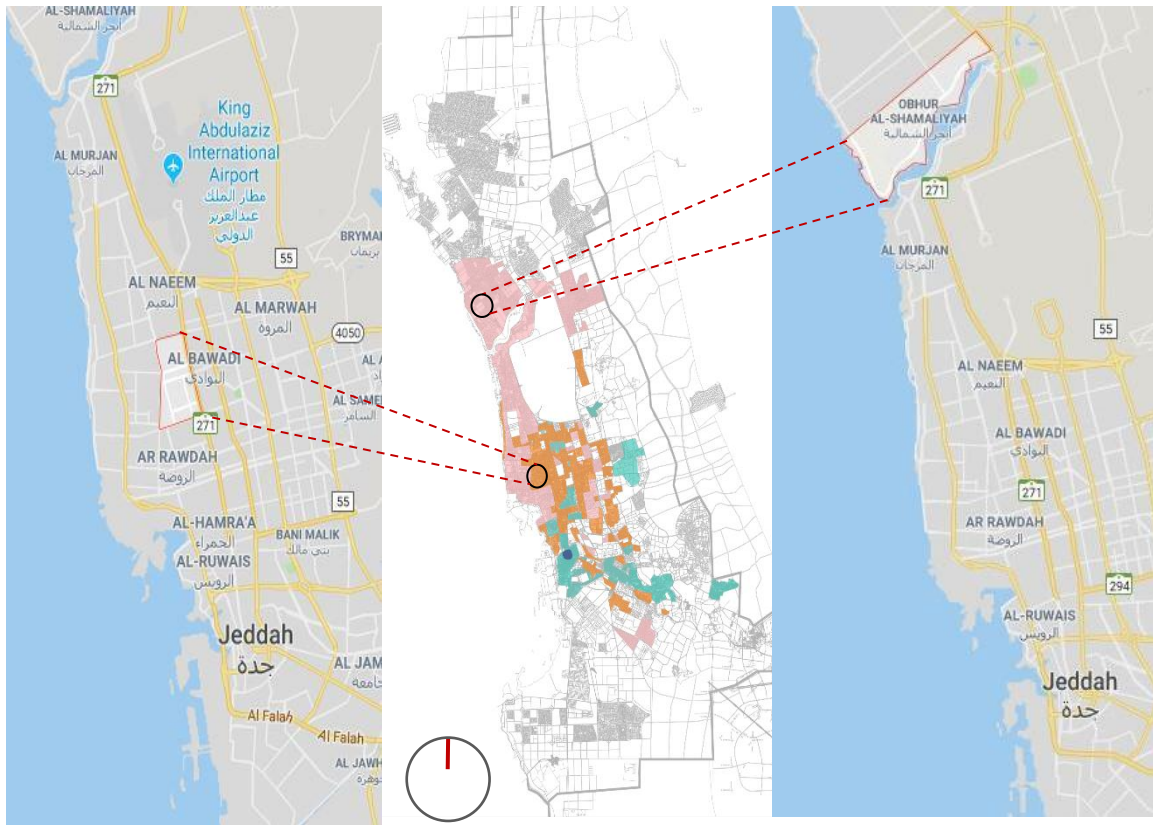


Figure 2.15. Mid- rise buildings area (AlSalamah), Case A (left). Map of the low-rise buildings area of Jeddah (Obhur AlShamalya), Case B (right).

Both chosen urban layouts have a similar gridiron plan, but they have different characteristics related to density, H/W, and plot orientation.

CASE STUDY A: MID-RISE BUILDINGS (ALSALAMAH)

The selected case in the modern area is residential. The Al-Salamah district is located in the North of Jeddah (Figure 2.16). It is one of the biggest districts in Jeddah with an area of 693 hectares, a population of 90,000 inhabitants, and a population density equal to 129.94 persons per hectare (Jeddah-Municipality, 2006). The district is enclosed by four major arteries: Medinah Road on the Eastern edge, Prince Sultan on the Western edge, Heraa Street on the Northern edge, and Sari Street on the Southern edge. The area of the district is mainly flat terrain and does not have drastic topographical changes. Therefore, the design of the settlement adapts the gridiron straight street pattern. The subdivision of the AlSalamah district was developed by a private owner called Ba-Salamah and an estate agent called Al-Howaish.

It is interesting to look at the morphology of the district. The layout was designed by professionals with a completely different pattern in relation to the grid pattern of the AlSharafeyah district. The introduction of new forms can be seen in the creation of new urban areas and public parks and squares. This is as a result of the modernist influence in the city that took place around the 1970s, and the creation of new streets called boulevards within the boundary of the district instead of the previous narrow grid street pattern. According to the subdivision of the district, about 33% of the total land area was allocated for streets and community facilities as a compulsory land dedication as stated in the land development policy.

As is the case in the modern residential areas of the new periphery, the housing in the AlSalamah district consists of seven stories of detached apartment buildings. The typical lot size is 20x30 m and most blocks are 60x 180 m. The district was laid out in a rectangular grid system with rectangular and square lots. Such development consists of parallel alignments, simple and geometrically shaped patterns of streets which provided for adequate vehicle movement with a width ranging from 10 to 20 m. The architecture is distinctly American in style and built according to zoning regulations that stipulate distances from the street, detached rather than attached buildings. The regulations were changed in 1985 to allow mixed use buildings along the main streets when their width exceeded 30 m. These regulations attracted private sector investment such as the development of unorganized retail activities which appeared in the form of extensive ribbon developments along the major road surrounding the district and throughout the wide local roads within the district. As Daghistani (1993) points out that the development of a ribbon development resulted in traffic congestion and a diffusion of retail services in an unorganized way and reflects a series of individual decisions without clear planning guidelines from the municipality. Figure 2.16 shows the chosen layout demonstrating the streets and the surrounding buildings. Moreover, Figure 2.17 provides a schematic sketch of the layout illustrating the buildings heights and some streets sections.

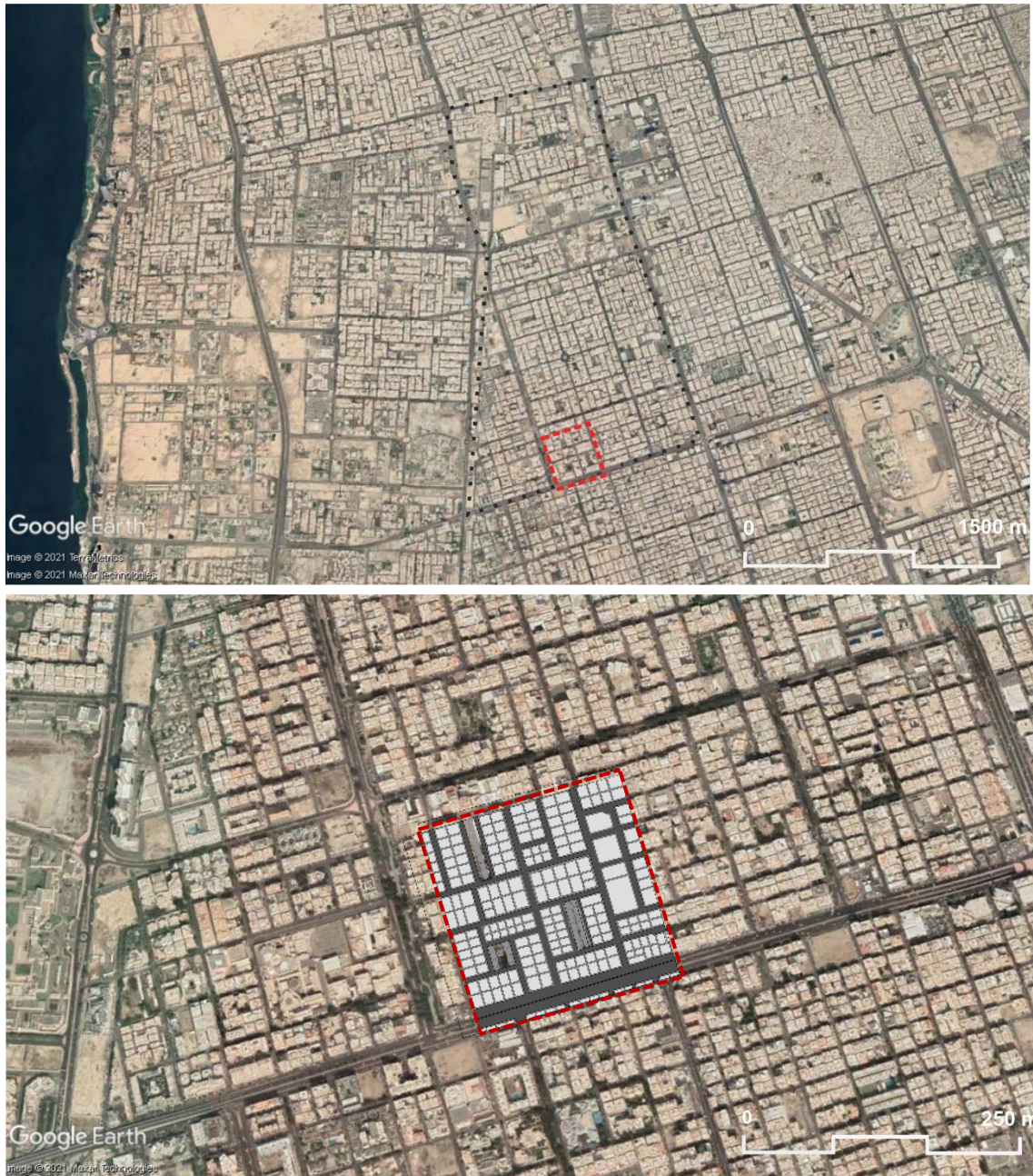


Figure 2.16. The case study Alsalamah Mid-rise buildings layout Case A (Source: Google Earth).

CASE A (ALSLAMAH)

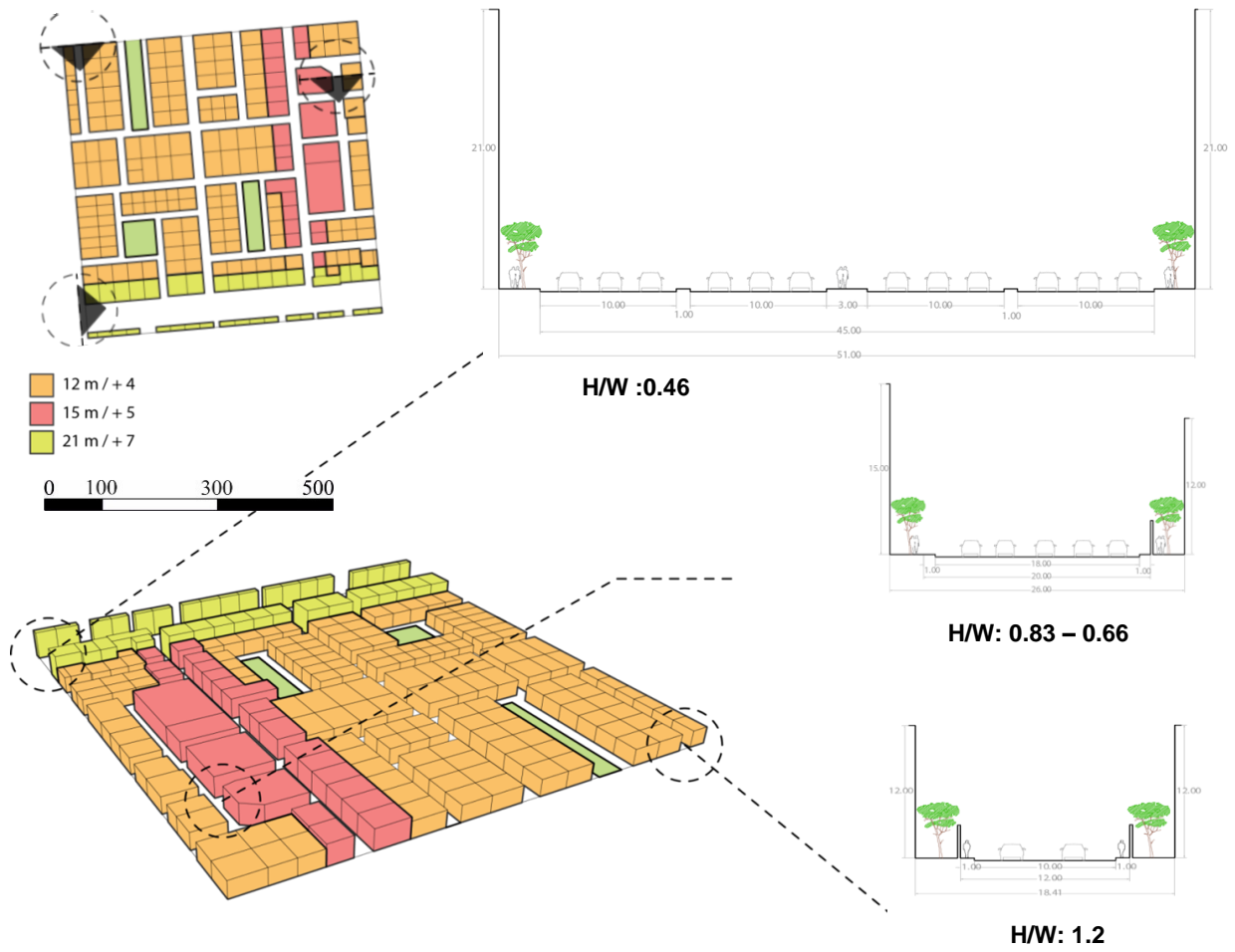


Figure 2.17. The Mod-rise layout of Jeddah (AlSalamah) schematic drawings in 500m x 500m sections and plans. (Source: Author elaboration)



Figure 2.18. The pictures show the actual streets of the layout of Case A.

CASE STUDY B: LOW-RISE BUILDINGS (OBHUR ALSHAMALYAH)

The new area Obhur AlShamalya (Figure 2.19) is located 30 Kilometers north of Jeddah. The area is characterized by its 2 to 3 story. Also, the development consists of parallel alignments in simple geometrically shaped patterns. The area consists of detached villas, segregated from the commercial area, simple geometrically shaped patterns of streets designed for adequate vehicle movement, with width ranging from 10 to 20 meters. Both layouts consist of lots with a typical size of 20 x 30 meters, and most blocks are 60 x 180 meters. The district was laid out in a rectangular grid system, with rectangular and square lots. The architecture is distinctly American in style and built according to zoning regulations that stipulate distances from the street and detached rather than attached buildings. Besides, each villa is surrounded by a fence with a height of 3 to 4 m. The simulation and analysis were on the streets and the envelope (façades) of the layouts.



Figure 2.19. The case study Obhur AlShamalyah Low-rise buildings layout Case A (Source: Google Earth).

CASE B (OBHUR ALSHAMALYA)

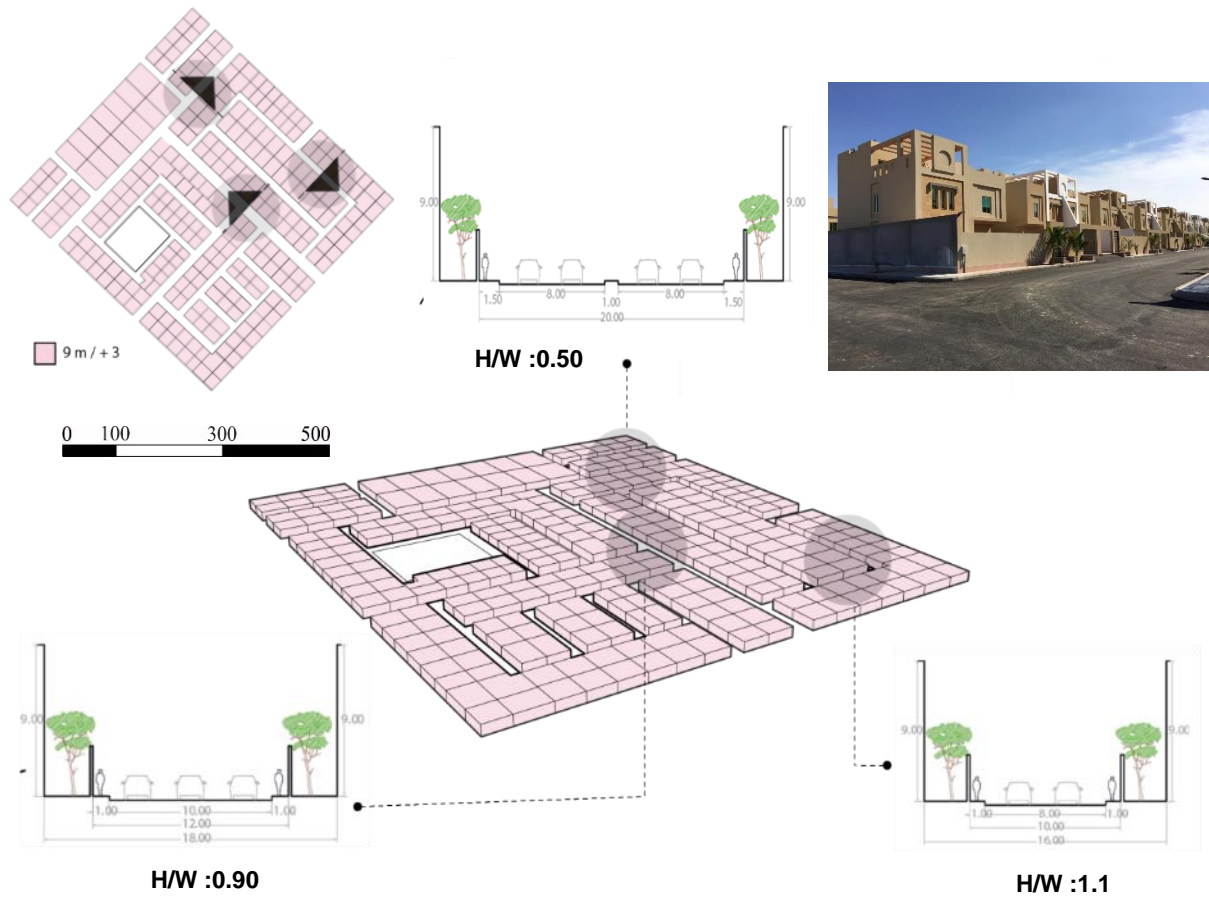


Figure 2.20. The contemporary area of Jeddah (Obhur AlShamalya) in 500m x 500m sections and plans. (Source: Author elaboration)



Figure 2.21. The picture shows the actual streets of the layout of Case B.

2.4 SOLAR ACCESS IN THE URBAN PUBLIC SPACE

2.4.1 *The Direct Solar Radiation (Case A and B)*

the AlSalamah neighborhood, Case A, and the Abhor AlShamalya neighborhood, Case B, both receive almost equal amounts in high average solar intensity in summer (Case A: 5.905 kWh/m²/day and Case B: 5.83 kWh/m²/day). This can be explained by the same solar angle in summer being higher than in winter and because of the wide streets in both layouts. Case A has an N-S orientation as all street axes are directed towards N-S and E-W. For Case B, the layout is on a rotation of 45° with all street axes being oriented to the intermediate orientations NE-SW and NW-SE. Therefore, the solar access on both layouts is different due to their orientation. During winter, Case A receives less incidence of solar flux due to higher abstractions on the layout than Case B. The numerical formulas used do not take other climatic variables into account. The differences between the measured values and estimated solar irradiation could also impact the solar flux during summer and winter. During winter, Case A received 1.89 kWh/m²/day and Case B 2.38 kWh/m²/day. The difference of solar radiation intensity between both cases is 20%.

For Case A (modern layout), Figure 2.22 shows that the horizontal surface of the (streets) receives a direct solar radiation in summer from 5:30 o'clock to 18:00 o'clock with a total of 13 hours. Here, the sun period is higher due to less obstructions and a lower density. The simulation reveals that the streets receive a direct solar radiation in summer ranging from 50 Wh/m² to 950 Wh/m². The level peaks from 10:00 o'clock to 14:30 o'clock ranging from 800 Wh/m² to 953 Wh/m² at noon. During winter, solar radiation occurs between 7:00 o'clock and 17:00 o'clock, which is 10 hours, showing at noon the highest amount with 420 Wh/m².

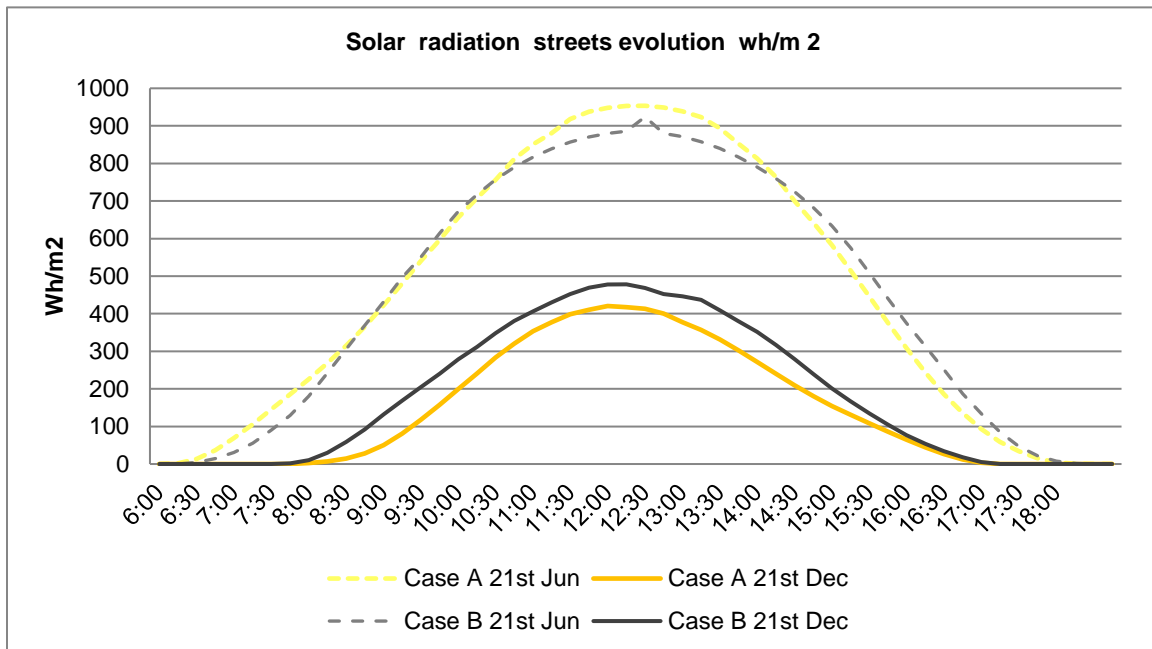


Figure 2.22. Solar flux evolution of the horizontal surface (streets) for the two layouts with a maximum and a minimum in summer 21st June and winter 21st. December.

Moreover, the findings show that Case A receives approximately the same amount of incident solar radiation in summer as Case B (contemporary layout) with a 5.2% difference between direct solar radiation in Case A and Case B at noon. However, the streets in Case B receive in winter 16% more direct solar radiation with almost 500 Wh/m² at noon which is higher due to the orientation of the layout with lower solar obstructions. The simulation also shows that in summer Case A received at noon the highest incident solar radiation of the two case studies with almost 1000 Wh/m² whereas Case b received the highest amount in winter with almost 500 Wh/m². These results clearly indicate a direct correlation between the solar obstruction then the exposure to direct solar radiation: solar radiation increases as the buildings' heights and street width decreases.

2.4.2 Case A: Mid-rise Mix use buildings (AlSalamah)

The SVF Influence of the Urban Morphology in Case A:

The simulation shows that the average SVF for the whole layout of the horizontal surface (streets) is 66.40% (Figure 2.23). Due to obstructions, the SVF on the streets level increases from the center to the side of the streets.

Also, based on the simulation results in Case A, the building-height-to-street-width ratio is at $0.46 < 1$. Thus, the streets with orientation N-S have a lower average SVF value than those with E-W orientation. Notably, building heights and street widths remain the same. As mentioned previously, the E-W orientation generally provides a greater degree of vision towards the celestial vault with respect to the street's orientations. The simulation reveals in the map that the N-S streets orientations have an H/W ratio from 0.66 to 1 which equals an average SVF of 60% to 100% (Figure 2.23). Additionally, on the E-W street orientation with an H/W ratio from 0.46 to 1, the SVF is between 60% to 100%. The evaluation of these layout types with mid high-rise buildings where the SVF is higher or closer to the buildings indicates that these obstruct the view and the closer to the center of the street the lower the SVF becomes (Masoud et al., 2019).

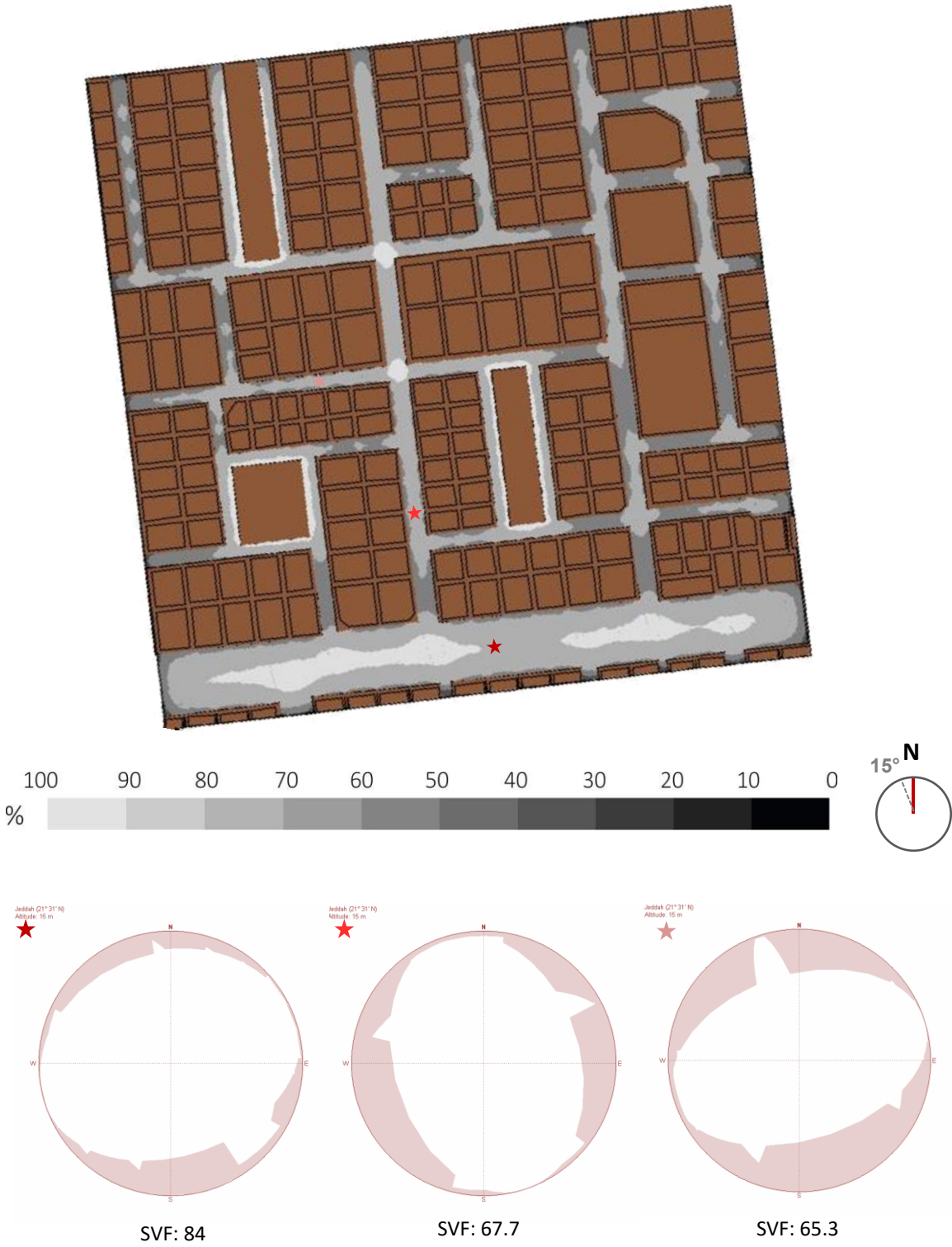


Figure 2.23. Case A: Sky View Factor distribution on streets. The different colored asterisks on the map are used to illustrate examples of the SVF for that particular point with the orthographic projection. Source: Heliodon software.

**Case A: Solar Radiation Time Interval Influence of the Horizontal Surface (Streets)
- Summer and Winter Solstice:**

The results of the Heliodon simulation disclose that the N-S orientations have an H/W ratio ranging from 0.66 to 1 and an average SVF ranging from 60% to 100% with a high sun period due to the urban sprawl system (Figure 2.23). This impacts the time interval of solar radiation received on the streets (Figure 2.24). It faces 5,18 h to 12 h of direct sun per day in summer and 2,28 h to 7,23 h in winter. The E-W-oriented streets in Case A receive direct solar radiation with about 10-12,3 h in summer and 1-10h in winter. Consequently, E-W streets are more exposed to incident solar radiation hours almost all day.

Moreover, as mentioned previously, the closer to the building the lower the sun period as shown on the maps in the Figures 2.25 for summer and 2.26 for winter. These maps quite clearly indicate the impact of street orientation on the solar time interval as for summer, the E-W-oriented streets show a longer time interval compared to the N-S-oriented streets (Figure 2.25). Interestingly, the map looks different for winter as in summer, the N-S-oriented streets exhibit longer sunny periods than the E-W oriented streets (Figure 2.26). These results clearly indicate that street orientation impacts the solar radiation time intervals.

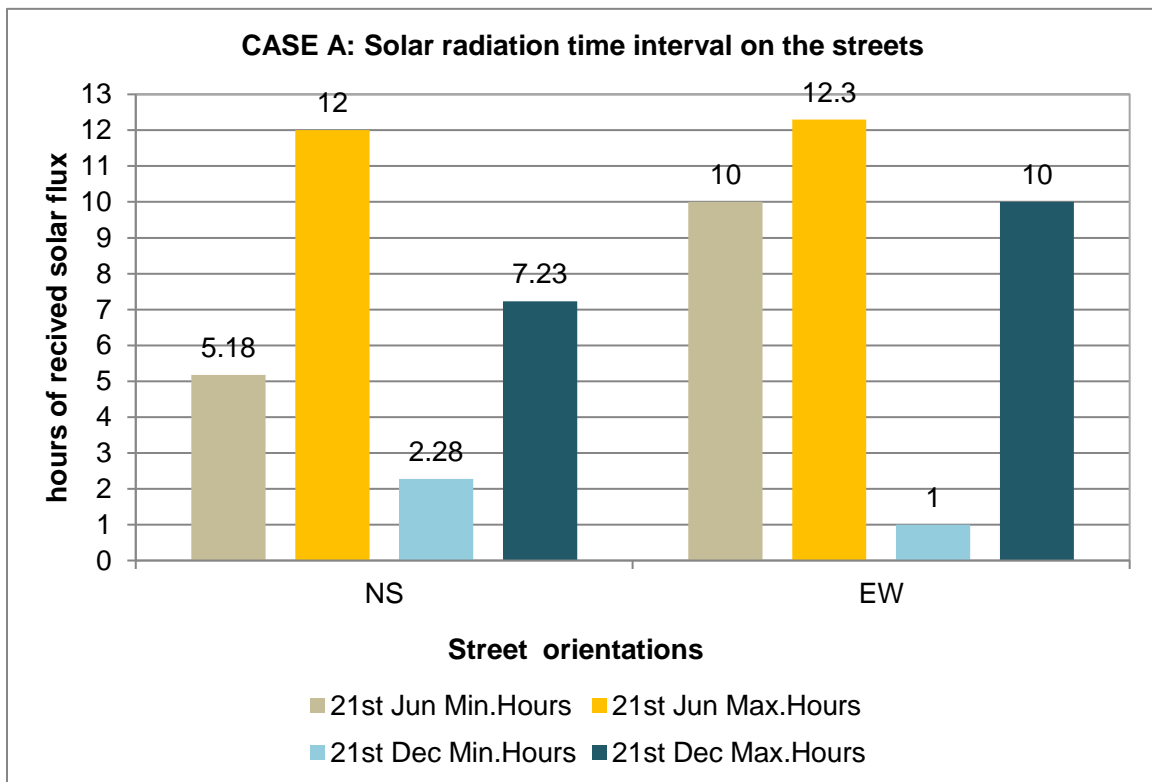


Figure 2.24. Case A: Solar radiation time interval on the two street orientations.

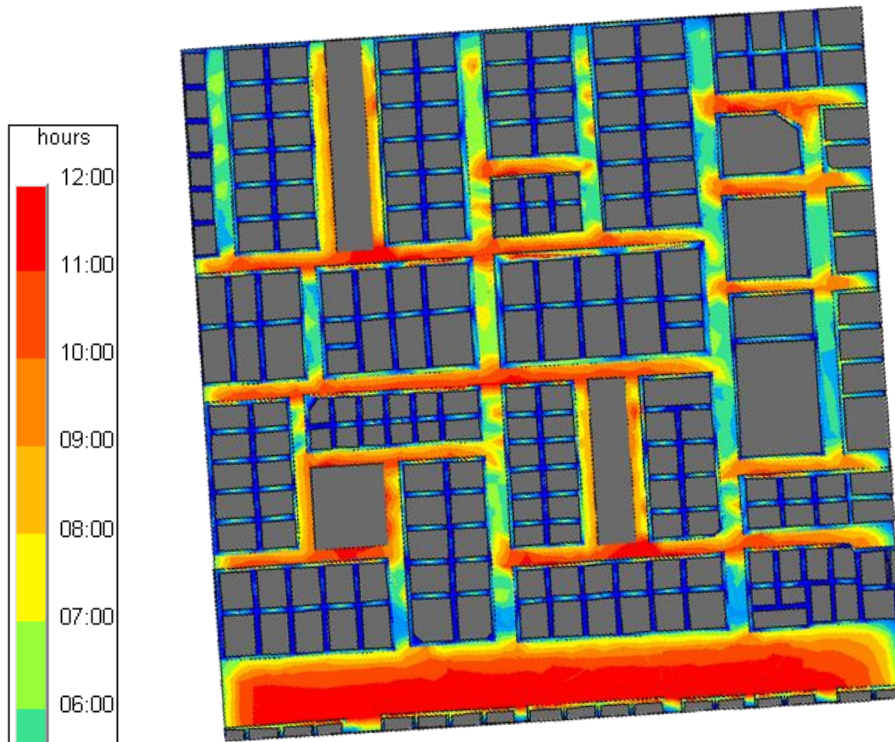


Figure 2.25. Case A: summer, 21st of June, solar radiation time interval (sun period). Source: Heliodon software.

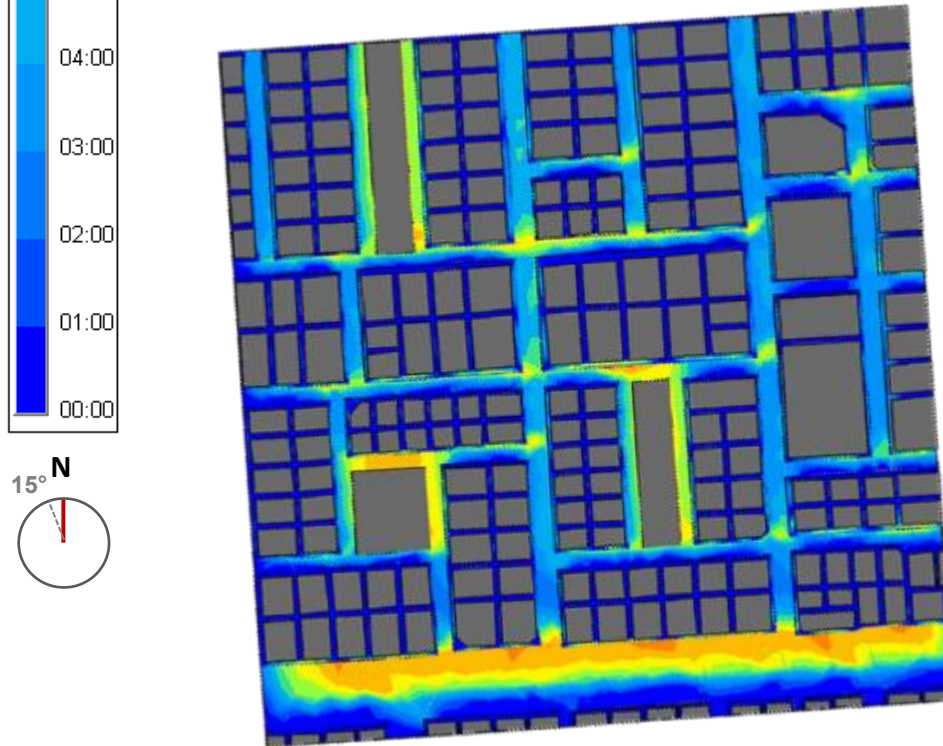


Figure 2.26. Case A: winter, 21st of December, solar radiation time interval (sun period). Source: Heliodon software.

Case B: Direct Solar radiation Value and Sky View Factor:

In Case A, the solar energy value of each street orientation is depicted using SVF and sunshine duration. The spatial distribution of Sky View Factor describes the obstruction of sky exposure by each street. The simulation reveals in the below Table 2.1 and graph Figure 2.27, show the Sky View Factor increases from the center to the sides of the streets. The streets oriented North-South with an H/W ratio from 0.26 to 1 receive an average solar flux in the summer ranging from 7 to 2 kWh/m²/day (Figure 2.28). And in winter from 3 to 1 kWh/m²/day (Figure 2.29) with an average Sky View Factor between a minimum of 40 % to a maximum of 100 %.

Additionally, on the East-West street orientation with an H/W ratio from 0.46 to 1, it receives an average solar flux ranging from 7 to 6 kWh/m²/day (Figure 2.28). And in the winter ranging from 2 to 0 kWh/m²/day (Figure 2.29) with an average Sky View Factor between minimum 50 % to a maximum 100 %. Furthermore, in summer the East-West orientation receives a higher solar flux value than the North-South orientation, and in winter the opposite is true (Masoud et al., 2019).

Table 2.1. Average solar flux, H/W ratio, and SVF on each street orientation in Case A.

Orientations	H/W Ratio	AV. SVF (%)	Range AV. Solar Flux 21st June (kWh/m²/day)	Range AV. Solar Flux 21st DEC (kWh/m²/day)
N-S	0.26	70 < 100	5 - 7	1-3
	0.60	60 < 90	5 - 7	1-3
	0.83	50 < 90	4 - 6	1-3
	1	40 < 60	2 - 5	1-3
E-W	0.46	70 < 90	6 - 7	0-2
	0.66	60 < 90	6 - 7	0-2
	1	50 < 60	6 - 7	0-2

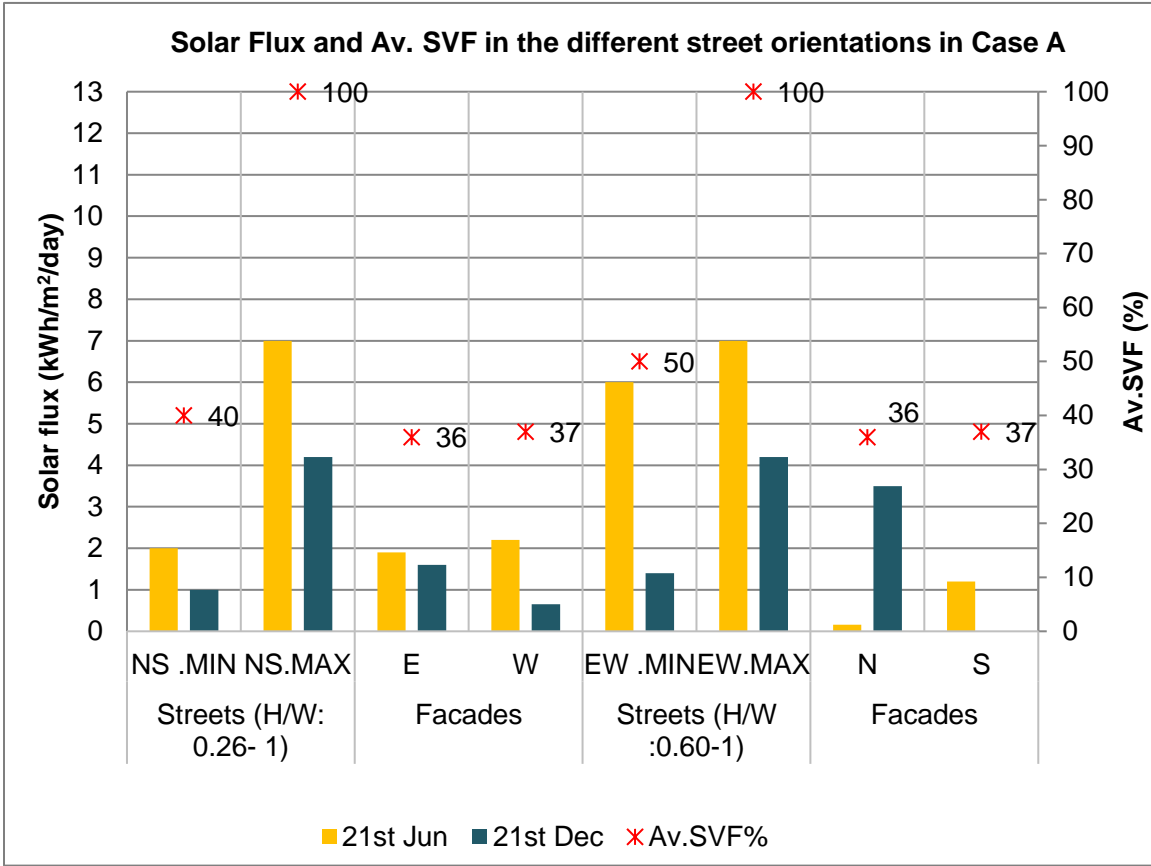


Figure 2.27. Case A: average solar flux and SVF on the different street orientations and facades.

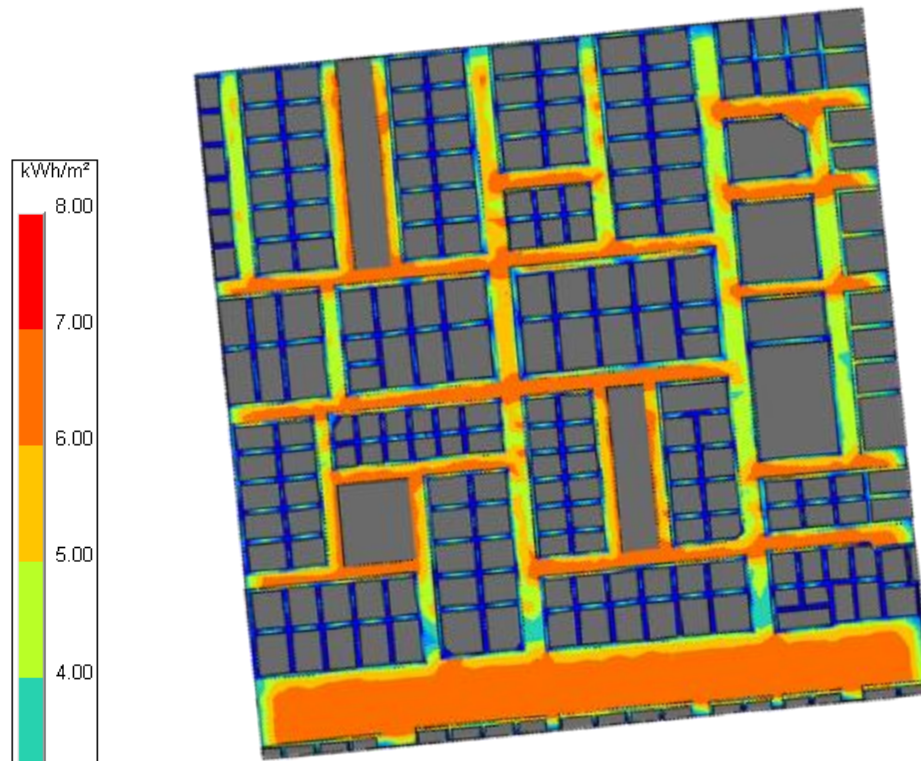


Figure 2.28. Case A: summer, 21st of June, solar flux. Source: Heliodon software.

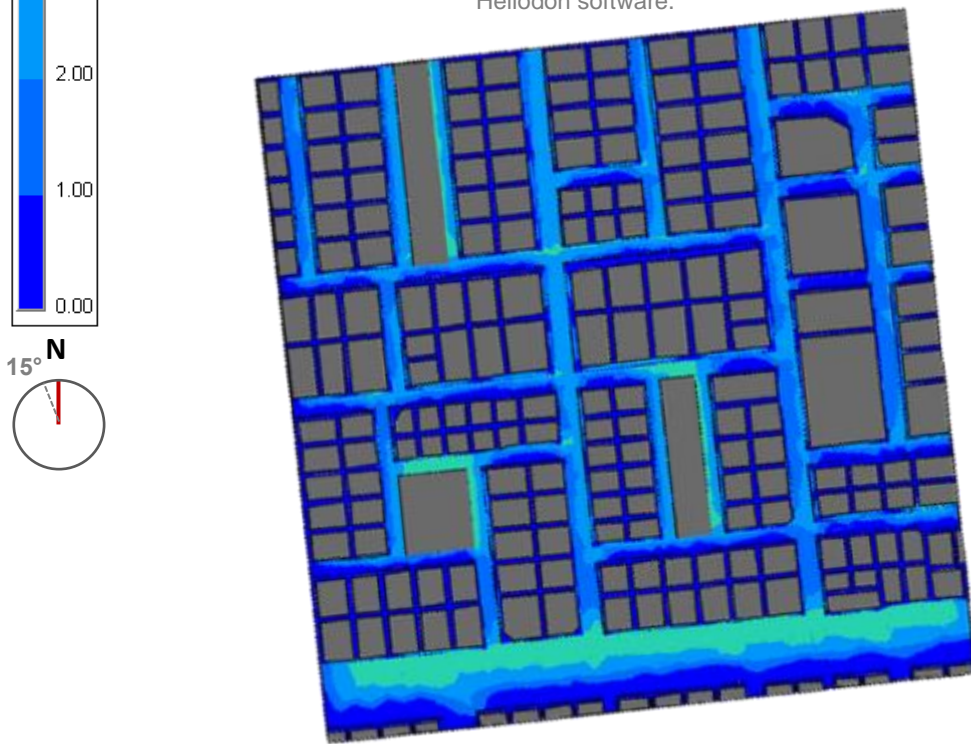


Figure 2.29. Case A: summer, 21st of December, solar flux. Source: Heliodon software.

2.4.3 Case B: Low-rise Residential buildings (Abhor AlShamalya)

The SVF Influence on the Urban Morphology in Case B:

The less dense the urban settlement is, the more visible the sky becomes. The urban layout in Case B has a dispersed low built-up density characteristic. The streets are symmetrical and have an aspect ratio ranging from $H/W = 0.90 < 0.45$. The simulation of all street orientations has approximately the same SVF value, indicating that the whole layout has the same amount of visible sky and the same number of obstructions.

In general, the simulation shows an average SVF for the whole layout 71.50 % (Figure 2.30). Therefore, this type of layout may have the same solar radiation intensity, the simulation reveals that the NE-SW and NW-SE average Sky View Factor is ranging between 60% minimum and 100%. As was mentioned previously, the higher the SVF value the higher is the solar intensity on a surface. Therefore, the urban development of these modern city types is disadvantageous when considering the climate in the built-up environment as an important factor. The factors considered in this layout are the automobiles and the individuality of the people living here.

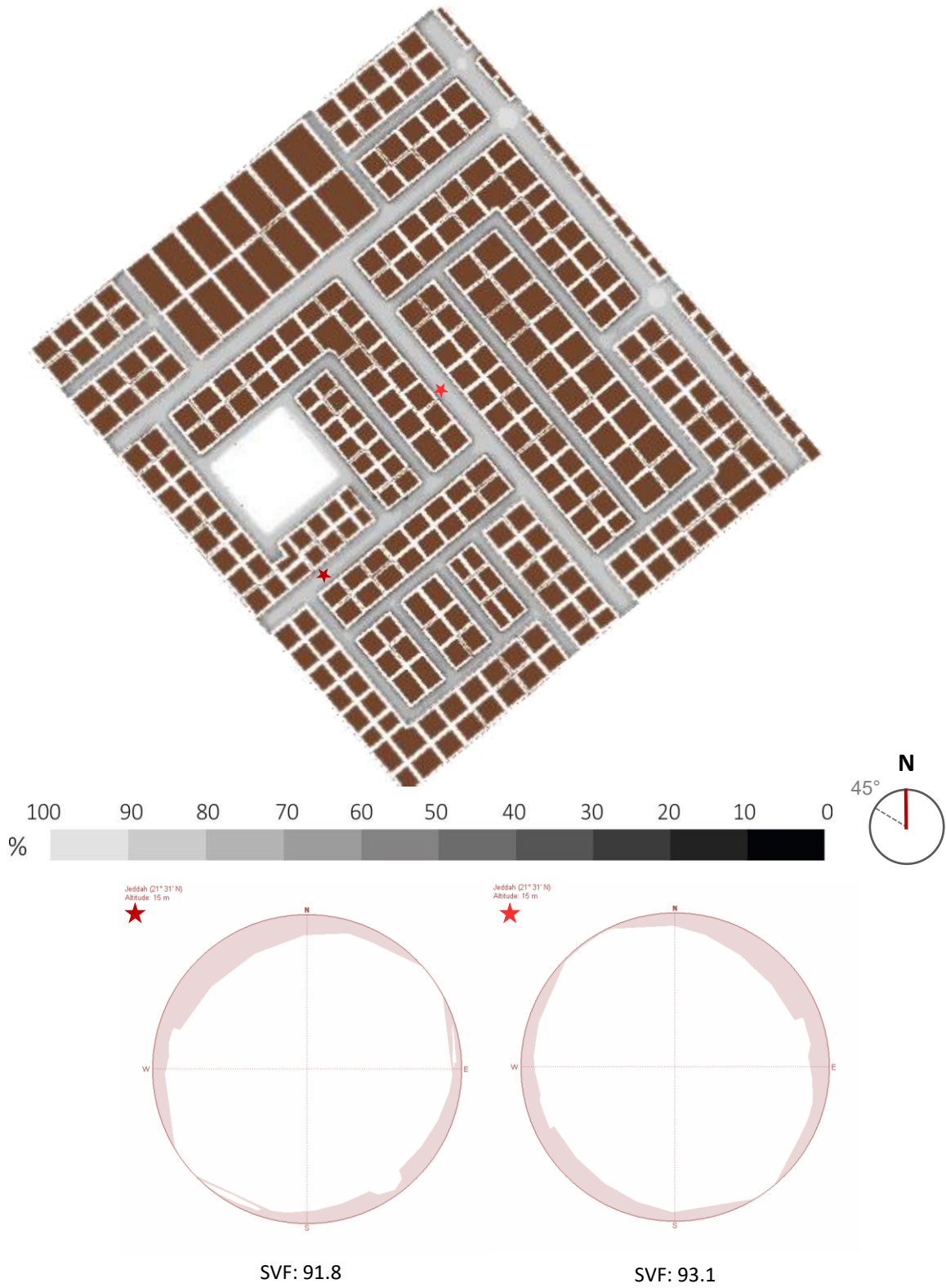


Figure 2.30. Case B: Sky view factor distribution on streets. The different colored asterisks on the map are used to illustrate examples of the SVF for that particular point with the orthographic projection. Source: Heliodon software.

**Case B: Solar Radiation Time Interval Influence on the Horizontal Surface (Streets)
- summer and Winter Solstice:**

The graph in Figure 2.31 shows the number of hours in summer and winter on the horizontal surface (streets) in the Case B layout consisting of low built-up density with low-rise buildings (residential). Obviously, the streets are highly exposed to direct solar radiation with more than 10 h of perceived sun. Only in the NE-SW orientation the maximum time of solar radiation is less than 8 h.

Figure 2.32 shows an orange color on the streets simulated map of Heliodon which almost covers all street surfaces in summer indicating that the street surfaces receive almost 10 h of direct solar radiation on both orientations NE-SW and NW-SE. The NE-SW street orientation even has a 2-h-longer sun period and a total of 12 h direct solar radiation (red color). The distribution of the color is almost equal as no higher obstructions are present which would diminish the solar radiation.

The low-rise buildings are not providing any shade to the streets. And whenever the street is wider the red color becomes clearer indicating that this type of morphology of building heights is constant without any obstructions that mitigate the harsh solar radiation, unless the streets become narrower. During winter, the findings show that due to a low solar angle the sun period is reduced in this urban layout especially for its layout orientation at 45° (Figure 2.33). The degradation of colors is more visible in winter than summer. Here, the streets receive almost 7 h sun and a minimum of 2 h when the street parts are located closer to S-E facades and S-W facades.

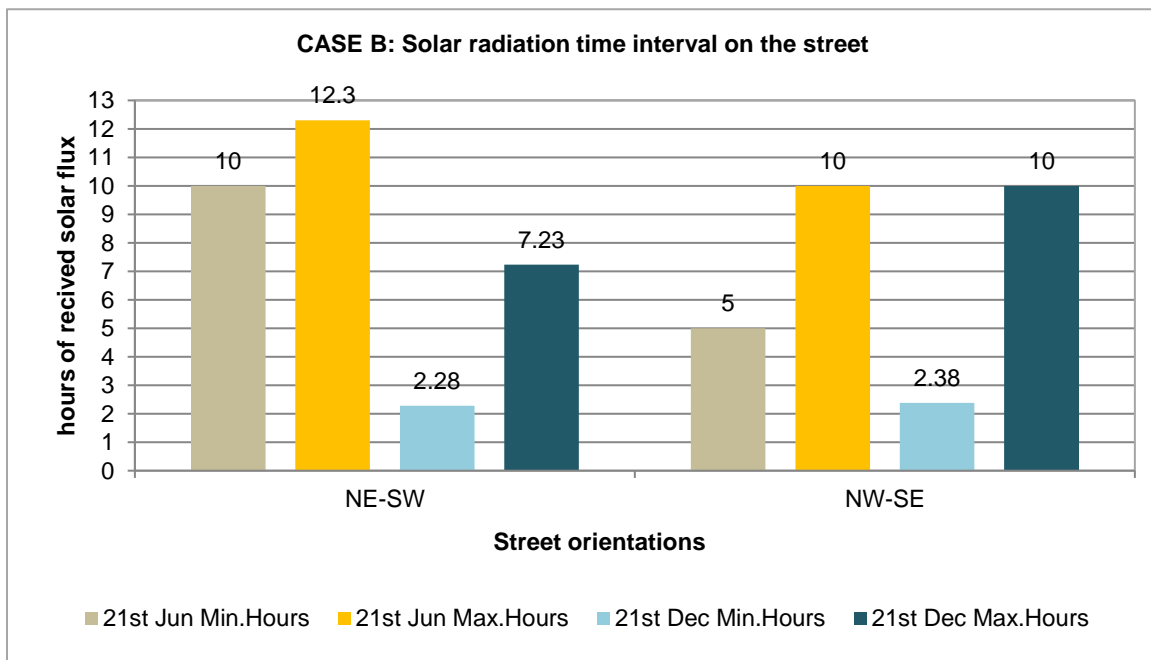


Figure 2.31. Case B: Solar radiation time interval on the two street orientations.

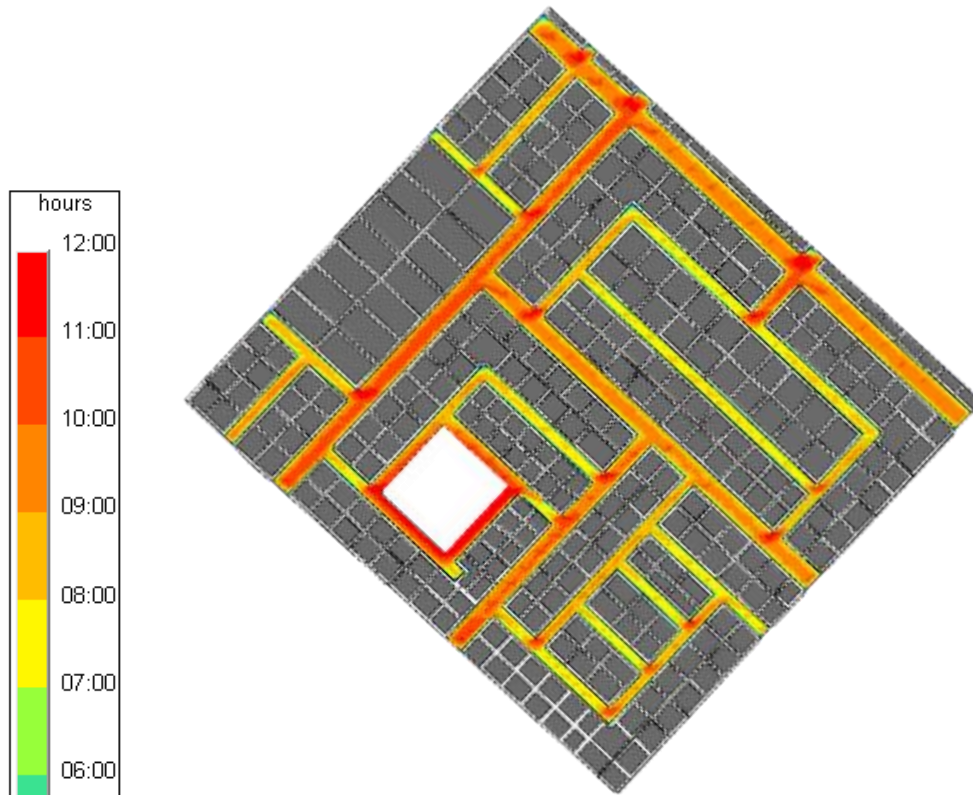


Figure 2.32. Case B: summer, 21st of June, solar radiation time interval (sun period).
Source: Heliodon software.

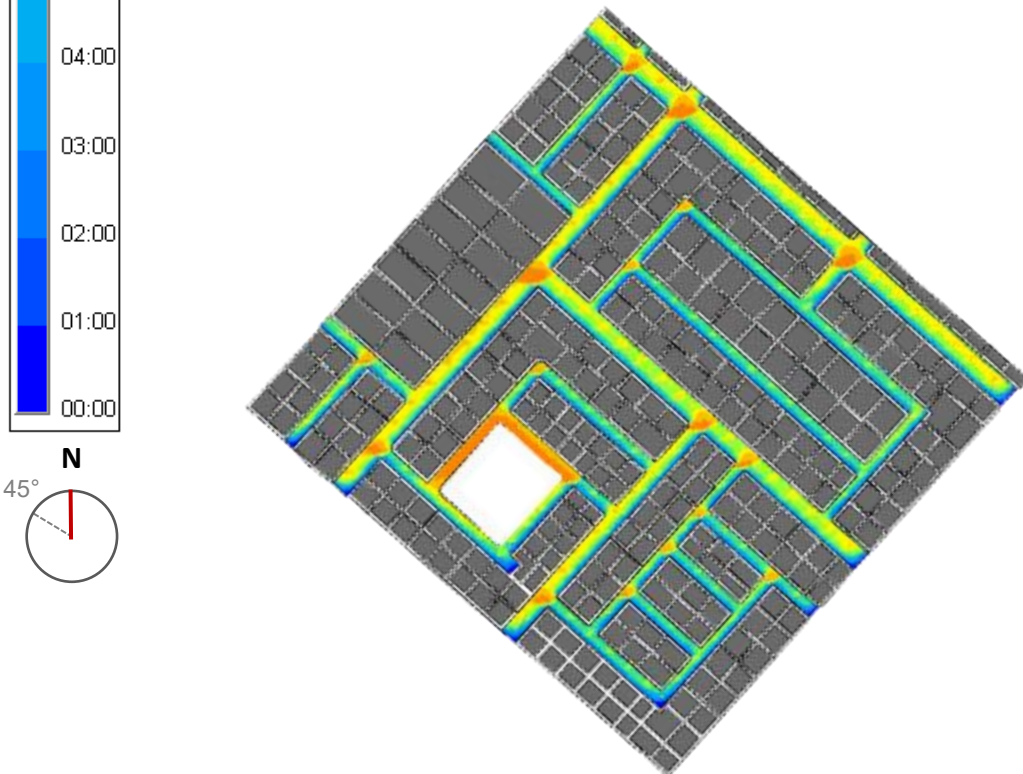


Figure 2.33. Case B: summer, 21st of December, solar radiation time interval (sun period).
Source: Heliodon software.

Case B - Solar Flux Value and Sky View Factor:

In Case B, the layout is oriented at 45° and no obstructions are affecting the exposure of the layout surface to solar radiation. As a result of the low-density solar angle, and the plot orientation, Figure 2.34 reveals that the average solar flux on the entire layout is the same amount in general. It has a high solar flux value throughout the whole day on the 21st of June ranging from 7 to 6 kWh/m²/day (Figure 2.35). And in winter on the 21st of December both streets' orientations receive a direct solar radiation ranging between 2.90 kWh/m²/day minimum and 4.2 kWh/m²/day maximum (Figure 2.36).

Moreover, it shows that the average SVF is between a minimum of 60 % and of 80 % of the streets-oriented Northwest-Southeast. Northeast-Southwest orientation presents a higher average SVF, between 80 % and 100 %. Besides, the solar radiation shows similar intensity due to the lack of obstruction. Consequently, the sun penetrates from all directions.

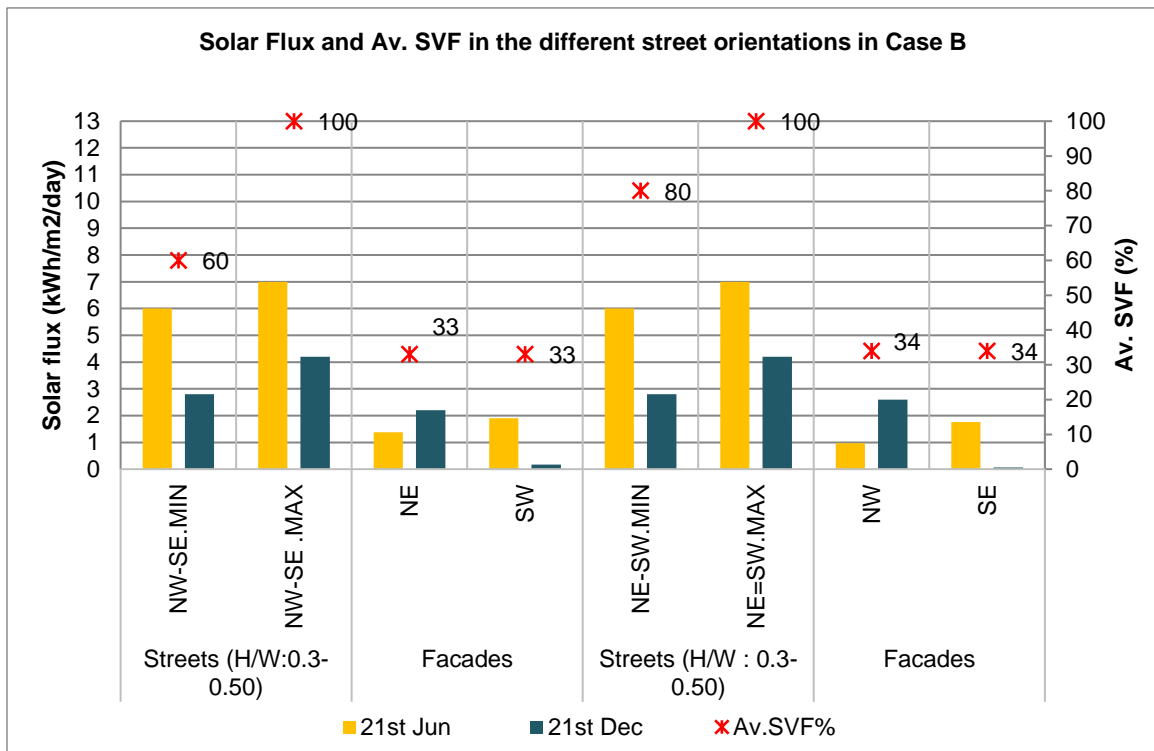


Figure 2.34. Case B: average solar flux and sky view factor (SVF) on the streets and facades.

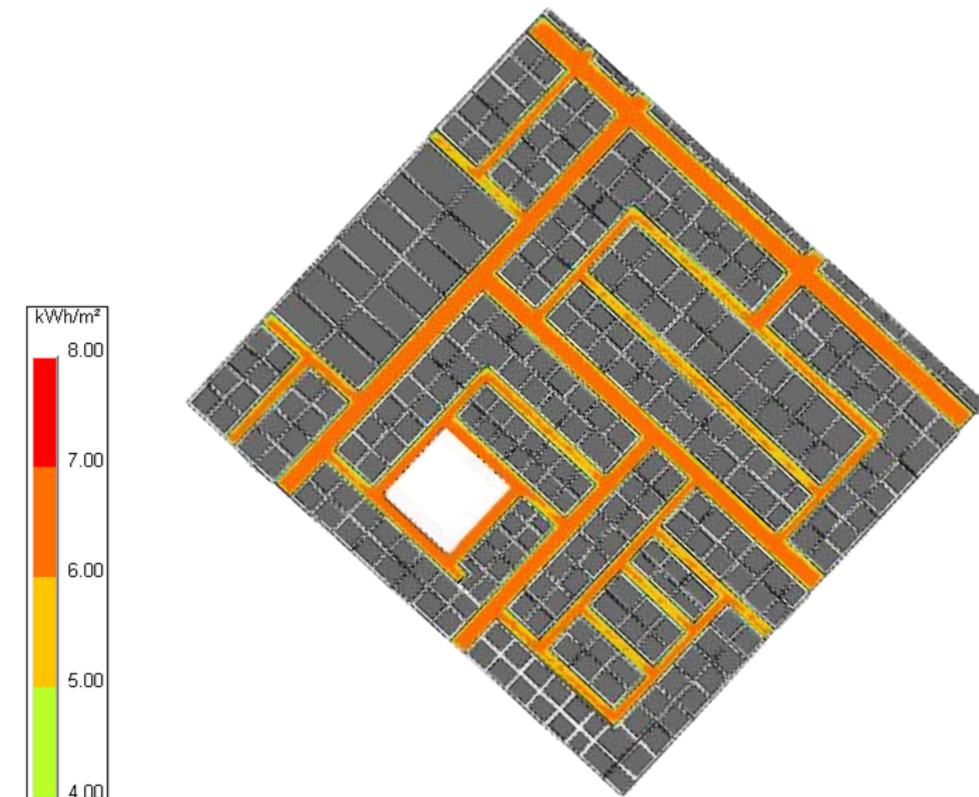


Figure 2.35. Case B: summer, 21st of June, solar flux. Source: Heliodon software.

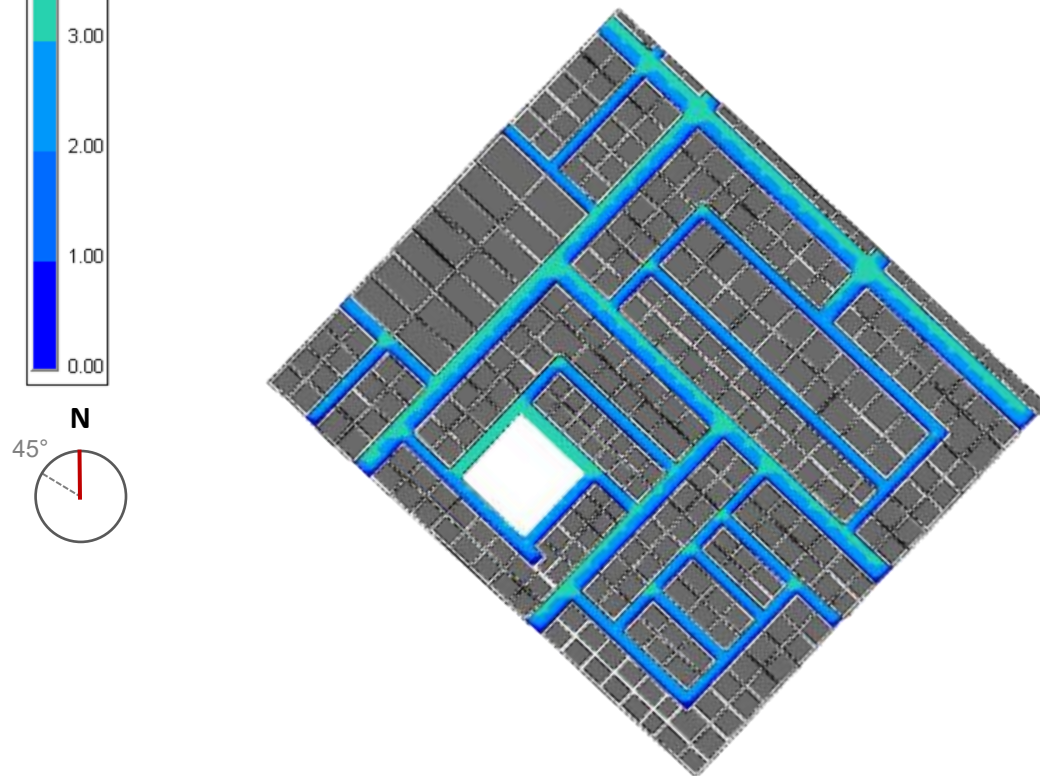


Figure 2.36. Case B: winter, 21st of December, solar flux. Source: Heliodon software.

The overall quantitative analysis of the results for the Cases A and B shows that in the selected urban layouts with wider streets and fewer obstructions, the vertical surfaces (facades) receive less solar radiation than the horizontal ones (streets) (Figure 2.37-2.38). Additionally, vertical surfaces receive in both cases a different solar radiation depending on the facade orientation and the solar angle due to the layout orientation.

Accordingly, on 21st June, the facades in **Case A** that show the highest solar flux value are the West facades receiving 2,20 kWh/m²/day with an average SVF of 37% (Figure 2.37). Following that are the East facades receiving 1.90 kWh/m²/day with an average SVF of 36%. Somewhat lower is the solar flux value for the South facades with 1.2 kWh/m²/day and an average SVF of 37%. The lowest numbers are to find for the North facades which receive 0.16 kWh/m²/day and an average SVF of 36%. This contrasts with winter, when the South facade obtains on the 21st of December the highest amount of solar flux value with 3.5 kWh/m²/day.

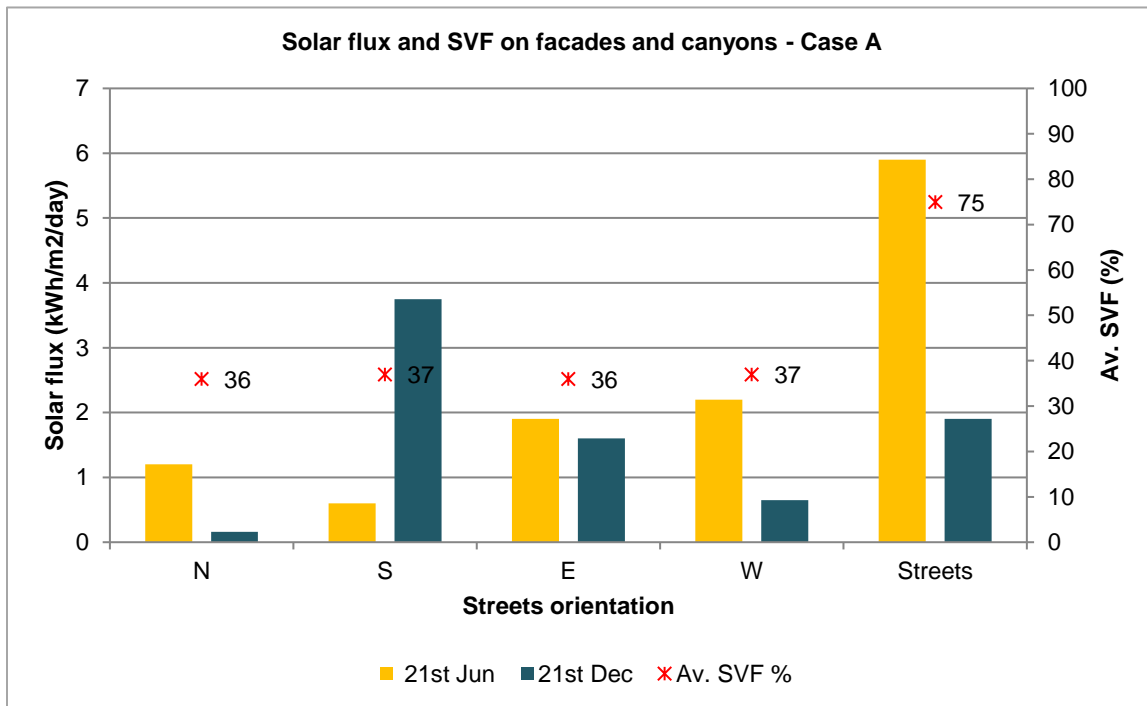


Figure 2.37. Summer and winter solar flux and the average SVF of the streets and the different-oriented facades in Case A.

Looking at **Case B**, the Southwest facades receive on 21st of June the highest solar flux value with 1.90 kWh/m²/day and an average SFV of 33% (Figure 2.38). The Northwest facades receive a lower solar flux value with 0.97 kWh/m²/day and an average SFV of 34%. In contrast, on 21st of December, the Northwest facades show the highest SFV amongst the facades with 2.6 kWh/m²/day. The Southeast facades receive the lowest incident solar energy of 0.067 kWh/m²/day. This is because the solar angle is on the summer solstice is higher than on the winter solstice. Additionally, due to the low-density and dispersed urban layout, the average sky view factor is constant in all vertical (facades) and horizontal (streets) surfaces. Check Appendix 2 (section 2.4) for all the facades Heliodon simulation.

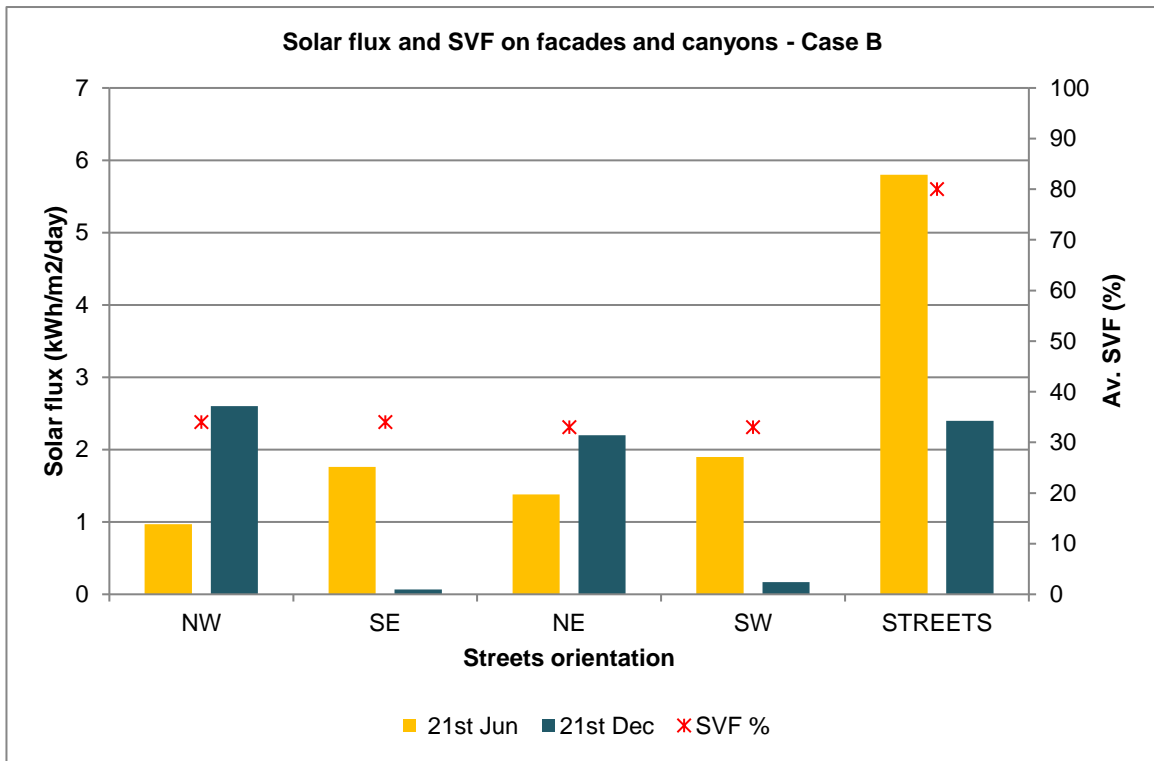


Figure 2.38. Summer and winter solar flux and the average SVF of streets and the different-oriented facades in Case B.

2.5 SUMMARY OF THE RESULTS

The results showed that with the compact morphology the old layout (AlBalad) receives an average solar flux of 3.2 kWh/m²/day. Case A has a dispersed urban morphology characterized by mid-rise buildings. The streets on this layout receive an average solar flux of 5.9 kWh/m²/day. On the other hand, the layout in Case B has an equally dispersed urban morphology characterized by low-rise buildings and receives an average solar flux of 5.8 kWh/m²/day. Together, the urban layouts of Case A and B receive approximately the same average amount of solar radiation intensity on their street surfaces.

The difference in solar intensity reveals a 44% decrease in summertime for AlBalad layout in comparison to Case A and Case B. During wintertime, the difference of incident solar radiation intensity between AlBalad and Case A is 69% and between AlBalad and Case B 75%. Regarding the characteristics and environmental requirements of the hot-desert climate of Jeddah, the observation is that AlBalad could be classified as the most efficient layout during the hot season. For the Cases A and B, the urban layouts are less efficient during the hot season.

Moreover, the simulations in all three case studies revealed that the average SVF depends on the studied urban geometry parameters, the obstruction of the buildings (height of buildings), width of street, and their street orientation. Thus, the old area in (AlBalad) has the lowest average Sky View Factor with a 28%. Only in plazas and street crossings the average SVF increases up to 60%. The mid-rise buildings layout in Case A and Case B the average SVF is relatively high. For Case A it is 66.40% and for in Case B 71.50 %. For both cases, the intersections have an Av. SVF of 80% to 100%.

CHAPTER 3

THE PUBLIC TRANSPORTATION AND URBAN FORM

“The most vibrant cities are ones that prioritize the one element that gives them their character - its people. If more places reduce the space for cars and give it back to people, then any city can become a more social, healthy, and happy place for everyone.”

Melissa & Chris Bruntlett

3.1 TRANSPORTATION AND URBAN FORM

3.2 TRANSPORTATION ISSUES ON THE URBAN ENVIRONMENT

3.3 PUBLIC TRANSPORTATION AND CITIES

3.4 JEDDAH PUBLIC TRANSPORTATION PROJECT

3.5 ASSESMENT OF PROPOSED PUBLIC TRANSPORT SYSTEM

3.6 JEDDAH FUTURE URBAN DENSITY

3.1. TRANSPORTATION AND URBAN FORM

The evolution of transportation has generally led to changes in urban form. The more radical the changes in transport technology, the more alterations on the urban form. The planning of recent times is committed to constructing mass transit infrastructure, in some cases the underground.

Therefore, Transport and urban form are one of the central aspects of urban development; the two shapes access to people, goods, services, and cities' information. The more efficient this access, the greater the economic benefits through economies of scale, agglomeration effects, and networking advantages. Different urban accessibility pathways directly impact other measures of human development and environmental sustainability (van Audenhove, et al. 2014).

Jeddah's existing infrastructure cannot support the city's needs. There is an urgent need for a public transport network to encourage economic development, enhance social well-being, and improve life quality. Therefore, Jeddah city will shortly start constructing a public transportation program (JPTP) in response to the city's needs. This will radically change the habits of Jeddah's inhabitants.



Figure 3.1. Future infrastructure scheme: the idea of a multifunctional urban ecology of horizontal and vertical transport (Tottenham Court Road station – London) (Source: Global Schindler Award 2015)

In every city, the evolution of urban transport and mobility is inseparable from urban development patterns. Likewise, urban transport cannot be regarded separately from urban forms (Newman and Kenworthy 1989, Houghton 1995, Rode et al. 2014, UN Habitat 2013).

The rapid development of the urban planning system has resulted in a significant grouping of people and buildings between metropolises, which have created new urban growth centers. From a monocentric to a polycentric model, the development of the urban structure always follows economic and urban development. Uncontrolled development creates urban problems, most of which stem from supply-demand imbalances. The static supply side is urban elements such as land and transport, and human behavior is always part of demand. (Jing and Zhentao 2007).

To implement access to people, goods, and information, each city has developed its own unique spatial structure and transportation system. However, the most popular combinations of urban spatial structures and transport have evolved in different principal patterns of development. The extent to which accessibility is based on the physical proximity between the sources and the destinations, or on transport solutions capable of overcoming spatial separation. These solutions involved private or public motorized transport and defines these pathways. (Bottles 1987; Cervero 1998).

Initially, transit systems allowed for horizontal growth, which encouraged and demanded dense, compact urban development while maintaining human-scale urban environments. The urban design acknowledged that all public transport passengers remained pedestrians at some point in their journey, navigating through public urban space. The advent of the automobile, on the other hand, encouraged suburban growth at far lower densities and introduced a mode of transportation that required considerably more space to function than any previous mode of transportation. To summarize, public transportation requires urban density, while car usage requires space. The inefficient use of scarce urban space by private vehicles has resulted in extraordinary tensions in most cities. This poses a particular problem in densely populated developing cities, where modern motorization significantly outpaces the development of road infrastructure and public transportation alternatives (Hickman and Banister 2014).

Car-based systems occupy much more space than any other mode of urban transportation. For example, for a 50 km/h vehicle, over 160 sq.m is required, in comparison to 4 sq.m. for buses ((based on average occupancy levels) (Rode, et al. 2014). Car parking space is an additional need, with cars being inactive for most of the time. The average car in the United States is parked 96 percent of the time, and the aggregate parking space in car-oriented central business districts (CBD), such as Los Angeles, is more than 80 percent of the CBD land area (Manville and Shoup 2004). Globally, an additional 45,000-77,000 km² would be required for car parking alone by 2050 (Dulac 2013), an area equivalent to the size of Denmark. As a result, the space requirements of private vehicle traffic not only mean further de-densification of cities but

are also a major contributor to public space congestion and parking pressures, as the provision of road infrastructure is often unable to keep up with rising vehicle traffic levels (Kersys, 2011)

The difference in transport intensity between high and low-density areas can be more than 40% per capita of the vehicle-miles-traveled area (Ewing, Bartholomew, et al. 2008). The US National Research Council estimates that doubling densities in metropolitan areas can reduce vehicle-kilometer-travel (VKT) travel by up to 25% while also concentrating employment (National Research Council 2009). Overall, the dependence on cars is negative (Figure 3.2).

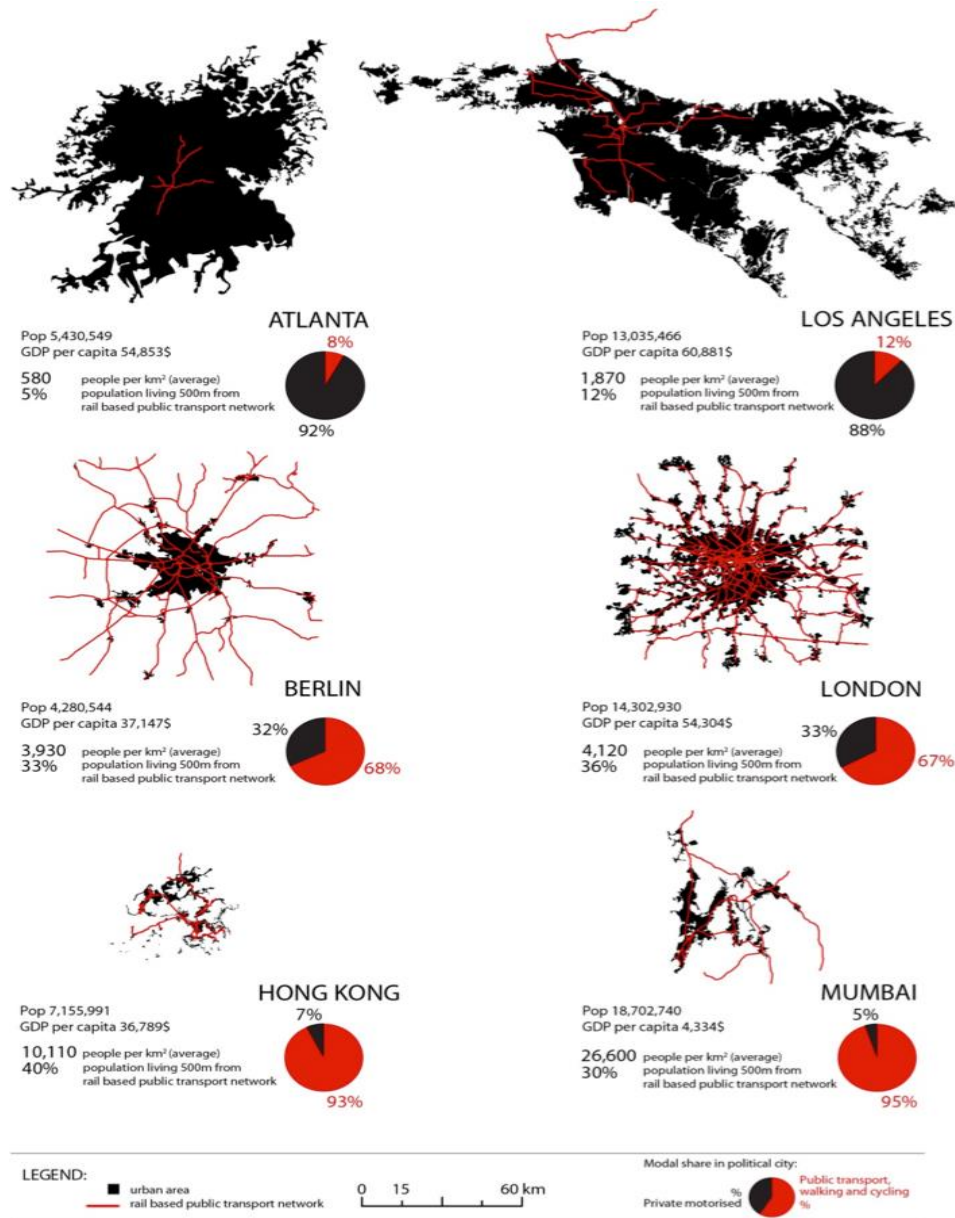


Figure 3.2. Urban form and modal share (black in pie chart is private motorized) of selected cities (Source: concept and information design based on Sorensen and Hess 2007)

3.2 TRANSPORTATION ISSUES ON THE URBAN ENVIRONMENT

The relationship between transportation and the environment is fundamentally contradictory; transportation activities support growing passenger and goods mobility demands. However, increased motorization and pollution have resulted from transportation activities. As a result, the transportation industry is becoming more strongly associated with environmental issues. Climate change, air quality, noise, water quality, soil quality, biodiversity, and land take are the most significant environmental impacts of transportation (Rodrigue, 2006).

Urban transport systems' co-dependence with the urban form also plays a central role in the global transition to a low-carbon economy (Hickman and Banister 2014). Around ten billion trips are made every day in urban areas around the world. Of these, a significant and increasing proportion is undertaken using high carbon and energy-intensive private motorized vehicles. About 80 percent of the increase in global transport emissions since 1970 has been due to road vehicles (IPCC 2014a).

As a result, transport is one of the major sources of carbon emissions in cities. Overall, the transport sector produces around 23 percent of global energy-related CO₂ emissions, equivalent to 6.7 gigatons of CO₂ in 2010 (IPCC 2014a). While urban car use is the single largest contributor to transport carbon emissions, freight transport accounts for up to 20 percent of urban traffic and up to 50 percent of urban transport GHG (greenhouse gas) emissions - is often underrepresented (Savy 2012). Emissions are growing more rapidly in the transport sector than in any other sector and are projected to increase by 50 percent by 2035 and almost double by 2050 under a business-as-usual scenario (Dulac 2013; IPCC 2014a).

While urban transport emissions correlate strongly with income, there are major differences between cities with similar wealth levels. The carbon intensity of urban accessibility is determined by two main factors: the overall distance of motorized travel required (which is largely informed by urban form characteristics) (Figure 3.3-a) and the carbon intensity of these modes (Figure 3.3-b). The energy intensity informs the latter of different transport modes and the carbon intensity of their fuels.

The well-known research findings figure 3.3-a shows linking urban form with transport energy use in larger cities across the world, which initially established a strong negative correlation between population density and annual gasoline consumption (Newman and Kenworthy 1989). Overall, more recent research has confirmed this relationship when controlling for wealth, and they also apply for carbon emissions (OECD 2012; Qin and Han 2013; UN-Habitat 2013; IPCC 2014b). For example, sprawling Atlanta produced six times more transport-related carbon emissions at similar wealth levels than relatively compact Barcelona (ATM, 2013; D'Onofrio, 2014; LSE Cities 2014). This finding aligns with analysis conducted for 30 cities in China, which showed that compact cities have higher CO₂ efficiency, particularly supporting non-motorized transport (Liu, Chen, et al.

2012). The IPCC suggests that an urban accessibility pathway consisting of more public transport-oriented compact cities, combined with improved infrastructure for non-motorized transport, could reduce GHG intensities by 20 to 50 percent over the medium to long-term compared to 2010 levels (IPCC 2014a).

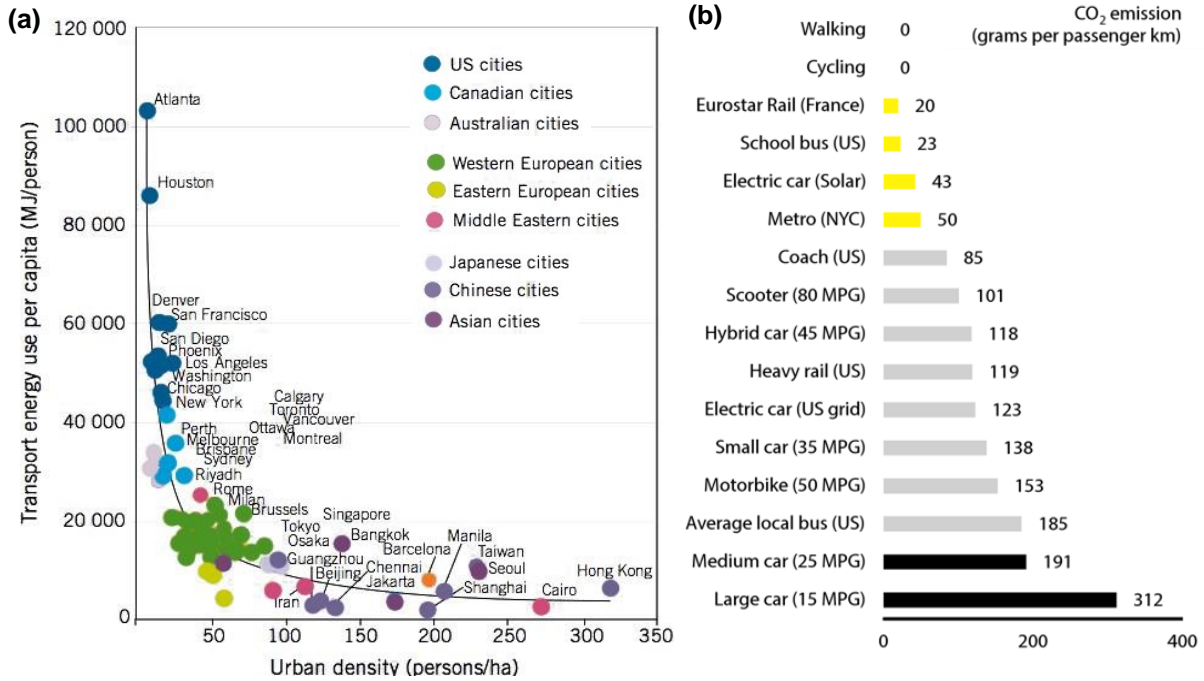


Figure 3.3. Population density and transport energy use per capita for selected cities (left) (Source: WHO 2011). Emissions per passenger km by urban transport mode (right) (Source: STF 2014)

These relationships matter for the developmental choices which rapidly growing cities face today. A scenario study for US metropolitan areas in cities such as Atlanta and Phoenix suggests a reduction of 7 to 10 percent in carbon emissions due to a 20 to 40 percent reduction in vehicle-miles-traveled due to compact urban development (Ewing, et al. 2008).

The positive correlation between energy or carbon efficiency and urban density can also be observed outside the transport sector and, together with affluence levels, can impact variations in carbon emissions at the national level (Figure 3.4). For instance, compact and taller building types can improve heat energy efficiency at the neighborhood level by a factor of six compared to detached houses (Rode et al., 2014). According to the Residential Energy Consumption Survey (RECS) in the US, households in suburban areas use more energy on average both in total (22.5 percent) and per capita (12.7 percent) compared to those in cities (Estiri, 2012), which translates to 36 percent higher electricity, 19.5 higher natural gas and 29 percent higher consumption per household in suburban areas (EIA, 2001).

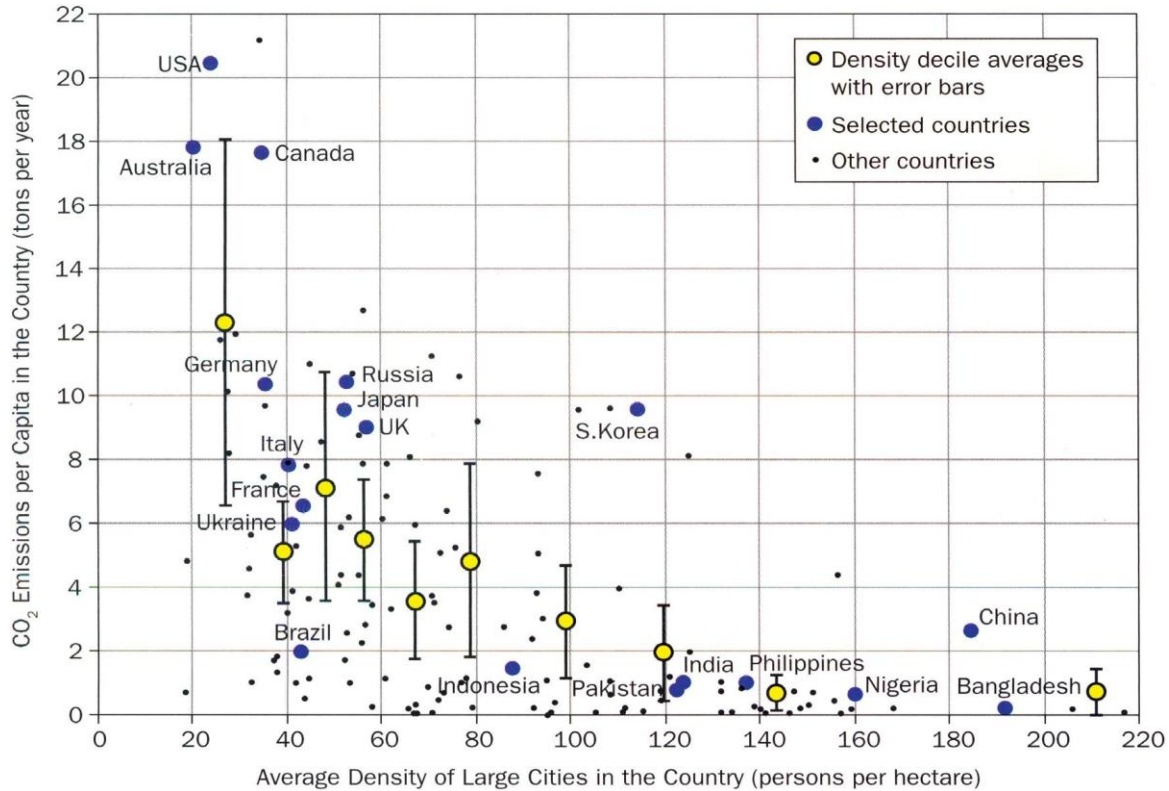


Figure 3.4. Average urban densities in large cities and average carbon emission per capita (Source: Angel 2012)

Given the significant negative externalities of urban accessibility pathways characterized by sprawling and car-oriented urban agglomerations, many commentators cite major market failures as the cause of sprawl whilst recognizing that these are extremely complex and interrelated. Among the most obvious are significant subsidies of related infrastructure and operations, as well as unpriced negative externalities ranging from congestion to health and environmental impacts (Wheaton 1998; Brueckner, Mills, et al. 2001; Wu 2006).

3.3 PUBLIC TRANSPORTATION AND CITIES

Over the last decade, investment in public transport, including BRT (Bus Rapid Transit) and rail systems, has also increased, indicating a shift away from primarily investing in roads as was common in earlier decades (Owens 1995; Goodwin, Hass-Klau, et al. 1998; Vigar 2001; Owens and Cowell 2011).

Despite the global trend towards increasing motorization, new and alternative urban forms and transport planning patterns have emerged in recent years. In the developed world, several cities have increased their share of public and non-motorized transport and reduced car ownership while creating more attractive and economically prosperous inner cities. For example, between 2000 and 2010, car ownership levels in New York, London, and Berlin have been declining (Burdett and Rode 2012).

Simultaneously, alternative urban development and accessibility pathways are beginning to emerge, and re-densification is recorded in many European and North American cities. Examples of well-planned compact cities include Copenhagen, Stockholm, and Hong Kong, whereas other cities such as London, Brussels, Boston, Tokyo, Hamburg, and Nagoya have re-densified and moved back towards more concentrated forms (Floater, Rode et al. 2013; Floater, Rode et al. 2014). Since 2000, population growth in London has been concentrated within a 10 km radius of the city center; and between 2004 and 2011, 53 percent of all newly constructed floor area was located within walking distance (0-500 meters) of the nearest rail or underground station (Rode 2014). Even cities in China have already started to increase densities: population density in Beijing's core has already increased by 50 percent over the past decade (World Bank 2014). This 'return to the city' has multiple socio-economic reasons, many of which are related to the agglomeration effects discussed above. Besides, changing demographics and family structures, greater participation of women in the labor market, and related lifestyle changes have all been identified as significantly reducing suburban living attraction (Lovejoy, Handy et al. 2010)

Within urban transport infrastructure provision, massive capital cost savings can be generated due to a shift away from private car infrastructure towards public transport,

3.4 JEDDAH PUBLIC TRANSPORTATION PROJECT

The city of Jeddah did not develop as a radical structure, whereas the old town was previously protected by walls, which have been replaced by a ring road. The city's overall footprint is more deeply expressed by longitudinal development along the coast. Overtime, a series of highways were installed to facilitate access between the two furthest sides of the city; however, these infrastructures have, in fact, caused clear fragmentation between neighborhoods (Mandeli, 2017).

The car is the dominant transportation mode in Jeddah as mentioned in previous chapters. This represents over 96% of all daily travel, and concurrently, many of Jeddah's roads experience high congestion levels (Aljoufie 2012).

The enormous traffic volume and resultant congestion threaten not only the quality of the environment and the safety of road users but, in the long term, can additionally undermine the economic prosperity of the city. Dealing effectively with traffic congestion and its effects will be critical to ensuring an environment in which the population can live, work, and move about comfort and safety (UN-Habitat, 2019).

To determine the functionality of the city's current road network, UN-Habitat conducted a study to calculate access to the two city centers of Al Balad and Al Rawdah within a 15-minute, 30-minute, and 60-minute drive distance from anywhere in the city. For the analysis, the driving speed was calibrated at two-thirds of the designated road speed, taking into account traffic congestion in the city. Figure 3.5 depicts the accessibility study, which reveals travel times between these centers and the city only via private

transportation modes. According to the study, 48 percent of the population, equivalent to two million people, have access to the urban core within a 15-minute drive. Within 30 minutes of driving, this access increased to 73%. Only 7% of the population was found to be without access to the urban core, with drive times of more than 60 minutes (UN-Habitat, 2019).

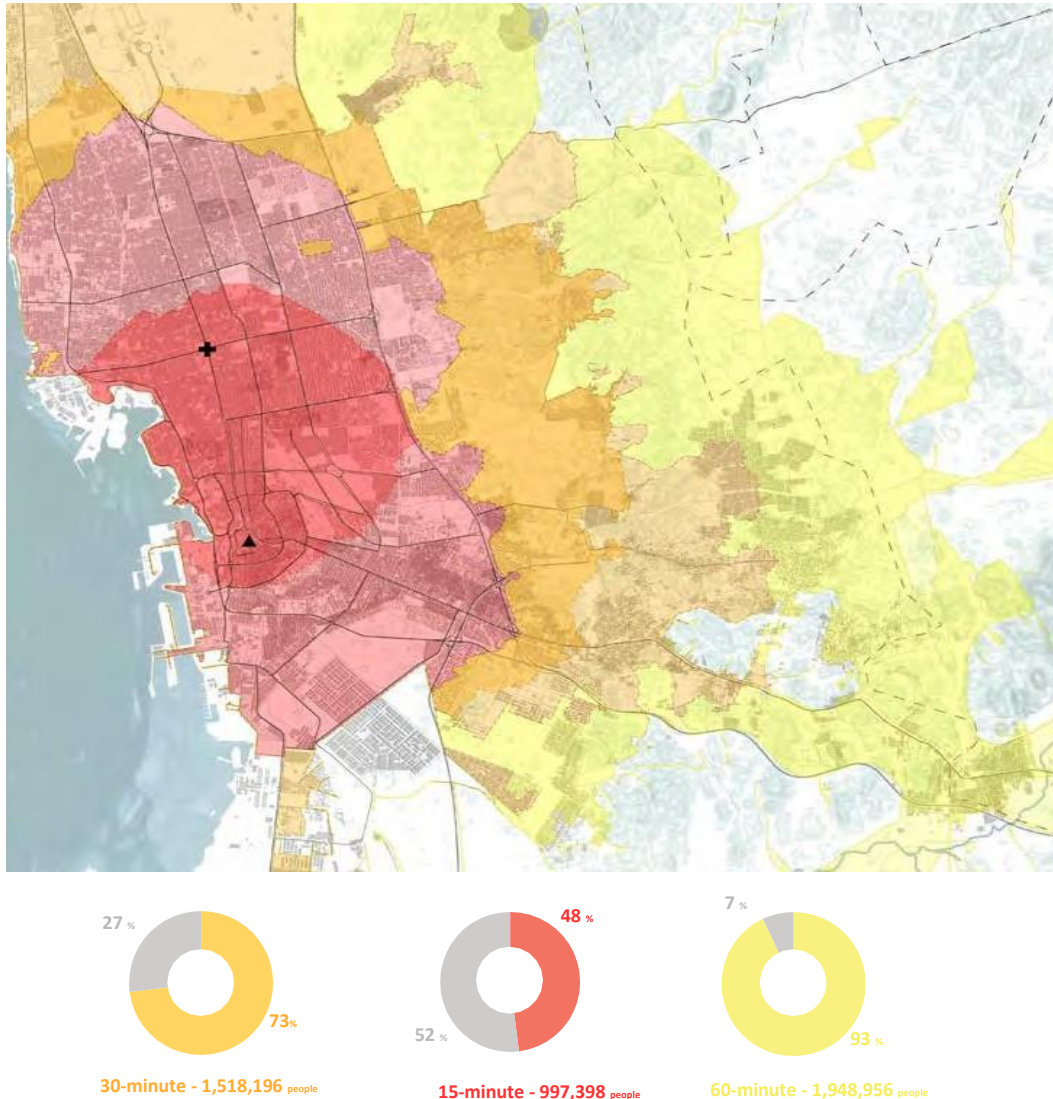


Figure 3.5. Drivability to the commercial city centers (Source: UN-HABITAT 2019)

Additionally, a pedestrian accessibility analysis shown in Figure 3.6 has been applied to three central areas of the city. The results are as follows:

- Waterfront - 14,397 people living within a 10-minute walking distance from the selected center. This is attributed to low density as large residential villas dominate the neighborhood.
- Al Rawdah - 82,376 people, living within a 10-minute walking distance.
- Al Balad - 175,069 people living within a 10-minute walking distance.



Corniche

The Jeddah Corniche is the **30 kilometers coastal resort area** of the city of Jeddah. Located **along the Red Sea**, the corniche features a coastal road, recreation areas, pavilions, and large-scale civic sculptures — as well as **King Fahd's Fountain**, the highest fountain in the world.

Al Rawdah

Al Rawdah District of Jeddah nestled in the heart of the city, amidst residential buildings and considered the **main shopping and business area**.

Al Balad

Al Balad - the **historical city center** of the city of Jeddah, As explained in chapter 1.

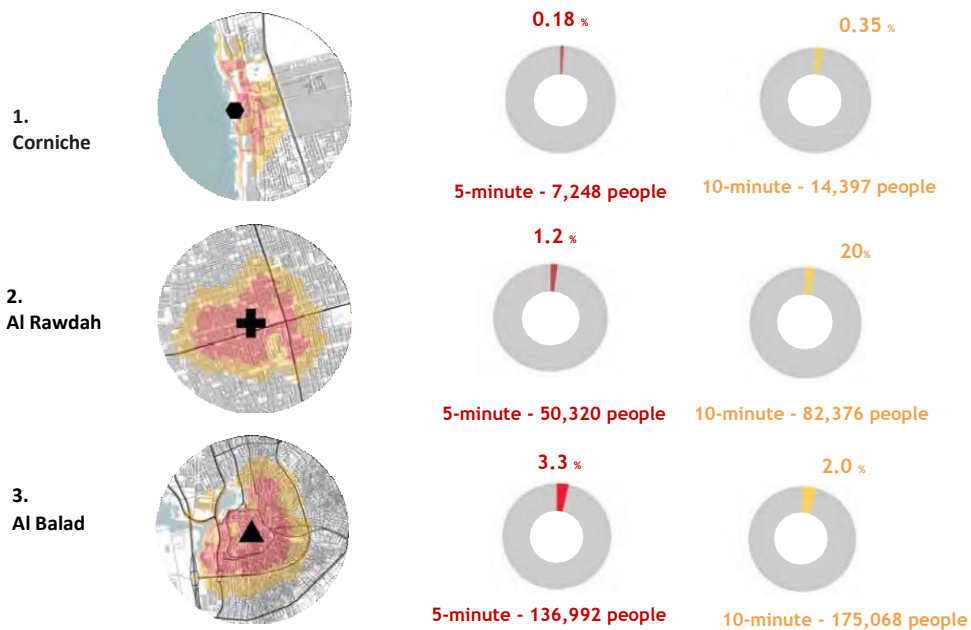


Figure 3.6. Walking accessibility to the city centers (Source: UN-HABITAT 2019)

3.5 ASSESSMENT OF PROPOSED PUBLIC TRANSPORT SYSTEMS

The Future Saudi Cities Program is a jointly implemented project managed by the Deputyship of Town Planning of the Ministry of Municipality and Rural Affairs of the Government of the Kingdom of Saudi Arabia and the United Nations Human Settlements Program (UN-Habitat). Foster and Partners has been appointed through an international competition to develop the “architectural vision” for Jeddah’s city-wide public transport plan.

The two driving initiatives of the Jeddah Structural Plan are TOD (transit-oriented development) and Public Transit. Core to this approach is the introduction of an Express Metro Route (the Red Line). This would be supplemented by three Metro routes (the Orange, Blue, and Green Lines) (Figure 3.7), concentrating on connecting the city's highest residential density areas to key facilities and attractions (airport, port, and CBD). The Metro and Express Metro Lines, together with a regional commuter rail route, converge on the main employment center (CBD) to create a dense, high-capacity network capable of sustaining the high employment levels proposed.

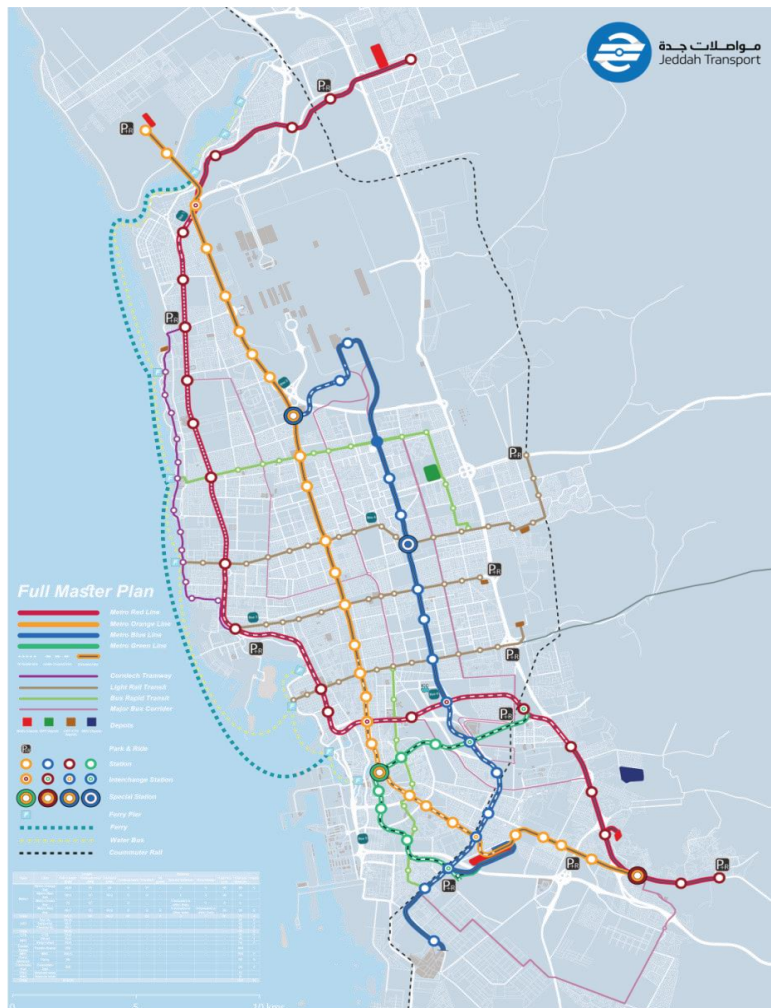
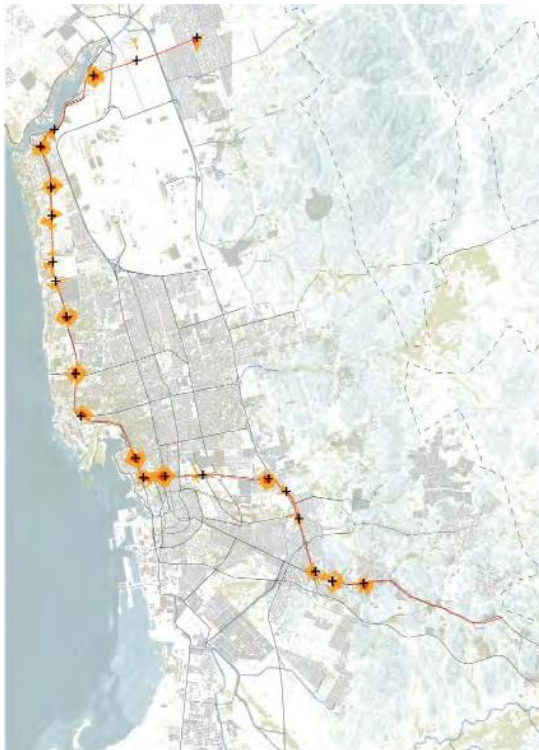


Figure 3.7. Jeddah public transportation Master Plan (Source: <http://www.metrojeddah.com.sa/>).

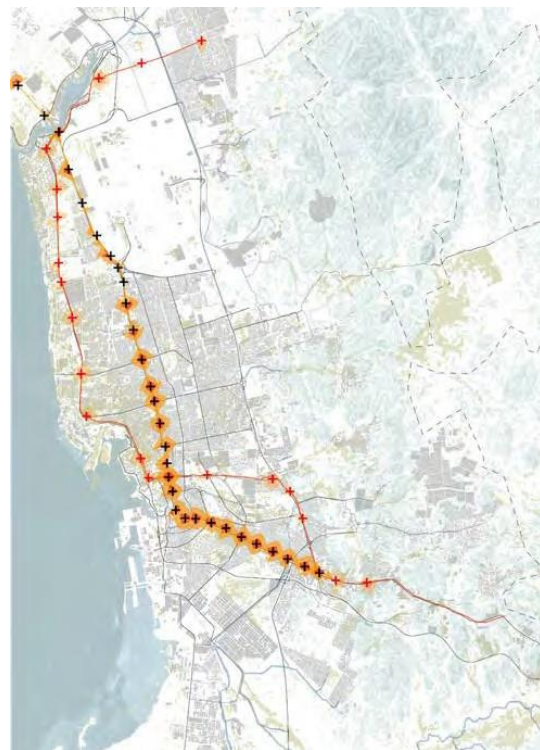
Moreover, express Bus and BRT (Bus Rapid Transit) routes' local networks would connect centers to the Metro and Regional Commuter rail interchanges outside the core city area. In some cases, such as East Jeddah and Salaman Bay, LRT (Light Rail Transit) routes would form the spine for development and local movement. The four new lines, yet to be built, will combine to create an extensive public transport network, it will be introduced through phases (Figure 3.8), and composed as follows:

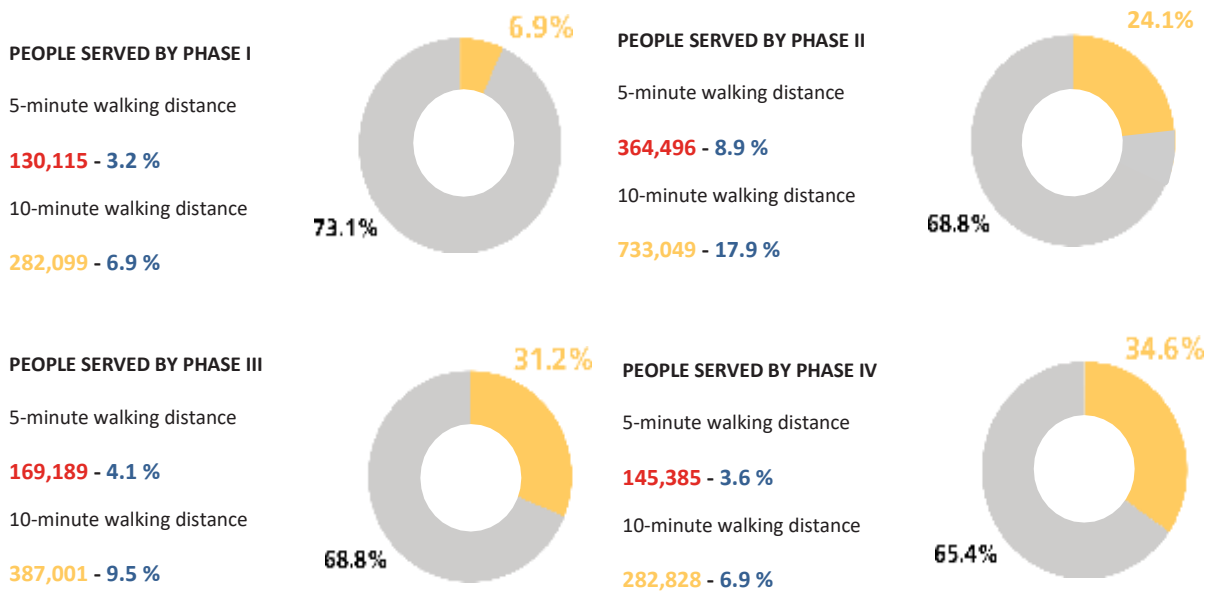
Line I - Express Metro (red): from the North to the South of the city, running along the waterfront and concluding at the old Makkah road. This line will serve 6.9% of the existing population within a 10-minute walking catchment area; The Express Metro provides a high capacity, high speed, limited-stop service. It connects the Town Centers in the urban core (Telal Jeddah, Jeddah Al- Jadeedah (contemporary area), Markaz Al Madinah (the center of the city), and Moulaisaa). Major interchange stops are provided at King Abdullah Sports City in Telal Jeddah, Jeddah Al Jadeedah on the western coast, three stops throughout the CBD at Markaz Al Madinah, and a final interchange at Moulaisaa. Typically, these are 1-2 km apart. They will serve multi-district centers and provide interchange with level 3 LRT / BRT transit and local bus services. A minimum net density of 100 dwellings per hectare is required to support an Express Metro interchange. Its speed in service will be 25- 30 kph (including stops) and hold a capacity of 30,000 pphd (passenger per hour per direction).

Metro Line Phase I: 67 km and 22 stops



Metro Line Phase II: 41 km and 30 stops





Metro Line Phase III: 35 km and 19 stops

Metro Line Phase IV: 16.7 km and 12 stops

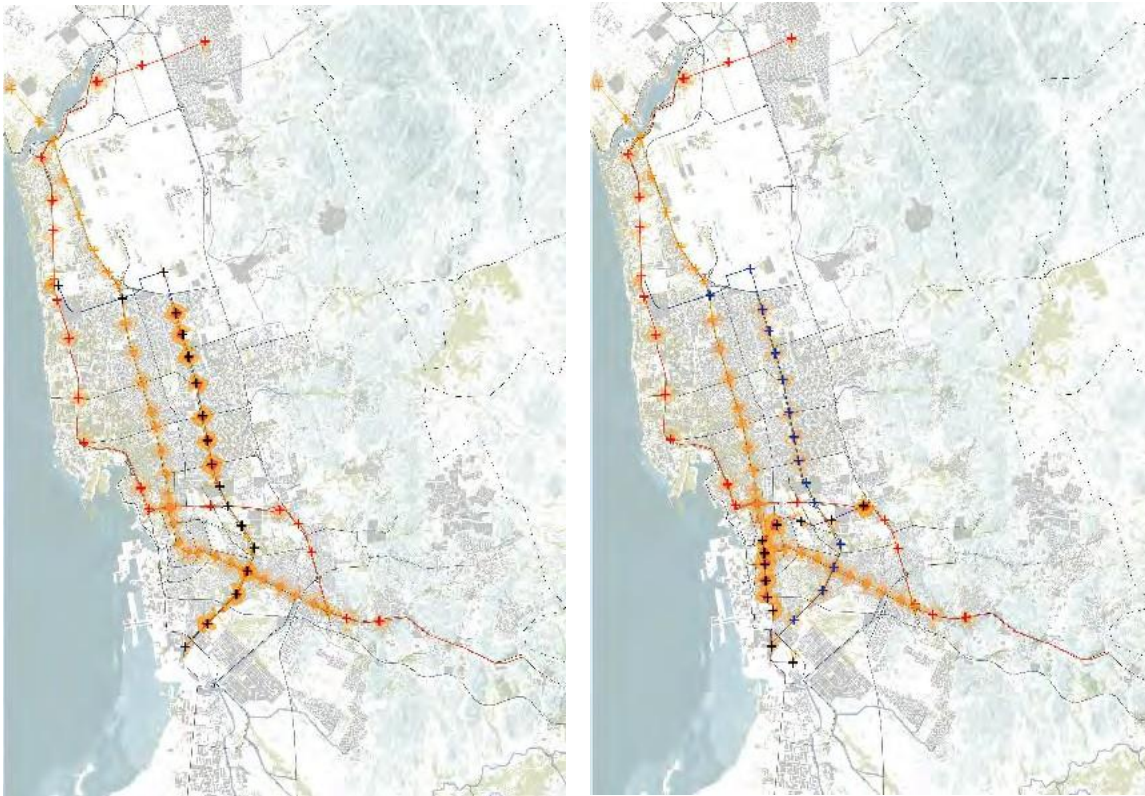


Figure 3.8. Phases of proposed transportation system (metro lines) (Source: UN-HABITAT 2019).

Line II (orange): The service runs in partial alignment with the Express Metro and serves all major interchanges to further distribute traffic across the city to stations that connect into the LRT / BRT networks. This line will serve 17.9% of the existing population within a 10-minute walking catchment area.

Line III (blue): This metro line will connect the international airport to the old city center of Al Balad. The line will serve 9.5% of the existing population within a 10-minute walking catchment area.

Line IV (purple): This line will connect the HSR station with Al Balad's center. The line will serve 6.9% of the existing population within a 10-minute walking catchment area.

The proposed metro lines will constitute a high-capacity urban transport system that aims to form the backbone around which to organize further networks. The BRT lines that will connect on an East-West axis will be essential to support the overall functionality of the North-South orientated metro lines.

3.6 JEDDAH FUTURE URBAN DENSITY

Firstly, FSCP (Future Saudi Cities Program) conducted scenario-analysis for increased urban density, which cut through the diagnosis of existing urban conditions and the approved/submitted project proposals. Initially, the city's current state was investigated to identify conditions within a benchmark density that could be used to compare alternative scenarios. Secondly, based on projections and accepted planning instruments, a scenario has been created. Finally, a scenario has been established in which the density distribution complies with UN-Habitat guidelines. The Five Principles for Sustainable Neighborhood Planning, as outlined by UN-Habitat, are as follows:

- Enough space for streets and a well-functioning street network: The street network should cover at least 30% of the land and have a street length of at least 18 kilometers per square kilometer.
- High density: at least 15,000 people per square kilometer, or 150 people per hectare or 61 people per acre
- Mixed-use land: In every neighborhood, at least 40% of floor space should be set aside for economic purposes.
- Social mix: The availability of houses in various price ranges and tenures in each neighborhood to accommodate people of various income levels; low-cost housing should account for 20% to 50% of the total residential floor area, and each tenure form should not account for more than 50% of the total.
- Limited land-use specialization: This is to keep single-function blocks or neighborhoods to less than 10% of each neighborhood's total area.

It is easy to identify how sprawling development on the Northern edge of the city has left patches of vacant undeveloped land. The 2015 Structural Plan echoes this condition and identifies areas for expansion most prominently in the city's South and North extremities; the hexagon forms on the Jeddah map in Figure 3.9 show the growth and vacant undeveloped lands.

The plan simultaneously considers new developments and public transit on an expanded basis, throughout the city has massive scope for densification within the current footprint. The over-dimensioned Development Protection Boundary, overlapping with the Makkah municipal boundary, encourages a sprawling growth pattern, as it is viewed more as a prompter for new development than as a buffer area for protection from development. The aim of this boundary should be to keep the city compact and organized, rather than providing legal and spatial authorization for sprawled development.

The developmental pattern of the city is composed of:

- Fragmented development: Many districts and blocks are isolated from one another.
- Inconsistent density: Pockets of higher density are interspersed at random with vacant or significantly underutilized land.
- A dominant highway network: This uses large quantities of land while isolating city blocks from one another.

At the urban scale, the population density is 48.21 p/ha (Population per hectare), which is not an uncharacteristically low value compared to other Saudi cities. However, it remains far lower than the UN-Habitat recommended average of 150 p/ha, which is key to supporting sustainable neighborhood planning and design. As the vacant land within the current urban footprint amounts to approximately 24% of the total urban area, the city needs to concentrate further development in these areas through punctual infill and densification strategies rather than promote new developments on the outskirts of the city.

At the neighborhood scale, this reads like a series of excluded (or secluded) patches of the urban fabric, often on the outskirts of the denser city and far from mixed-use areas. Entire neighborhoods are singularly residential, and the overall percentage of mixed-use development is deficient. In the future, the ways that new neighborhoods are considered will have a critical effect on the city's finance, which will be challenged by infrastructure costs for settlements located far away from city centers.

The appearance of these new infrastructures may provide an opportunity to reverse the trend of extensive growth in the surrounding territory. In conclusion, Jeddah Public transportation project will enhance the enormous traffic volume and resultant congestion. It will improve the quality of the environment and the safety of road users, and in the long term, it will also undermine the city's economic prosperity. It will deal effectively with traffic congestion, and its effects will be critical to ensuring an environment in which the population can live, work, and move about comfort and safety.

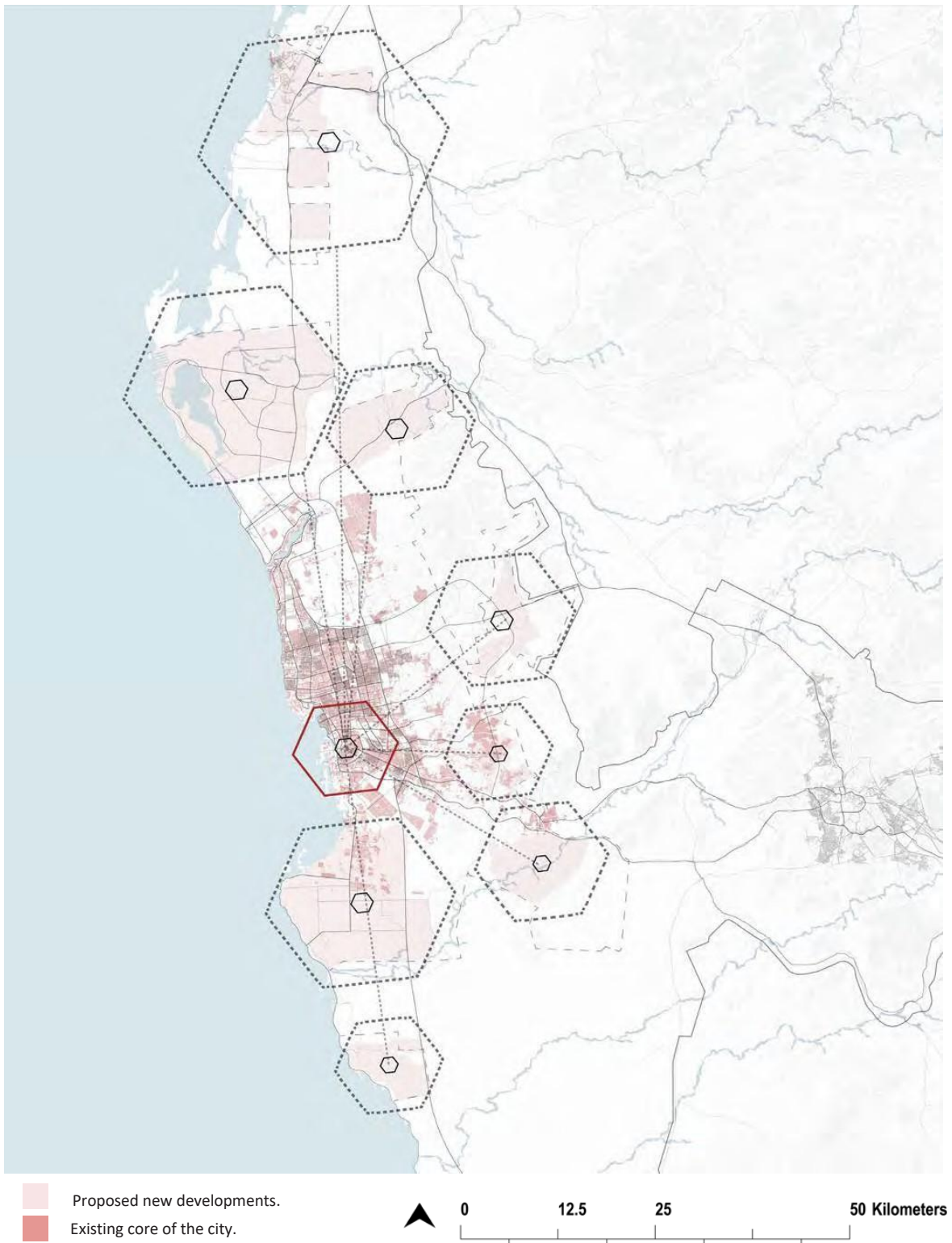


Figure 3.9. Jeddah's unbalanced growth and development patterns (Source: UN-HABITAT 2019)

CHAPTER 4

THE OASIS EFFAT

“All the cities of the world are going to expand. We need a better understanding of what makes good urban habitat for home sapiens. We have an obligation to make the new places more livable, more sustainable, and healthier. We have the tools.” ~

Jan Gehl

4.1 INTRODUCTION

4.2 DEFINITION OF TRANSITIONAL SHADED SPACES

4.3 OUTDOOR THERMAL COMFORT IN TRANSITIONAL SPACES

4.4 THE COMPACT CITY: JEDDAH'S DEVELOPMENT CONSOLIDATION AND DENSIFICATION

4.5 FOSTER DENSIFICATION AROUND METRO NODES

4.6 CONCLUSION

4.1 INTRODUCTION

The appearance of the new transport infrastructures may be an opportunity to improve the pedestrian public space's environmental conditions around the stations and nodal links. Considering the main stations of the future metro as nodes creating more densely inhabited fabric around them, would provide transitional spaces for pedestrian activities.

The concept is to provide an 'oasis effect,' mainly attributed to shading. Microclimate generated in and around these activity nodes must be mainly well designed, to encourage residents and visitors to reclaim a pedestrian life that was noticeable in the old city. However, it has virtually disappeared in newer neighborhoods, entirely devoted to automobile transport. Services and facilities around metro nodes should become the transitional thermal comfort areas of the metro station exits.

This section of the thesis deals with the comfort of the transitional spaces in hot climate cities. Many studies of the urban environment showed the significance of architecture and thermal diversity in urban life. Architectural diversity is obtained by various spatial characteristics identified in urban spaces, such as geometry, orientation, urban structure, and materials. With spatial diversity comes thermal diversity, defined as the variety of microclimate conditions regarding air temperature, radiation, and humidity in the thermal space. Modifications of the urban structure and building elements can create thermally comfortable outdoor spaces (Steemers et al. 1997, Ratti et al. 2003).

Furthermore, Jeddah's future metro plan advocates for a TOD policy to be introduced around major interchanges and metro stations. Following the development of a public transit system, the city should facilitate residential densification in selected major nodes to create new centers. Incentives for mixed-use growth and clusters of services and facilities surrounding them. This plan reinforces the Oasis effect proposed in this thesis.

Subsequently, creating an 'Oasis effect' concept by densifying the urban fabric around the metro nodes, and applying building geometric design solutions, could be an acceptable approach to reducing the harsh solar radiation penetration on the streets and improve pedestrian thermal comfort.



Figure 4.1. An oasis in a desert.

4.2 DEFINITION OF TRANSITIONAL SHADED SPACES

A variety of terms refer to the environmental conditions within a space. However, one of the popular typologies defines transitional spaces as sheltered outdoor spaces formed by building elements or tree covers (Numan, 2005). In architecture, these kinds of spaces cannot be classified as interior or exterior, and their existence cannot be explained in terms of a precise and specific function. They are found worldwide and constitute an important element of different architectural typologies (Coch, 2003).

Transitional spaces interacting with the interior and exterior are also known as interstitial or intermediate spaces. They are categorized according to their spatial characteristics as semi-outdoor, semi-open, or semi-closed. They are also classified concerning the degree of integration into the main part of the building, i.e., they are attached or added (Cadima, 2000). For some authors, the transitional space is a "mediator, a link between the interior spaces, and the natural environment with its uncontrolled climate, sun, wind, and rain" (Kapstein, 1988). Some examples are shown in Figure 4.2.

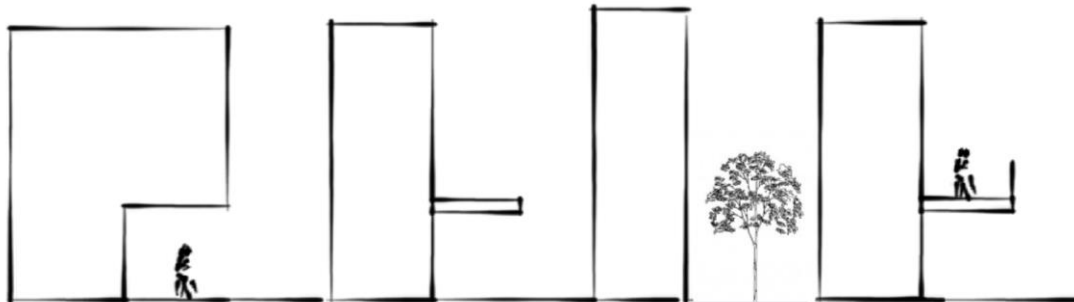


Figure 4.2. Transitional spaces examples

Throughout the history of architecture, innumerable solutions of transitional spaces have been used worldwide, especially in warm regions. Arcades, porticos, cloisters, loggias, large eaves, and even some shading devices with the extra protection of lattices have been present in the Mediterranean and Islamic, Eastern, and Indian cultures. The sun became a factor to be controlled, and spaces were available to take advantage of the sunbeams in winter, while they were shaded in summer (Coch, 2003).

4.3 OUTDOOR THERMAL COMFORT IN TRANSITIONAL SPACES

Several urban design experiences illustrate a real concern and consciousness in designing with the climate either by taking advantage of the potential of natural energy or by protecting the living spaces from adverse climatic conditions. These can be observed throughout history in the traditionally built heritage (Ali-Toudert, 2000, Knowles, 1981, Golany, 1982, Krishan, 1996) as well as in contemporary urban projects (Asimakopoulos et al., 2001, Hawkes and Forster, 2002, Thomas, 2003), some examples are shown in Figure 4.3. Many of these arrangements deal directly with street geometry, confirming its structural role.

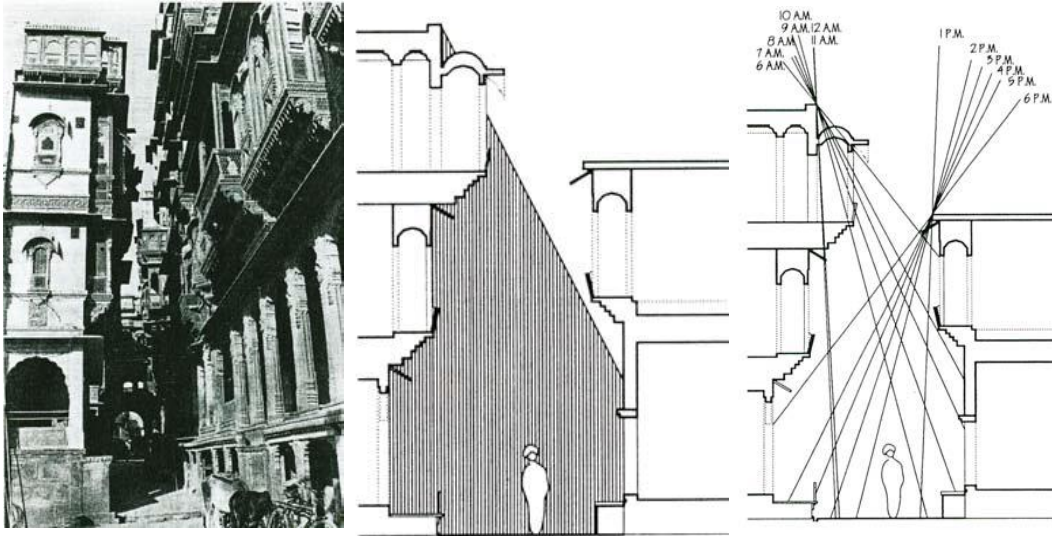


Figure 4.3. Solar control through self-shading facade in a hot-dry climate (Krishan, 1996).

The street canyon design affecting pedestrian thermal comfort could be categorized into two groups: urban geometry and green infrastructure. The main variations in urban geometry include canyon aspect ratio (H/W), sky view factor, and orientation (discussed in previous chapters).

Lee et al. (1994) compared the shading effect of buildings, umbrellas, and trees in an open area. In a warm-summer desert climate, the measurement results confirmed that the tree-shading strategy has a less effective cooling performance ability than the building-shading strategy since the buildings block shortwave radiation. Nevertheless, Santamouris et al. (1999) and Nakamura and Oke (1988) reported that planting trees are the most efficient strategy for decreasing air temperature, even though these changes are limited. However, in hot climate cities, solar radiation is the most important variable to enhance pedestrian comfort; it is of prime importance in the thermal sensation (Mayer and Höpfe, 1987, Mayer, 1993). The air temperature was found to be a secondary factor influencing human thermal comfort since it is only moderately affected by urban geometry changes (Ali-Toudert, Mayer, 2006).

In another study done by Matzaraki et al. (1999), the PET (Physiological Equivalent Temperature) was reduced due to the trees providing shade to direct solar radiation. However, in desert hot climate cities, big, rounded trees that would provide a big shading area are not available. Also, such trees need a lot of water, which is not

possible in desert climates and cities. This contrasts with the tropical hot climate cities with much rain.

Regardless of the outcomes of the other studies, transforming this knowledge into practice is still challenging. As Erell et al. (2011) mentioned, urban planning and design are complicated processes as the designer deals with various parameters at multiple levels. The capacity to improve thermal stress and the outdoor environment helps designers deal with geometric manipulation to balance outdoor thermal comfort.

Investigations based on actual scientific methods, which prove the efficiency of commonly used street design concepts on outdoor thermal comfort, are lacking. Therefore, the current knowledge on this subject is mainly qualitative. Some available studies are outlined and discussed below.

Ali-Toudert and Meyer (2006) investigated in **Ghardaia, Algeria, latitude 31°N** the effects of a vertical street profile, including symmetrical and asymmetrical canyon shapes, using galleries and other shading devices on the facades, taking various orientations into account. The studied galleries are 4 m in height and 3 m wide. The study employed numerical modeling using the three-dimensional microclimate model ENVI-met 3.0, predicting the microclimatic changes within urban environments. The thermal comfort was evaluated for the daytime hours across the canyon using the physiologically equivalent temperature (PET) (Höppe, 1999).

The results showed that all investigated design aspects have a moderate impact on the air temperature and a strong effect on the heat sensed by a human body and, hence, on the resulting thermal sensation. Galleries and further shading through overhanging facades enable a decrease of exposure time and thus of thermal discomfort. However, this efficiency varies with the orientation and the vertical proportions of the canyon.

Using galleries (Figure 4.4) reveals to be beneficial for mitigating thermal stress. This is due to the reduced direct solar radiation received by a human body and to less long-wave irradiation emitted by the surrounding surfaces, in particular the ground. The galleries of an E-W street are best protected, and a SE gallery in a NE-SW oriented street. The asymmetry, as expected, increases the sun exposure of the street and hence the thermal stress.

Overhanging facades as horizontal shading devices (can also be balconies) increase the area and duration of shade substantially at the street level and reduce further heat stress, as shown in Figure 4.4. Maximal values of PET also slightly decrease. This design solution is advisable if combined with an asymmetrical profile: On one hand, there is more shading at street level in summer, and on the other hand, more internal solar access is ensured in winter. Moreover, these "self-shading" facades reduce indoor spaces' overheating by less warming of their surfaces and hence less heat conduction towards indoors.

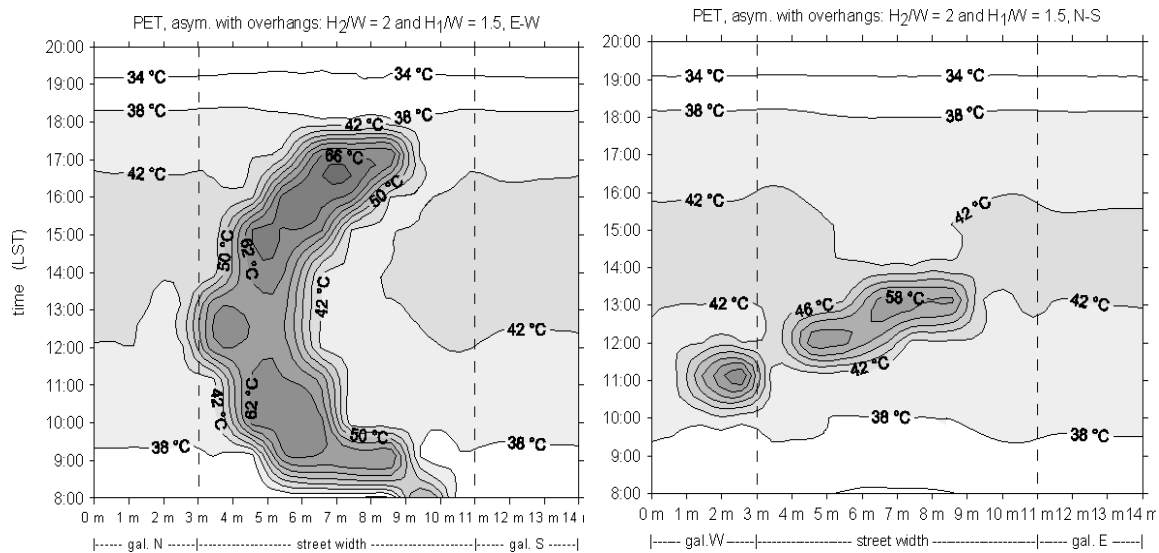


Figure 4.4. Spatial and temporal distribution of the thermal index PET at street level in an asymmetrical urban canyon with galleries and overhanging facades for E-W and N-S orientations, typical summer day (1st August) in Ghardaia, Algeria (32.40° N, 3.80° E)

Therefore, if appropriately combined, all investigated design elements can effectively mitigate heat stress in summer and promote thermal comfort. PET patterns give a good picture of the corrective measures for improving an urban street's climate quality. For example, a large street in E-W orientation appears to be where comfort is the most difficult to ensure. However, in this case, galleries are efficient and therefore advisable. Planting trees in E-W-oriented streets is sensible as they also reduce the duration and area of discomfort. For all other orientations, a judicious combination of all design details, i.e., asymmetry, gallery, overhangs, vegetation, along with an appropriate H/W and orientation, can substantially ameliorate the microclimate at street level. These details improve the quality in summer and provide in winter, to a certain level, indoor solar access for the upper parts of the street canyon. Moreover, findings revealed that the PET increases with the increase of direct solar radiation under typical hot and sunny summer conditions.

In another study, Johansson and colleagues (2006) evaluated different street designs from a thermal comfort perspective and suggested possible improvements in **Colombo, Sri Lanka, latitude 6.9°N**. The outdoor thermal comfort was estimated by calculating the PET. In canyons, the PET decreases with an increasing H/W ratio: the highest maximum PET values were found for H/W ratios of about 0.5, which were about 10°C higher than for H/W = 4.0 (Figure 4.5). N-S-oriented streets have lower PET values than E-W-oriented streets. This trend increases with increasing the H/W ratio. PET also increases with higher surface albedo, but the effect is small, with only 5°C between the darkest and lightest alternative.

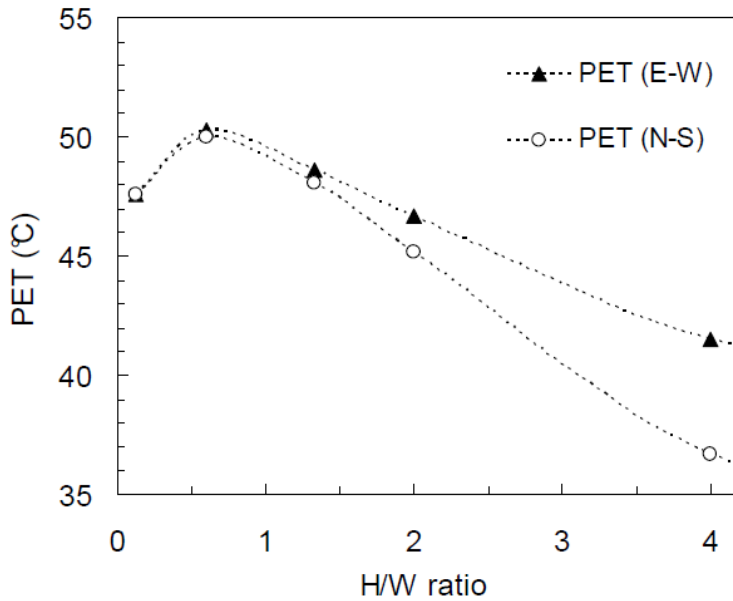


Figure 4.5. The maximum daytime PET (at 14:00 h) as a function of the H/W ratio (Source: Johansson and Emmanuel, 2006).

The effect of shading by pedestrian arcades and trees on the maximum PET is considerable, as shown in Figure 4.6. Opaque shading is slightly more efficient than trees since the tree canopies let some solar radiation through.

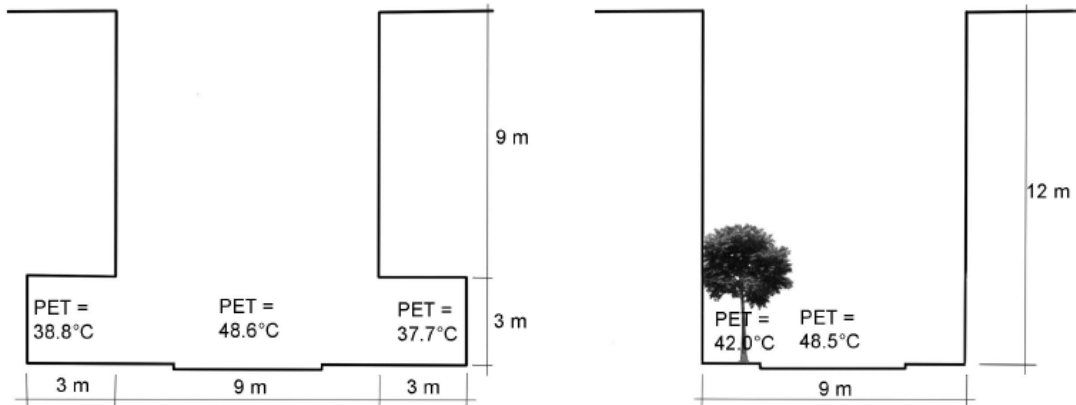


Figure 4.6. Effect of shade on the maximum PET (at 14:00 h) in an E-W-oriented canyon (Source: Johansson and Emmanuel, 2006).

The relation between H/W ratio and gallery in a single orientation on pedestrian thermal comfort was studied in another research in **Canton City, China, latitude 23°N** (Yin and Xiao, 2016). They chose a traditional shophouse street with a typical vernacular architecture type common in the South of China and in Southeastern Asian cities. Using the simulation software (ENVI-Met), two groups of experiments were conducted by varying only the width of the road and verandah to a certain scale range. The PET values from monitoring points in different streets were compared (Figure 4.7). From this analysis, conclusions on a range of scale were made, which will contribute to a better microclimate in the Shophouse Street.

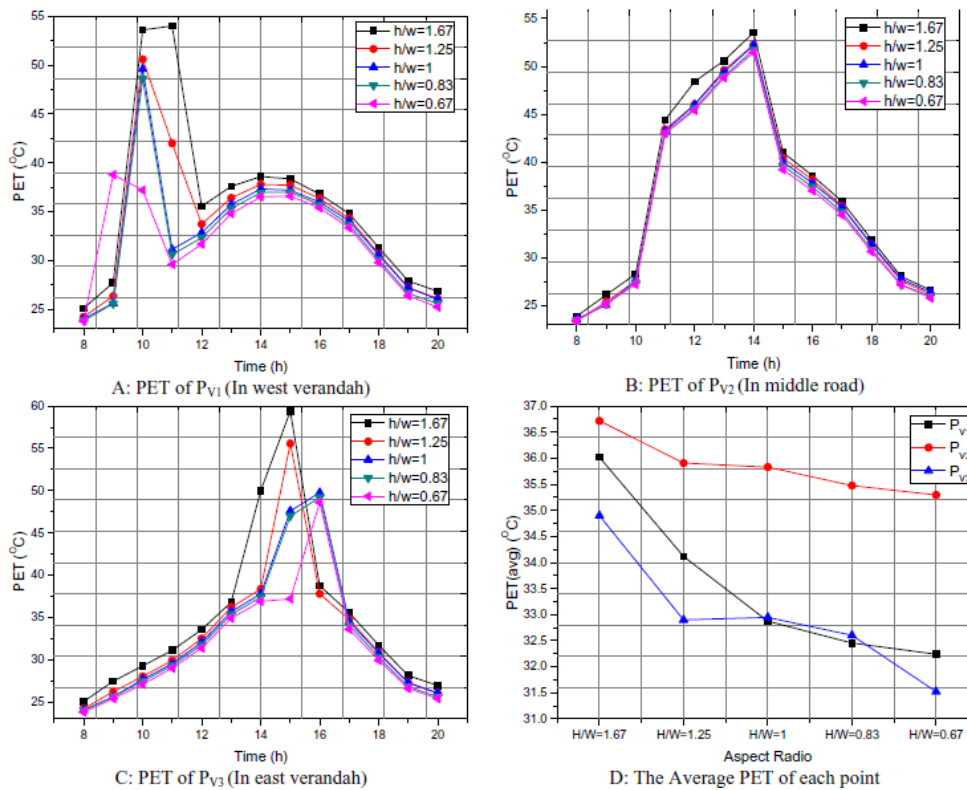


Figure 4.7. The PET of the different measuring points (Source: Yin and Xiao, 2016).

They discussed that a narrower road could lead to a better thermal environment but will deteriorate the wind environment when the street width is less than 9 m. The most comfortable microclimate is provided when the height of the beside building is 15 m and the road width 12 m to 15 m (or the aspect ratio at 1 to 1.25).

Furthermore, a wide verandah will form a more comfortable microclimate. When the height of the first story is 5 m, a better microclimate will be achieved with a verandah width of more than 5 m (or the aspect ratio of less than 1). The authors concluded that traditional shophouse streets in Canton offer a comfortable microclimate for residents in the urban public space (Yin and Xiao, 2016).

Another interesting investigation was carried by Garcia and Coch (2019). They investigated in **Cordoba, South of Spain, latitude 37°N**, the effect of different types of textile elements (Toldos), which are typically used in summer to shade the pedestrians from the sun, on the amount of direct solar radiation received on the horizontal surface (canyon).

The analysis was based on simulations using Heliodon on an N-S-oriented and an E-W-oriented canyon in a compact urban layout. Both street orientations were simulated and evaluated with and without the textile elements. Their findings showed that the textile shading device significantly reduced the direct solar radiation the entire day in the N-S canyon, especially at the South-facade foot area (Figure 4.8). The reduction of solar radiation on the N-S canyon was greater than on the E-W canyon. Moreover, the textile element type's opacity significantly affects the amount of solar radiation received at the pavement, an encouragement to study self-shading systems through buildings.

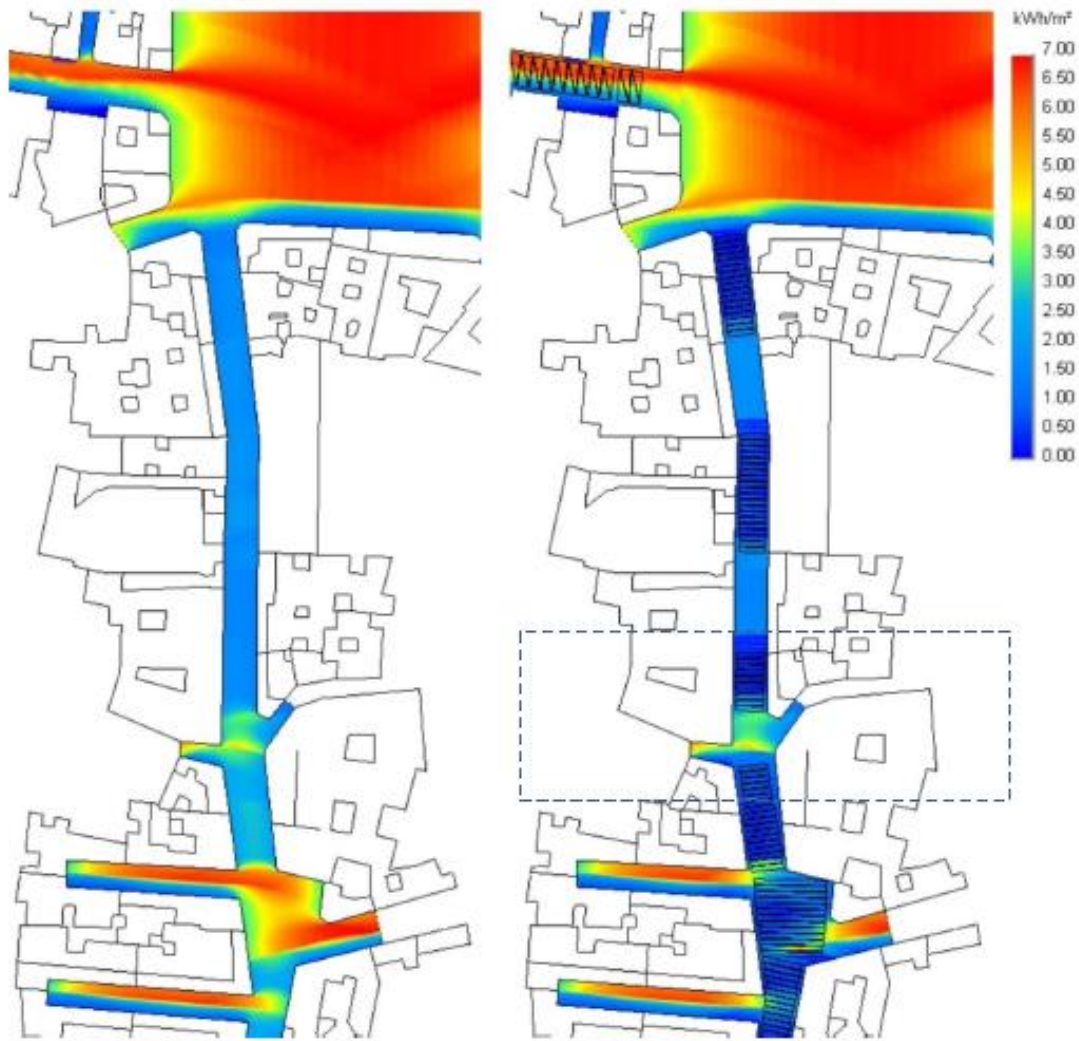


Figure 4.8. The comparison results of the direct solar radiation in canyon with and without the textile (Source: Coch and Garcia, 2018).

Yin et al. (2019) investigated the impact of shading strategies and configurations in traditional shophouse neighborhoods on **Guangzhou's** outdoor thermal comfort, **South China, latitude 23.1°N, 113.3°E**. Three street canyons with different shading strategies were selected as basic cases for microclimatic measurement in summer, e.g., alleys, streets with an-arcade for pedestrians, and streets with high-density greenery (boulevard).

Further parametric simulations investigated five group models based on the three types of street canyons which are alley, arcade for pedestrians, arcade proportion, greening for pedestrians, and covered area by trees. These five models were analyzed for their PET including parameters such as street orientation, CHW (canyon aspect ratio), AHW (arcade aspect ratio), and TCA (tree covered area). They were simulated with ENVI-met. The data was then compared with the scale data from traditional shophouse neighborhoods (TSN). The correlations among them were revealed after analyzing the results (Figure 4.9).

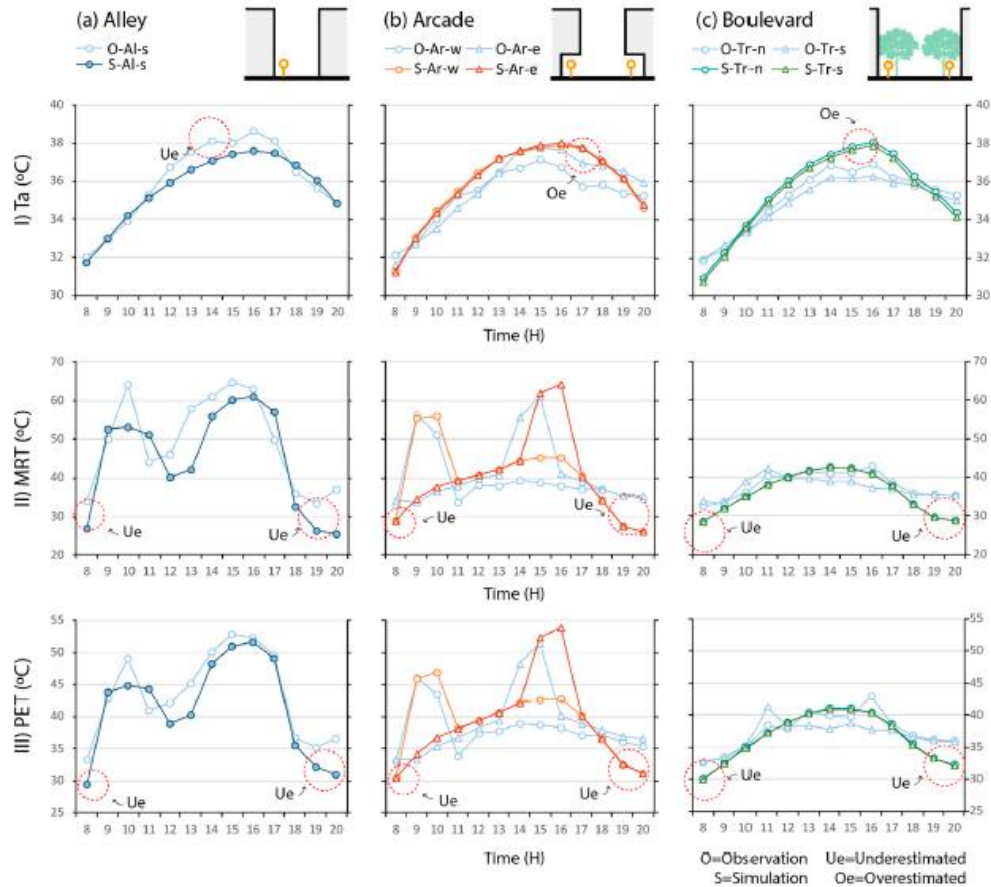


Figure 4.9. The comparison between the results from measurement and simulation in different street canyons: (a) Alley, (b) Arcade and (c) Boulevard (Source: Yin et al., 2019).

The microclimatic measurement results illustrated the features of the thermal environment of canyons with different pedestrian shading strategies. Among these strategies, arcade shading with SE-NW orientation could not avoid direct exposure to solar beams during the daytime, and pedestrians suffered extreme thermal stress at certain times. However, despite the same intensity, the duration of extreme thermal stress was shortened compared to points in the E-W-oriented alley. Furthermore, the best amelioration in thermal conditions was found in boulevards with many trees. There were no obvious fluctuations in PET under the high-density tree canopy as the tree canopy area blocked the sun path throughout the day at the E-W-oriented boulevard. The canyon-axis orientation significantly influenced the pedestrian thermal comfort level only in alleys and arcaded streets.

Their findings showed that the pedestrian thermal stress increased dramatically when the H/W ratio was lower than 1.5 in alleys and 0.78 in boulevards. If the H/W ratio was higher than 1, this indicates a remarkable reduction of the PET for arcade pedestrians. For the other periods without fluctuations, MRT and PET were similar. In E-W-oriented streets with arcades, the shading improved pedestrians' thermal conditions compared to shading in alleys. In fact, arcades demonstrated to have a rather uniform temperature in all street orientations. This was only impaired when the AHW was higher than 1.33.

After the above discussion, the mechanism of climate adaptation in TSN was also reintroduced. The canyons of TSN integrated shading and applied proper street configuration variables to achieve a desirable environment for pedestrians. The results in Yin et al. (2019) could serve as guidelines for non-climatic designers in the early phases of urban design or planning. These principles help predict the thermal conditions in street canyons and optimize selected measurements and street configurations. For example, the E-W-oriented street with arcades and greening design prominently ameliorates thermal stress for pedestrians. Furthermore, the fluctuations in N-S-oriented streets can be avoided by applying arcade and greening with a proper AHW and TCA.

4.4 THE COMPACT CITY: JEDDAH'S DEVELOPMENT CONSOLIDATION AND DENSIFICATION

Enhancing the climatic environment around metro nodes by introducing more shading solutions to protect from heat stress in hot climate cities like Jeddah is necessary. According to the previous studies, the environmental condition in transitional spaces is evident. Through improving the environmental condition, pedestrians will walk around these nodes having a better thermal sensation.

Therefore, to translate scientific studies into real-life, Jeddah city's future metro plan introduced the new metro nodes and lines. The following explanation will show the proposed nodes that will be densified to reinforce the oasis effect's idea.

The city center's urban areas, particularly between the airport and Makkah Road, have a population density of 100 people per hectare or higher. This has major consequences for the transformation of city transit systems in the future. High population densities put many people within walking distance of important local facilities, and they usually support more efficient and compact public transportation systems, which pedestrian priority communities can supplement. Nevertheless, very low-density suburban areas also make up a significant portion of the metropolitan area. Wherever possible, these low-density areas within the current urban structure should be redeveloped, in-filled, and higher-density mixed-use areas introduced (Jeddah Municipality, 2015).

New construction outside the urban footprint should be limited to achieve more compaction, while dense new and revitalized developments within the city should be encouraged by using available vacant land. Vacant land plays an important role in this strategy, as it helps to consolidate growth and increase current density while also offering an additional opportunity to incorporate public space in strategic locations within the existing urban fabric.

The city should follow a polycentric model by encouraging high-density mixed-use centers to be built around major public transportation station interchanges, following the Transit-Oriented Development concept in the Jeddah Structural Plan (Figure 4.10). TOD gives pedestrians quick access from public transportation to work and employment. Except for the main city center, Jeddah's current concentration of mixed land use is relatively weak. Clusters are forming along the major axes, but they are unstructured. Previous proposals sought to promote mixed-use development along

key corridors that would be ideal for potential public transportation networks. Though, in some parts of the city, such as Tahliyah Street, these goals have only been partially met. The designated corridors are often too long to support commercial demand, resulting in fragmented growth. Furthermore, corridors are not aligned to suitable highway types, making access to services and employment more difficult (UN-Habitat 2019).

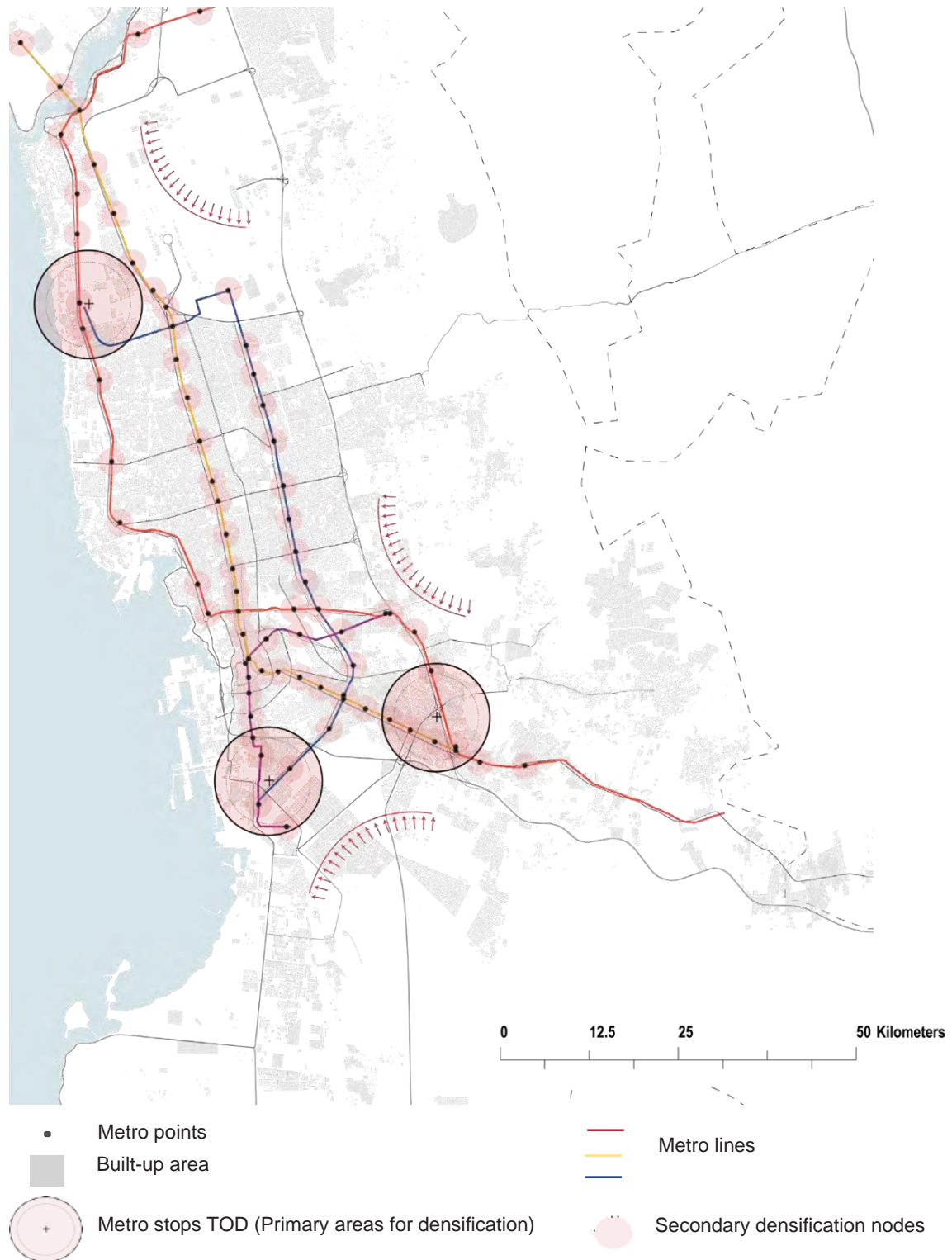


Figure 4.10. The Compact City: Consolidating and densifying Jeddah's development

Transforming conceptual guidelines into specific operational plans requires a series of detailed institutional actions that can gradually cause spatial, economic, and social changes. As a result, an action plan for Jeddah based on the three strategic recommendations and based on a series of systematically scaffolded interventions will direct the creation of a more integrated and resilient region.

The action plan outlines four systemic actions customized to Jeddah. Although all the strategic actions are aimed at specific interventions (that can cause a structural shift in Jeddah's development trajectory), there are conceptual differences between them. The four actions are as follows:

- ACTION 1: Establish the planned public transportation system.
- ACTION 2: Promote Foster densification around major nodes and transportation corridors (TOD).
- ACTION 3: Preserve, improve, and integrate historic and vernacular areas.
- ACTION 4: Reconnect natural elements to one another and to the city by establishing a well-integrated network of green public spaces.

Therefore, the Action Plan creates synced effects on two levels: The Metropolitan Area of Jeddah and the neighborhood. It supports the rehabilitation of existing infrastructures for several purposes, the reinforcement of the relationships between different city users, the integration of the urban outskirts with the city Centre, the enhancement of transport and the networks of mobility, the development of conservation programs, and extended financing and legal instruments to support vernacular and historic settlements (UN-Habitat 2019).

4.5 FOSTER DENSIFICATION AROUND METRO NODES

Jeddah Plan advocates for a TOD policy to be introduced around major interchanges and metro stations (Figure 4.11). This strategic intervention will relieve congestion in Jeddah's CBDs and reduce car dependence among residents on the city's outskirts. Following the development of a public transit system, the city should facilitate residential densification in selected major nodes to create new centers. Incentives for mixed-use growth and clusters of services and facilities surrounding them will help accomplish this.

The city should begin supporting TOD growth, focusing incentives on residential densification in areas where public transportation is easily available. By preparing for potential population growth within the existing urban footprint, unplanned settlements with limited infrastructure distribution, and low density could be avoided. As a result, one of the plan's activities suggests which areas should be prioritized in putting a Transportation Oriented Development approach to Jeddah's strategic densification into action:

1. Promote mixed-use around the main public transport nodes identified.

2. Define new urban centers at strategic points along the public transport system to promote densification. Promote dense and mixed-use development along the entire public transport system (TOD).
3. Promote dense and mixed-use development along the entire public transport system (TOD)

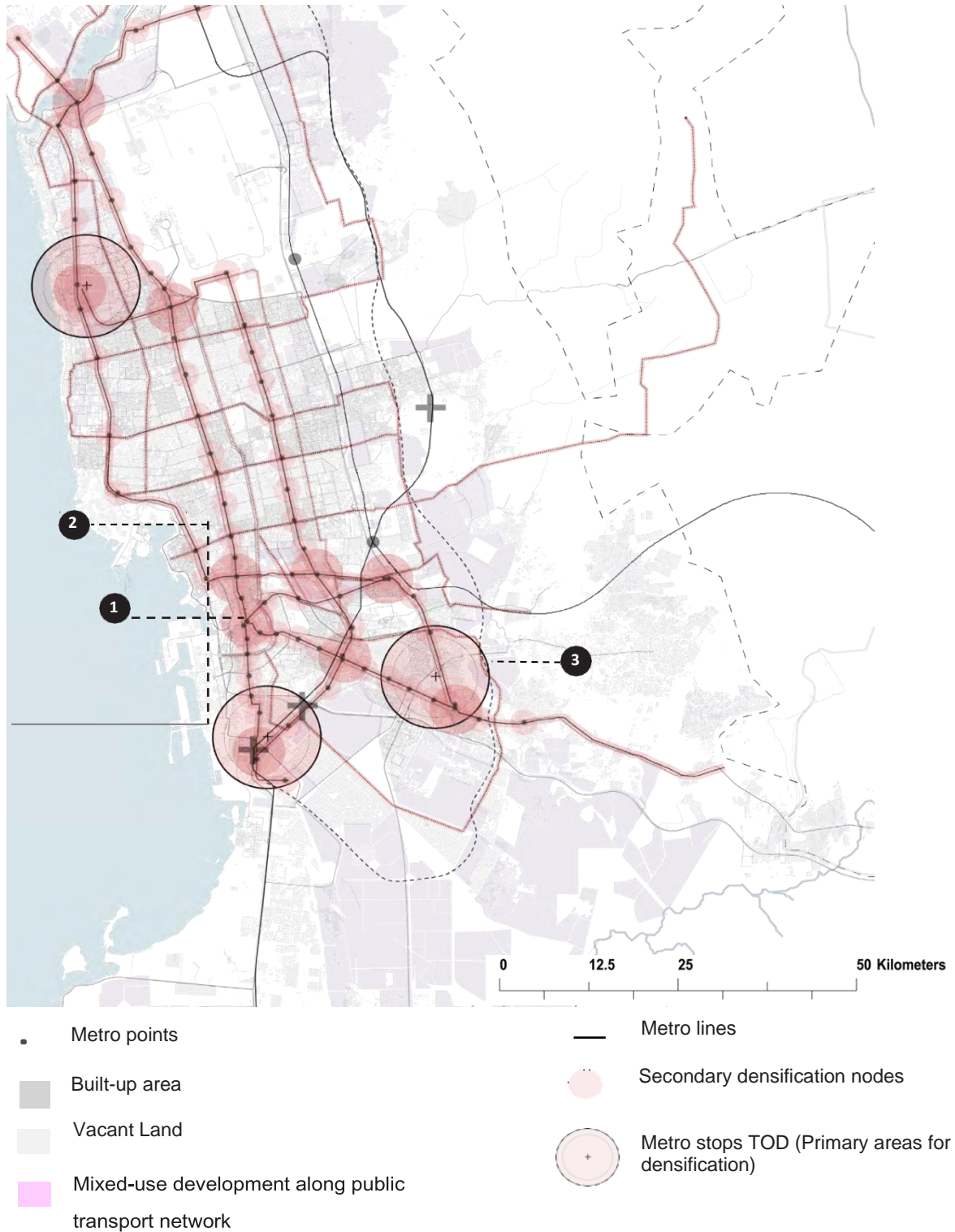


Figure 4.11. Action 2: Foster densification around major nodes and transport lines (TOD)

4.6 CONCLUSION

The city's planned design can recover suitable environmental qualities that can be implemented if limited to areas of limited dimensions.

The implementation of infrastructure such as the metro can propose regulating the buildings forms around its stations.

The subway is an underground transport system for users who move on foot; therefore, the stations along its route become the origin and end of pedestrian mobility, and the design of a comfortable public space becomes a necessity and an opportunity.

To apply new approaches based on the analysis of the traditional city's urban characteristics and applying building geometric design solutions. This will create Shaded spaces that protect the user from excess solar radiation, the main factor of discomfort in these climates.

CHAPTER 5

SOLAR RADIATION IN THE SHADED URBAN GEOMETRY

“Streets and their sidewalks-the public places of a city-are its most vital organs.”

Jane Jacobs

5.1 THE RAWWASHIN AND THE COVERED STREETS

5.2 SUN PROTECTION AS A STRATEGY TO PROTECT THE BUILDING AND / OR THE PEDESTRIAN SPACE

5.3 OVERHANGING FAÇADE SHADING PEDESTRIANS

5.4 EVALUATION OF THE SHADING URBAN GEOMETRY

Evaluating the relationship between existing urban morphologies and direct solar radiation opens an entirely new study scope. Applying the urban solar control through transitional shading elements will affect the street shading design and create semi-outdoor or transitional spaces. Transitional shading elements might be one of the essential strategies to improve shading in the urban morphology to protect pedestrians from solar radiation and enhance their thermal comfort in hot climate cities.

Therefore, this chapter endorses the importance of having horizontal shading on the pedestrian walkways through architectural and urban regulations that will improve pedestrian comfort by reducing the direct solar radiation penetration. However, the complex geometry of urban design and architecture makes it difficult to find an optimal solution.

This chapter will test geometry design solutions in streets. Assessing different horizontal shading systems provided a clear scientific idea of the proportion needed to avoid and protect from solar radiation. Moreover, proposing a new factor, the shading view factor, which will assist in proposing better layouts in urban design by including the human factor of pedestrian comfort.

Considering this the influence on the neighborhood's existing urban settings, different proposals on existing urban layouts were made. The research evaluates two types of street design solutions: the first in the old area building characteristics with extruded windows (Rawashin) and applies them to the entire facade model of the studied old urban layout in chapter 1 (section 1.3). The second is a hypothetical overhanging facade applied to the mid-rise layout studied in chapter 2, Case A (Section 2.3).

These two building construction forms simplify the complexity of the vertical urban texture found in existing urban areas and facilitate examining and comparing the geometry's impact to determine external incident solar radiation conditions on the street level.

The results will provide and add helpful insights for planning high density and compact 'Oasis effect' around the metro nodes.

The abbreviation of the terminologies used in the analysis is similar to the previous chapters, additional ones are listed in Table 5.1.

Table 5.1. Abbreviations of the hypothetical geometry.

Abbreviation	Explication
N-S-E-W-NS-EW-SE-NW	North-South-East-West-Northeast-Southeast-Southwest-Northwest
OVHF	Overhanging facades
E _{OVHF} -W _{OVHF} -N _{OVHF} -S _{OVHF}	East - West - North - South Overhanging Facade
SHVF	Shading View Factor

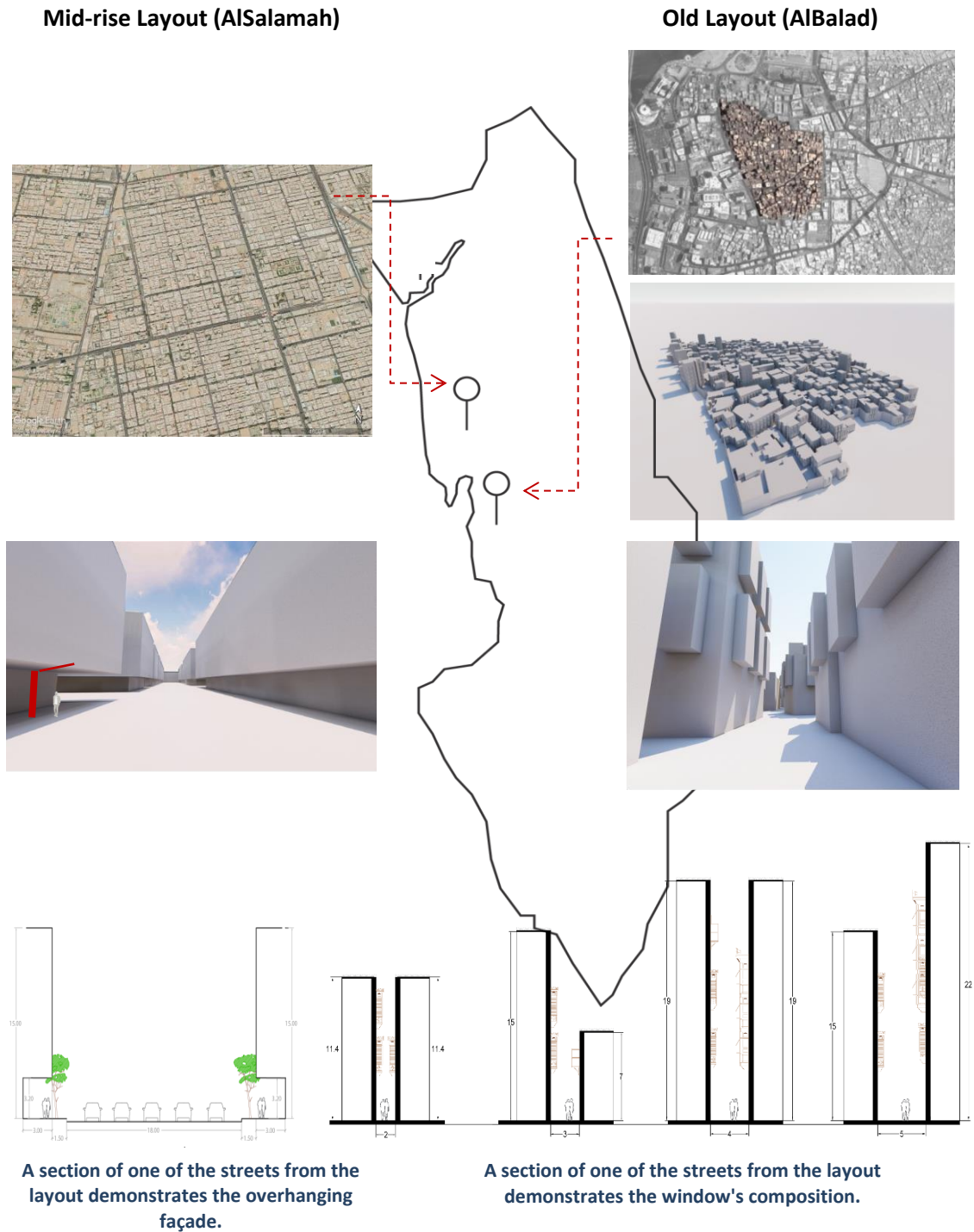


Figure 5.1. Characteristics of the two geometric hypothetical studies for the old (AlBalad) and the modern (AlSalamah) layout.

5.1 THE RAWASHIN AND THE COVERED STREETS

Case H₁ (Old layout- AlBalad)

For the old compact area in the Case of AlBalad, the entire horizontal surface (streets) is calculated with Heliodon2 to demonstrate the average received direct solar radiation after applying the extruded windows (Rawashin).

Four streets chosen from the main simulated layout were investigated in more detail to analyze the direct solar radiation effect under the Rawashin as shown on the right of Figure 5.2; the SVF graph plan is used in chapter one Albalad case (left, see also Chapter 1). These four streets selected upon the results obtained from the previous chapter one as the N-S street had an average SVF between 18% to 25%, E-W 20% to 30%, NE-SW 20% to 50 %, and the NS-EW between 30% to 50%. Additionally, the amount of solar radiation received on the horizontal surface was compared with or without the Rawashin. Heliodon Plus then calculated these streets to provide valuable additional information for decision making.

The old compact layout with extruded windows (Rawashin) was unified in size due to the layout size; it is challenging to model each exact geometry size. The extruded windows on facades in the old compact-dense urban layout (AlBalad) with a similar extruded thickness (0.60 cm) as shown in the section of the old street in Figure 5.1. They are allocated on facades of the buildings starting from the first floor, similar to the actual allocation in the real condition. Moreover, in this case study only the summertime, the 21st of June, is analyzed and evaluated. The extruded windows were applied to the entire model, and the simulation was done on the horizontal surface (street).

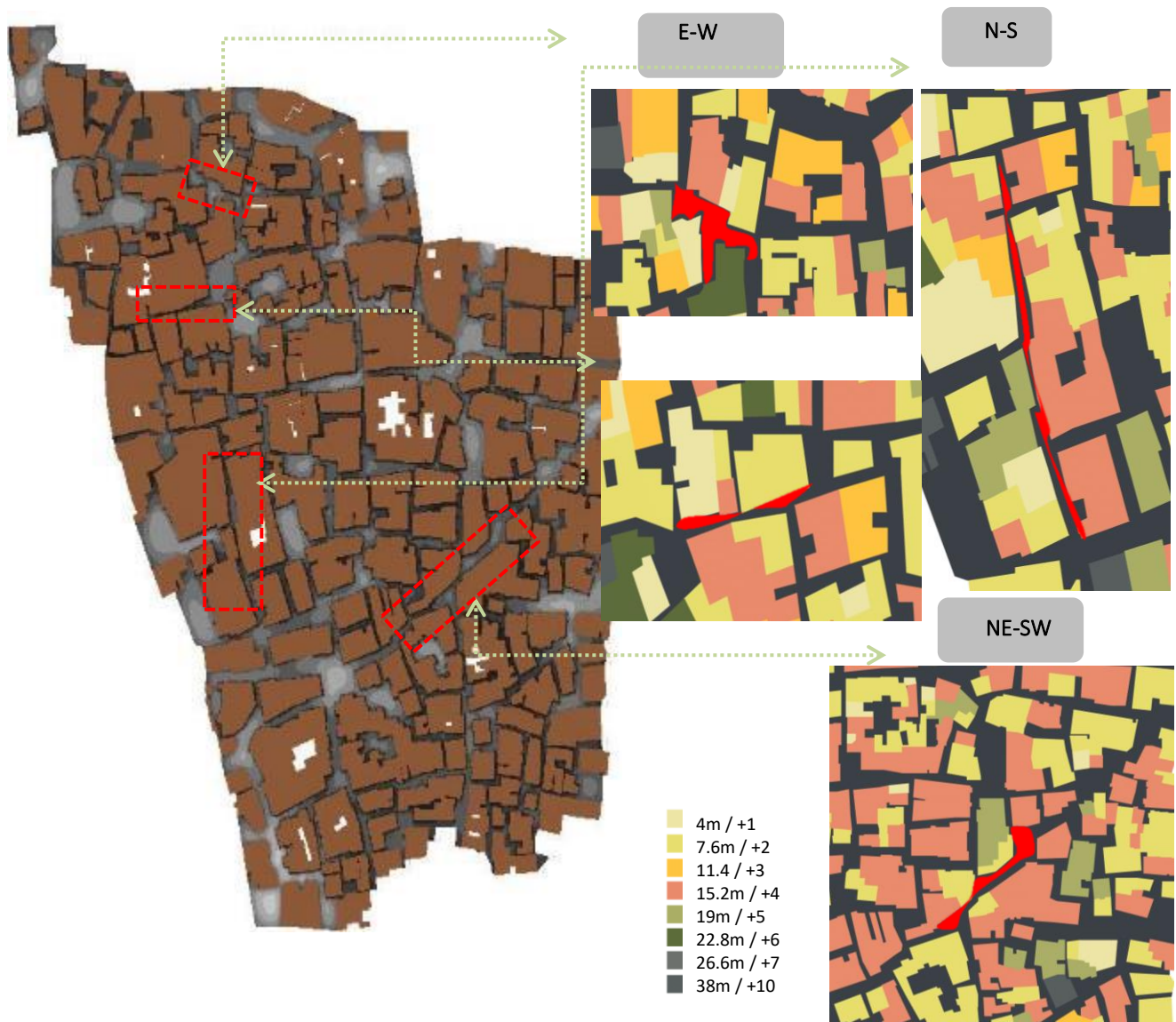


Figure 5.2. SVF plan of Jeddah old area (AlBalad) showing the four zoomed-in street selections (left). The selected analyzed streets from the layout (right).

5.1.1 Effect of Extruded Windows (Rawashin) on the Amount of Solar Flux Received on the Horizontal Surface

In the simulation with the extruded windows (Rawashin) on AlBalad (old layout), the first observation of the overall results shows that this modification reduces the overall average solar flux on the horizontal surface (streets) by 12% as compared to the old AlBalad compact layout without extruded windows on the vertical surface (facades) (Figure 5.3). The solar radiation reduction is more obvious under windows than in the overall reduction of the layout of each street design.

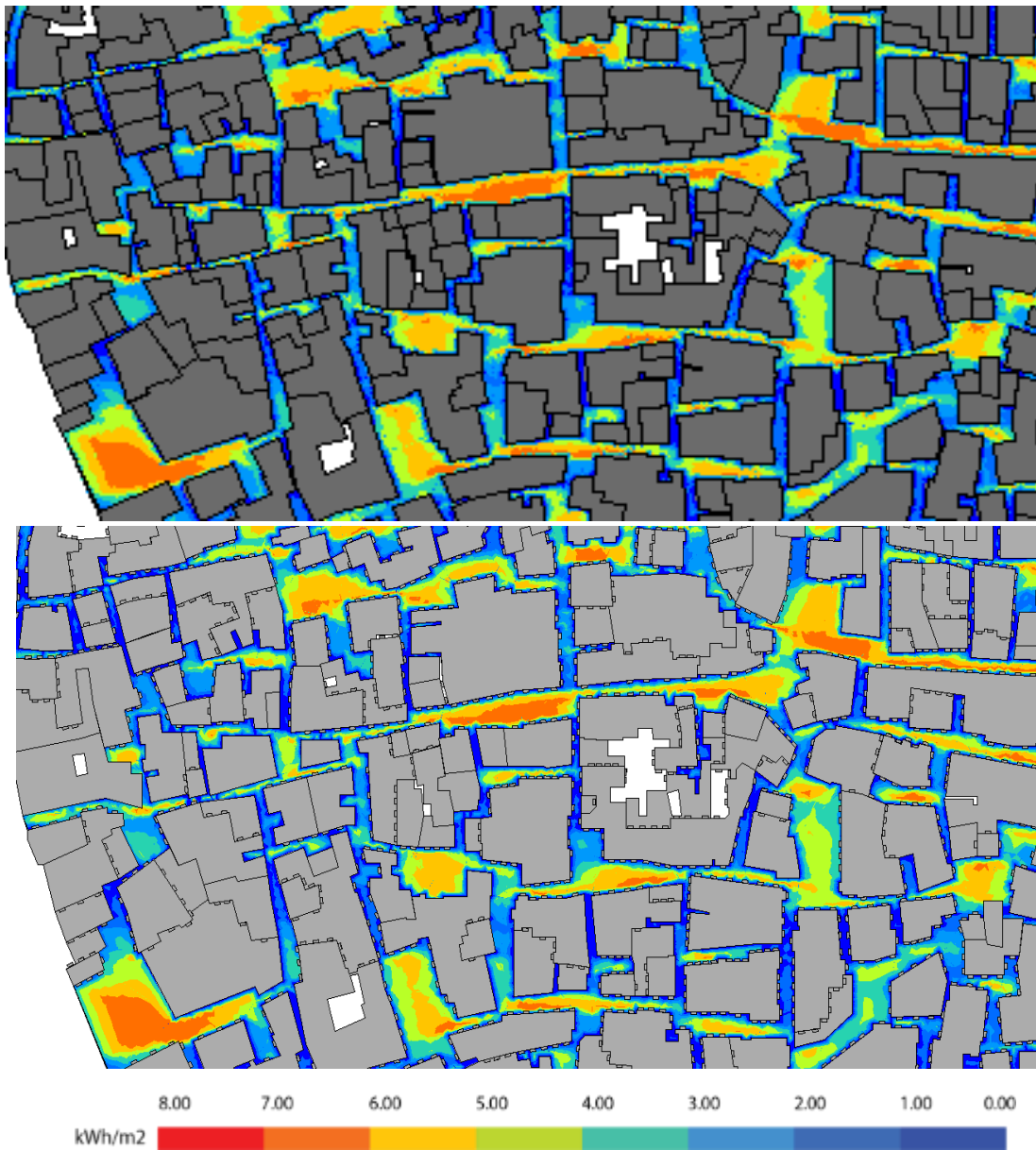


Figure 5.3. Solar flux in Case A with (bottom) or without (top) applying Rawashin.

5.1.2 Impact of Extruded Windows (Rawashin) on all Different street Orientations

The following different street orientations (N-S, E-W, NE-SW, and NW-SE) in the simulation compared the received direct solar flux on the horizontal surface with and without the effect of the extruded windows. The selected streets have asymmetrical building heights with H/W ratios ranging from $H1/W = 3.1 \geq 7.6$ and $H2/W = 1 \geq 8$ and an average SVF ranging from 10% to 50%.

Figure 5.4 shows the amount of incident solar flux received at the horizontal surface in the N-S street, comparing the street with and without applying the Rawashin. The N-S streets have a H/W ratio ranging from $H1/W = 2.2 \geq 8.6$ and $H2/W = 2.5 \geq 5.7$ and an average SVF of 25%. The solar flux received in the street (horizontal surface) without applying the Rawashin fluctuates due to the asymmetrical buildings. The highest amount of solar flux starts from the center and gradually reduces until it reaches the facades. When the H/W ratio is high, the direct solar radiation distribution is almost even, but when the H/W ratio is low, the street Eastside receives a higher solar flux than the Westside.

When applying the Rawashin, the main observation is, as expected, an apparent reduction of solar flux below them. The covered area has a minimal solar flux value ranging between 1 to 3 kWh/m²/day. However, these covered spaces also experience high incident solar radiation periods due to the relation between the street parameters and the solar movement during the day or the season.

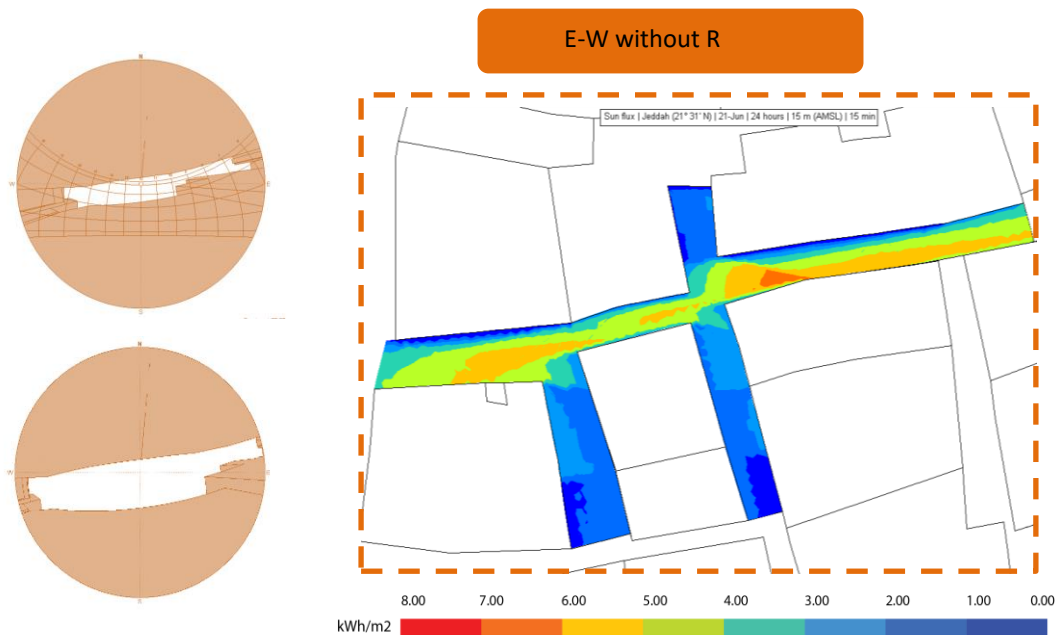
Moreover, the results reveal that the Eastside spaces under the Rawashin in an N-S street are more exposed to direct solar flux than the Westside spaces, but the reduction is 1 kWh/m²/day. Looking at the different points in the street, as shown in Figure 5.4, reveals that Point A, the Eastside of the street with 4 kWh/m²/day, was reduced by the Rawashin to 3 kWh/m²/day. In Point B, the solar flux reduction was meager due to the low H/W ratio and an average SVF of 50%. Point C has a higher H/W ratio and a lower average SVF. Here, the reduction under the covered spaces is remarkable. The street's Eastside with 3 kWh/m²/day was reduced to average solar radiation between 1 to 0.50 kWh/m²/day in some areas of this side of the street. On the Westside, the reduction was noticeable under all the covered spaces.



Figure 5.4. The amount of solar flux in an N-S street: comparison of the street with and without the Rawashin. The circles on the top indicate the street projection (stereograph and orthograph) with and without the Rawashin, whereas the bottom pictures show the solar flux without (left) or with Rawashin (right) highlighting the three different Points A, B, and C.

For the E-W street, the solar flux received on the street without applying the windows models (Rawashin) is as follows: in summer, the 21st of June, the solar flux fluctuates starting from the Southern part and reaching the Northern part of the street ranging from 7-5 kWh/m² per day to 2 kWh/m² per day (Figure 5.5). The Southern part receives in summertime more solar flux than the Northern part of the street. In winter, it is the contrary as the Northern part of the street receives more solar flux than the Southern part due to the solar angle in both seasons.

Moreover, the solar flux received in the streets with the application of extruded windows (Rawashin) the reduction of solar flux is evident as observed in the picture at the bottom of Figure 5.5. Here in the street, the solar flux fluctuates in summer, starting from the street center, reaching under the windows, going from the center with 7-5 kWh/m² per day, and reducing to 1 kWh/m² per day under the extruded windows. In the Southern part, the solar flux reduction under the windows from 7-6 kWh/m² per day to 3 kWh/m² per day, whereas in the Northern part of the street, the reduction was from 3 kWh/m² per day to 1-0 kWh/m² per day. Findings revealed a solar flux reduction between 57% up to 77% in the E-W streets in the Southern part of the street. Thus, the horizontal shading forms on the horizontal surface are highly efficient and should be considered when designing cities in hot climate cites as it is not enough to modify the morphology of the urban layout to reduce direct solar radiation.



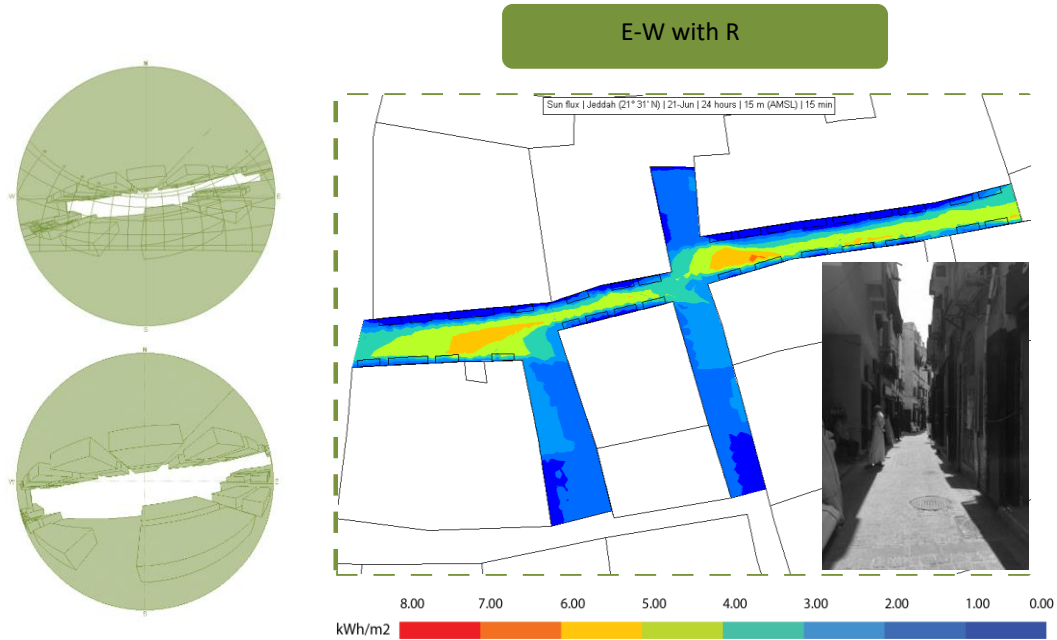


Figure 5.5. The amount of solar flux in an E-W street. Comparison of the street with (bottom) and without (top) the Rawashin (R).

Heliodon plus simulation reveals the solar radiation in kW/m² the entire year-round, specifically for the direct solar radiation with and without meteorological data, and shows the diffuse solar radiation and the global irradiance. Each graph in Figure 5.6 is numbered accordingly to help with the explanation of the results.

Moreover, as the research concentrates on evaluating the direct solar radiation, the comparison focused on the received direct solar radiation on the street's horizontal surface without and with applying horizontal shading elements on the facades (the extruded windows, Figure 5.7). Nevertheless, the first part is a general explanation of the solar radiation results of the Heliodon simulation, and the second part applies the metrological data (measured) results, showing why they are performing in this way.

Due to the slight differences in the received direct solar flux between the Heliodon simulation and the street's horizontal surface measured data, the figures below only explain the East-West street orientation. The other simulated streets are outlined in Appendix 3 (Section3.3).

In the following graphs of Figures 5.6 and 5.7, the Y-axis on the left represents the 12 months of the year, and on the right, it describes the amount of solar radiation received in kW/m². The X-axis represents the hours of the day. Furthermore, to obtain the kWh/m² during one day from the graphs below, add the values (in kW) per hour during a specific day from the Y-axis on the left graph, then taking a specific hour and adding it to the value, the result provides the kWh/m² that corresponds to the chosen day.

Graph one in Figure 5.6 reveals that the street receives a direct solar flux six months a year from March to September for 6 hrs per day, ranging between 0.2 to 0.7 kW/m². The

street also receives within this period its highest solar flux two hrs around noon ranging between 0.5 to 0.7 kW/m². Nevertheless, Heliodon plus results after applying the metrological data show an apparent decrease in received direct solar flux from March to September, ranging from 0.3 to 0.6 kW/m².

Moreover, the graph on the right of Figure 5.6 shows the street's simulation considering the metrological data showing an apparent effect in the other variables on the results. The graph indicates a reduction of 0.1 kW/m² of the total value between the Heliodon simulation and the measured results, which is not high due to cloudiness turbidity. Also, graph 4 shows that the global irradiance results are remarkably close to receiving direct solar radiation; this means that Jeddah has an almost clear sky, as explained previously and in chapter 1.

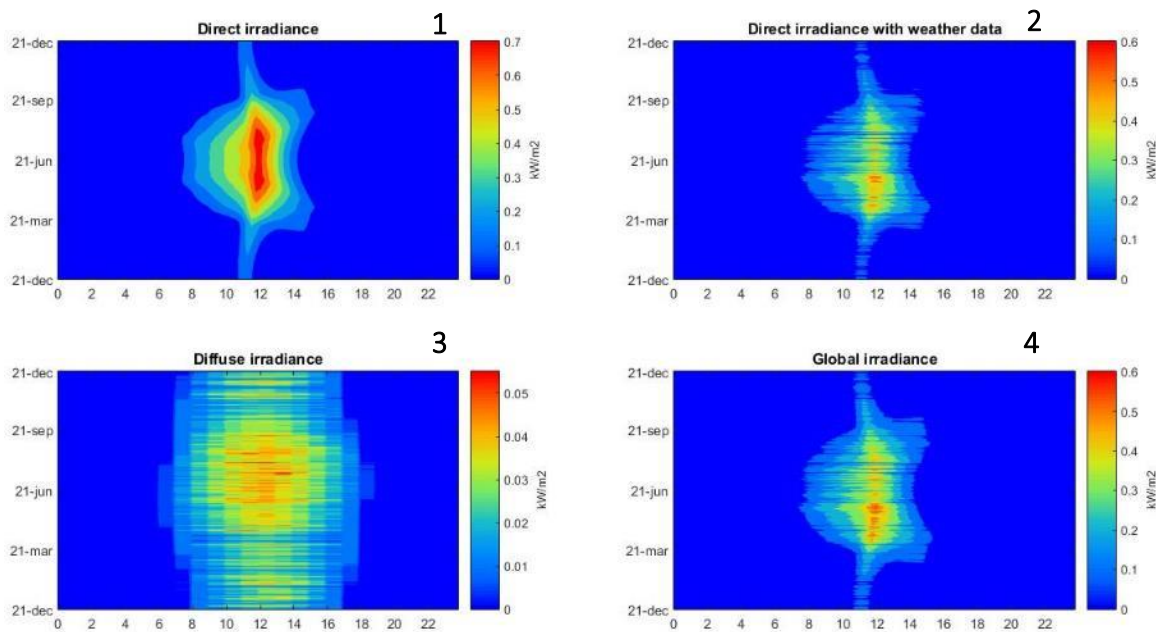


Figure 5.6. Heliodon Plus simulations on the East-West street without applying the Rawashin.

The study about the presence of clouds was obtained from the meteorological station in Jeddah, the theoretical energy data obtained are compared with the actual data measured by the local weather station using Heliodon and a correction factor is established. Seeing the differences between the theoretical values and means of direct radiation, Heliodon proceeds to establish a correction factor with the following formula outlined in Table 5.2 (Nahon, 2016). Check Appendix 1 (Section 1.2) for cloud effect in other cities (e.g., Barcelona, London, Paris, and Montreal).

$$\text{Correction factor} = \frac{\text{Solar radiation calculated from the measured value.}}{\text{Solar radiation calculated by Heliodon.}}$$

Table 5.2 Heliodon plus correction factor of each month.

Months	Jan	Feb	Mar	Apr	May	Jun	July	Aug	Sep	Oct	Nov	Dec
Correction	0.59	0.78	0.84	0.82	0.72	0.57	0.53	0.53	0.69	0.82	0.74	0.66

After applying the extruded windows to the simulated model, the direct solar radiation results fluctuate and decrease. After also including the meteorological data, simulating the models reveals a difference as well from the Heliodon simulation. The result numbers on the graphs show the difference between the received direct solar radiation on the street with and without the Rawashin. The graphs in Figure 5.7 illustrate the exported images.

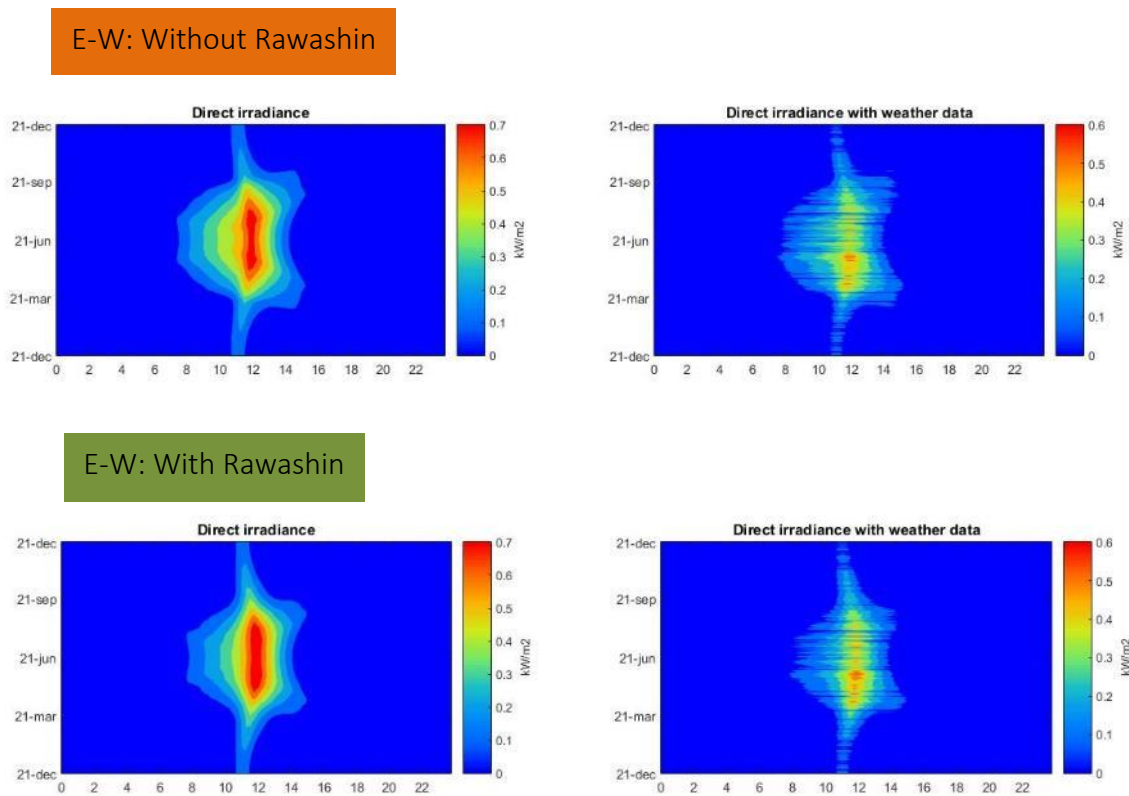


Figure 5.7. Heliodon Plus simulations comparing the East - West street with and without applying the Rawashin.

Further, tracing the simulated image graph of the direct solar radiation without or without applying the Rawashin demonstrates the differences between both results (Figure 5.8). The dashed red line in Figure 5.8 shows the results without and the black traced line with the Rawashin. Additionally, it must be mentioned here that the difference in the received direct solar radiation between both simulations is not as high due to the size of the dimension of the extruded windows as the size of the designed horizontal shading elements affects the results of the received solar radiation on the horizontal surface.

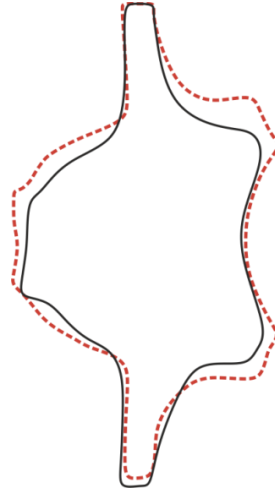


Figure 5.8. Trace of the Heliodon Plus simulations of direct solar radiation of the East-West street with (black line) and without (red line) applying the Rawashin.

Figure 5.9 shows that the NW-SE street has a H/W ratio ranging from $H1/W = 0.66 \geq 4.5$ and $H2/W = 1.45 \geq 3$, and an average SVF from 30% to 50%. The solar flux received on the street without applying the Rawashin is fluctuating, starting from the SE side to the NW side of the street with a solar flux ranging between 5-7 kWh/m²/day (SE side) to 2-3 kWh/m²/day (NW side). The street center experiences a high amount of solar flux ranging from 6 - 7 kWh/m²/day. On the other hand, applying the Rawashin confirms that the covered spaces reduce the incident solar flux for the street's NW side to 0.5-2 kWh/m²/day and for the SE side to 2-5 kWh/m²/day.

The SE side receives more solar flux than the NW side of the street. In summary, the street's orientation, the average SVF, the H/W ratio of the street, along with the size of the horizontal shading element all together affect the amount of shading under these extruded facade design elements in a compact urban settlement. Considering all the parameters together that affect pedestrians' amount of shading is significant to enhance pedestrian's comfort because all of them work together. When one is not considered, then the puzzle is not complete.

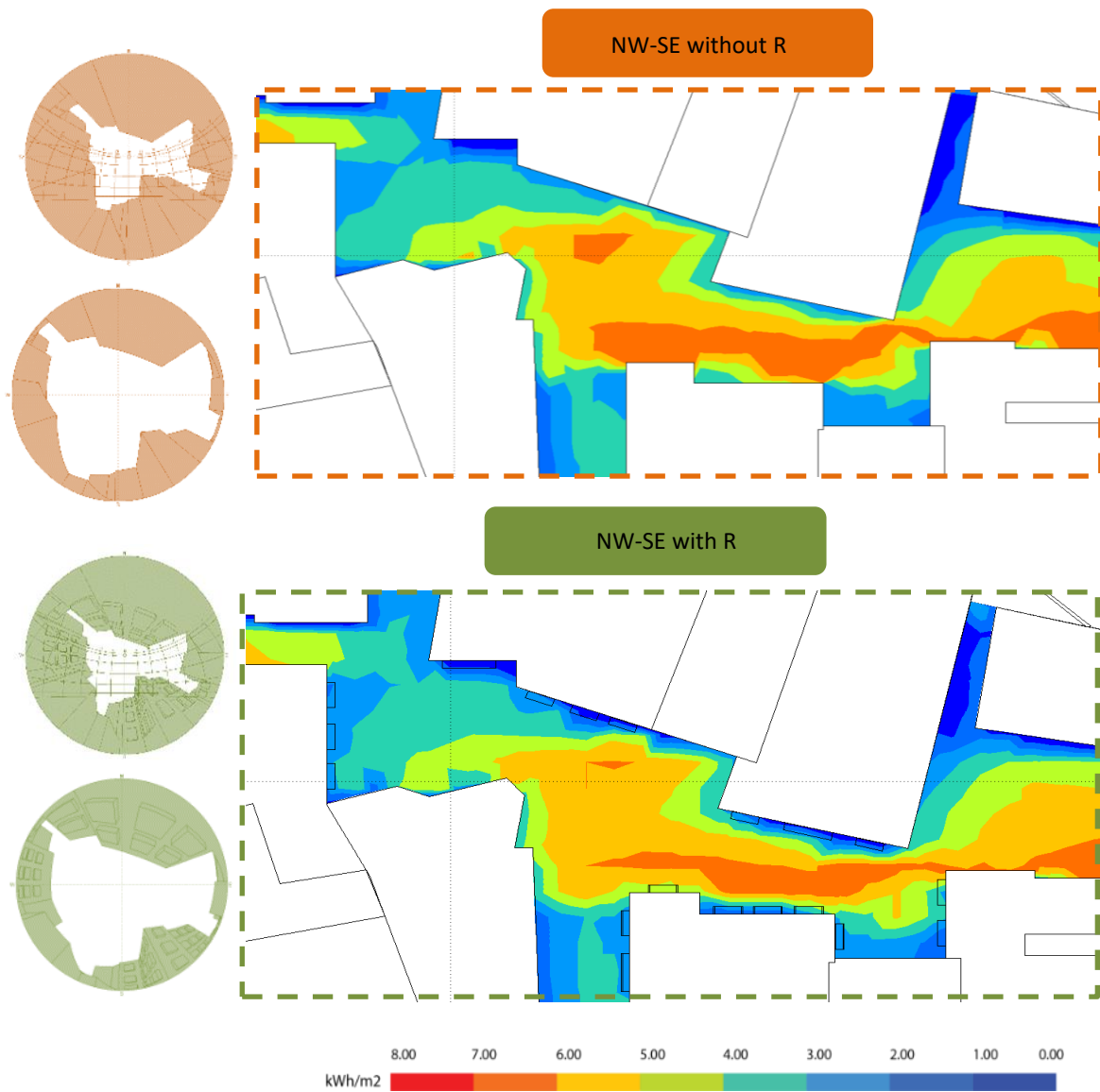


Figure 5.9. The amount of solar flux in an NW-SE street. Comparison of the street with (bottom) and without (top) the Rawashin.

Figure 5.10 demonstrates that the NE-SW street has a H/W ratio ranging from $H1/W = 1.52 \geq 2.5$ and $H2/W = 0.74 \geq 2.5$, with an average SVF from 30% to 70%. The solar flux received ranges from 7 kWh/m²/day in the areas with a low aspect ratio, like at Point A, and reaches 4 kWh/m²/day on the end of both sides of the street. Point B has a high aspect ratio and receives a solar flux of 2-3 kWh/m²/day. After applying the Rawashin model, the simulation revealed a more reduced solar flux on the street's NW side than for the SE side. The street's NW side received an incident solar flux ranging from 1-2 kWh/m²/day and the SE side 2-3 kWh/m²/day. Interestingly, the reduction was not even under all covered spaces due to the asymmetrical H/W ratio.

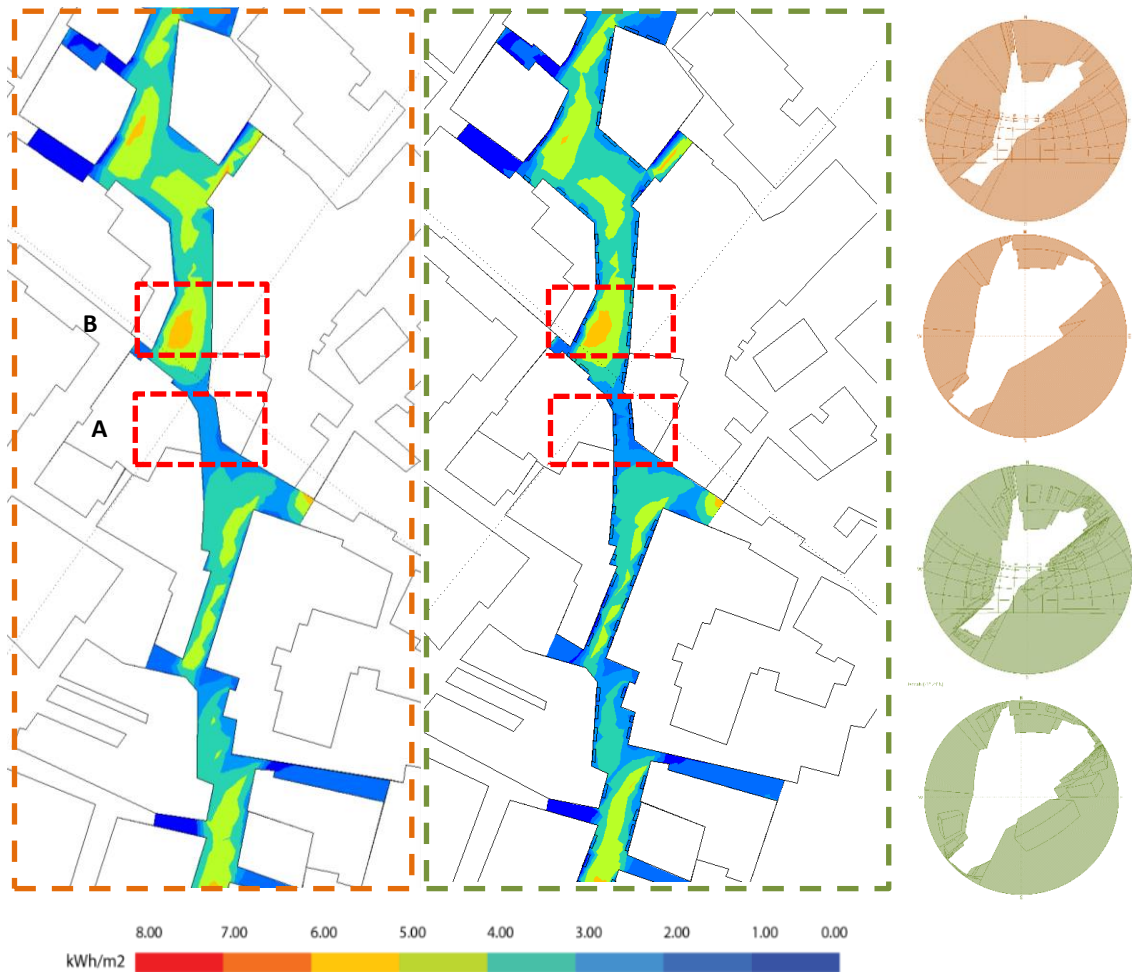


Figure 5.10. The amount of solar flux in an NE-SW street. Comparison of the street with (left) and without (right) the Rawashin. The red boxes indicate the two highlighted areas Point A and B.

5.2 SUN PROTECTION AS A STRATEGY TO PROTECT THE BUILDING AND / OR THE PEDESTRIAN SPACE

The **Shading View Factor (SHVF)** shall provide clear regulations for shading spaces. Due to the dispersed modern morphology and the climate being too hot and dry, modifying the urban morphology will take place at the pedestrian level to provide enough shade on the street to enhance pedestrians' comfort.

The **shading view factor (SHVF)** represents at a particular viewing point the ratio between the invisible sky and a hemisphere centered over the analyzed location (**SHVF = $180^\circ - \text{SVF}$**) (**SHVF = $1 - \text{SVF}$**) (Figure 5.11).

At SHVF = 1, this point indicates that the entire sky is blocked, there is no short-wave reflection and there is no long-wave nocturnal interference if no obstacles are blocking the sky view. If the SHVF = 0, then the entire space is unshaded. The shading view factor depends on the pedestrian's position. Its value changes when being at the center of the walkway or being lateral to the wall or at the edge of the walkway closer to the streets.

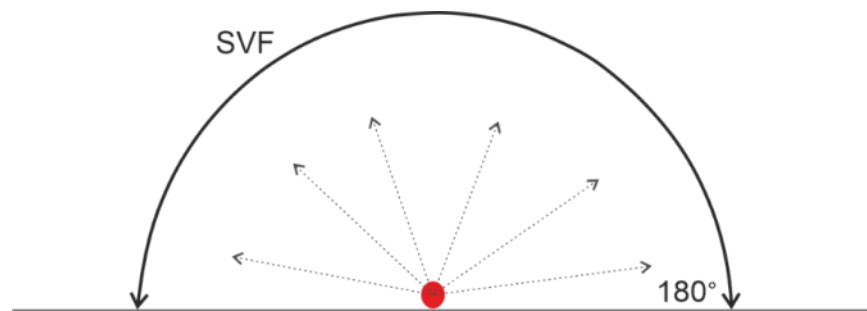


Figure 5.11. The Sky View Factor, the red circle is the receptor point.

The SHVF can be applied to streets or spaces characterized by low or medium obstruction to protect from direct solar radiation, mainly when using horizontal shading systems in outdoor spaces. Also, architects could use this parameter when they want to protect the building users from solar radiation when using terraces on building facades.

Moreover, the SHVF indicates the amount of shade given by a horizontal or vertical surface to enhance pedestrian comfort in hot climate cities or prevent rain in tropical hot climate cities. It can consider the streets' complexity and obstructions, but the SHVF simulation can also be done without any obstructions (Figure 5.12). This investigation focuses on analyzing and creating shaded spaces in hot desert climate cities and finding out the efficiency of these spaces.

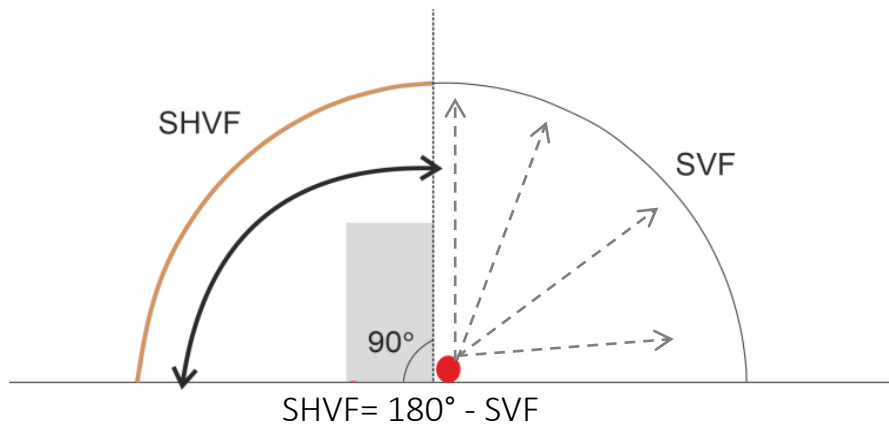


Figure 5.12. The shading view factor vs. the sky view factor, the red circle is the receptor point.

Furthermore, the amount of the shading view factor on a given surface depends on the **surface's orientation**: consequently, the amount of the SHVF changes. Figure 5.13 shows a horizontal shading element centered over a receptor point and a vertical shading element.

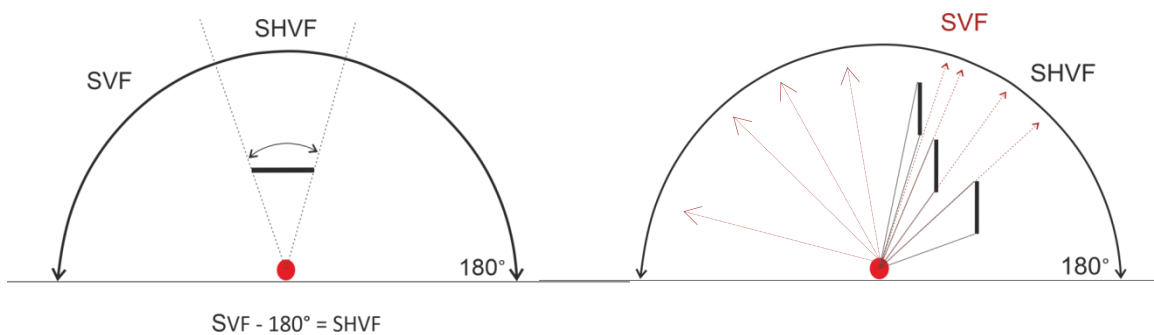


Figure 5.13. The horizontal shading element (left) and the vertical shading element (right) showing the sky view factor vs. the shading view factor. The red dot is the receptor, the marked black lines show the shading view factor angles, and the red lines the amount of the visible sky.

Also, in an urban context, some factors affect the value of the shading view factor. One of them is the **height of the building** (obstruction height). When a receptor is standing close to the building, the obstruction's side is covering a part of the hemisphere, and any other obstructions surrounding the receptor will affect the value of the shading view factor. Figure 5.14 shows the receptor's effect besides a vertical obstruction in the center of the hemisphere and another building on the other side, providing more shading to the receptor.

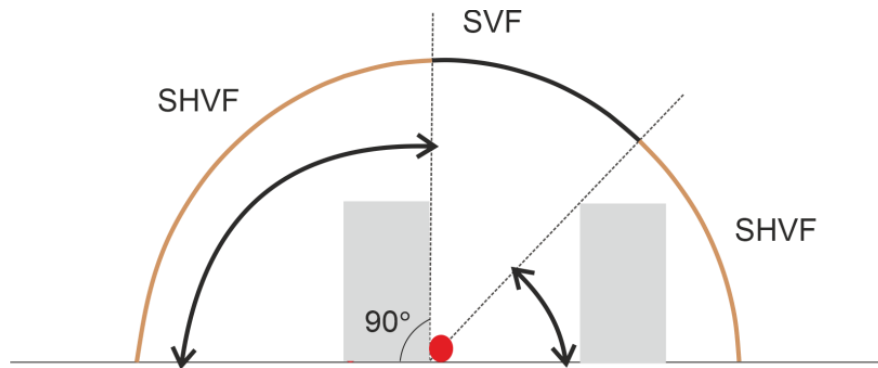


Figure 5.14. Explanation of the shading view factor that is contrary to the sky view factor.

Furthermore, Figure 5.15 shows that applying horizontal shading elements to the urban context will increase the shading view factor. Consequently, the amount of direct solar radiation received on the space under the horizontal shading element decreases. An essential factor in this case that will affect the amount of the shading view factor value and the amount of direct solar radiation received is **the horizontal shaded element's dimension**.

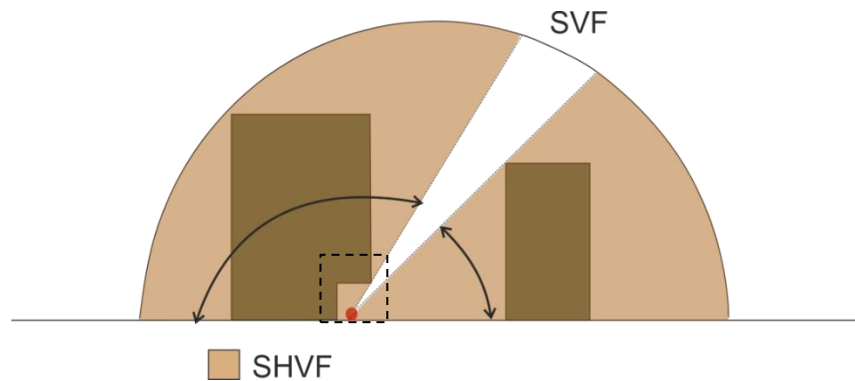


Figure 5.15. The amount of shading view factor versus the amount of sky view factor. The red circle represents the receptor under the horizontal shading element.

Correspondingly, the amount of the shading view factor on a given surface depends on the **receptor's location on the surface, if it is vertical or horizontal**—consequently, the amount of the shading view factor changes (Figure 5.16). Figure 5.16 shows the change of SHVF amount versus the location of the receptor on a **horizontal surface**. The receptor's location (red circles 1 to 3) and the associated different angle lines going out from each receptor point to represent the change of SHVF. All these factors affect the amount of shading for pedestrians. Also, Figure 5.17 explains how other obstructions around the receptors' different locations can further affect the amount of the shading view factor.

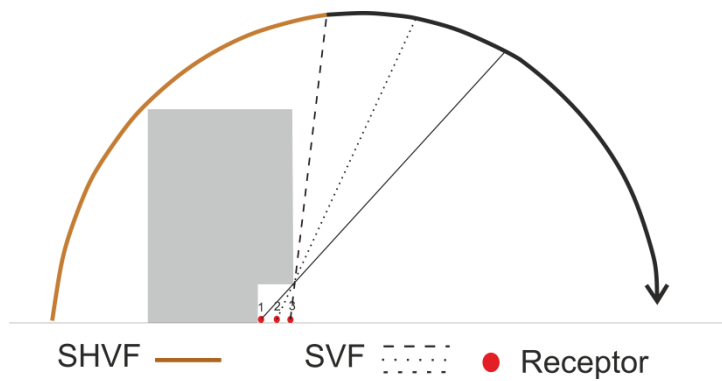


Figure 5.16. The different amounts of shading view factor from one receptor to another in different locations. The red circles represent the receptors and their different locations numbered from 1 to 3.

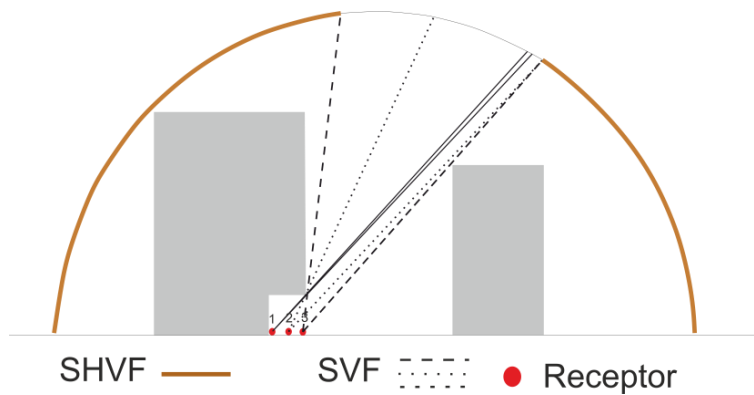


Figure 5.17. The different amounts of shading view factor from one receptor to another in different locations. The red circles represent the receptors and their different locations numbered from 1 to 3.

In addition to the previous explanation, Figure 5.18 shows the receptor's location on a **vertical surface** and how the sky view factor differs between the receptors 1, 2, and 3 displayed by the different angle lines to the hemisphere showing the change of the SHVF. Besides, Figure 5.19 demonstrates the effect of obstructions around the different receptors. As explained previously, the obstructions influence the amount of SHVF on the vertical space. Further, this figure shows another factor that affects the amount of SHVF in space: the **distance of the surrounding obstructions** from the receptors.

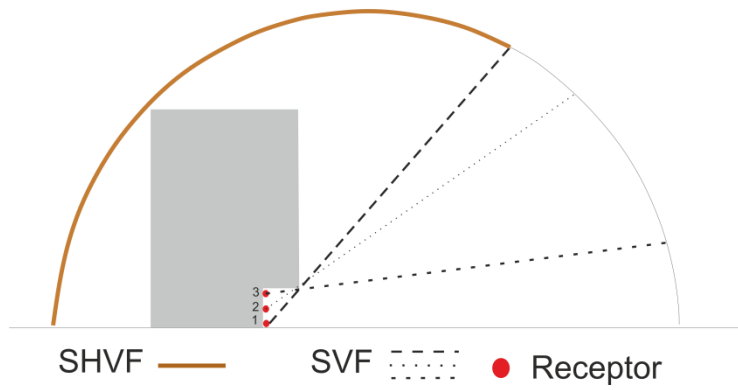


Figure 5.18. The relationship between the shading view factor and the location of the receptor on the horizontal surface. The red circles demonstrate different points on the pedestrian walkway.

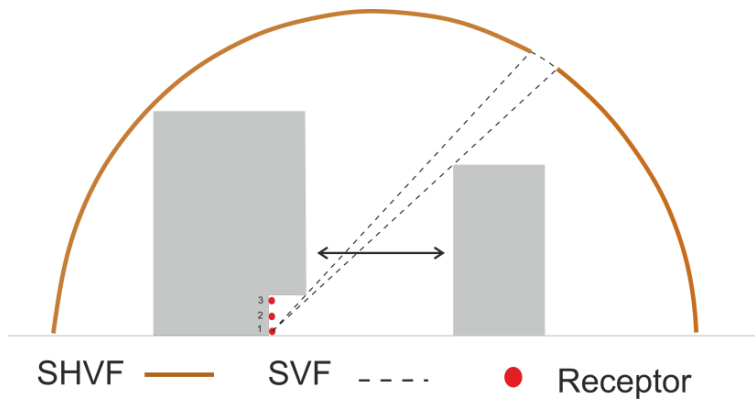


Figure 5.19. The relationship between the shading view factor and the location of the receptor on the horizontal surface. The red circles demonstrate different points on the pedestrian walkway.

5.3 OVERHANGING FAÇADE SHADING PEDESTRIANS

Case Study H₂ (Modern Layout – AlSalamah)

The general observation of the extruded windows' overall results (Rawashin) in the old area shows that the simulation appears efficient. The numerical values demonstrate a lower incidence of solar radiation on the horizontal surface (street) and a shorter sun period under the extruded windows. Nevertheless, this also depends on the solar angle to the geometry's angle.

The second proposal encompasses overhanging facades applied to the modern mid-rise building's urban layout of AlSalamah.

This section will evaluate the different overhanging facades' geometry, and the effect of the shading view factor on the amount of direct solar flux received on the horizontal surface.

The main chosen layout in Figure 5.20, an area (dashed black lines), was modified with OVHF to simulate the horizontal surface below. Nevertheless, not the entire street strip was simulated, and only certain OVHF were chosen from each side of each street orientation. This hypothetical geometry was applied and tested in the modern sprawl system on all wide streets if sprawling systems are in continuous development. There are wide streets to a limit that its buildings are not obstructed and create shaded spaces. Therefore, this type of horizontal system should be considered for these types of streets in these latitudes.

Moreover, an area of the layout was chosen from the existing urban layout of Case A with N-S orientations and a H/W ratio of 0.80, respectively, an E-W street orientation with a H/W ratio of 1 (Figure 5.20).

In terms of overhanging facades' physical characteristics, the present study utilizes two different overhanging facades typologies to evaluate their geometrical influence on outdoor direct solar radiation. Two different series of overhanging facades were considered the first series with a setback of the ground floor from each building with the following angles θ 22° - θ 34° - θ 45° and the second series with θ 17° - θ 27° - θ 37°.

To generate new urban regulations and to evaluate their impact on the external microclimate condition, the simulation adopted the following settings regarding the urban and building regulations used in Jeddah city:

- *Some settings were used and applied, such as overhanging facades from the street side, kept constant in the model within the acceptable range at 3 m.*
- *Moreover, a 1.2 m width of the pedestrian walkway was used as geometry for the overhanging facade to evaluate its impact.*

The purpose of using several dimensions is to evaluate each in its effect in creating shading spaces. The height of overhanging facades used in the present study is the

minimum height for residential buildings as defined in the regulation guide, which is one story equaling 3 m for apartment buildings.



Figure 5.20. Case A: the existing urban layout (above), showing the building heights and the applied proposal represented in the dotted square. The pictures at the bottom show the actual streets of the layout.

Before analyzing the second hypothetical type, we address a question: **To what extent does this type of geometry enhance pedestrian comfort through the produced given shade?**

Additionally, the description of the overhanging facade applied to the proposal as outlined in Figure 5.21. I must mention here that the following discussion will not discuss or consider the streets. The focus will be on the sides of the streets under the overhanging facades.

As shown in Figure 5.21, the angle remains constant in the overhanging facade series 1 (θ 22°) with a change in height and width of the horizontal geometry. This works on all other chosen geometries or will be applied in the future when designing a horizontal shading geometry.

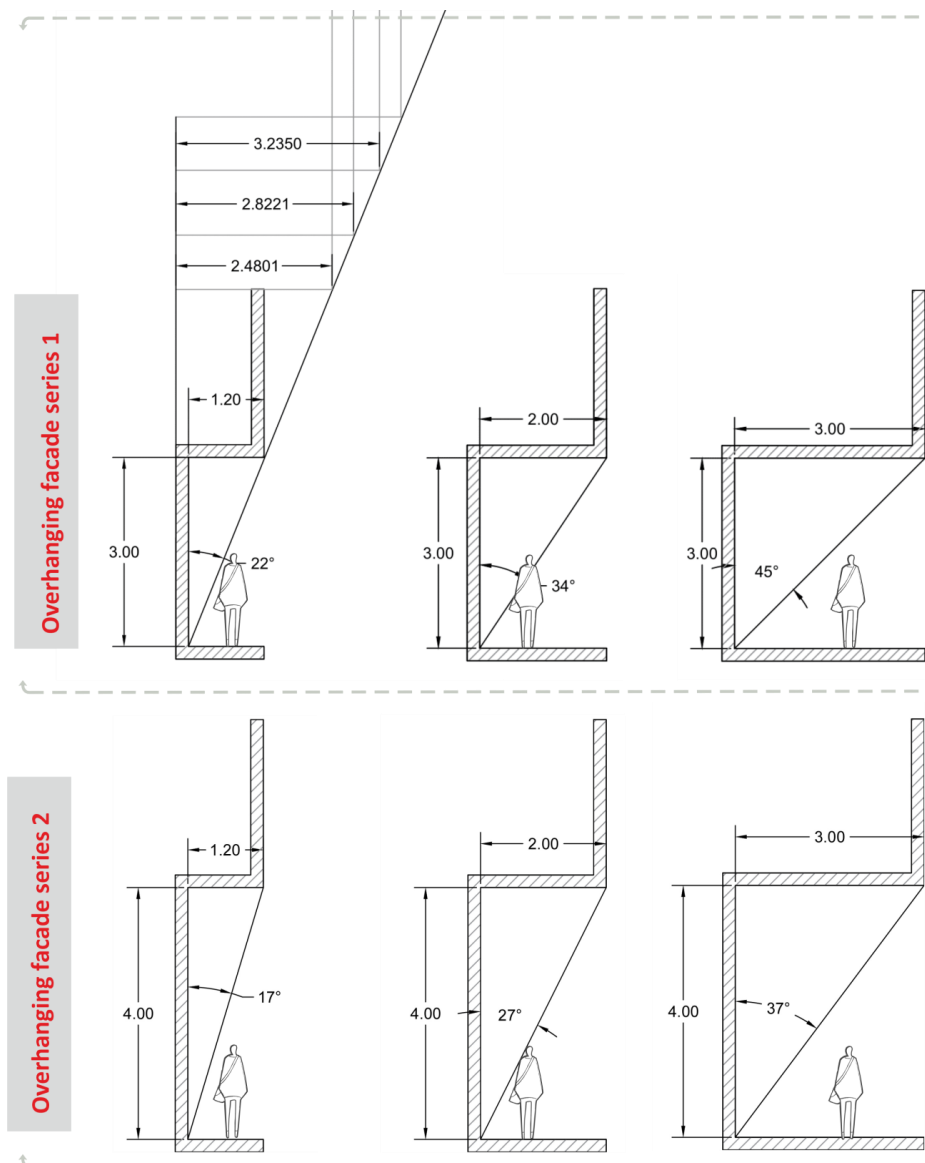


Figure 5.21. Overhanging facades description of both series.

The simulation of the shading view factor and the solar radiation is done only on the horizontal surface (pedestrian walkways) of the OVHF, excluding the setbacks of the plot (Figure 5.22). Also, Figure 5.22 shows the chosen overhanging facades' horizontal surfaces. Further, the simulation of the stereographic and the orthographic projections was executed by locating the receptor 1 m above the ground level, which gave a more extensive projection of the OVHF geometry to show and simplify the idea of the SHVF.

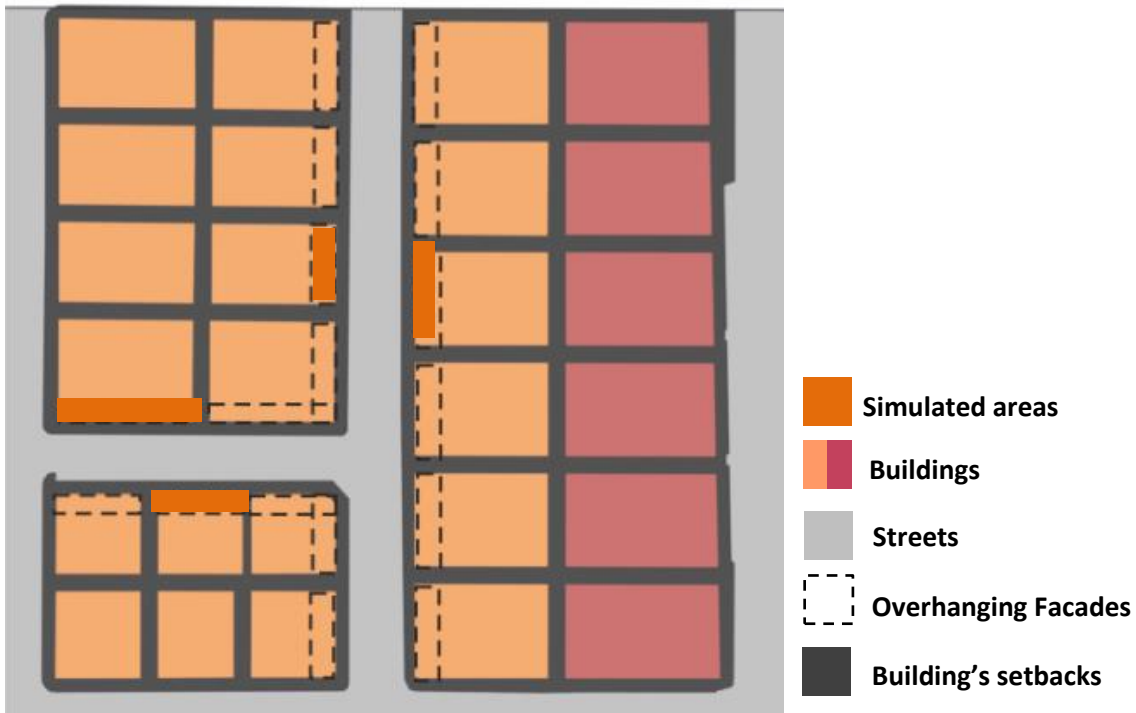


Figure 5.22. The studied urban layout of Case A, showing the simulated surfaces under the overhanging facades.

5.3.1 Shading View Factor in Relation to the Chosen Overhanging Facades

In order to provide an overview of the direct solar radiation in this type of geometry, the shading view factor was simulated on four different orientations (series 1 and 2), locating the receptor 1 m above the ground. These images were generated from the 3D model of the study area, using HELIODON 2 software. An orthographic projection shows the amount of shade that these spaces generate for pedestrians, the so-called shading view factor (SHVF). Moreover, the shading view factor is considered as the first step to compute solar radiation. Further, it depends on the surface orientation where it is computed and is the primary ingredient of the radiative exchange between the sky and the surface. Besides, stereograph projection shows the projected obstructions in the analyzed space for each area and the solar access throughout the day and the year.

Figures 5.23 to 5.26 explain the shading view factor on three different geometries of overhanging facades that are designed on each side of the streets in all orientations.

The chosen explanation is on a N_{OVHF} , characterized by 1.2 m width, 3 m height, and by having a 22° angle to demonstrate the shading view factor at a certain point on a horizontal surface (under the OVHF). The section shows the overhanging facades' geometry and its angle concerning the amount of shading view factor. As mentioned in Chapter 2, the street orientations in Case A are not precisely oriented E-W having an angle of 15° , limiting a change in orientations as shown in the polar diagram on the left of Figure 5.22. Therefore, the following projections show these differences, which also affect the results.

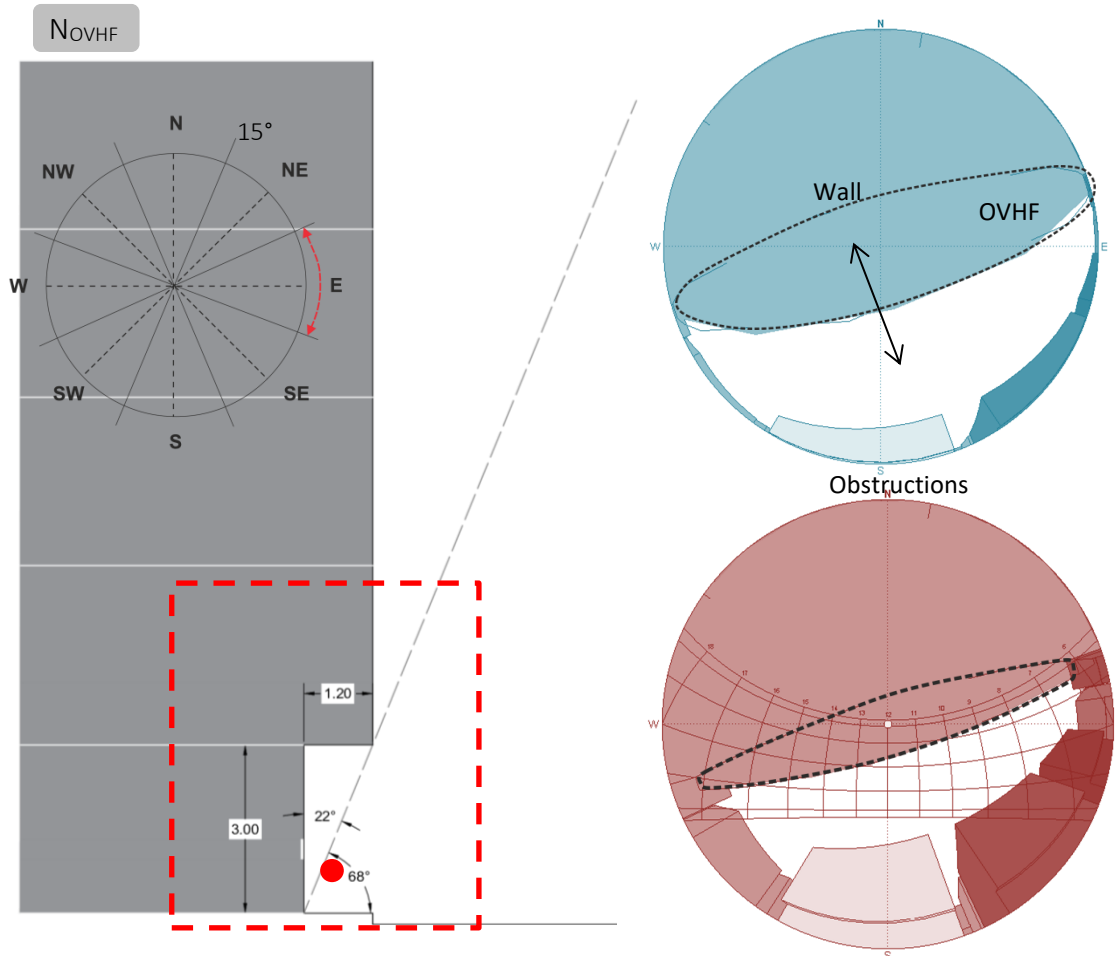


Figure 5.23. Overhanging facade series 1 on an E-W street, $\theta 22^\circ N_{OVHF}$, the orthographic projection is in blue and the stereographic projection in red (right) with sections of the streets showing the overhanging facade dimensions (left).

The amount of shade given by the horizontal shading element on the horizontal surface depends on its dimension, as shown in the section of Figure 5.23. Further, the red circle in the section is the receptor located in the center of the walking area, 1 m above the ground level. From this point all the projections of the shading view factor were created as well as the stereograph. The projection on the right of Figure 5.23, the dotted lines indicate the amount of shade given via the overhanging facades to the receptor space.

In this case, the $\theta 22^\circ$ provides shade in summer to the receptors throughout almost the entire day in June, July, and August (Figure 5.23). In winter, the shading element provides less shade to the receptor space during November, December, January, and February.

In the remaining months, the shading element provides shade almost half of the day: the receptor space is shaded one hour before noon until the end of the day. And in other months, the space is shaded from afternoon until the end of the day.

The shading element decisions concerning the hour, day, and month changes depending on the orientation of the overhanging facades (Figure 5.24). The projections show that the $\theta 22^\circ$ of the S_{OVHF} indicates a definite change. The horizontal shading element performance on this side with respect to the receptor space is different than for the N_{OVHF} . I must mention here that the shading view factor value of the S_{OVHF} is the same as for N_{OVHF} , despite the solar flux changes, due to the sun movement. The right stereograph in Figure 5.24 shows the effectiveness of the shading element, especially of the S_{OVHF} , as the shading is almost 70% throughout the entire year except for the last few hours of the day in a couple of months.

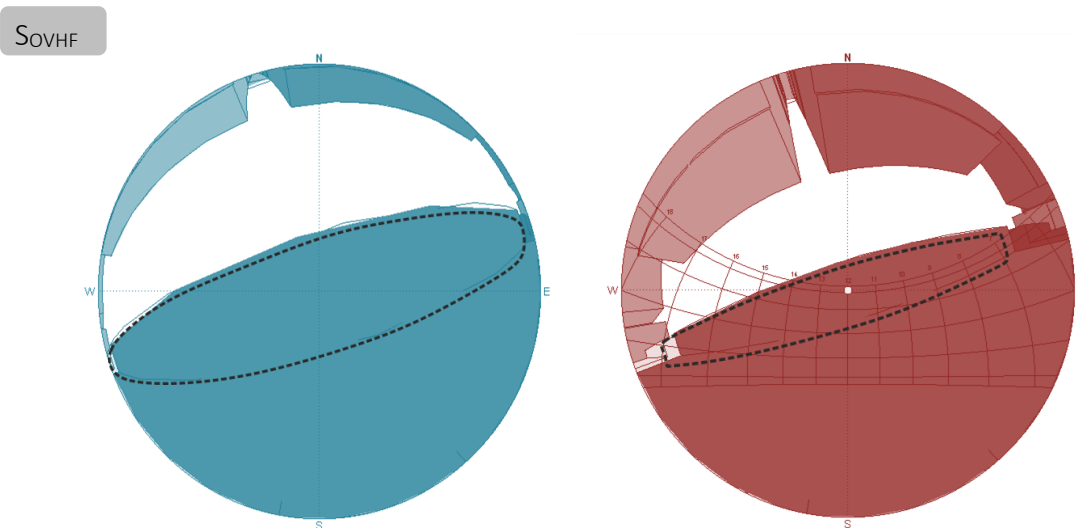


Figure 5.24. Overhanging facade series 1: $\theta 22^\circ S_{OVHF}$. The orthographic projection is in blue (left) and the stereographic projection in red (right).

Also, as the dimension of the overhanging facade geometry changes, the shading view factor increases or decreases, and consequently, the solar flux will penetrate or decrease. In Figure 5.25, the OVHF orthographic and stereograph projection represent the effect of the geometrical change on the amount of shading on the horizontal space and receptor. The projections are presented in such a way to have a clear vision about the change of shading view factor between the three different geometries in series 1 of the N_{OVHF} . Besides, the projections clearly show the effectiveness of the geometry in enhancing shading spaces and the protection given to the receptor.

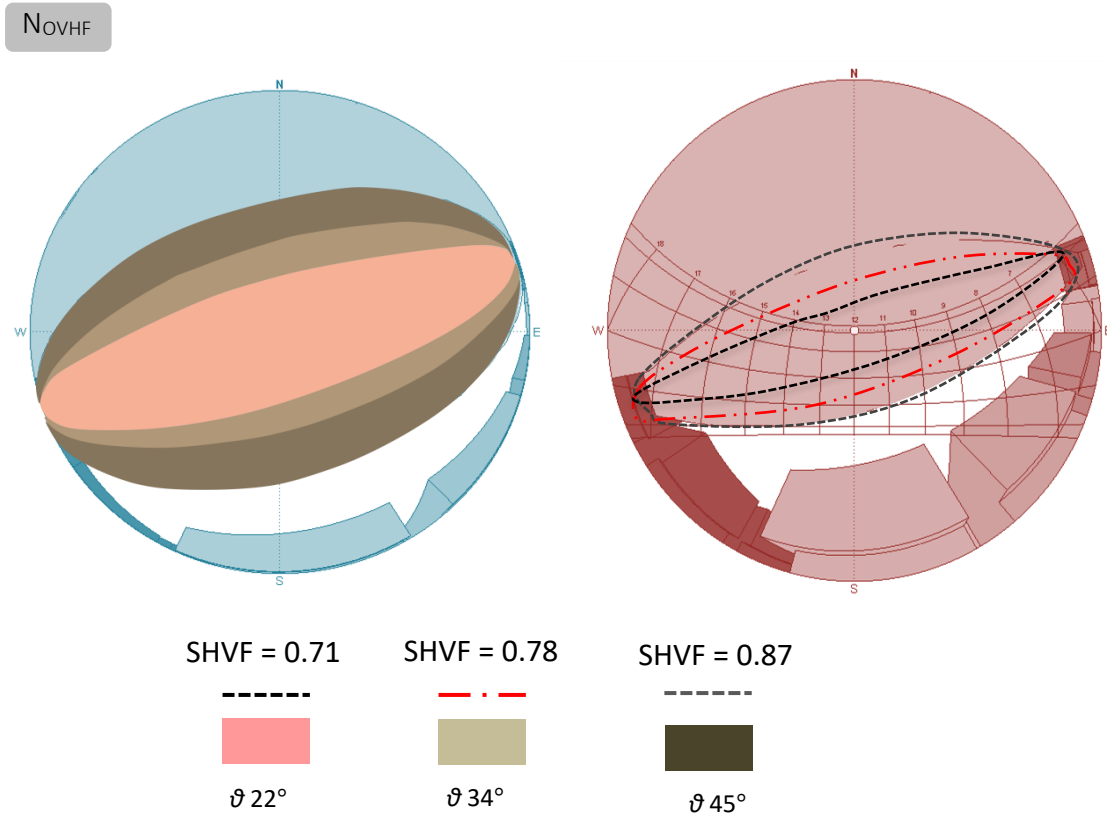


Figure 5.25. Overhanging facade series 1: N_{OVHF} representing the three geometries on an orthographic projection in blue (left) and stereographic projection in red (right).

The demonstrated comparison of the two geometrical series to comprehend the different effects and the changes of them on the horizontal surface is outlined in Figure 5.26. The orthographic projection shows the different SHVF of all geometries. The outcomes show that the proportion of the geometry of the overhanging facade or any horizontal shading element affects the shading view factor value. The difference of the SHVF is more evident between one geometry to the other, highlighting its efficiency. When comparing one with the other, then the difference of the SHVF is not as high, and it is expected that even the amount of direct solar flux between series 1 and series 2 is not that high either.

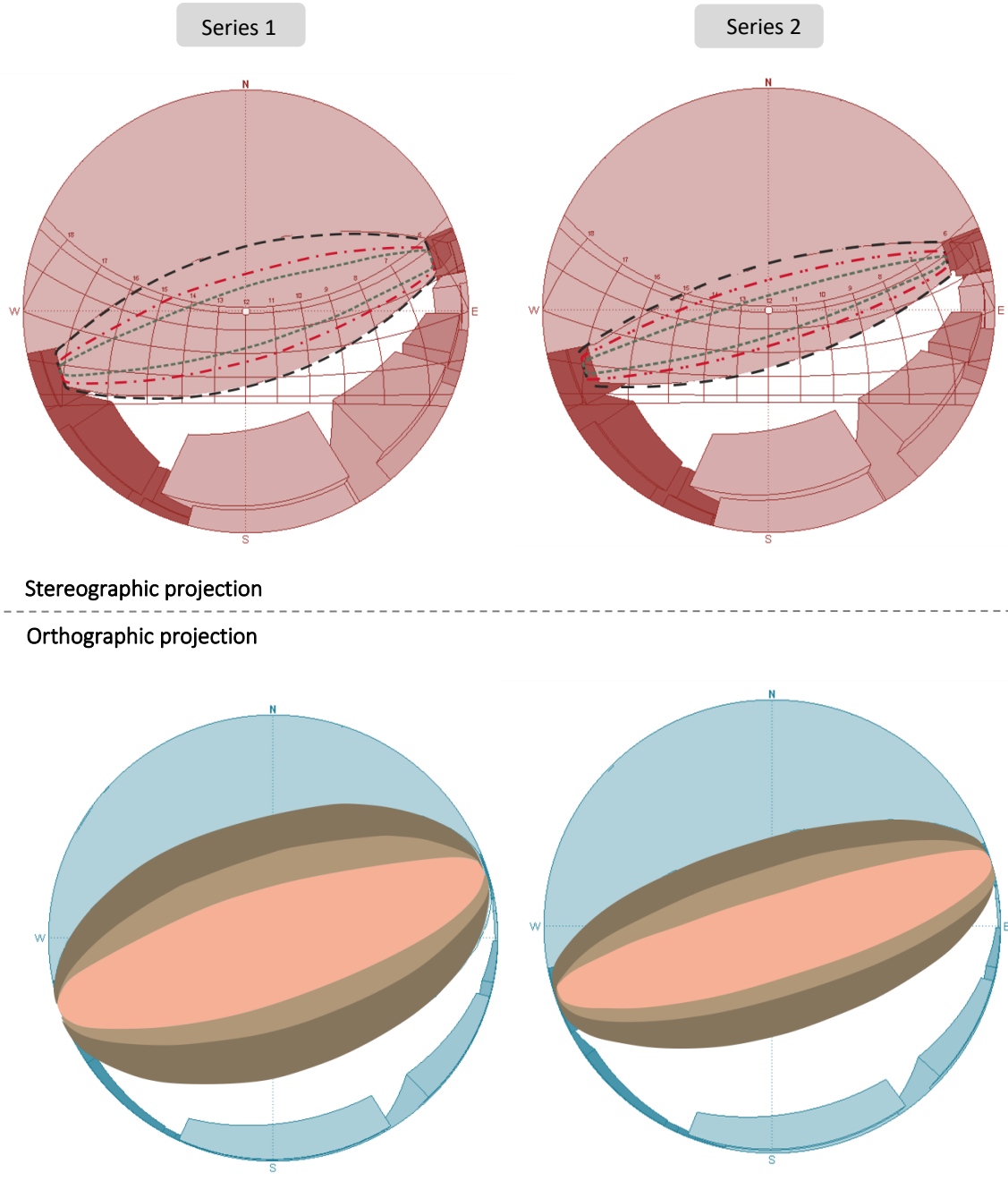





Figure 5.26. Shading view factor (SHVF) of the overhanging facade series 1 and 2 of the No_{VHF} representing the three geometries represented by θ in Table 5.3 of each series on the stereographic and orthographic projection series 1 (left) and series 2 (right).

Table 5.3. Shading view factor of the overhanging facades geometry represented by θ .

$\theta 22^\circ$		SHVF = 0.71	$\theta 17^\circ$	SHVF = 0.67
$\theta 34^\circ$		SHVF = 0.78	$\theta 27^\circ$	SHVF = 0.72
$\theta 45^\circ$		SHVF = 0.87	$\theta 37^\circ$	SHVF = 0.80

Interestingly, when the angle of the overhanging facade is small, then the shading view factor has a low value with respect to the solar angle. Figure 5.27 demonstrates the mean average shading view factor for all geometries of series 1 and 2 to illustrate the differences between all of them and to show the relationship between the shading view factor and the geometrical angle θ of the shaded horizontal element. From Figure 5.27 it is clear that when the OVHF angle is small then, consequently, the shading view factor is also reduced. The X-axis represents the SHVF percentage and the Y-axis the chosen geometrical angles. Hence, from all the simulated geometries, the 45° θ geometry has the highest SHVF among all the simulations.

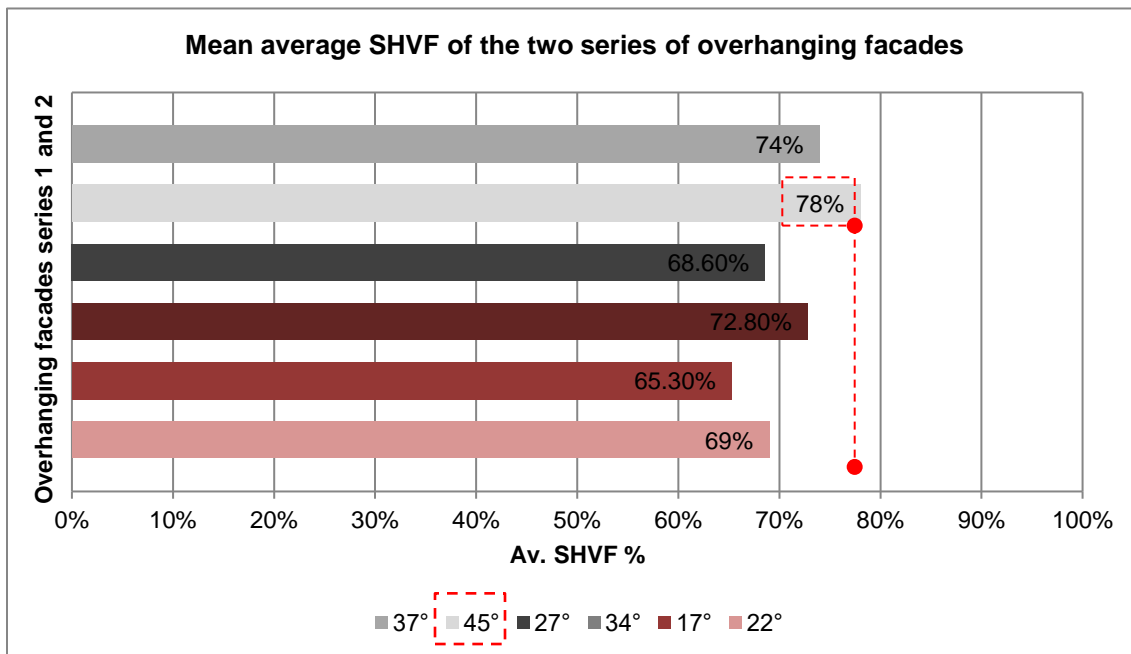


Figure 5.27. Average shading view factor of series 1 and 2 of all overhanging facades on the horizontal surface (pedestrian walkway).

All the analyzed geometries of series 2 with their shading view factor (orthographic projections), their stereographic projections, and their sections can be found in the Appendix 3 (Section 3.5).

In general, the findings show that it is vital to increase the shading of pedestrian walkways to enhance their comfort so that the direct solar flux can be reduced. The influence of the analyzed geometries concerning the direct solar radiation will be explained in more detail in the following section. Similarly, the correlation between the shading view factor and the direct solar flux on the horizontal surface (pedestrian walkways) will be demonstrated in more detail.

5.3.2 Results Overhanging Facades Received solar flux in relation to Shading View Factor

The results of series 1 and 2 were very close to each other, with only a few percentages of difference in receiving solar flux on the horizontal surface. Therefore, the following explanation will focus only on series 1, evaluating its three types of overhanging facades geometry. Due to the results, we decided to leave the results of series 2 in Appendix 3 (Section 3.5) for future in-depth study of this topic. Moreover, this section will start by demonstrating the different influences of the overhanging facades' geometries on the direct solar radiation of the horizontal surface E_{OVHF} , W_{OVHF} , N_{OVHF} , and S_{OVHF} and comparing them with the results of the existing urban geometry in Case A that was given on the horizontal surface (streets) in Chapter 2. Further, simulation was done on the 21st of June and the 21st of December.

5.3.3 Results of the Overhanging Facade Geometry Influencing the Amount of Solar Flux Received on the Pedestrian Walkway in E_{OVHF} and W_{OVHF}

The results obtained from the horizontal surface under the E_{OVHF} and W_{OVHF} are shown in Figure 5.28. In **summer**, both sides show on the 21st of June a dramatic increase in direct solar flux at a particular time and a decrease on the horizontal surface (pedestrian walkways). Both orientations appear to have reasonably symmetric results. In contrast, the received direct solar flux under the OVHF of 22° and 45° are symmetrical on the 21st of June. Simultaneously, the OVHF with 34° has a slight difference between the E_{OVHF} and the W_{OVHF} . Here, both sides of the OVHF behave differently in the received solar time interval shifts. The W_{OVHF} starts receiving a direct solar flux from sunrise until noontime from 6:30 hrs to noon, indicating that it receives five hours of direct solar radiation.

In contrast, for the E_{OVHF} orientation, the solar flux starts penetrating from noontime until midday, from 11:45 hrs to 16:30 hrs, which are also almost five hours of direct solar radiation. Further, while the solar time interval remains the same when comparing the three proposed geometries, the solar flux values themselves are changing. In total, the solar flux was, as expected, higher at the horizontal surface of 22°, and the OVHF with 45° registered the lowest received solar flux when comparing the proposed geometry.

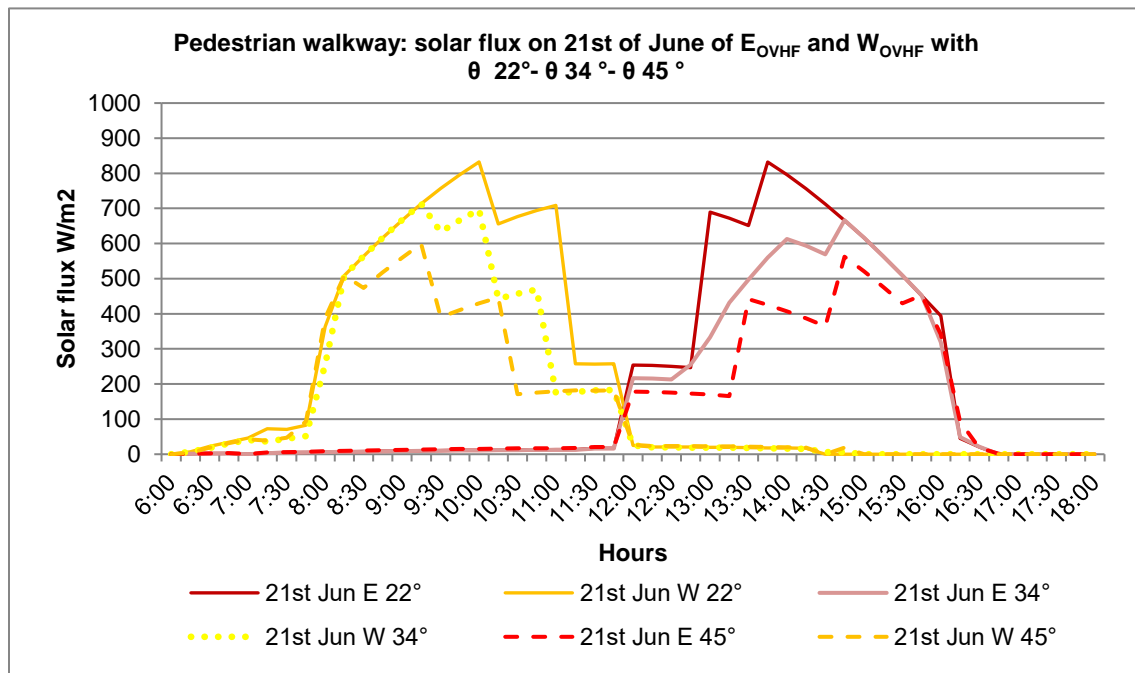


Figure 5.28. Received direct solar flux on the 21st of June of the overhanging facades on the horizontal surface (pedestrian walkways) of W_{OVHF} (W) and E_{OVHF} (E).

Furthermore, the graph in Figure 5.29 reveals that both sides exhibit asymmetrical results in **winter** on the 21st of December. Besides, direct solar flux received on the horizontal surface of E_{OVHF} in winter is contrary to that from the summertime. The results show that the solar flux increases dramatically from 11:30 hrs to 16:30 hrs, whereas the W_{OVHF} increases significantly from 8:00 hrs to 11:00 hrs, having asymmetric effects with respect to the three different geometrical OVHF designs. The solar flux on the W_{OVHF} is higher than the E_{OVHF} in all proposed geometries. Therefore, the W_{OVHF} receives 3 hrs of direct solar flux from the morning until one hour before noon. Moreover, the E_{OVHF} receives almost 4.5 hrs. of direct solar flux starting one hour before noon until two hours before sunsets. Also, for the three proposed geometries, the time interval in solar radiation remains the same as mentioned in summer, and only the solar flux values change in the spaces.

Moreover, as the sun angle is different in summer than winter, each side of the overhanging facades reacts differently from one season to another. In other means, in summer, the solar penetration on the horizontal space is different than in winter. See Appendix 3 (Section 3.4)

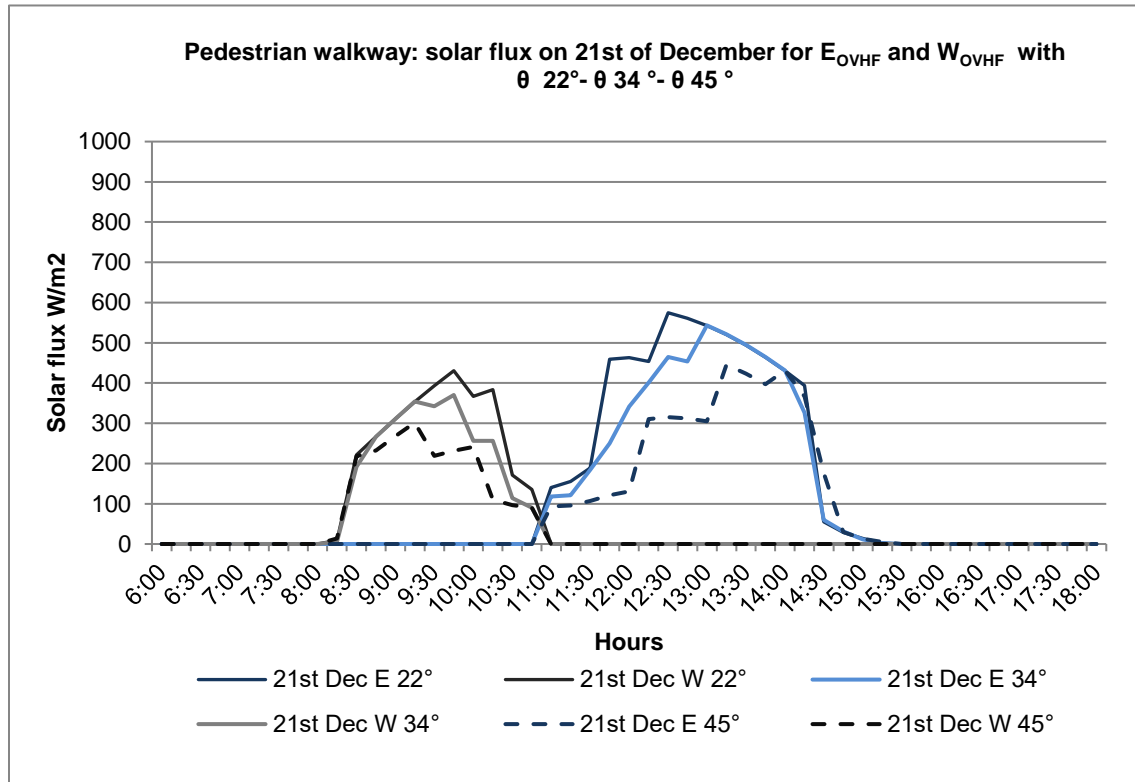


Figure 5.29. Received direct solar flux on the 21st of Dec, on the horizontal surface (pedestrian walkways) of the W_{OVHF} (W) and E_{OVHF} (E).

The influence of the overhanging facade geometry on solar flux received is different from one proportion to another, as mentioned previously in this chapter. Figure 5.30 shows the correlation between the shading view factor and the solar flux received on the horizontal surface, indicating the peak hour of solar flux on that day for the three OVHF geometrical types on the 21st of June. The simulation confirms that the proportion of the geometry affects the penetration of direct solar radiation and that the shading view factor increases when the direct solar flux decreases. In the E_{OVHF} and the W_{OVHF} orientations, the solar flux decreases on the horizontal surface as the angle increases. This correlation is apparent for the OVHF θ 45° (Figure 5.29).

When the proportion of the overhanging facade changes, also the amount of received solar flux changes. In other means, when the angle increases by 6°, the solar flux decreases by 20%. The reduction of solar flux in summer on both sides from the OVHF of θ 22° to θ 34° was 20%. However, the difference from the OVHF of θ 34° to θ 45° is 13% less, and the difference of received solar flux between θ 22° and θ 45° is 30%. Consequently, this shows that the received solar flux on the horizontal surface of the OVHF highly depends on the angle θ of the OVHF. Nevertheless, Figure 6.42 indicates that the W_{OVHF} horizontal surface of θ 22° and θ 34° appears to have similar amounts of solar flux at their peak hour.

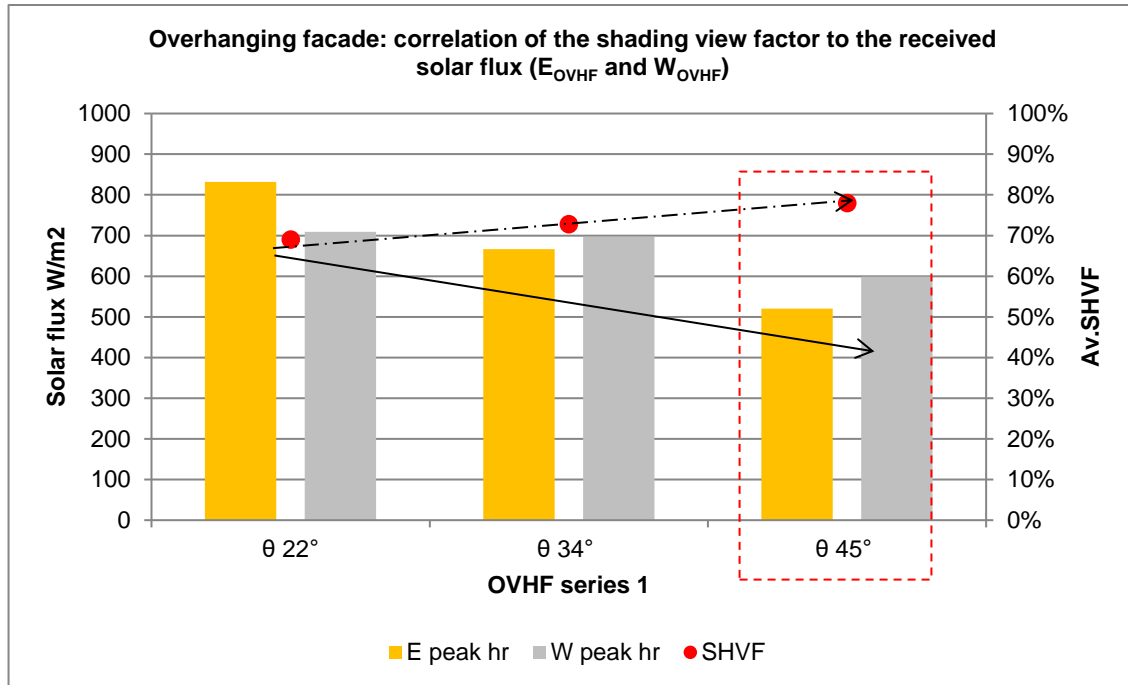


Figure 5.30. Overhanging facades: received direct solar flux on the 21st of June and its correlation to the average SHVF on the horizontal surface (pedestrian walkways) (W_{OVHF} (W) and E_{OVHF} (E)).

Figure 5.31 compares the solar flux received on streets in Case A (Chapter 2) to the solar flux on the horizontal surface (pedestrian walkways) of the E_{OVHF} and the W_{OVHF} applied on the existing layout of Case A in summer. The graph shows an apparent reduction in the solar flux of all three types of geometries. Nevertheless, the OVHF with $\theta 45^\circ$ is the most efficient geometric proportion for reducing the direct solar flux and enhancing the shading space for pedestrians. The observation between both simulations shows that the OVHF created a shaded space protecting the pedestrians from direct solar radiation. Moreover, Figure 5.31 shows a solar flux reduction during summer of almost 40% for the entire day on both orientations compared to Case A. Further, the solar flux results on both orientations indicate an 80% of solar flux reduction at noon. Also, the difference of the solar flux in the peak hour between the existing streets in Case A in N-S street orientation and the shaded spaces under the OVHF has changed due to the horizontal shading element.

The irregularity of the solar flux results shown in Figure 5.31 is due to urban development setbacks. Jeddah urban regulations permit a setback between one building and another from both sides of each building. Consequently, the direct solar radiation penetrates from both sides of the setbacks to the OVHF, causing the irregularity in the solar flux results, whereas in Case A, there is a smooth curve line.

Figure 5.31 also shows the difference between the overhanging facade results of $\theta 45^\circ$ and the existing Case A for the 21st of December. It reveals that, in winter, the E_{OVHF} has a different peak hour than the existing N-S street in Case A. The received solar flux time has been moved from noon in Case A to 2 hrs before noon on the horizontal surface of

the OVHF. Further, the E_{OVHF} horizontal surface receives slightly more solar flux in the peak hours than the existing streets in Case A. Moreover, the W_{OVHF} receives 25% less solar flux than the existing streets in Case A. As observed before, the solar flux curve has an irregular form due to the setbacks and the solar penetration from the geometrical design side.

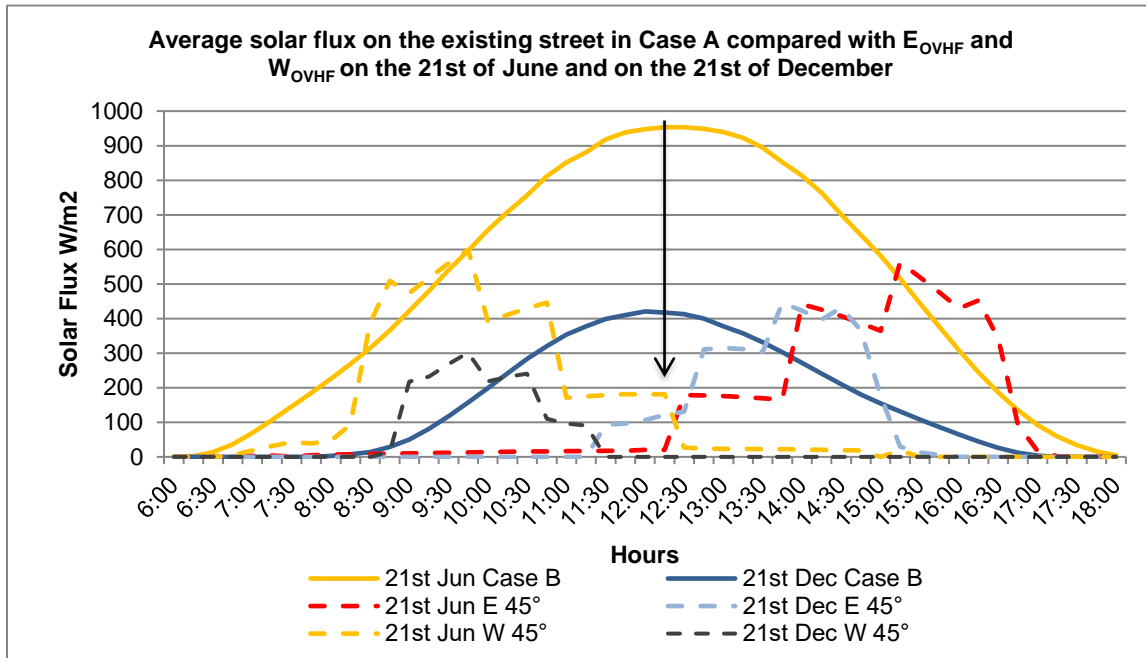


Figure 5.31. Comparison of the received direct solar flux on the 21st of June and on the 21st of December between the overhanging facades on the horizontal surface (pedestrian walkways) for W_{OVHF} (W) and E_{OVHF} (E) and the existing street geometry in Case A.

5.3.4 Results of the Overhanging Facade Geometry in Influencing the Amount of Solar Flux Received on the Pedestrian Walkway for N_{OVHF} and S_{OVHF}

Before showing the amount of solar flux, this section will reveal the influence of overhanging facades on the solar flux response. Using graphs, the explanation with one angle the reaction as it is affected equally on all different chosen angles though with a different amount of solar flux.

The graph in Figure 5.32 illustrates the received direct solar flux at different times in the day of 21st of June for N_{OVHF} and the S_{OVHF} for an OVHF with $\theta 22^\circ$, $\theta 34^\circ$, and $\theta 45^\circ$. It reveals the opposite effects of received solar flux on both orientations. Due to sun movement and orientation of the overhanging facades, as was observed on the E_{OVHF} and the W_{OVHF} . Consequently, the N_{OVHF} receives a direct solar flux from sunrise until before noon and the S_{OVHF} from noon until sunset. Each orientation behaves differently during the day as well as in different seasons. Moreover, the result shows that orientations appear to be reasonably asymmetrical. S_{OVHF} receives in some moments of the day a higher solar flux than N_{OVHF} .

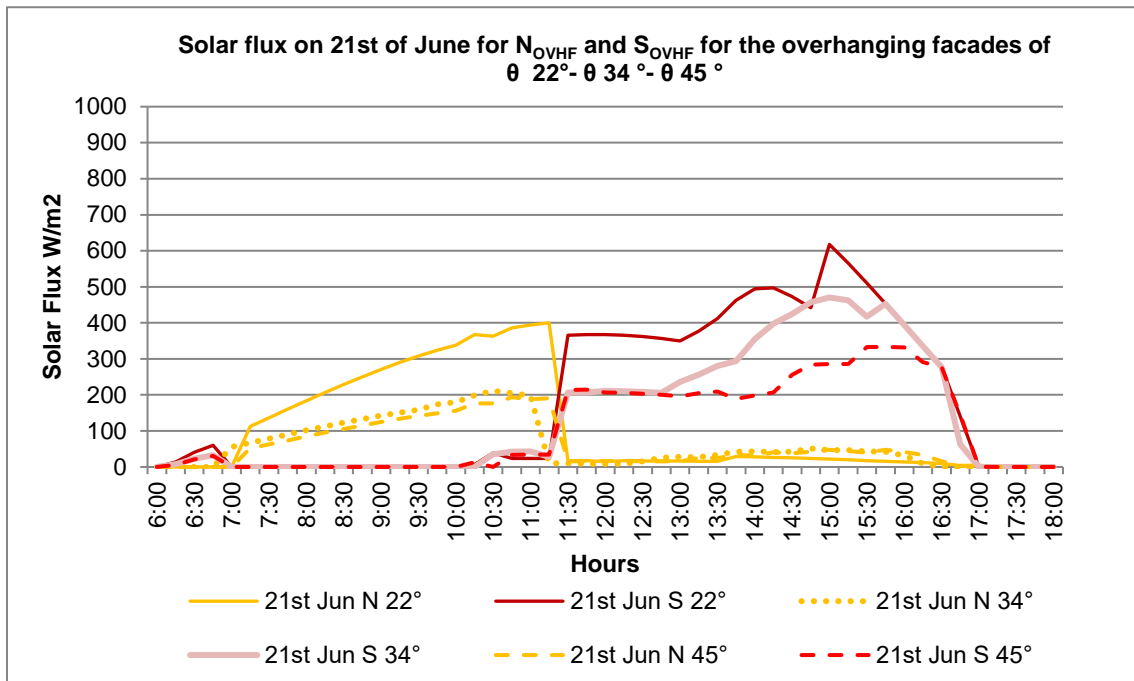


Figure 5.32. Received direct solar flux on the 21st of June of the overhanging facades on the horizontal surface (pedestrian walkways) of N_{OVHF} (N) and S_{OVHF} (S).

Furthermore, Figure 5.33 shows the three geometrical angles on both orientations and how they perform under the direct solar flux during 12 hours in wintertime on the 21st of December. On the one hand, the simulation reveals that S_{OVHF} appears to have almost no solar flux on the horizontal surface for all three overhanging facade geometries. On the other hand, the N_{OVHF} demonstrates a contrary result, with S_{OVHF} having a dramatically high solar flux during the day, decreasing after noontime. Nevertheless, comparing the performance of the three geometrical angles, the chart in Figure 6.45 illustrates that there is no solar flux reduction in wintertime between θ 22° and θ 34°. Both angles receive almost the same amount of solar flux.

Nevertheless, θ 45° shows a reduction of 16% of direct solar flux than the other two angles starting at 11:00 am. After that time, the direct solar flux decreases. See Appendix 3 (Section 3.4).

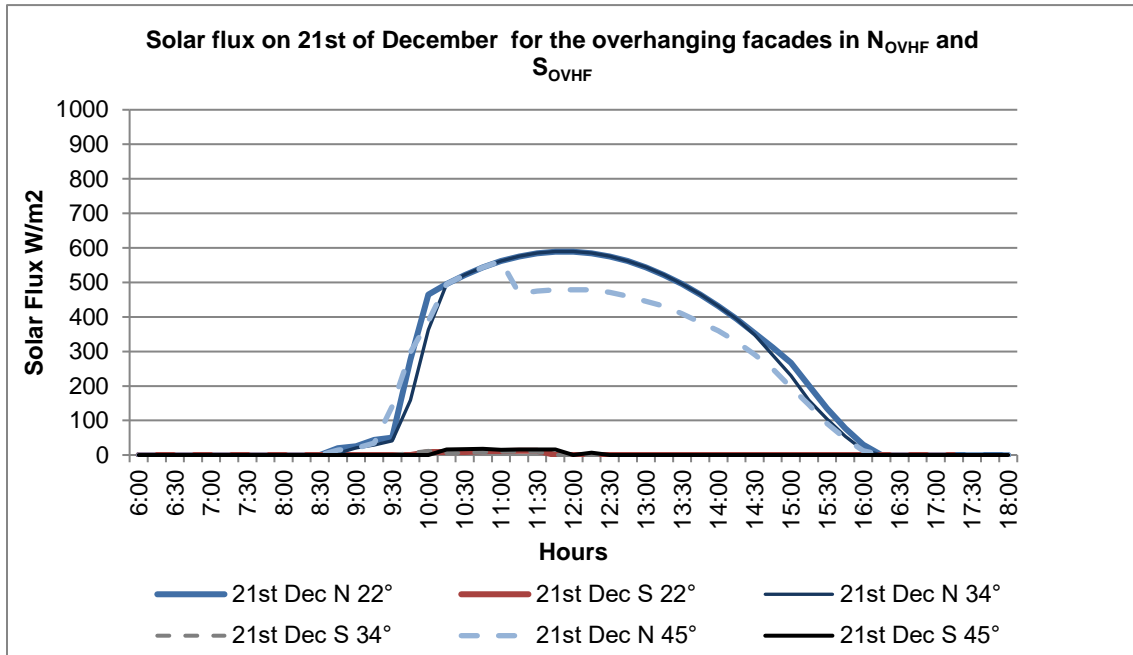


Figure 5.33. Received direct solar flux on the 21st of December of the overhanging facades on the horizontal surface (pedestrian walkways) of N_{OVHF} (N) and S_{OVHF} (S).

Comparing the received solar flux in summertime (21st of June) between N_{OVHF} and S_{OVHF} , the N_{OVHF} receives 20% less solar flux than S_{OVHF} in the three studied geometrical angles ($\theta 22^\circ$, $\theta 34^\circ$, and $\theta 45^\circ$). In contrast, in wintertime (21st of December), the S_{OVHF} side receives 90% less than N_{OVHF} . Hence, when comparing the horizontal surface of N_{OVHF} in the chosen geometrical angles, there is no reduction in the direct solar flux apart from the $OVHF \theta 45^\circ$ where it is by 16% reduced.

The bar chart in Figure 5.34 shows the correlation between the shading view factor and the direct solar radiation on the horizontal surface of all different chosen geometries' angles ($\theta 22^\circ$, $\theta 34^\circ$, and $\theta 45^\circ$) for N_{OVHF} and S_{OVHF} .

The direct solar flux dropped slightly on the horizontal surface of the N_{OVHF} from 290 W/m² for $\theta 22^\circ$ to 200 W/m² for $\theta 34^\circ$ to 190 W/m² for $\theta 45^\circ$. However, while the amount of solar flux slightly decreased in N_{OVHF} , the amount of direct solar flux in S_{OVHF} decreased, but the reduction was higher than for N_{OVHF} . In S_{OVHF} , the solar flux decreased from 617 W/m² for $\theta 22^\circ$ to 470 W/m² for $\theta 34^\circ$ to a low 333 W/m² for $\theta 45^\circ$.

Therefore, the reduction of solar flux of the horizontal surface of N_{OVHF} for the three angles is 30%. Further, S_{OVHF} had almost a reduction of 50% from $\theta 22^\circ$ to $\theta 45^\circ$. Consequently, when the shading view factor increases, the direct solar flux decreases. This indicates that **considering the parameters that affect this increase and decrease is a must. Firstly, the orientation is a crucial parameter and, secondly, the angle of the designed geometry. These two parameters affect the amount of received solar radiation and the amount of shading protection provided to pedestrians.** Hence, with

a 10% increase in the shading view factor, there is a 50% reduction of direct solar flux on the horizontal surface of S_{OVHF} . For N_{OVHF} , a 10% increase of the shading view factor results in 30% of solar flux reduction.

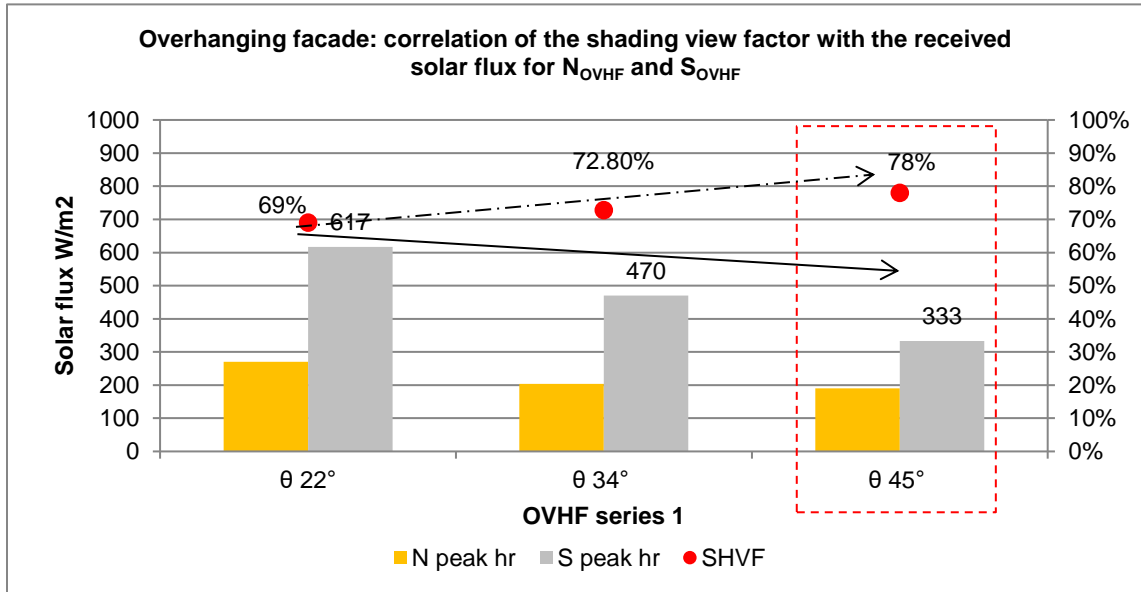


Figure 5.34. Overhanging facades: received direct solar flux on the 21st of June and its correlation to the average SHVF on the horizontal surface (pedestrian walkways) for N_{OVHF} (N) and S_{OVHF} (S).

Furthermore, the graph in Figure 5.35 illustrates a comparison of the received solar flux between the horizontal surface of N_{OVHF} and S_{OVHF} of $\theta 45^\circ$ and the existing streets in Case A during summer and winter.

Additionally, there is an apparent reduction of the solar flux on the horizontal surface of N_{OVHF} and S_{OVHF} than in the existing streets in Case A. On the one hand, there is a decrease of 70% between the existing streets and N_{OVHF} in the summertime, whereas, in wintertime, N_{OVHF} received a 10% higher solar flux than the existing streets in Case A. On the other hand, S_{OVHF} reveals a solar flux reduction of 60% in summer compared to the existing streets in Case A. However, in winter, the decrease was almost 100%.

As mentioned in Chapter 2, the summer of Case A is 12 hours, and the solar flux peak hour is at noon. Here, we must mention that the overhanging facade's geometry enhanced the existing situation as the solar flux reduced dramatically, especially around noontime. The solar time interval for both orientations of N_{OVHF} and the S_{OVHF} is 4 hrs. In wintertime, the existing streets in Case A and N_{OVHF} have a solar time interval of 9 hrs. S_{OVHF} has an almost zero solar time interval.

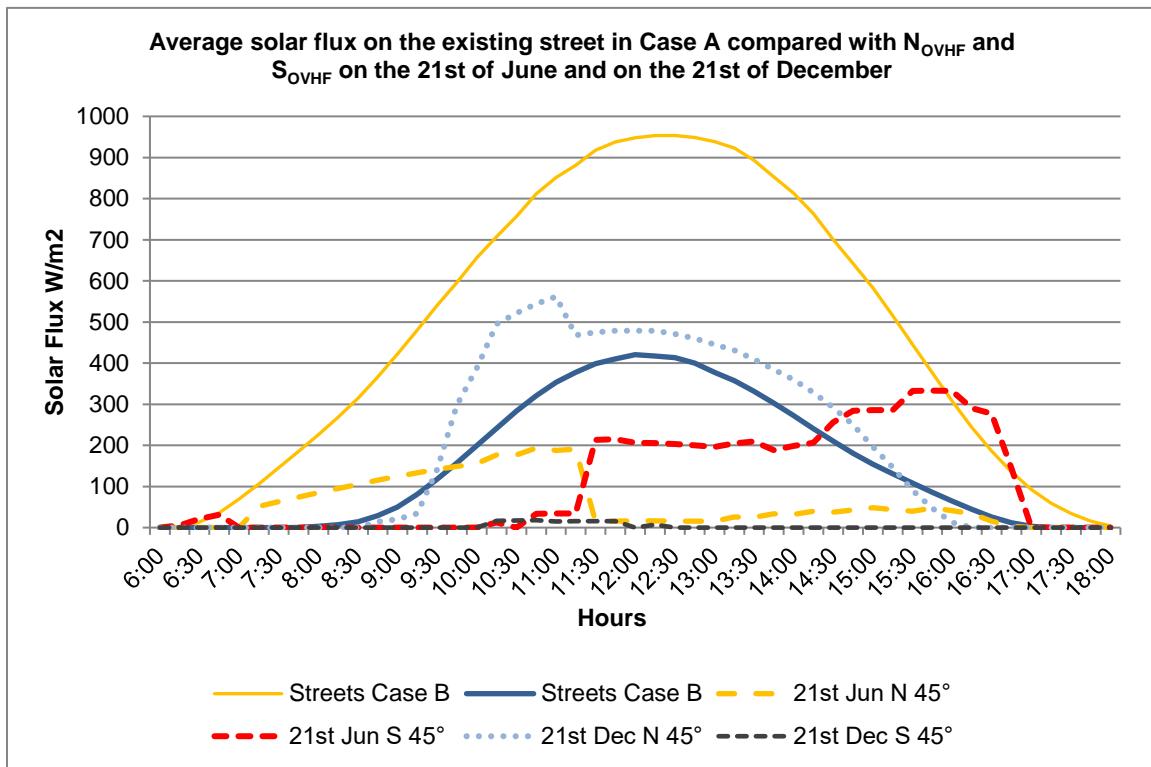


Figure 5.35. Comparison of the received direct solar flux on the 21st of June and on the 21st of December between the overhanging facades on the horizontal surface (pedestrian walkways) (N_{OVHF} (N) and S_{OVHF} (S)) and the existing street geometry in Case A.

5.3.5 Effect of Overhanging Facades on the Amount of Solar Flux Received on the Horizontal Surface of E_{OVHF} and W_{OVHF}

The graphs in Figure 5.36 compare the received direct solar radiation during the entire day of the 21st of June (summer solstice) and the 21st of December (winter solstice) on the horizontal surface of the OVHF in both orientations of E_{OVHF} and W_{OVHF} . This comparison shows the impact of the geometry on the amount of direct solar radiation received under the covered area and the amount of shade provided to the pedestrians.

The horizontal surface of the E_{OVHF} is only partly stressful in the afternoons in both analyzed seasons. In summer, the E_{OVHF} with $\theta 22^\circ$ receives at 14:00 hrs the highest amount of solar flux with 820 W/m². For the $\theta 34^\circ$, the duration is slightly reduced, with its peak of solar flux at 15:00 hrs. Due to the change in the size of the OVHF, the solar flux with 660 W/m² is 20% less than for $\theta 22^\circ$. Further, on the horizontal surface of the OVHF of $\theta 45^\circ$, the time for the highest peak of solar flux was the same as for the OVHF of $\theta 34^\circ$. However, the solar flux was reduced to 570 W/m², which is 13% less than for the $\theta 34^\circ$ and 30% less than for $\theta 22^\circ$. The difference of the direct solar flux on the horizontal surface between the $\theta 34^\circ$ - and $\theta 45^\circ$ - sized OHVF of E_{OVHF} in summer is not that high. However, between $\theta 22^\circ$ and $\theta 45^\circ$, the difference in solar flux reduction is high as $\theta 45^\circ$

provides more shade for the pedestrians. Though this was clear from the beginning, $\theta 22^\circ$ offers sufficiently more shade for the pedestrians than the actual situation without shade. On the other hand, the winter solstice is as stressful in the afternoon as observed for summer. The E_{OVHF} with an OVHF of $\theta 22^\circ$ receives its highest solar flux value at 13:00 hrs with 580 W/m². For the $\theta 34^\circ$, solar flux peak time delayed 20 min due to the change of the size of the OVHF having a flux of 530 W/m² which is 8% less than for $\theta 22^\circ$. As for the $\theta 45^\circ$, solar flux peak is 450 W/m² and thus 15% less than the solar flux for $\theta 34^\circ$ and 22% less than for $\theta 22^\circ$. In summary, the wider the OVHF, the shorter is the solar period and the lower the solar flux as more shade is provided to the pedestrians.

For the OVHF on the W_{OVHF} , a general observation is that in both seasons, the solar flux on the horizontal surface of the OVHF is most stressful before noon, and it fluctuates. Further, in the summer solstice, the solar flux value of the $\theta 22^\circ$ OVHF remains the same as observed for E_{OVHF} of the OVHF. Its peak time is at 10:15 hrs, whereas $\theta 34^\circ$ has peak time at 9:25 hrs, which is a 55 min time difference. The $\theta 34^\circ$ OVHF has with 700 W/m² 14% less solar flux than $\theta 22^\circ$ in W_{OVHF} but still 5% more than $\theta 34^\circ$ in E_{OVHF} . For the $\theta 45^\circ$ OVHF, the solar flux is 600 W/m² which is 14% less solar flux than for the $\theta 34^\circ$ OVHF and 26% less than for the $\theta 22^\circ$ OVHF.

For the winter solstice, the picture is different. Here, the $\theta 22^\circ$ OVHF receives at 10:15 hrs its highest peak value of solar flux with 410 W/m². Nevertheless, we must mention here that the W_{OVHF} $\theta 22^\circ$ OVHF at the winter solstice has 30% more solar flux than the E_{OVHF} . Further, the $\theta 34^\circ$ OVHF receives its highest peak value at 10:00 hrs with 380 W/m² and thus 7% less of the solar flux than observed for the $\theta 22^\circ$ OVHF. The $\theta 45^\circ$ OVHF received at 9:15 hrs its highest value with 300 W/m². This is 30% less solar flux than for the $\theta 22^\circ$ OVHF.

The simulation reveals that at the summer solstice, both the $\theta 34^\circ$ and the $\theta 45^\circ$ OVHF in E_{OVHF} receive 5% less solar flux than in W_{OVHF} . As mentioned before, the $\theta 22^\circ$ OVHF has the same solar flux values as for E_{OVHF} . In winter solstice, the E_{OVHF} has a higher solar flux than W_{OVHF} .

Taken together, as the objective was to provide shade in summer from the harsh direct solar radiation, a wider OVHF on the West orientation is recommended to have more protection and shaded spaces.

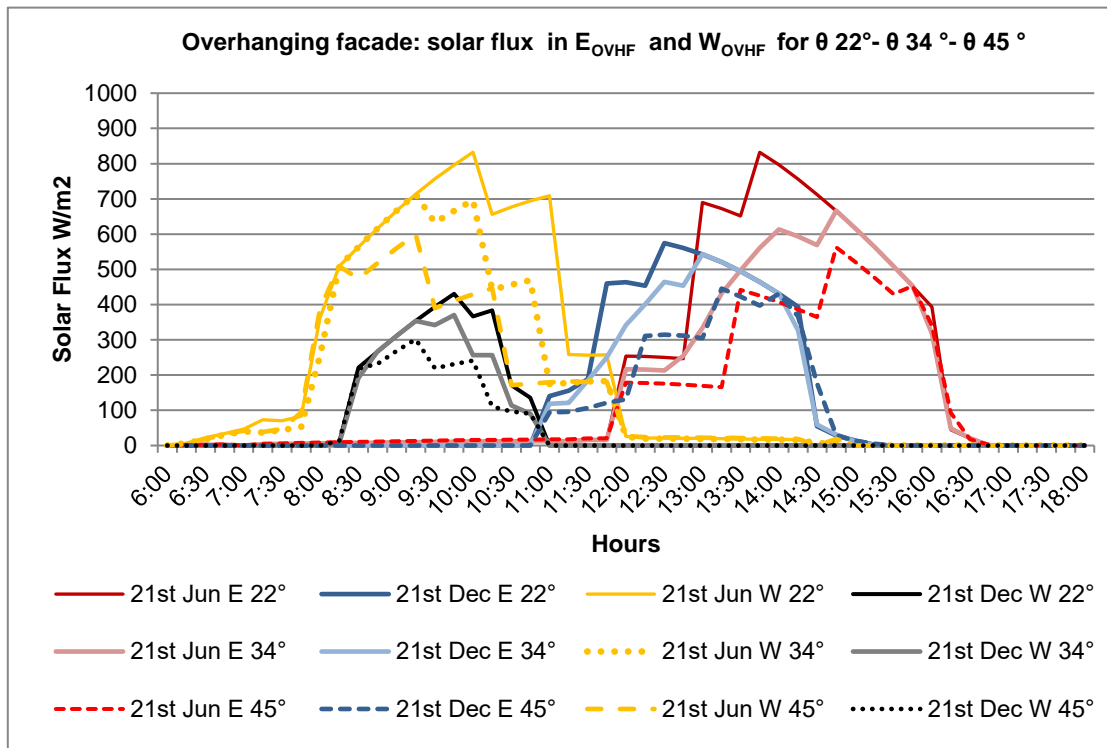


Figure 5.36. Received direct solar flux in E_{OVHF} (E) and W_{OVHF} (W) for $\theta = 22^\circ, \theta = 34^\circ$, and $\theta = 45^\circ$.

5.3.6 Effect of Overhanging Facades on the Amount of Solar Flux Received on the Horizontal Surface in N_{OVHF} and S_{OVHF}

The overall observation concerning the N_{OVHF} and S_{OVHF} orientations is that the solar flux was reduced when applying this OVHF proposal compared to the actual situation without OVHF. Nevertheless, due to the sun trajectory and angle on the summer solstice and the sun close to the zenith, the pedestrian walkways under the S_{OVHF} receive a more extended sun period and a higher solar flux than under N_{OVHF} (Figure 5.37).

Moreover, the OVHF geometry effect is efficient in reducing the direct solar flux and creating shaded spaces for pedestrians. Notably, the solar flux is generally higher when the OVHF angle is lower concerning the vertical surface (facades).

The direct solar flux on the horizontal surface of the $\theta = 22^\circ$ OHVF in S_{OVHF} fluctuates. It receives between 20 and 610 W/m^2 in summer and winter between 10 and 20 W/m^2 . In N_{OVHF} , the simulated direct solar flux fluctuates and receives between 10 and 390 W/m^2 and in winter between 20 and 600 W/m^2 .

The direct solar flux on the horizontal surface of the OVHF with $\theta = 34^\circ$ receives in S_{OVHF} between 20 and 460 W/m^2 in summer, which is 24% less than observed for the $\theta = 22^\circ$ OVHF. In winter, the horizontal surface receives between 5 and 10 W/m^2 . As aforementioned, the amount is meager, as almost no direct solar radiation is received. Nevertheless, N_{OVHF} receives between 50 and 210 W/m^2 in summer, which is a 46% solar

flux reduction compared to the $\theta 22^\circ$ OVHF. In winter, the solar flux ranges between 10 and 600 W/m².

Moreover, the direct solar flux of the $\theta 45^\circ$ OVHF on the horizontal surface in S_{OVHF} provides an intensity ranging between 10 and 330 W/m² in summer, thus 21% less than observed for the $\theta 34^\circ$ OVHF and 40% less than for the $\theta 22^\circ$ OVHF. In winter, it receives between 0 and 5 W/m². On the other hand, the direct solar flux in N_{OVHF} ranges between 50 and 200 W/m² in summer, a 4% solar flux reduction compared to the $\theta 34^\circ$ OVHF. In winter, N_{OVHF} receives between 10 and 600 W/m².

The findings indicate that in winter, the received solar flux in N_{OVHF} is almost constant and higher than in summer. Further, the difference of direct solar flux received on the horizontal surface of the $\theta 22^\circ$, and the $\theta 45^\circ$ OHVF in S_{OVHF} is almost 40% in summer and almost 50% less in N_{OVHF} . Interestingly, the difference between the $\theta 34^\circ$ and the $\theta 45^\circ$ OVHF is only 4% in summer.

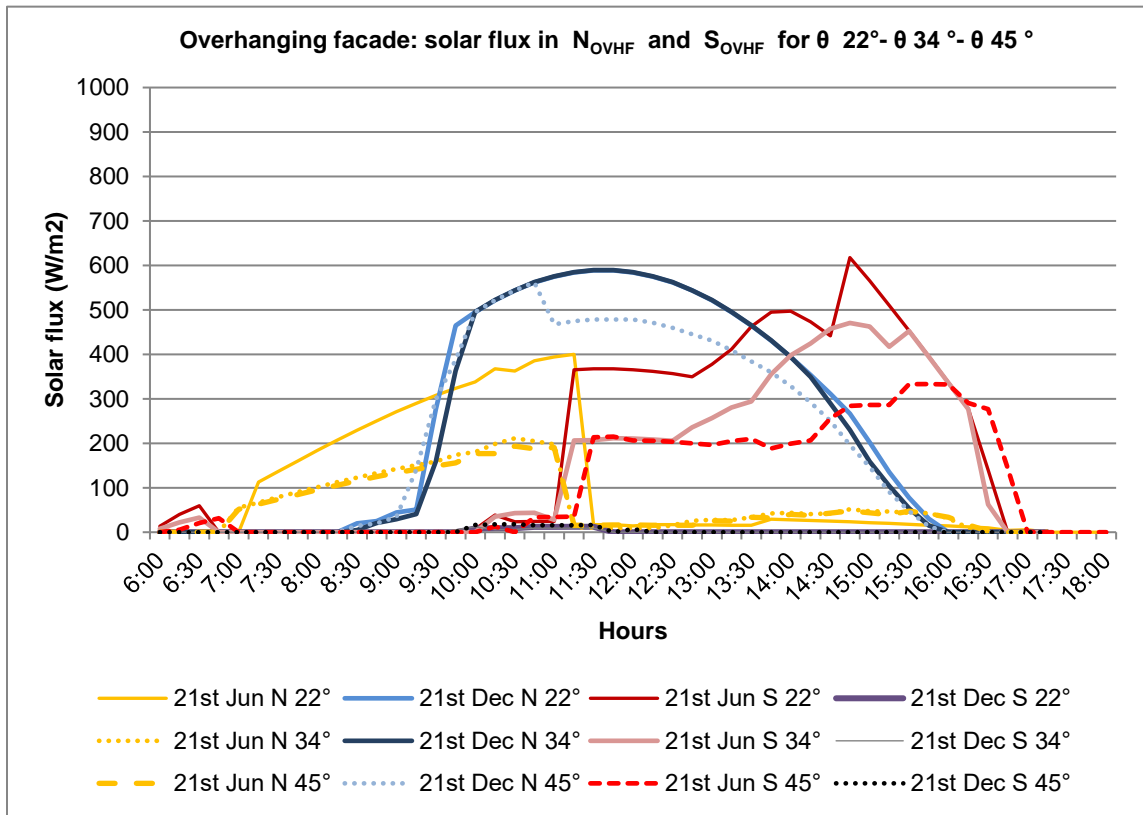


Figure 5.37. Received direct solar flux in N_{OVHF} (N) and S_{OVHF} (S) for $\theta 22^\circ$, $\theta 34^\circ$, and $\theta 45^\circ$.

5.4 Evaluation of the Shading Urban Geometry

5.4.1 Evaluation of the Extruded Windows (Rawashin) in the Compact Urban Layout H1

By comparing direct solar radiation in the old layout AlBalad with and without the Rawashin, the effects of the Rawashin applied on the streets are quantified. A reduction of direct solar radiation was expected on the ground surface under the Rawashin by providing shade for the pedestrians. The shade of these extruded windows on the street's horizontal surface is different from one side of the street to the other, depending on the street orientation.

In the E-W streets during summer, when the sun angle is exceptionally high, the N side of the street has more shadow under the Rawashin than the S side. The direct solar radiation reduction on the horizontal surface under the Rawashin on the N side was 60%, and under the S side 40% (Figure 5.38). In the N-S streets, the W side had more shadow in summer than the E side. Here, the direct solar radiation reduction on the W side was 60%, and for the E side, 25% (see Appendix 3, Section 3.2). In the NW-SE streets, the shade was more evident on the SW side with a direct solar radiation reduction of 60% and less shade on the NE side with a 40% reduction (see Appendix 3, Section 3.2). For the NE-SW street, the created shade was more when applying the Rawashin on the SE side with a direct solar radiation reduction of 50%, whereas the NW side had only 25% direct solar radiation reduction (see Appendix 3, Section 3.2)

Remarkably, the extruded windows in the compact layout were efficient in reducing direct solar radiation and creating shade for pedestrians. However, one must consider the complex dimensional proportions of the morphology structure in the old compact layout with the dimensional geometry of the Rawashin.

The solar radiation analysis on the horizontal surface (streetss) demonstrated that applying horizontal shading elements offers different opportunities to enhance pedestrian comfort. Consequently, a structured analysis of the existing urban layout with and without applying the Rawashin allows detecting the efficiency of the horizontal shading elements and their possible improvement of the street, especially in compact urban layouts.

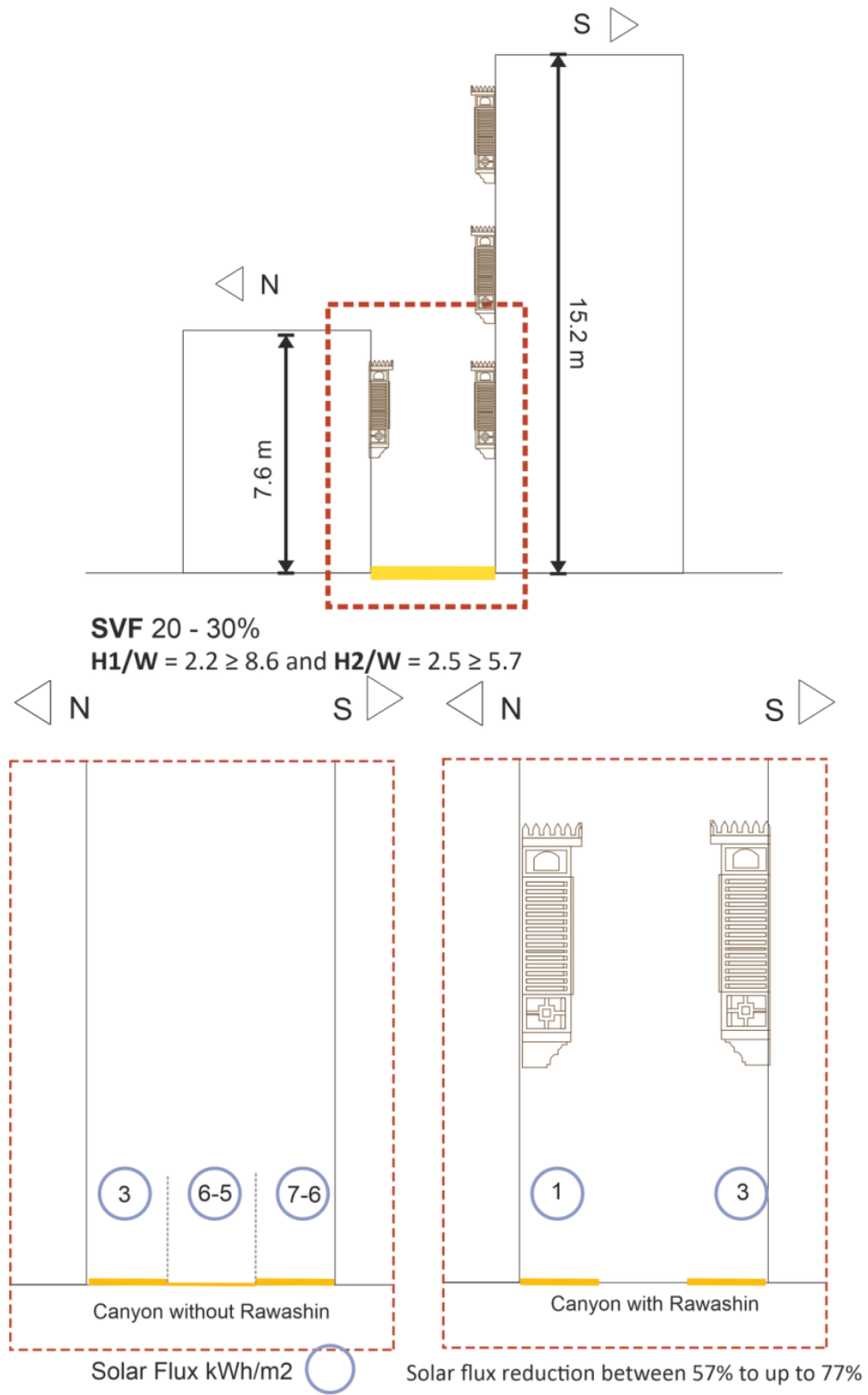


Figure 5.38. Received direct solar flux on the E-W street in the old area Jeddah demonstrating the results of the street before and after applying the Rawashin.

5.4.2 Evaluating the Shading View Factor in the Outdoor Environment

Enhancing pedestrian comfort in hot-desert climate cities shading is one of the crucial and fundamental design aspects in outdoor spaces to protect from the harsh solar radiation. Therefore, this research was dedicated to enhancing this design aspect in improving pedestrian comfort.

The Shading View Factor is one of the new inventions of this study and an eye-opener for architects and urban designers to consider in their future designing of pedestrian walkways or open spaces (plazas). Hence, it opens a new research topic to improve outdoor spaces in hot climate cities.

The shading view factor parameter helps to simplify the complex outdoor environment. It shows a clear correlation between the value given in a shaded space and the amount of direct solar radiation received when applying a horizontal shading element. A particular modification is applied to enhance pedestrian comfort (see also the examples given in Figures 5.39 and 5.40).



Figure 5.39. Designed by Oscar Niemeyer and Hélio Uchôa, Biennale Pavilion, São Paulo, Brasil, 1957. The overhanging facade clearly shows the shading view factor effect.



Figure 5.40. Designed by Le Corbusier, Palace of Assembly, Chandigarh, India, 1951. The designed shading element protecting the different entrances of the building: people can move from one access to another under the overhanging facade.

The benefit of this new parameter is that it facilitates enhancing shading spaces in hot climate cities. It gives the urban designer and the architect a flexible and rigid tool to enhance outdoor spaces and human thermal comfort. Moreover, this parameter could be tested in-depth with other types of horizontal geometries. Nevertheless, the first steps to evaluate the parameter were done in this study, and the first attempt was to find a new way to enhance thermal comfort.

The newly established shading view factor (SHVF) offers new perspectives on an existing modern dispersed urban layout. Comparing the SHVF in the analyzed series 1 and 2 provided an opportunity to explore different horizontal geometry dimensions and test their effect on direct solar radiation.

The comparison illustrated a small difference percentage of received direct solar flux on the horizontal surface at the summer solstice on the 21st of June and at the winter solstice on the 21st of December between both series. Still, due to the proportion of the studied overhanging facade geometries with the solar angle, there was no significant difference between both series. Nevertheless, it provided a starting point to understand how horizontal shading systems in the outdoor environment behave concerning direct solar radiation.

This research sheds light on a few types of geometries using the SHVF, and the study could be extended by examining more geometrical angles. The results indicate that the novel parameter shading view factor will open doors for new research and investigations. The evaluation of both series was not to compare; it was more to evaluate different geometrical angles and how they perform under the harsh solar radiation. Furthermore, it was to analyze how the horizontal shading elements can enhance human thermal comfort.

5.4.3 Evaluation of Overhanging Facades in the Mid-Dense Modern Urban Layout H2

The second type of horizontal shading geometry is the overhanging facade. This type's evaluation was on the modern mid-rise existing urban layout with wide streets exposed to direct solar radiation. Two types of geometric series were simulated. Each series had three different overhanging facades to evaluate the influence on the horizontal surface (pedestrian walkways) and the amount of created shading.

Further, a quantified comparison was made on both series to evaluate their geometry and determine their different effects on the pedestrian walkways. The analysis is based on two geometrical image projections: the stereographic projection and the orthographic projection, which evaluate the SHVF for pedestrians under these created spaces and the solar access shown for the entire year. The simulations also analyzed the direct solar radiation under the overhanging facades. The solar radiation simulations were generated for the 21st of June (summer solstice) and for the 21st of December (winter solstice) from the 3D model of the study area using the Heliodon2 software.

Therefore, in terms of geometry's impact, the SHVF changes when the overhanging facade angles change. If the OVHF angle is high, the SHVF is also high, and space below receives a lower amount of solar flux. Similarly, when the angle is low, the shade is low, and the horizontal surface under the overhanging facade receives a higher direct solar flux.

Furthermore, the overhanging facade analysis showed the efficiency of the shading element in creating shaded spaces to reduce solar flux. The results show that the studied urban shading elements regulate the average direct solar radiation condition. These spaces still experience peak moments with high direct solar flux.



Figure 5.41. Designed by Marcel Breuer, Whitney Museum of American Art, New York, 1966. The overhanging facade of the building protects pedestrians from solar radiation. (Source: Photographer Ezra Stoller)



Figure 5.42. Designed by Lúcio Costa, Oscar Niemeyer, Affonso Reidy, and Carlos Leão, Education and Health Ministry building, Rio de Janeiro, Brazil, 1940.



Figure 5.43. Designed by Carlos Cascaldi, College of Architecture and Urbanism, Sao Paulo, Brazil, 1961. A massive overhanging facade protects the entrance of the building.

The overhanging facade analysis revealed more than 50% of solar flux reduction in summer and winter, mainly in the critical hours around noon, as observed in series 1. Further, the OVHF geometry with $\theta 45^\circ$ performed better than the other proposed OVHFs. The difference between solar radiation reduction and shading view factor between $\theta 45^\circ$ and $\theta 34^\circ$ was between 7% and 15%, which is low.

The overhanging facades reduced the direct solar radiation, especially for the highest angle of $\theta 45^\circ$ (shadow view factor 80%) in summer and winter for all four orientations ($N_{OVHF} - S_{OVHF} - E_{OVHF} - W_{OVHF}$). Here, $E_{OVHF} - W_{OVHF}$ received less direct solar radiation in summer than $N_{OVHF} - S_{OVHF}$. However, in winter, $N_{OVHF} - S_{OVHF}$ is protected at noontime and receives less direct solar radiation, whereas for $E_{OVHF} - W_{OVHF}$, the direct solar radiation at noontime is at its highest. $E_{OVHF} - W_{OVHF}$ received on all studied geometrical angles the same amount of direct solar radiation in summer. However, from all the four overhanging facades, the N_{OVHF} received the least direct solar radiation. For $E_{OVHF} - W_{OVHF}$, the direct solar penetration was almost symmetrical in summertime and wintertime, whereas only in summer for $N_{OVHF} - S_{OVHF}$ was the penetration symmetrical but not in wintertime.

Figures 5.44 and 5.45 show the summary result of the effect of the $\theta 45^\circ$ OVHF on both orientations, the W_{OVHF} and E_{OVHF} , in wintertime and summertime demonstrating the solar flux on the ground level of the pedestrian street with and without OVHF.

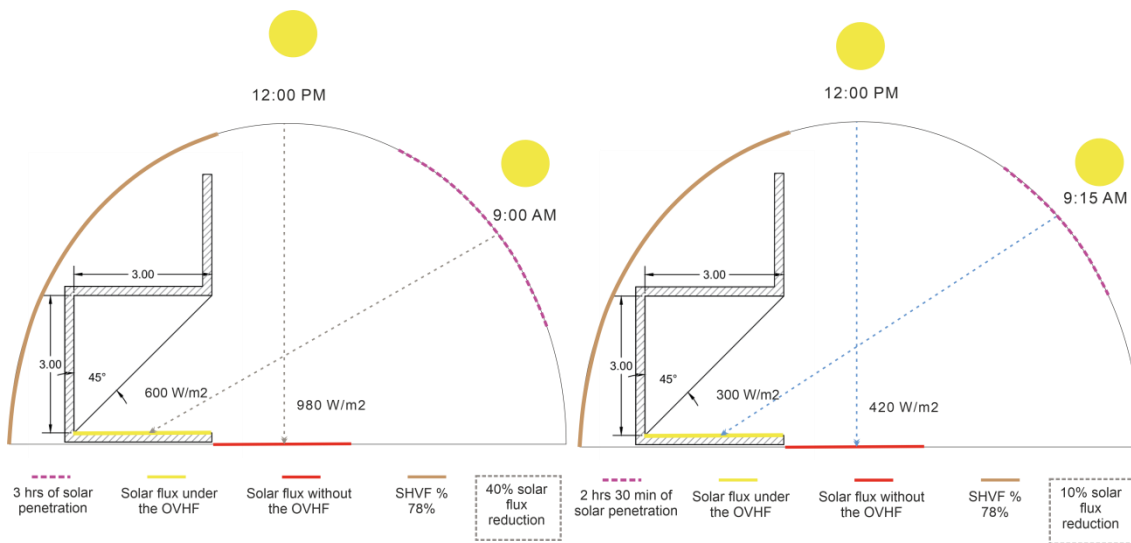
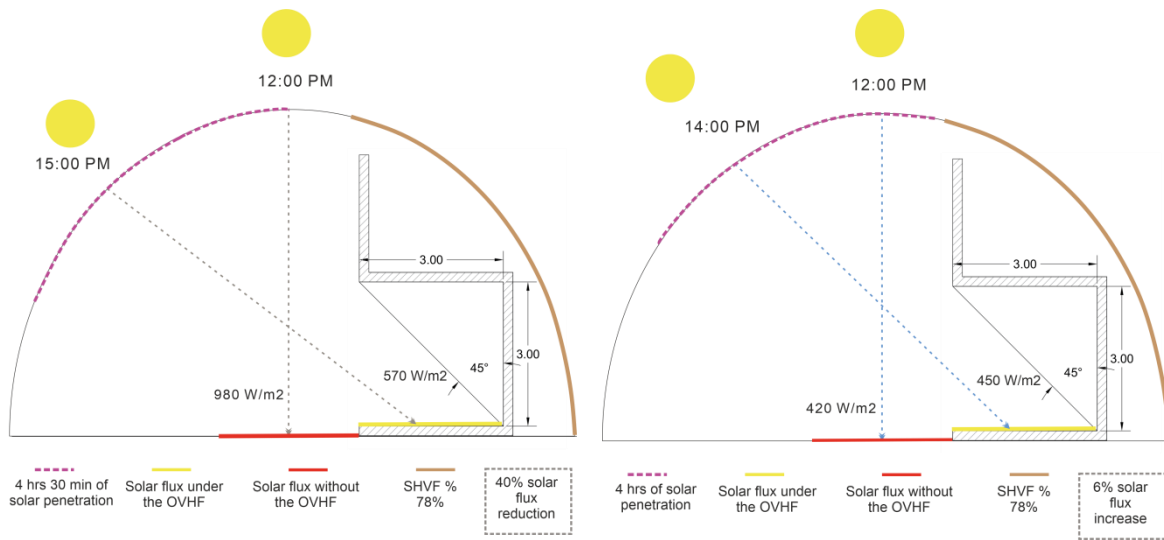


Figure 5.44. Received direct solar flux on the W_{OVHF} orientation on the pedestrian street before applying and after the OVHF in summertime (right) and wintertime (left).



5.45. Received direct solar flux on the E_{OVHF} orientation on the pedestrian street before and after applying the OVHF in summertime (right) and wintertime (left).

Figures 5.46 and 5.47 show the summary result of the effect of the $\theta 45^\circ$ OVHF on both orientations, the N_{OVHF} and S_{OVHF} , in wintertime and summertime, demonstrating the solar flux on the ground level of the pedestrian street with and without OVHF.

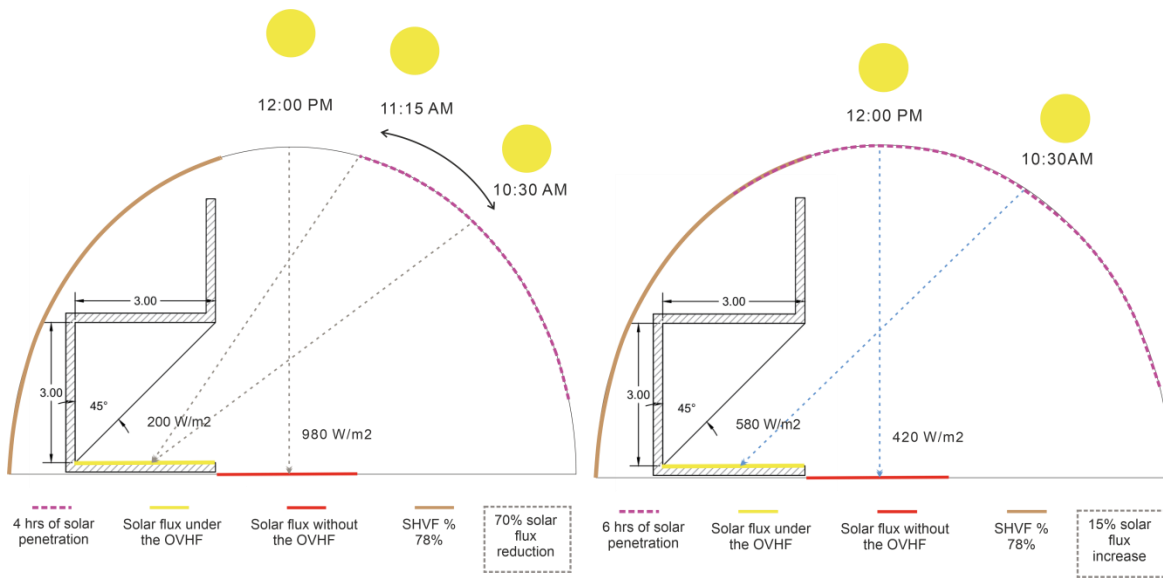


Figure 5.46. Received direct solar flux on the N_{OVHF} orientation on the pedestrian street before and after applying the OVHF in summertime (right) and wintertime (left).

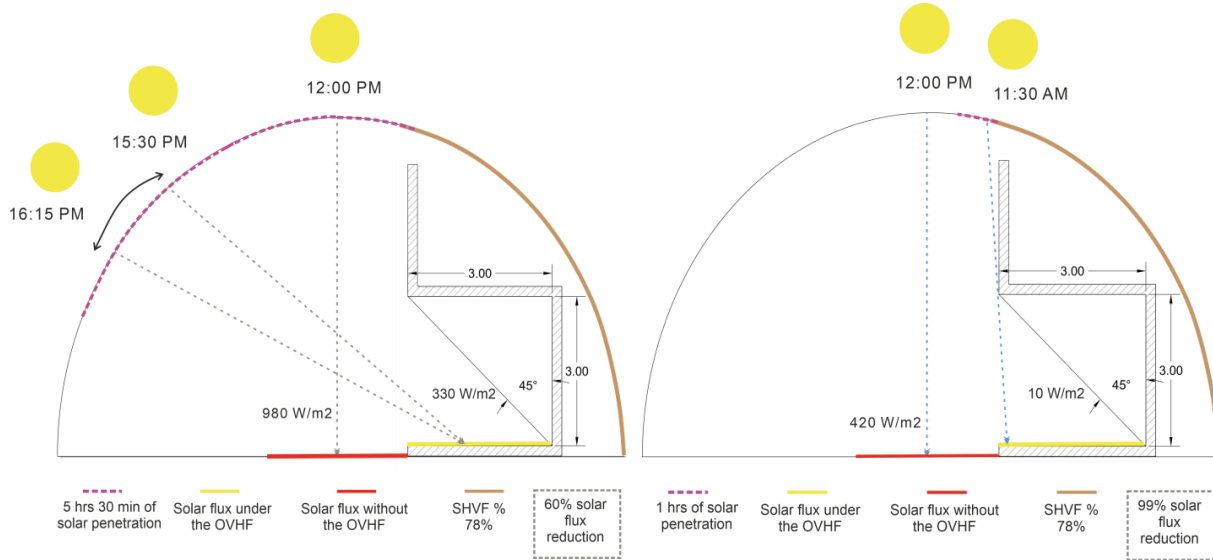


Figure 5.47. Received direct solar flux on the S_{OVHF} orientation on the pedestrian street before and after applying the OVHF in summertime (right) and wintertime (left).

The use of the SHVF is an additional indicator providing information about shading effects. In the end, it is not about which side or orientation of the overhanging facade is better than the other side; it is about how these horizontal elements are performing in hot climate cities and that they are enhancing the human thermal comfort and about protecting the pedestrians from direct solar radiation.

CONCLUSIONS AND FUTURE INVESTIGATIONS

CONCLUSION

This thesis sheds light on the urban form in hot-desert climate cities and how urban morphology affects the microclimate and pedestrian comfort. In hot climate cities solar radiation is the climatic factor with the most significant influence on energy behavior in outdoor spaces. In the context of the architecture and urban sustainability the current study confirms the significance of analyzing the built environment's different categories; outdoor shading spaces are essential to improve the environmental conditions to enhance pedestrian thermal comfort. The study set up and identifies relationships between urban morphology and direct solar radiation performance to answer this thesis's research questions: **To what extent can urban morphology modifications in hot-climate cities be necessary to improve pedestrian comfort? Is the compact urban fabric the only solution to enhance pedestrian comfort in hot climate cities to protect outdoor spaces from solar penetration?**

From the analysis of results obtained from this work, several conclusions have been drawn:

Avoiding direct solar radiation in modern urban layouts

The morphology parameters of street aspect ratio, street orientation, and the sky view factor are intimately related to energy performance.

A numerical modelling simulation was used to assess the solar radiation in the urban layout of the old area (AlBalad), analyzing its solar radiation time interval, Sky View Factor and direct incidence. The existing morphology significantly undermines the intensity of solar energy and solar access time interval, in summer and winter on the horizontal surfaces (streets) and vertical surfaces (walls).

This investigation also analyses the effect of direct solar radiation on two different existing urban layouts in the modern area of Jeddah city characterized by sprawling urban development. In sprawling urban design, the urban morphology does not provide shade for pedestrians. Therefore, in these modern urban layouts to enhance pedestrian comfort other solar radiation protection measures should be considered, especially on hot summer days. Modifying the vertical morphology creating horizontal-shaded walkways for pedestrians would be a wise and skillful guidance.

The direct solar radiation and the Sky View Factor (SVF) have been calculated considering the solar radiation intensity and solar obstructions determined by different urban situations.

Public transportation and applying the “oasis effect.”

Jeddah city is expected to construct a new subway in 2020 that will dramatically change the inhabitants' behavior. The current urban morphology and climatic situation are not suitable for transit and commuting from one metro point to the destination location.

Therefore, after assessing and analyzing Jeddah's different existing urban morphologies, the future metro stations could be considered nodes with more densely inhabited fabrics, providing transitional spaces for pedestrian activities.

The concept of creating an 'oasis effect' attributed to shading would be applied. A lively and well-designed microclimate will encourage residents and visitors to reclaim a noticeable pedestrian lifestyle present in the old city, which virtually disappeared from newer neighborhoods due to the shift towards automobile transportations.

Services and facilities around the metro nodes should become transitional thermal comfort areas around the metro station exits. Given that the prevailing climate condition in Jeddah city during the daytime in the summer season is extremely hot, thermal comfort is challenging to achieve passively. However, employing appropriate street geometry can be achieved by limiting the duration of exposure to solar radiation.

Urban horizontal shading geometry (Rawashin) in the old area AlBalad

The use of horizontal shading elements revealed beneficial to reduce direct solar radiation by the surface covered (the ground). In the old urban context, one of the crucial conclusions is that the street area below the extruded windows (Rawashin) decreased the average solar flux potential on the 21st of June, summer solstice, between 57 % and in some areas 77 % on E-W canyons, compared to the E-W canyons without extruded windows. Extruded windows on the vertical morphology should be encouraged.

Building regulations on building codes should be modified to provide outdoor shade from harsh sun penetration. In other words, due to the results and findings obtained in this investigation and for the necessity of shading pedestrian walkways in low latitudes, it is advised to apply horizontal shading to protect from the direct solar radiation, not only considering the modification of the urban morphology.

Nevertheless, it is recommended that when designing horizontal shading devices (extruded windows, balconies, arcades, galleries, or overhanging facades), the south façade extruded element should be more comprehensive due to the penetration of direct solar radiation in the summer season that is considered essential to be protected from at that time of the year to enhance pedestrian comfort. Also, always consider the aspect ratio of the streets and canyons while designing them.

Shading view factor and overhanging facades

An indicator to evaluate horizontal shading elements effect in an urban context is defined: The Shading View Factor. It quantifies the avoided direct solar radiation under horizontal shading elements as arched, overhanging facades, extruded windows and balconies.

The variables considered to calculate the shading view factor are the building height, distance of other obstructions, orientation of the horizontal shading element, dimension of the horizontal shaded element (angle θ).

The use of horizontal-shading elements on the vertical morphology should be encouraged. Building regulations around metro nodes should be modified to promote outdoor shade from the harsh sun penetration. Consequently, this will reduce the direct solar radiation to protect pedestrians and the surrounding surfaces from the longwave solar radiation.

Assessing different horizontal shading systems would provide criteria about the proportion needed to avoid and protect the pedestrian urban space from direct solar radiation.

SUGGESTIONS FOR FUTURE INVESTIGATIONS

The current research focused on connecting urban microclimate theoretical understanding with the practical design method. Direct solar radiation simulations carried out in this thesis provided information about the thermal behavior of existing urban morphologies during specific days. The aim was to analyze the relationship between direct solar radiation (shortwave) and urban morphology. The literature review also showed an absence in the investigation, either experimental or numerical, to directly address the urban geometry's impacts on human comfort in hot climate cities. This instantly highlights the significance and, on the other hand, the complexity of this research. It also highlights that much additional work is necessary, as outlined below. Several exciting questions for future investigations arose during this study:

- This study examined the impact of urban geometries and the spatial arrangement between buildings on direct solar radiation. Future studies should include indoor measurements to develop a more detailed knowledge of the effect of the thermal mass of the streets and other facets (walls and ground) on its microclimate conditions and building energy consumption.
- In addition to the barriers preventing vegetation and water use as design alternatives in this desert climate area due to the scarcity of water sources, future studies may examine the impact of chosen trees typically found in desert areas on internal microclimate conditions and thermal outdoor comfort. Plants as *Albizia lebbbeck*, *Delonix regia*, and *Prosopis juliflora* are some of the prevalent drought-tolerant species that are efficient and can be used for environmental management.
- Human comfort is a multifaceted problem that incorporates physical, physiological, and psychological dimensions. An overview of available research highlighted significant differences in assessing comfort. It is still difficult to understand the actual human thermal sensation from the currently used thermal indices. Complementing energy-based techniques with adaptive techniques (social surveys) is required in future studies to better comprehend human comfort and eventually provide a widely relevant comfort evaluation tool.
- More links between the architectural and urban scales are highly recommended as urban buildings are mainly designed to handle indoor comfort in practice. A promising option would be to develop microscale numeric instruments that simultaneously evaluate the outdoor and indoor climate impacts of urban geometry (i.e., buildings' energy efficiency).
- Future investigations should shed light on reflected and lightweight materials on the roofs of buildings, streets, and wall facades as this plays a role in the outdoor thermal comfort. The material properties should also be investigated under this climate conditions in the relationship between thermal conductivity and human thermal comfort.

- Studying the relationship between density indicators and the reflected longwave radiation flux will provide more detailed insights on outdoor thermal comfort solutions.
- This thesis thus provided some basics for further studies and guidelines for design by proposing a new factor, the shading view factor, which will offer better layouts in urban design by including the human aspect of pedestrian comfort.

BIBLIOGRAPHY

A

Abu-Ghazzeah, T., 1994. Built form and religion: underlying structures of Jeddah Al-Qademah. *Tradit. Dwellings Settlements Rev.* V.

Abdulaal, W.A., 2012. Large urban developments as the new driver for land development in Jeddah. *Habitat International*, 36, 36-46.

Abreu-Harbich, L.V., Labaki, L.C., and Matzarakis, A., 2015. Effect of tree planting design and tree species on human thermal comfort in the tropics. *Landsc. Urban Plan.* 138, 99–109. <https://doi.org/10.1016/j.landurbplan.2015.02.008> .

Alharbi, T.H., 1989. The Development of Housing in Jeddah: Changes in Built Form from the Traditional to The Modern. Doctorial Study, University of Newcastle.

Ali-Toudert, F. 2000. Integration of the climate dimension in town planning. Magister's memory, EPAU, Algiers.

Ali-Toudert, F., & Mayer, H., 2006. Numerical study on the effects of aspect ratio and orientation of an urban street canyon on outdoor thermal comfort in hot and dry climate. *Building and Environment*, 41(2), 94–108. doi:10.1016/j.buildenv.2005.01.013

Asimakopoulos, D. N., Assimakopoulos, V. D., Chrisomallidou, N., Klitsikas, N., Mangold, D., Michel, P., Santamouris, M., Tsangrassoulis, A. 2001. Energy and climate in the urban built environment. James–James, London.

Al-Hathloul, S., and Mughal, M., 2004. Urban growth management—The Saudi experience. *Habitat International*, 28, 609–623

Al-Ajlan, S.A., Al-Ibrahim, A.M. Abdulkhaleq, M., and Alghamdi, F., 2006. Developing sustainable energy policies for electrical energy conservation in Saudi Arabia. *Energy Policy* 34, 1556-1565.

ATM., 2013. Observatori de la mobilitat. Barcelona, Area de Barcelona, Autoritat del Transport Metropolita.

Aljoufie, M., Zuidgeest, M., Brussel, M., and Van Maarseveen, M., 2013. Spatial-temporal analysis of urban growth and transportation in Jeddah City, Saudi Arabia. *Cities*, 31, 57-68.

Antoniou, J., 1981. *Islamic cities and conservation*. United Nations Educational, Scientific and Cultural Organization, 7 place de Fontenoy, 75700 Paris. Printed. <https://doi.org/10.1192/bjp.111.479.1009-a>

B

Batty, M., Besussi, E., & Chin, N., 2003. *Traffic, urban growth and suburban sprawl*. Retrieved from University College London website: http://www.casa.ucl.ac.uk/working_papers/paper70.pdf

Baik, A., & Boehm, J., 2017. Jeddah Heritage Building Information Modelling (JHBIM). *Heritage Building Information Modelling*, 132–153. <http://dx.doi.org/10.4324/9781315628011-11>.

Beckers, B., and Masset, L., 2006. *Heliodon2 Software and user's guide*. <http://www.heliodon.net>

Baik, A., & Boehm, J., 2017. Jeddah Heritage Building Information Modelling (JHBIM). *Heritage Building Information Modelling*, 132–153. <http://dx.doi.org/10.4324/9781315628011-11>.

Ben-Hamouche, M., 2009. Complexity of urban fabric in traditional Muslim cities: Importing old wisdom to present cities. *URBAN DESIGN International*, 14(1), 22–35. doi:10.1057/udi.2009.7

Beckers, B., 2012. *Solar Energy at Urban Scale*. ISTE-John Wiley.

Beckers, B., 2012. Worldwide aspects of solar radiation impact *in Solar energy at urban scale*, Hoboken: Wiley, .99-118

Besueievksy, G., Beckers, B., Patow, G., 2016. Skyline-control Based LoD Generation for Solar Analysis in 3D Cities. *First Int. Conf. Urban Phys.*, 32–44.

Bianca, S., 2000. *Urban form in the Arab world past and present*. Thames and Hudson, New York.

Bokhari, A., 1979. *Jeddah. A Study in Urban Formation*. Ph.D. Dissertation, University of Pennsylvania, Philadelphia

Brueckner, J. K., Mills, E., Kremer, M., 2001. "Urban Sprawl: Lessons from Urban Economics." *Brookings - Wharton papers on urban affairs*: 65-97.

Bruegmann, R., 2005. *Sprawl*. doi:10.7208/chicago/9780226076973.001.0001

Bottles, S. L., 1987. *Los Angeles and the automobile: The making of the modern city*. Berkeley, California, University of California Press.

Bokhari, A., 1979. *Jeddah. A Study in Urban Formation*. Ph.D. Dissertation, University of Pennsylvania, Philadelphia.

Burchell, R. W., Shad, N. A., Listokin, D., Phillips, H., & Downs, A., 1998. *Costs of sprawl revisited. Final report*. United States.

Burdett, R., Rode, P., 2012. The Electric City. Urban Age Electric City Conference. Burdett, R. and Rode, P. London, LSE Cities. London School of Economics.

C

Cadima, P., 2000. *Transitional Spaces: the potential of semi-outdoors spaces as a means for environmental control with special reference to Portugal*. Doctoral thesis (Environment Energy). Architectural Association Graduate School of London, Open University.

Costa, F., Noble, A., & Pendleton, G., 1991. Evolving planning systems in Madrid, Rome, and Athens. *GeoJournal*, 24(3). doi:10.1007/bf00189030

Coch, R.H., and Serra, F.R., 1995. *Arquitectura y energía natural* (I.). Barcelona: Edicions UPC.

Coch, H., & Serra, R., 1995. *Arquitectura y energía natural* (1st ed.; Universitat Politècnica de Catalunya, Ed.). Barcelona: Universitat Politècnica de Catalunya.

Cervero, R., 1998. *The transit metropolis: a global inquiry*. Washington DC, Island Press.

Coch, H., 1998. Bioclimatism in vernacular architecture. *Renewable and Sustainable Energy Reviews*, 2(1–2), 67–87. [https://doi.org/10.1016/s1364-0321\(98\)00012-4](https://doi.org/10.1016/s1364-0321(98)00012-4)

Coch, H., 2003. *La Utilitat dels Espais Inútils – una aportació a l'avaluació del confort ambiental a l'arquitectura dels espais intermedis*. Doctoral Thesis (Àmbitos de Investigación en la Energía y el Medio Ambiente en la Arquitectura). Universitat Politècnica de Catalunya (UPC).

Compagnon, R., 2004. Solar and daylight availability in the urban fabric. *Energy and Build.* Vol.36, 321–328.

Couch, C., Leontidou, L., & Petschel-Held, G., 2007. *Urban Sprawl in Europe: Landscapes, Land-Use Change and Policy*. Blackwell: London, UK. <https://doi:10.1002/9780470692066>

D

Daghistani, A., 1991. Urban growth management in Jeddah. *Planning Outlook*, 34

D'Onofrio, D., 2014. Understanding the regulatory environment of climate and the impact of community design on greenhouse gas emissions. Atlanta, GA, Atlanta Regional Commission.45

Duncan, G.O., 1987. *The planning and development of the city of Jeddah 1970-1984*. Unpublished PhD Thesis, University of Durham.

Dulac, J., 2013. Global land transport infrastructure requirements - Estimating road and railway infrastructure capacity and costs to 2050. Information paper. Paris, OECD/IEA.

E

EIA., 2001. Total Energy Consumption in US households by urban-rural location, 2001. Washington DC, US Department of Energy.

Elkabir, Y.A., 1983. The study of urbanization in the Arab world: a theoretical perspective. *Ekistics*, 50, 232-236.

Erell, E., Pearlmutter, D., & Williamson, T., 2012. *Urban Microclimate*. doi:10.4324/9781849775397

Erell, E., Pearlmutter, D., and Williamson, T.T.J., 2011. *Urban microclimate: designing the spaces between buildings*. Taylor & Francis, Abingdon.

Estiri, H., 2012. Residential Energy Use and the City-Suburb Dichotomy, University of Washington.

Ewing, R., 1997. Is Los Angeles-Style Sprawl Desirable? *Journal of the American Planning Association*, 63(1), 107–126. <https://doi:10.1080/01944369708975728>

Ewing, R., Bartholomew, K., Winkelman, S., Walters, J., Anderson, G., 2008. "Urban development and climate change." *Journal of Urbanism* 1(3): 201-216.

Ewing, R., 2008. Characteristics, Causes and Effects of Sprawl: A Literature Review. In *Urban Ecology an International Perspective on the Interaction Between Humans and Nature*, 1st ed. Springer USA: New York, NY, USA. https://doi:10.1007/978-0-387-73412-5_34

F

Faden, Y.M.O., 1977. *Urban Dwelling Environments: Jeddah, Saudi Arabia, in Architecture*. Massachusetts Institute of Technology. 86.

Fathy, H., 1986. 'Natural Energy and Vernacular Architecture: Principles and Examples with Reference to Hot Arid Climates', University of Chicago Press, Chicago and London.

Fathy, Hassan., 1971. ' Urban Arabic Architecture in the Middle East', lecture in Beirut university. (In Arabic).

Floater, G., Rode, P., Zenghelis, D., Montero Carrero, M., Smith, D. A., 2013. Stockholm: Green Economy Leader Report. London, LSE Cities - London School of Economics and Political Science.47

Floater, G., Rode, P., Zenghelis, D., Ulterino, M., Smith, D., Baker, K., Heeckt, C., 2014a. Copenhagen: Green Economy Leader Report. London, LSE Cities - London School of Economics and Political Science.

Foruzanmehr, A., 2017. Thermal Comfort in Hot Dry Climates. <https://doi.org/10.4324/9781315527130>

Frenkel, A., & Ashkenazi, M., 2008. Measuring Urban Sprawl: How Can We Deal with It? *Environment and Planning B: Planning and Design*, 35(1), 56–79. doi:10.1068/b32155

G

Galster, G., Hanson, R., Ratcliffe, M. R., Wolman, H., Coleman, S., & Freihage, J., 2001. Wrestling Sprawl to the Ground: Defining and measuring an elusive concept. *Housing Policy Debate*, 12(4), 681–717. <https://doi.org/10.1080/10511482.2001.9521426>

Gargiulo Morelli, V.; Salvati, L., 2010. *Ad Hoc Urban Sprawl in the Mediterranean City: Dispersing a Compact Tradition?* Nuova Cultura: Rome, Italy.

García-Nevado, E., 2019. *Termografía del cañón urbano. Uso de la perspectiva para una evaluación térmica global de la calle* (Universitat Politècnica de Catalunya). Retrieved from <http://hdl.handle.net/2117/132766>

Gehl, J., 2011. *Life between buildings: Using public space* (6th ed.; Island Press, Ed.). <https://doi.org/10.1016/j.eicb.2006.01.005>

Givoni, B., 1998. *Climate considerations in building and urban design*. Van Nostrand Reinhold, New York.

Giannakourou, G., 2005. Transforming spatial planning policy in Mediterranean countries: Europeanization and domestic change. *European Planning Studies*, 13(2), 319–331. doi:10.1080/0365431042000321857

Gibelli, M.C.; Salzano, E., 2006. *No Sprawl*; Alinea: Firenze, Italy.

Golany, G. 1982. *Design for arid regions*. Van Nostrand Reinhold, New York.

Golany, G. S., 1996. Urban design morphology and thermal performance. *Atmospheric Environment*, 30(3), 455–465. [https://doi.org/10.1016/1352-2310\(95\)00266-9](https://doi.org/10.1016/1352-2310(95)00266-9)

Goodwin, P., Hass-Klau, C., Cairns, S. (1998). “Evidence on the effects of road capacity reduction on traffic levels.” *Traffic Engineering+ Control* 39(6): 348-354.

H

Hakim, B. S., 1986. *Arabic-Islamic Cities: Building and Planning Principles*. London: KPI.

Hakim, B. S., 2001. Urban Form in the Arab World: Past and Present. *Cities*, 18(6), 426–427. doi:10.1016/s0264-2751(01)00036-1

Hawkes, D. – Foster, W. 2002. Energy efficient buildings, *Architecture, Engineering, and*

Environment. Norton, New York.

Hickman, R., Banister, D., 2014. *Transport, Climate Change and the City*, Routledge.

Höppe, P., 1999. The physiological equivalent temperature - a universal index for the biometeorological assessment of the thermal environment. *International Journal of Biometeorology*, 43(2), 71–75. doi:10.1007/s004840050118

Houghton, S. J., 1995. *18th Report of the Royal Commission on Environmental Pollution: Transport and the Environment*. Oxford, Oxford University Press.

I

IPCC., 2014a. *Climate Change 2014: Mitigation of Climate Change - Transport*. Working Group III: Mitigation of Climate Change. Potsdam, Intergovernmental Panel on Climate Change.

IPCC., 2014b. *Climate Change 2014: Mitigation of Climate Change - Human Settlements*. Working Group III: Mitigation of Climate Change. Potsdam, Intergovernmental Panel on Climate Change.

J

Jacobs, J., 1993. *The Death and Life of Great American Cities*, New York: Vintage Books.

Jaber, S., 2013. 'URBAN STREETS Towards Sustainable Mobility in Arabic Cities', 4 (19). <http://dx.doi.org/10.18419/opus-100>

Jeddah Municipality, 2004. *Jeddah structure plan*. Saudi Arabia: Jeddah Municipality.

Jeddah Municipality, 2006. *Transportation and traffic development plan*. Saudi Arabia: Jeddah Municipality, Aljoufie.

Jeddah Municipality, 2008. *Jeddah transportation urgent plan*. Okaz Daily, Electronic version. <<http://www.okaz.com.sa/okaz/osf/20080721/Con20080721211291.htm>> Accessed 05.08.11.

Jeddah Municipality, 2015, "The Jeddah Plan – Structural Plan", Volume 3

Jing, Z.; Zhentao, Z., 2007. Hierarchy Analysis and Strategies on the Imbalance between Supply and Demand of Urban Tra_c. *J. Transp. Syst. Eng. Inf. Technol.*, 7, 24–29.

Johansson, E., and Emmanuel, R., 2006. The influence of urban design on outdoor thermal comfort in the hot, humid city of Colombo, Sri Lanka. *Int J Biometeorol* 51, 119–133. doi:10.1007/s00484-006- 0047-6

K

Kapstein, G., 1988. *Espacios Intermedios – respuesta arquitectónica al medio ambiente: II Región*. Santiago de Chile: Universidad del Norte, Fundación Andes.

Kazepov, Y., 2005. *Cities of Europe: Changing Contexts, Local Arrangements, and the Challenge to Social Cohesion*. *Cities of Europe*, Blackwell: Oxford, UK, 3–42. <https://doi:10.1002/9780470694046.ch1>

Kersys, A., 2011. “Sustainable Urban Transport System Development Reducing Traffic Congestions Costs.” *Engineering Economics* 22(1): 5-13.

Khan, S.M., 1981. The influence of Arabian Tradition on the old city of Jeddah: The urban setting, in I. Serageldin and S. El-Sadek. (eds.). *The Arab City: Its Character and Islamic cultural heritage*, (Riyadh: The Arab Urban Development Institute), pp: 191-197.

Kiet, A., 2011. Arab Culture and Urban Form. *Focus*, 8(1). doi:10.15368/focus.2011v8n1.4

Knowles, R., 1981. *Sun Rhythm Form*, Cambridge, Massachusetts: The MIT Press

Krishan, A. 1996. The habitat of two deserts in India: hot-dry desert of Jaisalmer (Rajasthan) and the cold-dry high altitude mountainous desert of leh (Ladakh). *Energy and Buildings* 23. 217-229.

L

Lapidus, I. M., 1973. The Evolution of Muslim Urban Society. *Comparative Studies in Society and History*, 15(1), 21–50. <https://doi:10.1017/s0010417500006903>

Lee, I. Y., & Park, H. M., 1994. Parameterization of the pollutant transport and dispersion in urban street canyons. *Atmospheric Environment*, 28(14), 2343–2349. doi:10.1016/1352-2310(94)90488-x

Lefèvre, B., 2009. Urban transport energy consumption: Determinants and strategies for its reduction an analysis of the literature. *Sapiens*, 2,3.

Lewis-Lettington, Robert, Ayman El-Hefnawi, M.B., 2019. UN-Habitat: Future Saudi Cities Programme City Profiles Series: Jeddah. ISBN 9786038279298. FIX THE CAPITAL LETTERS

Lewis-Lettington, Robert, Ayman El-Hefnawi, M.B., 2019. UN-Habitat: Future Saudi Cities Programme City Profiles Series: Jeddah.

Lin TP, Matzarakis A, Hwang RL., 2010. Shading effect on long-term outdoor thermal comfort. *Building and Environment*, 45:213e21.

Liu, Y., Chen, T., Song, X., 2012. Relationship between Urban Form and Urban CO2 Efficiency with Policies and Recommendations.

Lovejoy, K., Handy, S., Mokhtarian, P., 2010. "Neighborhood satisfaction in suburban versus traditional environments: An evaluation of contributing characteristics in eight California neighborhoods." *Landscape and Urban Planning* 97(1): 37-48.

LSE Cities., 2014. Transport related carbon emissions in Atlanta and Barcelona: Updated comparative calculations. Working paper. London, LSE Cities.

Lynch, K., & Rodwin, L. 1958. A Theory of Urban Form. *Journal of the American Institute of Planners*, 24(4), 201–214. doi:10.1080/01944365808978281

M

Mayer, H., & Höppe, P., 1987. Thermal comfort of man in different urban environments. *Theoretical and Applied Climatology*, 38(1), 43–49. doi:10.1007/bf00866252

Mayer, H., 1993. Urban bioclimatology. *Experientia*, 49(11), 957–963. doi:10.1007/bf02125642

Matzarakis A., Mayer H., and Iziomon M.G., 1999. Applications of a universal thermal index:physiological equivalent temperature, *Int J Biometeorolo*, 43, 76–84.

Manville, M., Shoup, D., 2004. "People, parking and cities." *ACCESS Magazine*.

Marciotto, E. R., Oliveira, A. P., & Hanna, S. R.,2010. Modeling study of the aspect ratio influence on urban canopy energy fluxes with a modified wall-canyon energy budget scheme. *Building and Environment*, 45(11), 2497–2505. doi:10.1016/j.buildenv.2010.05.012

Masoud, B., Coch, H., Beckers, B., 2016. Sky Access versus Shading for Pedestrian Comfort in the Hot Tropical Climate of Jeddah. First international conference on urban physics, Quito-Galapagos.

Masoud, B., Coch, H., Crespo, I., Beckers, B., 2018. Effects of urban morphology on shading for Pedestrians Sky view factor (SVF) as an indicator of Solar Access. Passive and low energy architecture conference, Hong Kong.

Masoud, B., Coch, H., & Beckers, B., 2019. The Correlation Between Urban Morphology Parameters and Incident Solar Radiation Performance to Enhance Pedestrian Comfort, Case Study Jeddah, Saudi Arabia. *Smart Innovation, Systems and Technologies*, 543–554. doi:10.1007/978-981-32-9868-2_46

Mandeli, K., 2017. The significance of public open space to physical activity and prevention of obesity in Jeddah, Saudi Arabia. *Cities, communities and homes: Is the urban future livable*. UK22–23.

Morris, A.E.J., 1972. *History of Urban Form - Before the Industrial Revolutions*. 3rd Edition. Essex, U.K. & New York, USA. Longman Scientific & Technical.

Mubarak, F.A., 2004. Urban growth boundary policy and residential suburbanization: Riyadh, Saudi Arabia. *Habitat International*, 28, 567-591.

N

Nakamura, Y., & Oke, T. R., 1988. Wind, temperature and stability conditions in an east-west oriented urban canyon. *Atmospheric Environment* (1967), 22(12), 2691–2700. doi:10.1016/0004-6981(88)90437-4

National Research Council, 2009. *Driving and the Built Environment: The Effects of Compact Development on Motorized Travel, Energy Use, and CO2 Emissions -- Special Report 298*, The National Academies Press.

Nahon, R., Muñoz, D., and Beckers, B., 2016. *Heliodon Plus, 2016. Software and user's guide*. <http://www.heliodon.net>.

Newman, P., Kenworthy, J. R., 1989. *Cities and automobile dependence: a sourcebook*. Aldershot, Gower.

Neuman, M., 2005. The compact city fallacy. *Journal of Planning Education and Research*, 25(1), 11–26. <https://doi.org/10.1177/0739456X04270466>

O

OECD, 2012. *Compact City Policies: A Comparative Assessment*. OECD Green Growth Studies, OECD.

Oke, T. R., Kalanda, B. D., & Steyn, D. G., 1981. Parameterization of heat storage in urban areas. *Urban Ecology*, 5(1), 45–54. doi:10.1016/0304-4009(81)90020-6

Oke, T.R., 1988. Street design and urban canopy layer climate. *Energy and Buildings*, 11(1-3), pp.103–113.

Oke, T.R., 1987. *Boundary Layer Climates*. Methuen. London.

Olgay, V., 1963. *Design with climate: bioclimatic approach to architectural regionalism*. Princeton, N.J: Princeton University Press.

Oliveira, S., and Andrade, H., 2007. An initial assessment of the bioclimatic comfort in an outdoor public space in Lisbon. *International Journal of Biometeorology*, 52, 69e84.

Owens, S., 1995. "From 'predict and provide' to 'predict and prevent'? Pricing and planning in transport policy." *Transport Policy* 2(1): 43-49.

Owens, S., Cowell, R., 2011. *Land and limits: interpreting sustainability in the planning process*, Routledge.

P

Peel, M. C., Finlayson, B. L., McMahon, T. A. 2007. Updated world map of the Köppen-Geiger climate classification. *Hydrol. Earth Syst. Sci.* 11(5), 1636–1641

Pont, MB., and Haupt, P., 2012. *Spacematrix, Space, Density and Urban Form*. NAI Uitgevers ISBN 10: 9056627422.

Q

Qin, B., Han, S. S., 2013. “Planning parameters and household carbon emission: Evidence from high- and low-carbon neighborhoods in Beijing.” *Habitat International* 37: 52-60.

R

Ratti, C., Raydan, D., and Steemers, K., 2003. Building form and environmental performance: archetypes, analysis and an arid climate. *Energy Build*, 35, 49–59.

Rehman, S., Bader, M. A., & Al-Moallem, S. A., 2007. Cost of solar energy generated using PV panels. *Renewable and Sustainable Energy Reviews*, 11(8), 1843–1857. <http://dx.doi.org/10.1016/j.rser.2006.03.005>.

Rodrigue, J-P., 2006. *The Geography of Transport Systems*, First Edition, New York: Routledge. doi:10.4324/9780203884157

Rode, P., 2014. *The Politics and Planning of Urban Compaction: The Case of the London Metropolitan Region. The Economy of Sustainable Construction*. Ilka and Andreas Ruby, N. J. Berlin, Ruby Press.

Rode, P., Hoffmann, C., Kandt, J., Graff, A., Smith, D., 2014. *New Urban Mobility in London and Berlin*, LSE Cities and InnoZ.

S

Saqqaf, A. Y., 1987. *The Middle East City: Ancient Traditions Confront a Modern World*. Paragon House Publishers, New York.

Salagoor, J. Y., 1990. *The influence of building regulations on urban dwelling in Jeddah*. Ph.D. Thesis, University of New Castle Upon Tyne, UK

Santamouris, M., Papanikolaou, N., Koronakis, I., Livada, I., & Asimakopoulos, D., 1999. Thermal and air flow characteristics in a deep pedestrian canyon under hot weather conditions. *Atmospheric Environment*, 33(27), 4503–4521. doi:10.1016/s1352-2310(99)00187-9

Savy, M., 2012. Urban freight: a comprehensive approach. Urban Freight for Livable Cities, Gothenburg, Volvo Research and Education Foundation.

Shashua-Bar, L., Pearlmutter, D., & Erell, E., 2009. The cooling efficiency of urban landscape strategies in a hot dry climate. *Landscape and Urban Planning*, 92(3-4), 179–186. doi:10.1016/j.landurbplan.2009.04.005

Spronken-Smith, R., and Oke, T.R., 1999. Scale modelling of nocturnal cooling in urban parks. *Boundary Layer Meteorology*, 93, 287–312.

Squires, G., ed. 2002. Urban sprawl: Causes, consequences & policy responses. Washington, DC: Urban Institute Press.

Stemmers, K., Baker, N., Crowther, D., Dubiel, J., Nikolopoulou, M.H., and Ratti, C. 1997. City texture and microclimate. *Urban Des Stud*, 3, 25–50.

T

Thomas, R. 2003. Sustainable urban design: an environmental approach. Spon. London.

Tolmer, C.E., Castaing, C., Diab, Y., and Morand, D., 2013. *CityGML and IFC: Going further than LOD*. Proc. Digit. 2013 - Fed. 19th Int'l VSMM, 10th Eurographics GCH, 2nd UNESCO Mem. World Conf. Plus Spec. Sess. fromCAA, Arqueol. 2.0 al. 1, 645–648. <https://doi.org/10.1109/DigitalHeritage.2013.6743808>.

Torres-Quezada, J., 2018. *Comportamiento térmico de la cubierta en un clima cálido húmedo. Repercusión energética en el edificio* (Universitat Politècnica de Catalunya). Retrieved from <https://upcommons.upc.edu/handle/2117/125312>.

Tsai, Y. H., 2005. Quantifying urban form: Compactness versus “sprawl.” *Urban Studies*, 42(1), 141–161. <https://doi.org/10.1080/0042098042000309748>

U

UN Habitat, 2013. Planning and design for sustainable urban mobility: Global report on human settlements. United Nations Human Settlements Programme. New York, United Nations.

V

van Audenhove, F.-J., Kornichuk, O., Dauby, L., Pourbaix, J., 2014. The Future of Urban Mobility 2.0, Arthur D. Little and UITP.

Vigar, G., 2001. “Reappraising UK transport policy 1950–99: the myth of mono-modality ‘and the nature of ‘paradigm shifts.’” *Planning Perspectives* 16(3): 269-291.

W

World Bank., 2020a. Urban Population – Saudi Arabia. Retrieved June 28, 2020, from <https://data.worldbank.org/indicator/SP.URB.TOTL.IN.ZS?locations=SA>

World Bank., 2020b. Global Solar Atlas v2.3. Retrieved June 2020, from <https://globalsolaratlas.info/map>

W. Caves, R., 2005. *Encyclopedia of the City* (R. W. Caves, Ed.). New York: Routledge. Taylor & Francis Group.

Wheaton, W. C., 1998. "Land use and density in cities with congestion." *Journal of Urban Economics* 43(2): 258-272.

Wu, J., 2006. "Environmental amenities, urban sprawl, and community characteristics." *Journal of Environmental Economics and Management* 52(2): 527-547.

Y

Yin, S., & Xiao, Y., 2016. Scale Study of Traditional Shophouse Street in South of China Based on Outdoor Thermal Comfort. *Procedia Engineering*, 169, 232–239. doi:10.1016/j.proeng.2016.10.028

Yin, S., Lang, W., Xiao, Y., & Xu, Z., 2019. Correlative Impact of Shading Strategies and Configurations Design on Pedestrian-Level Thermal Comfort in Traditional Shophouse Neighbourhoods, Southern China. *Sustainability*, 11(5), 1355. doi:10.3390/su11051355

LIST OF FIGURES AND TABLES

INTRODUCTION

Figure 1. The world map showing the energy use per capita (Source: https://ourworldindata.org/grapher/per-capita-energy-use).....	13
Figure 2. Streets and pedestrian paths highlight where solar radiation penetrates for long hours (Source: http://www.metrojeddah.com.sa/).	14
Figure 3. Investigation Methodology.....	19

CHAPTER 1

Figure 1.1. Old compact urban form in the city of Tunis. (Source: https://arab-aa.com/2011/07/06/traditional-urban-fabric-in-the-arab-word-pic/).....	22
Figure 1.2. The Muslim city as a collection of homogenous areas (Source: Rapoport, 1977)	23
Figure 1.3. Old city of Erbil (ancient Arbela), example of the existing urban settlement types (Source: Morris, 1994).	24
Figure 1.4. The old city of Damascus. City example of the Greek and Roman planned origin types (left) (Source: Figure 1. https://archnet.org/authorities/3603/media_contents/96452). The street transformation process from the Roman colonnaded avenue to the later Islamic suqs (right) (Source: Bianca 2000, p.127, original Schoenauer, 1981).	24
Figure 1.5. Collector streets helping in breaking the way from the public areas to the residential quarters in Fez (left) (source: Bianca, 2000, p. 83). Saudi Arabia, AlQasim narrow streets, covered alleyways (right) (Source: Hakim, 1986).....	25
Figure 1.6. Old urban fabric of Riyadh city (Source: (left) Aina, et al. 2013 & (right) Al-Hemaidi, 2001).	26
Figure 1.7. Ghadames City, Libya (Source: Eltrapolsi and Altan 2017).....	26
Figure 1.8. Location of Jeddah on the Saudi Arabian map showing the latitude	27
Figure 1.9. Saudi Arabia on the world map highlighted in green	28
Figure 1.10. Classification of the BWh climate region (in red) (Source: Beck, 2018)	28
Figure 1.11. Temperature (Average maximum, Average and Average minimum), and average relative humidity of Jeddah city.	29
Figure 1.12. Comparison of the global solar radiation (Global-SR) (Airport station) (Source: http://www.meteonorm.com), with the simulated direct solar radiation (Direct-SR) (Heliodon2).....	30
Figure 1.13. Cloud coverage map satellite images Jun 2018 NASA (Source: https://earthobservatory.nasa.gov/global-maps/MODAL2_M_CLD_FR)	30
Figure 1.14. Monthly mean cloud cover (cloud cover %) (Heliodon plus cloud correction). compared with the temperature (Average maximum, Average and Average minimum), and average relative humidity of Jeddah city)	31
Figure 1.15. Stereographic (left) (Source: Masoud 2013) and isochronal solar figures for Jeddah (right) (Source: Heliodon software)	32
Figure 1.16. Orthophoto of Jeddah at different scales in 2021. (Source: Own elaboration based on Google Earth Pro).....	33
Figure 1.17. (A) The profile of the main commercial axis at the traditional district (Source: Osra, 2018) (B) the four main quarters. (C) Jeddah old urban maps on the and (Source: Historic Jeddah Municipality, Saudi Arabia, 2013, p. 241). And (D) 1938 aerial view of the Old City of Jeddah. (Source: Wikipedia. Retrieved May 2019)	34
Figure 1.18. Examples of Jeddah's old buildings showing the wooden extruded windows on the facades with different colors (from different Sources).....	35
Figure 1.19. The narrow street of old Jeddah city (AlBalad).....	36

Figure 1.20. Jeddah old area map (AlBalad). The dotted lines show the pedestrians paths (Source: Faden, 1977)	36
Figure 1.21. Examples of plazas highlighted in red lines on the left. On the right, the dotted lines demonstrate the path pattern of the pedestrian's walkways within the old area (Source: Alharbi, 1989)	37
Figure 1.22. Street orientation in AlBalad (left). Building heights in AlBalad (right)	37
Figure 1.23. Section samples of streets in the AlBalad layout without the projected windows (Rawashin)	38
Figure 1.24. The average Sky View Factor of the Streets and the different-oriented facades in the old compact layout (AlBalad)	40
Figure 1.25. AlBalad (the old layout) Sky View Factor (top) Sky View Factor orthograph projections some of the streets and plazas (bottom). (Source: Heliodon software)	41
Figure 1.26. Solar flux evolution of the horizontal surface (streets) for the old layout (AlBalad) with a maximum and a minimum in summer 21st June and winter 21st. December	42
Figure 1.27. AlBalad (the old layout) Solar radiation time interval on all street orientations.....	43
Figure 1.28. AlBalad (the old layout) summer, 21st of June, solar radiation time interval (sun period). Source: Heliodon software	44
Figure 1.29. AlBalad (the old layout) winter, 21st of December, solar radiation time interval (sun period). Source: Heliodon software	45
Figure 1.30. Summer and winter solar flux and the average sky view factor of streets and facades in the old compact layout (AlBalad).....	46
Figure 1.31. AlBalad (the old layout) summer, 21st of June, solar flux. (Source: Heliodon software)	47
Figure 1.32. AlBalad (the old layout) winter 21st of December, solar flux. Source: Heliodon software.....	48
Figure 1.33. Summer and winter solar flux and the average SVF of the streets and the different-oriented facades (AlBalad)	49
Table 1.1 (Latitude 21.32' N) Jeddah correction Factor Heliodon.....	31
Table 1.2 Jeddah meteorological cloud data from Meteoronorm (an okta is a unit of measurement of cloud)	31
Table 1.3 Sunrise, Sunset, and solar height at noon for 21st June and 21st December.....	32
Table 1.4 List of solar radiation indicators.....	39

CHAPTER 2

Figure 2.1. Riyadh, Saudi Arabia urban Sprawl (right) (Source: http://www.thereviewanddebatesatnyu.com/all/2016/4/27/l8isp66tz74in1sym27v4fc8ilup5g) Riyadh Satellite map (left) (Source: Google earth).....	52
Figure 2.2. Urban Sprawl of American cities as an example of Cape Coral in Florida. (Source: https://www.theguardian.com/cities/2017/apr/19/where-world-most-sprawling-city-los-angeles)..	53
Figure 2.3. Physical Patterns Defining Sprawl (Source: Galster et al., 2001)	54
Figure 2.4. Map showing the location of the historical city of Jeddah (Source: Jeddah Municipality, 2013, Jeddah Strategic Plan, Introduction, 16. Google Earth 2013. Jeddah)	55
Figure 2.5. Jeddah spatial-temporal changes (Source: Aljoufie et al., 2013)	56
Figure 2.6. Transitional urban development of Jeddah city	57
Figure 2.7. Transitional urban layout samples of Jeddah city (Source: Alharbi, 1987)	58
Figure 2.8. Transitional gridiron pattern of Al Nuslah and Al Sharqiah. (Source: Alharbi, 1987) ..	59
Figure 2.9. Jeddah transitional urban morphology. The dotted lines show the pedestrians paths (Source: Faden, 1977).....	59

Figure 2.10. Jeddah city map showing in blue the Highways and the main roads in red. (Source: Aljoufie, 2012)	60
Figure 2.11. Modern urban layout morphology showing different street levels. The dotted lines show the pedestrians paths (left). The gridiron pattern of Jeddah (right) (Source: Faden, 1977). 61	
Figure 2.12. distribution of population density in Jeddah City (Source: Ministry of Municipal and Rural Affairs King Fahd National Library, UNHabitat, 2019)	62
Figure 2.13. Types of urban morphologies that exist in Jeddah City.	64
Figure 2.14. Jeddah map showing the different streets orientations. Red lines: North-South street-orientation axis, blue lines: East-West, green lines: Northwest-Southeast, and orange: Northeast-Southwest	65
Figure 2.15. Mid- rise buildings area (AlSalamah), Case A (left). Map of the low-rise buildings area of Jeddah (Obhur AlShamalya), Case B (right).....	66
Figure 2.16. The case study Alsalamah Mid-rise buildings layout Case A (Source: Google Earth)	68
Figure 2.17. The Mod-rise layout of Jeddah (AlSalamah) schematic drawings in 500m x 500m sections and plans. (Source: Author elaboration)	69
Figure 2.18. The pictures show the actual streets of the layout of Case A	69
Figure 2.19. The case study Obhur AlShamalyah Low-rise buildings layout Case A (Source: Google Earth)	70
Figure 2.20. The contemporary area of Jeddah (Obhur AlShamalya) in 500m x 500m sections and plans.	71
Figure 2.21. The picture shows the actual streets of the layout of Case B. (Source: Author elaboration)	71
Figure 2.22. Solar flux evolution of the horizontal surface (streets) for the two layouts with a maximum and a minimum in summer 21st June and winter 21st. December	72
Figure 2.23. Case A: Sky View Factor distribution on streets. The different colored asterisks on the map are used to illustrate examples of the SVF for that particular point with the orthographic projection. (Source: Heliodon software)	74
Figure 2.24. Case A: Solar radiation time interval on the two street orientations	75
Figure 2.25. Case A: summer, 21st of June, solar radiation time interval (sun period). Source: Heliodon software	76
Figure 2.26. Case A: winter, 21st of December, solar radiation time interval (sun period). Source: Heliodon software	76
Figure 2.27. Case A: average solar flux and SVF on the different street orientations and facades	78
Figure 2.28. Case A: summer, 21st of June, solar flux. Source: Heliodon software.....	79
Figure 2.29. Case A: summer, 21st of December, solar flux. Source: Heliodon software	79
Figure 2.30. Case B: Sky view factor distribution on streets. The different colored asterisks on the map are used to illustrate examples of the SVF for that particular point with the orthographic projection. Source: Heliodon software.....	81
Figure 2.31. Case B: Solar radiation time interval on the two street orientations	82
Figure 2.32. Case B: summer, 21st of June, solar radiation time interval (sun period). Source: Heliodon software	83
Figure 2.33. Case B: summer, 21st of December, solar radiation time interval (sun period). Source: Heliodon software	83
Figure 2.34. Case B: average solar flux and sky view factor (SVF) on the streets and facades ...	84
Figure 2.35. Case B: summer, 21st of June, solar flux. Source: Heliodon software	85
Figure 2.36. Case B: winter, 21st of December, solar flux. Source: Heliodon software	85

Figure 2.37. Summer and winter solar flux and the average SVF of the streets and the different-oriented facades in Case A	86
Figure 2.38. Summer and winter solar flux and the average SVF of streets and the different-oriented facades in Case B	87
Table 2.1. Average solar flux, H/W ratio, and SVF on each street orientation in Case A	77

CHAPTER 3

Figure 3.1. Future infrastructure scheme: the idea of a multifunctional urban ecology of horizontal and vertical transport (Tottenham Court Road station – London) (Source: Global Schindler Award 2015)	90
Figure 3.2. Urban form and modal share (black in pie chart is private motorized) of selected cities (Source: concept and information design based on Sorensen and Hess 2007)	92
Figure 3.3. Population density and transport energy use per capita for selected cities (left) (Source: WHO 2011). Emissions per passenger km by urban transport mode (right) (Source: STF 2014)	94
Figure 3.4. Average urban densities in large cities and average carbon emission per capita (Source: Angel 2012)	95
Figure 3.5. Drivability to the commercial city centers (Source: UN-HABITAT 2019)	97
Figure 3.6. Walking accessibility to the city centers (Source: UN-HABITAT 2019)	98
Figure 3.7. Jeddah public transportation Master Plan (Source: http://www.metrojeddah.com.sa/).	99
Figure 3.8. Phases of proposed transportation system (metro lines) (Source: UN-HABITAT 2019)	101
Figure 3.9. Jeddah's unbalanced growth and development patterns (Source: UN-HABITAT 2019)	104

CHAPTER 4

Figure 4.1. An oasis in a desert.....	106
Figure 4.2. Transitional spaces examples.....	107
Figure 4.3. Solar control through self-shading facade in a hot-dry climate (Krishan, 1996)	108
Figure 4.4. Spatial and temporal distribution of the thermal index PET at street level in an asymmetrical urban canyon with galleries and overhanging facades for E-W and N-S orientations, typical summer day (1st August) in Ghardaia, Algeria (32.40° N, 3.80° E)	110
Figure 4.5. The maximum daytime PET (at 14:00 h) as a function of the H/W ratio (Source: Johansson and Emmanuel, 2006)	111
Figure 4.6. Effect of shade on the maximum PET (at 14:00 h) in an E-W-oriented canyon (Source: Johansson and Emmanuel, 2006)	111
Figure 4.7. The PET of the different measuring points (Source: Yin and Xiao, 2016)	112
Figure 4.8. The comparison results of the direct solar radiation in canyon with and without the textile (Source: Coch and Garcia, 2018)	113
Figure 4.9. The comparison between the results from measurement and simulation in different street canyons: (a) Alley, (b) Arcade and (c) Boulevard (Source: Yin et al., 2019)	114
Figure 4.10. The Compact City: Consolidating and densifying Jeddah's development	116
Figure 4.11. Action 2: Foster densification around major nodes and transport lines (TOD)	118

CHAPTER 5

Figure 5.1. Characteristics of the two geometric hypothetical studies for the old (AlBalad) and the modern (AlSalamah) layout	123
Figure 5.2. SVF plan of Jeddah old area (AlBalad) showing the four zoomed-in street selections (left). The selected analyzed streets from the layout (right)	125
Figure 5.3. Solar flux in Case A with (bottom) or without (top) applying Rawashin	126
Figure 5.4. The amount of solar flux in an N-S street: comparison of the street with and without the Rawashin. The circles on the top indicate the street projection (stereograph and orthograph) with and without the Rawashin, whereas the bottom pictures show the solar flux without (left) or with Rawashin (right) highlighting the three different Points A, B, and C.....	128
Figure 5.5. The amount of solar flux in an E-W street. Comparison of the street with (bottom) and without (top) the Rawashin (R)	130
Figure 5.6. Heliodon Plus simulations on the East-West street without applying the Rawashin .	131
Figure 5.7. Heliodon Plus simulations comparing the East - West street with and without applying the Rawashin.	132
Figure 5.8. Trace of the Heliodon Plus simulations of direct solar radiation of the East-West street with (black line) and without (red line) applying the Rawashin.....	133
Figure 5.9. The amount of solar flux in an NW-SE street. Comparison of the street with (bottom) and without (top) the Rawashin	134
Figure 5.10. The amount of solar flux in an NE-SW street. Comparison of the street with (left) and without (right) the Rawashin. The red boxes indicate the two highlighted areas Point A and B..	135
Figure 5.11. The Sky View Factor, the red circle is the receptor point.....	136
Figure 5.12. The shading view factor vs. the sky view factor, the red circle is the receptor point	137
Figure 5.13. The horizontal shading element (left) and the vertical shading element (right) showing the sky view factor vs. the shading view factor. The red dot is the receptor, the marked black lines show the shading view factor angles, and the red lines the amount of the visible sky	137
Figure 5.14. Explanation of the shading view factor that is contrary to the sky view factor.....	138
Figure 5.15. The amount of shading view factor versus the amount of sky view factor. The red circle represents the receptor under the horizontal shading element.	138
Figure 5.16. The different amounts of shading view factor from one receptor to another in different locations. The red circles represent the receptors and their different locations numbered from 1 to 3	139
Figure 5.17. The different amounts of shading view factor from one receptor to another in different locations. The red circles represent the receptors and their different locations numbered from 1 to 3	139
Figure 5.18. The relationship between the shading view factor and the location of the receptor on the horizontal surface. The red circles demonstrate different points on the pedestrian walkway	140
Figure 5.19. The relationship between the shading view factor and the location of the receptor on the horizontal surface. The red circles demonstrate different points on the pedestrian walkway.	140
Figure 5.20. Case A: the existing urban layout (above), showing the building heights and the applied proposal represented in the dotted square. The pictures at the bottom show the actual streets of the layout.	142
Figure 5.21. Overhanging facades description of both series	143

Figure 5.22. The studied urban layout of Case A, showing the simulated surfaces under the overhanging facades.	144
Figure 5.23. Overhanging facade series 1 on an E-W street, θ 22° NOVHF, the orthographic projection is in blue and the stereographic projection in red (right) with sections of the streets showing the overhanging facade dimensions (left)	145
Figure 5.24. Overhanging facade series 1: θ 22° SOVHF. The orthographic projection is in blue (left) and the stereographic projection in red (right)	146
Figure 5.25. Overhanging facade series 1: NOVHF representing the three geometries on an orthographic projection in blue (left) and stereographic projection in red (right)	147
Figure 5.26. Shading view factor (SHVF) of the overhanging facade series 1 and 2 of the NOVHF representing the three geometries represented by θ in Table 6.4 of each series on the stereographic and orthographic projection series 1 (left) and series 2 (right)	148
Figure 5.27. Average shading view factor of series 1 and 2 of all overhanging facades on the horizontal surface (pedestrian walkway)	149
Figure 5.28. Received direct solar flux on the 21st of June of the overhanging facades on the horizontal surface (pedestrian walkways) of WOVHF (W) and EOVHF (E)	151
Figure 5.29. Received direct solar flux on the 21st of Dec, on the horizontal surface (pedestrian walkways) of the WOVHF (W) and EOVHF (E)	152
Figure 5.30. Overhanging facades: received direct solar flux on the 21st of June and its correlation to the average SHVF on the horizontal surface (pedestrian walkways) (WOVHF (W) and EOVHF (E))	153
Figure 5.31. Comparison of the received direct solar flux on the 21st of June and on the 21st of December between the overhanging facades on the horizontal surface (pedestrian walkways) for WOVHF (W) and EOVHF (E) and the existing street geometry in Case A.	154
Figure 5.32. Received direct solar flux on the 21st of June of the overhanging facades on the horizontal surface (pedestrian walkways) of NOVHF (N) and SOVHF (S)	155
Figure 5.33. Received direct solar flux on the 21st of December of the overhanging facades on the horizontal surface (pedestrian walkways) of NOVHF (N) and SOVHF (S)	156
Figure 5.34. Overhanging facades: received direct solar flux on the 21st of June and its correlation to the average SHVF on the horizontal surface (pedestrian walkways) for NOVHF (N) and SOVHF (S)	157
Figure 5.35. Comparison of the received direct solar flux on the 21st of June and on the 21st of December between the overhanging facades on the horizontal surface (pedestrian walkways) (NOVHF (N) and SOVHF (S)) and the existing street geometry in Case A	158
Figure 5.36. Received direct solar flux in EOVHF (E) and WOVHF (W) for θ 22°, θ 34°, and θ 45°	160
Figure 5.37. Received direct solar flux in NOVHF (N) and SOVHF (S) for θ 22°, θ 34°, and θ 45°.	161
Figure 5.38. Received direct solar flux on the E-W street in the old area Jeddah demonstrating the results of the street before and after applying the Rawashin	163
Figure 5.39. Designed by Oscar Niemeyer and Hélio Uchôa, Biennale Pavilion, São Paulo, Brasil, 1957. The overhanging facade clearly shows the shading view factor effect.	164
Figure 5.40. Designed by Le Corbusier, Palace of Assembly, Chandigarh, India, 1951. The designed shading element protecting the different entrances of the building: people can move from one access to another under the overhanging facade.....	164
Figure 5.41. Designed by Marcel Breuer, Whitney Museum of American Art, New York, 1966. The overhanging facade of the building protects pedestrians from solar radiation. (Source: Photographer Ezra Stoller)	166

<i>Figure 5.42. Designed by Lúcio Costa, Oscar Niemeyer, Affonso Reidy, and Carlos Leão, Education and Health Ministry building, Rio de Janeiro, Brazil, 1940.....</i>	<i>167</i>
<i>Figure 5.43. Designed by Carlos Cascaldi, College of Architecture and Urbanism, Sao Paulo, Brazil, 1961. A massive overhanging facade protects the entrance of the building.....</i>	<i>167</i>
<i>Figure 5.44. Received direct solar flux on the WOVHF orientation on the pedestrian street before applying and after the OVHF in summertime (right) and wintertime (left).....</i>	<i>168</i>
<i>5.45. Received direct solar flux on the EOVHF orientation on the pedestrian street before and after applying the OVHF in summertime (right) and wintertime (left)</i>	<i>169</i>
<i>Figure 5.46. Received direct solar flux on the NOVHF orientation on the pedestrian street before and after applying the OVHF in summertime (right) and wintertime (left).....</i>	<i>169</i>
<i>Figure 5.47. Received direct solar flux on the SOVHF orientation on the pedestrian street before and after applying the OVHF in summertime (right) and wintertime (left)</i>	<i>170</i>
<i>Table 5.1. Abbreviations of the hypothetical geometry</i>	<i>122</i>
<i>Table 5.2 Heliodon plus correction factor of each month.....</i>	<i>132</i>
<i>Table 5.3. Shading view factor of the overhanging facades geometry represented by θ</i>	<i>149</i>

APPENDIX

CONTENT

APPENDIX 1	207
1.1 Table Summary Meteorological Data.....	207
1.2 Cloud Correction Factor.....	208
APPENDIX 2	214
2.1 Geometric Level of Details and Solar Radiation.....	214
2.2 Density indicator for the urban spaces calculation	215
2.3 Old Jeddah Urban Building Height References.....	219
2.4 Canyons and Streets Simulations Tables	225
2.5 Facade Simulations	228
2.6 Three Layouts: Average Solar Flux Received on Streets and Facades	254
APPENDIX 3	256
3.1 HELIODON 2 Summary Simulation of the Canyon Orientations with and without Rawashin	256
3.3 HELIODON PLUS Summary Simulation of the Canyon Orientations with and without Rawashin	259
3.4 Overhanging Facade Simulation Series 1	262
3.5 Overhanging Facade Stereograph Series 2.....	267

APPENDIX 1.

1.1 TABLE SUMMARY METEOROLOGICAL DATA

Table 1. Jeddah: Metrological data. Gh: Mean irradiance of global radiation horizontal, Bn: Irradiance of beam, Dh: Mean irradiance of diffuse radiation horizontal, N: Cloud cover fraction, Lg: Global luminance, Ta: Air temperature RH: Relative humidity: Dewpoint temperature DD: Wind direction, FF: Wind speed p: Air pressure.

Month	G_Gh	G_Bn	G_Dh	Lg	Ld	N
	[W/m2]	[W/m2]	[W/m2]	[W/m2]	[W/m2]	[octas]
Jan	170	170	73	18680	9866	4
Feb	217	226	77	23505	10487	2
Mar	267	270	81	28983	11204	2
Apr	301	292	85	33108	11724	2
May	305	263	108	33721	15509	0
Jun	284	209	127	31534	18606	2
Jul	272	196	127	30356	18384	2
Aug	269	188	124	30090	18193	1
Sep	263	230	99	29612	14774	1
Oct	240	249	75	26807	10957	2
Nov	191	206	69	21081	9592	3
Dec	163	173	68	17884	9051	4
Year	245	222	93	27114	13195	2
Month	Ta	Td	RH	p	DD	FF
Month	[C]	[C]	[%]	[hPa]	[deg]	[m/s]
Jan	25.0	19.9	73	1013	360	0.9
Feb	23.5	15.8	62	1012	360	1.0
Mar	25.1	16.9	60	1012	360	0.9
Apr	27.6	19.4	61	1012	360	0.8
May	29.6	21.2	61	1013	338	0.8
Jun	30.8	22.5	62	1013	360	0.8
Jul	32.4	23.0	58	1013	360	0.7
Aug	32.1	24.1	63	1012	338	0.9
Sep	30.7	24.5	70	1013	360	0.8
Oct	29.1	22.4	67	1012	360	0.6
Nov	27.0	19.6	64	1013	360	0.5
Dec	24.7	16.3	59	1013	360	0.5
Year	28.1	20.5	63	1013	356	0.8

Table 1 shows the climatological data recorded from the Jeddah meteorological station, which is located at the Airport, the Temperature: during the period from 1996-2005, Radiation: New period = 1998-2002. The data was collected from METEONORM Version 6.1.0.23.

1.2 CLOUD CORRECTION FACTOR

The effect of clouds is important in assessing how much solar radiation is received in a city during the day, as the earth is heated by the sun. If skies are clear, more heat reaches the earth's surface. This leads to higher temperatures. However, if skies are cloudy, some of the sun's rays are reflected off the cloud droplets back into space. Therefore, less of the sun's energy is able to reach the earth's surface, which causes the earth to heat up more slowly. This leads to cooler temperatures. When forecasting daytime temperatures, if cloudy skies are expected, lower temperatures are forecasted than one would predict if clear skies were expected.

At night, cloud cover has the opposite effect. If skies are clear, heat emitted from the earth's surface freely escapes into space, resulting in colder temperatures. However, if clouds are present, some of the heat emitted from the earth's surface is trapped by the clouds and remitted back towards the earth. As a result, temperatures decrease more slowly than if the sky was clear.

To determine the presence of clouds, the theoretical energy data obtained by Heliodon are compared with the real data measured by the local meteorological station and a correction factor is established. Seeing the difference between the theoretical and measured values of direct radiation, I proceed to establish a correction factor with the following formula:

Solar radiation calculated from the measured value.

$$\text{Correction factor} = \frac{\text{Solar radiation calculated from the measured value.}}{\text{Solar radiation calculated by Heliodon.}}$$

Thus, the following correction factor can be established on a percentage basis month by month. To obtain the values, the Heliodon Plus application (Nahon, 2016) is used, which through these three input elements allows to calculate a correction factor for the energy values in order to take into account the meteorology of the study area, leaving a figure closer to reality than would be given assuming the sky is always clear.

The table which can be attributed to this factor displays the cloud correction factor calculated all year round for Jeddah city by the software **HELIODON PLUS** (<http://www.heliodon.net/>) using meteorological data of each city from **METEONORM** (<http://www.meteonorm.com>).

In the following tables, the lower the value, the more clouds there are in that month. Months highlighted blue have a higher cloud coverage and could be considered the least favorable months to emit heat from the earth's surface in hot climate cities to cool the surface. On the other hand, in cold climate cities, it is favorable to have high cloud coverage to trap the heat emitted from the earth's surface, thereby retaining the heat at the surface. The months highlighted red have the lowest cloud coverage.

Table 2 Jeddah (Latitude 21.3 N) correction factor by Heliodon Plus.

Months	Jan	Feb	Mar	Apr	May	Jun	Jul	Aug	Sep	Oct	Nov	Dec
Correction	0.59	0.78	0.84	0.82	0.72	0.57	0.53	0.53	0.69	0.82	0.74	0.66

Table 3 Jeddah Metrological cloud data from Meteonorm.

Months	Jan	Feb	Mar	Apr	May	Jun	Jul	Aug	Sep	Oct	Nov	Dec
OCTAS	4	2	2	2	0	2	2	1	1	2	3	4

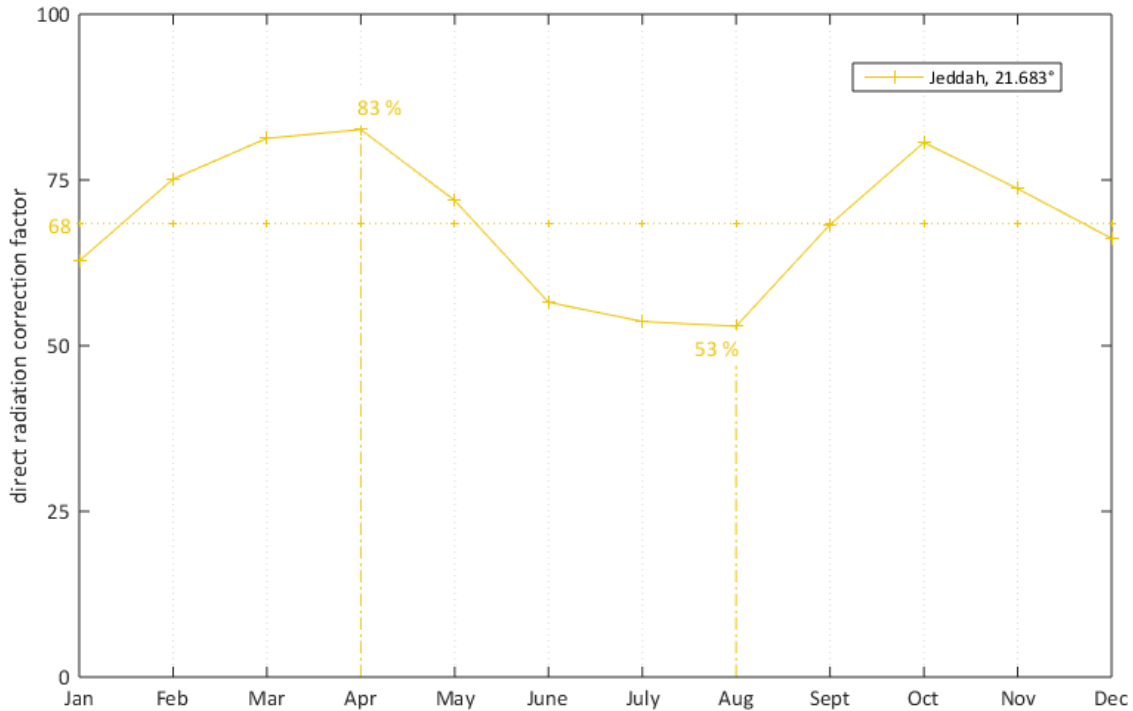


Figure 1. Correction factor for radiation values according to the presence of clouds in Jeddah

Clearly, the months of July and August are those that have more presence of clouds (53% correct on the theoretical calculation of direct solar radiation), while March is the least cloudy month (84% of the theoretical calculation). The annual mean cloud presence would then be 69%.

The attribute table displays clouds correction factor calculated all year round for different cities (Jeddah – Saudi Arabia, Barcelona, Paris, London, and Montreal - Canada) by the software HELIODON PLUS (<http://www.heliodon.net/>) using meteorological data of each city from METEONORM (<http://www.meteonorm.com>).

In the following tables, the lower the value, the more clouds are present in that month. Months (highlighted blue) have a higher cloud coverage and could be considered the lowest favorable months to emit heat from the earth’s surface in hot climate cities to cool the surface. On the other hand, in cold climate cities it is favorable to have high cloud coverage to trap the emitted heat from the earth's surface to heat the surface. Moreover, the months (highlighted red) have the low cloud coverage.

Paris-France.

Table 4 Paris (Latitude 48.8 N) correction factor by Heliodon Plus.

Months	Jan	Feb	Mar	Apr	May	Jun	Jul	Aug	Sep	Oct	Nov	Dec
Correction	0.28	0.21	0.27	0.35	0.36	0.29	0.31	0.42	0.41	0.35	0.47	0.21

Table 5 Paris metrological cloud data from Meteonorm.

Months	Jan	Feb	Mar	Apr	May	Jun	Jul	Aug	Sep	Oct	Nov	Dec
OCTAS	7	7	7	6	6	6	6	5	6	6	6	7

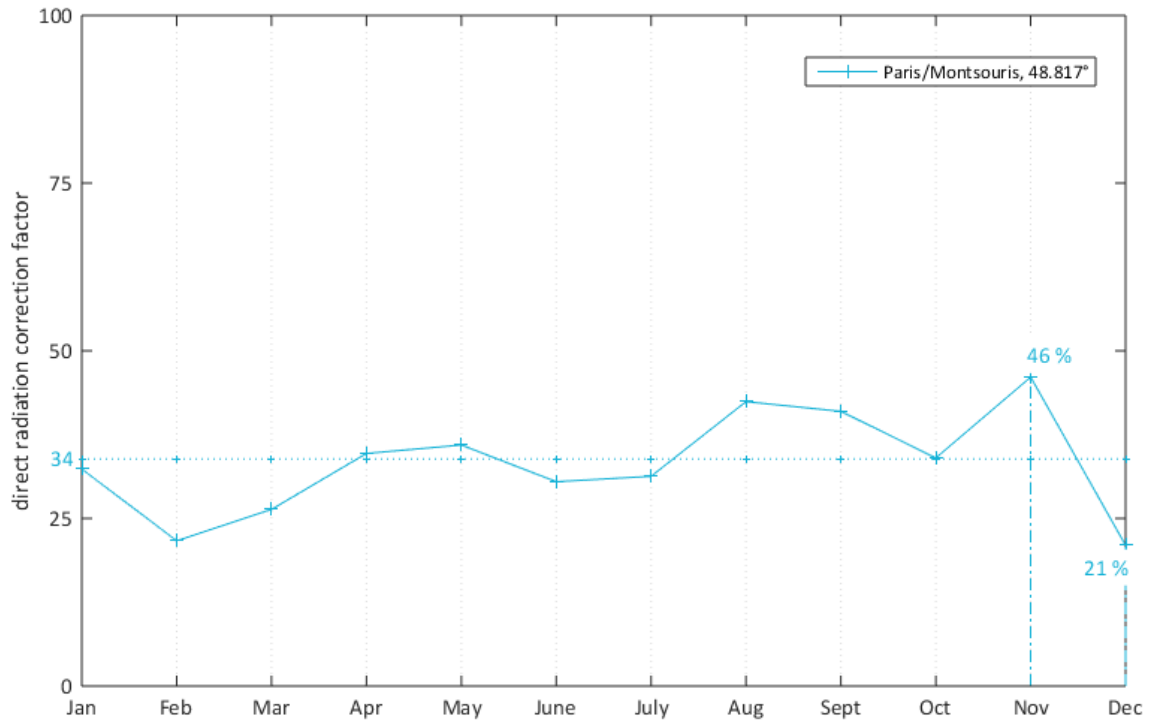


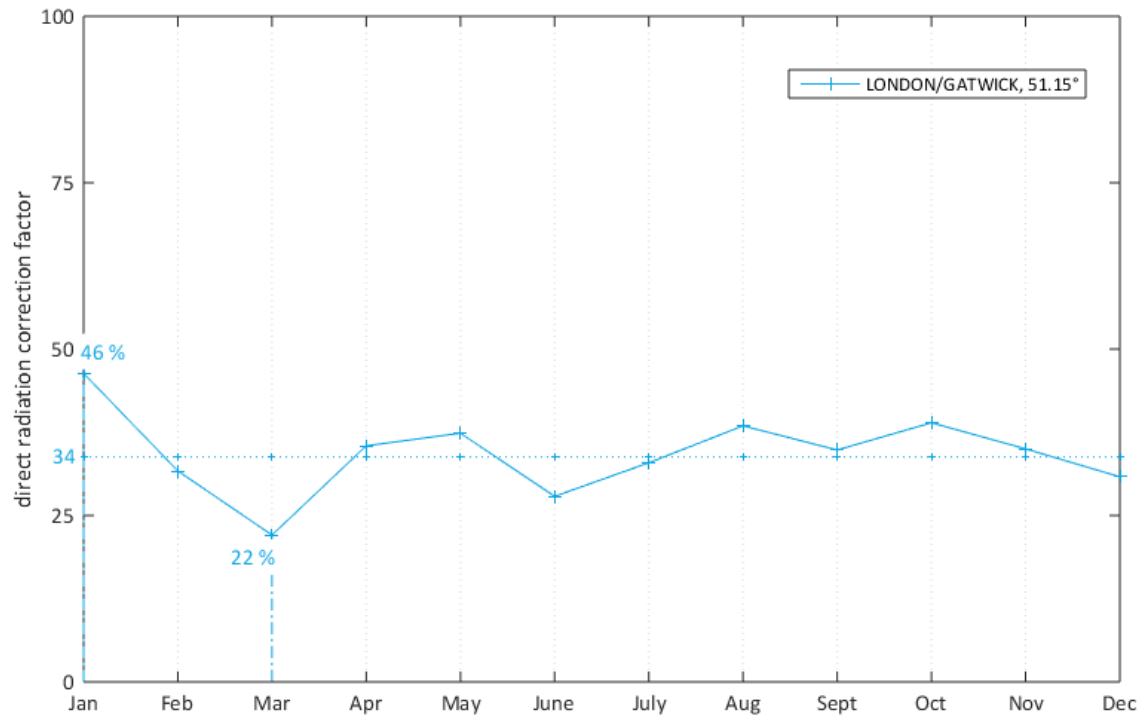
Figure 2. Correction factor for radiation values according to the presence of clouds in Paris.

At first glance, there is a high presence of clouds in Paris, even in the summer months. In winter, the correction factor reaches 21% in December and February being the coldest months. And between 29% - 31% in June and July, the month with the least presence of clouds is with 35% October. The average annual presence of clouds would be in this case 32.75%.

London.**Table 6** London (Latitude 51.5 N) correction factor by Heliodon Plus.

Months	Jan	Feb	Mar	Apr	May	Jun	Jul	Aug	Sep	Oct	Nov	Dec
Correction	0.45	0.36	0.22	0.35	0.37	0.27	0.33	0.38	0.37	0.41	0.38	0.32

London meteorological data were taken from energy plus software.

**Figure 3.** Correction factor for radiation values according to the presence of clouds in London.

It is observed in London that the month of January has less presence of clouds (45% correct on the theoretical calculation of direct solar radiation), while March is the coldest month (35% of the theoretical calculation). The annual mean cloud presence would then be 44.75%.

Barcelona.

Table 7 Barcelona (Latitude 41.3 N) correction factor by Heliodon Plus.

Months	Jan	Feb	Mar	Apr	May	Jun	Jul	Aug	Sep	Oct	Nov	Dec
Correction	0.89	0.77	0.76	0.63	0.64	0.58	0.72	0.63	0.58	0.68	0.67	0.84

Table 8 Barcelona Metrological cloud data from Meteonorm.

Months	Jan	Feb	Mar	Apr	May	Jun	Jul	Aug	Sep	Oct	Nov	Dec
OCTAS	5	3	4	4	3	4	3	4	5	4	5	5

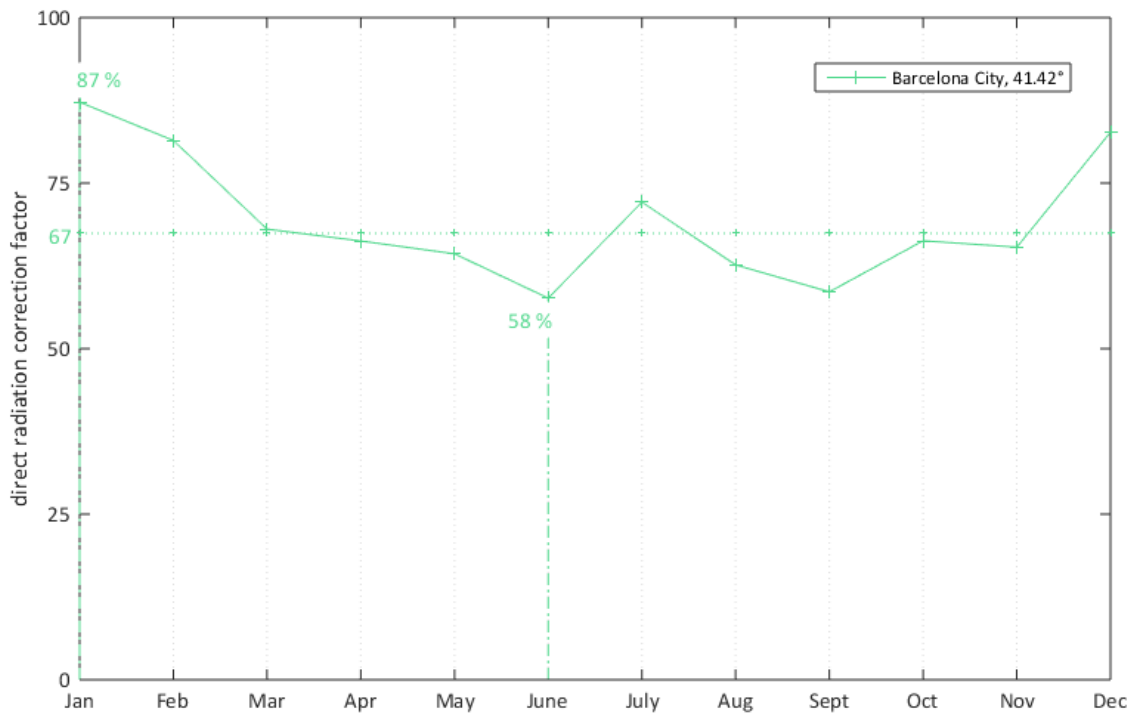


Figure 4. Correction factor for radiation values according to the presence of clouds in Barcelona.

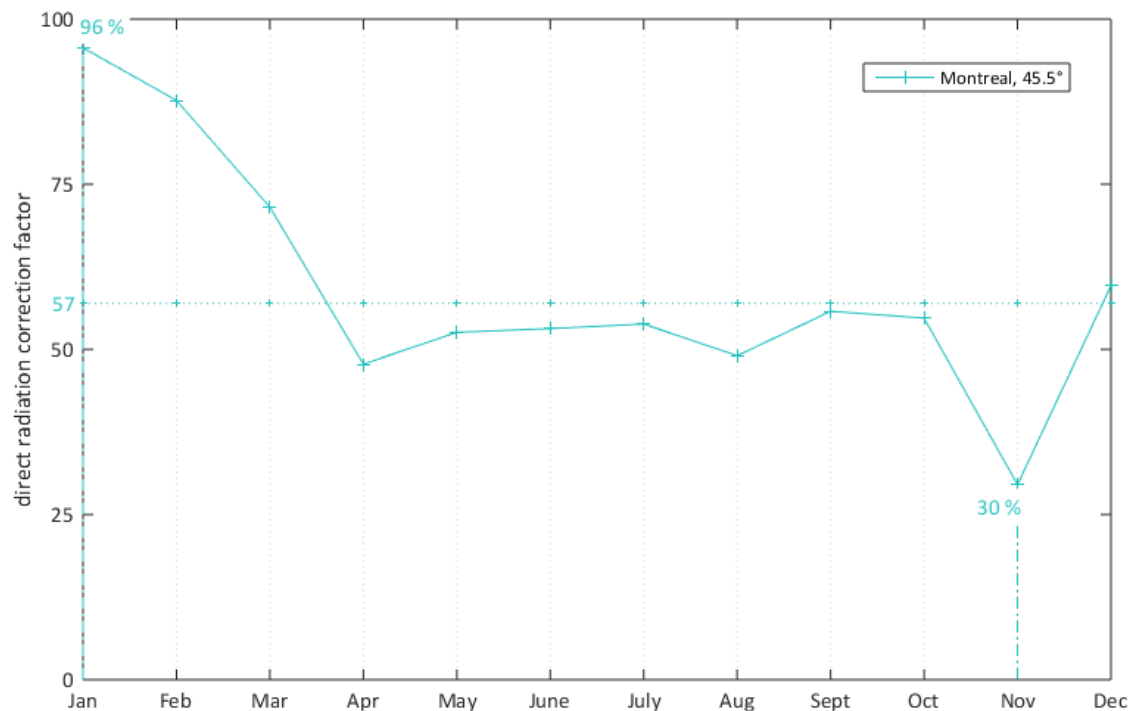
At the first glance of the tables has Barcelona less presence of clouds. In winter, the correction factor reaches between 84% and 89% in December and January. In summer 58% in June, with the months being the cloudiest in June and September. The average annual presence of clouds would be in this case 69.91%.

Montreal.**Table 9** Montreal (Latitude 45.5 N) correction factor by Heliodon plus.

Months	Jan	Feb	Mar	Apr	May	Jun	Jul	Aug	Sep	Oct	Nov	Dec
Correction	0.96	0.93	0.73	0.48	0.52	0.51	0.54	0.49	0.59	0.56	0.31	0.60

Table 10 Montreal metrological cloud data from Meteonorm.

Months	Jan	Feb	Mar	Apr	May	Jun	Jul	Aug	Sep	Oct	Nov	Dec
OCTAS	4	4	4	5	5	5	5	5	5	6	7	6

**Figure 5.** Correction factor for radiation values according to the presence of clouds in Montreal.

In Montreal, the months of January and February are those that have less presence of clouds (96% and 93% correct on the theoretical calculation of direct solar radiation), while November is the cloudiest month (31% of the theoretical calculation). The annual mean cloud presence would then be 60.1 %.

The most remarkable thing about this analysis is that, studying the real measurements of Jeddah city weather stations, it is observed that summer is much cloudier than winter. With these correction factors, it is possible to provide greater precision to the theoretical calculations of direct solar radiation by taking into account the climatic factor by means of real data collected at meteorological stations.

Moreover, The cloud cover fraction traduces the fraction of the sky that is covered by clouds, and doesn't take into account the 'thickness' of the clouds (thick dark clouds that block any direct radiation or semtransparent thin white clouds).

APPENDIX 2

2.1 GEOMETRIC LEVEL OF DETAILS AND SOLAR RADIATION

The CityGML 2.0 standard from the OGC 2012 defines five LODs. An improved LOD specification for 3D building models is LOD0, which is a representation of footprints and optionally roof edge polygons marking the transition from 2D to 3D GIS. LOD1 is a coarse prismatic model obtained by extruding an LOD0 model. LOD2 models a simplified roof shape and where the object's parts can be modelled into multiple semantic classes (e.g. roof, wall). LOD3 is an architecturally detailed model including windows and doors. Thus, LOD3 is considerably more complex than its preceding counterpart. LOD4 completes LOD3 by including indoor features (Kolbe, 2009). This taxonomy has been developed by the German Special Interest Group 3D (SIG 3D) initiative (Albert et al., 2003), and has been further described in Gröger and Plümer (2012). The five LODs have become widely adopted by the stakeholders in the 3D GIS industry and now describe the grade and the design quality of a 3D city model, especially its geometric aspect (i.e. "How much detail should be acquired?"). They are important in the computer graphics (Verdie et al., 2015; Musialski et al., 2013) and BIM communities (Tolmer et al., 2013) when dealing with 3D building models.

The identification of detail classes gives the possibility of choosing the degree of precision of a model regarding the different analytic requirements. Despite providing a global and immediate view of the physical structure of an urban environment, manual modeling is still complex because it requires considerable resources, in terms of tools and time as well as the amount of geometric data. Aliaga (2012) explained two more flexible alternative solutions: *"Traditionally, modelling cities has been a rather manual task that consumes significant amounts of resources. With the growing requirements of quantity and quality in urban content, there is an imperative need for alternative solutions that allow for fast, semi-automatic urban modelling."*

The first category refers to some geometric criteria and a few simple algorithms which describe the solar behavior of a represented environment in a simplified form, and which consider the relative position of the sun. This approach requires a process of abstraction and therefore a degree of approximation.

In this sense, procedural modeling techniques provide a more dynamic approach to define the level of detail in the reproduction of complex urban environments. Virtual models are not made up of volumes but are constructed through a hierarchy of algorithms that can be executed only when needed, allowing the storage and management of a high amount of data. Using this procedure (e.g. with CityEngine), it is possible to generate multi-scale models with different coexisting levels of detail which then can be adapted to the specific requirements of different applications.

Applying these procedural techniques in the solar analysis at an urban scale would simplify the management of the physical environment models and allow implementing simulation processes with greater flexibility and speed. In addition, multi-scale models

could provide interesting results regarding the evaluation of the influence of morphological details on the solar potential of a surface. Currently, some research focuses on precisely this issue of solar access to the urban scale.

2.2 DENSITY INDICATOR FOR THE URBAN SPACES CALCULATION

Here we must mention that in this section the case studies are indicated as following:

Case A for the old compact area (AlBalad), Case B and C for the sprawling morphology in jeddah, in the previous sections were Case A and B.

The basic geometric variables to be considered are the following:

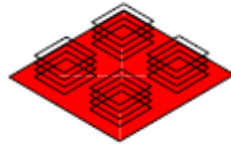
A = Floor area m^2

B = Built area m^2

C = Open areas or free area m^2

D = Total floor area m^2

Table 11. Density indicators for the urban space's calculation. (Source: Pont et al., 2010)



Building intensity (FSI):

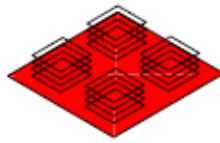
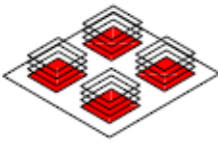
It reflects the building intensity independently of the programmatic composition and is calculated as follows for all levels of the scale:

$$\text{FSI} = D/A$$

F_x = gross area (m^2)

A_x = area of aggregation x (m^2)

X = aggregation (lot (L); island (I), fabric (F) or district (D)).



Coverage (GSI):

GSI, or coverage, demonstrates the relationship between built up and non-built space and is calculated as follows for all levels of scale:

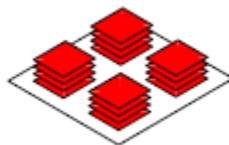
$$\text{GSI} = B/A$$

B = footprint of (m^2)

A = area of aggregation X (m^2)

X = aggregation (lot (L), island (I), fabric (F), or district (D))

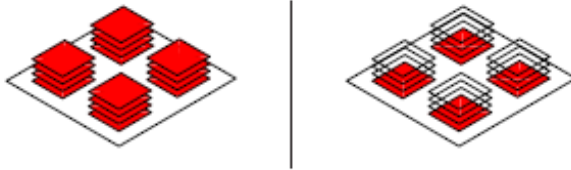
This unit uses the unit square meters per square meters (m^2/m^2)



Building height (L)

The average number of stories (or layers, L) can be achieved by ascertaining the intensity and coverage or FSI and GSI for the aggregation X . If more floor area is developed in a certain area, without changing the footprint, L will increase. If the building height should remain constant, then FSI and GSI have to increase.

$$L = \text{FSI} / \text{GSI}$$



Spaciousness (OSR):

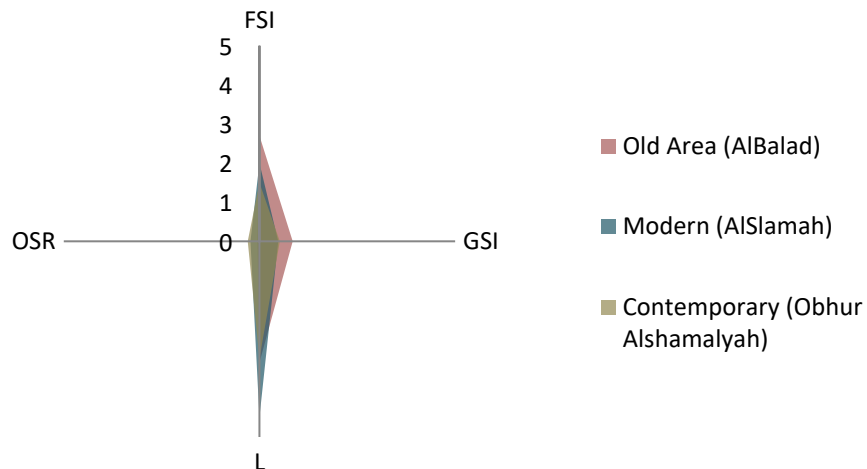
The variable OSR, or spaciousness, is a measure of the amount of non-built space at ground level per square meter of gross floor area. This figure provides an indication of the pressure on non-built space. If more floor area is developed in an area (with the same footprint), the PSR decreases and the number of people who will use the non-built space increase. The unit of OSR is m²/m².

$$OSR = (A - B)/FSI$$

Figure 6 demonstrates the density description of each case study (CaseA, Case B, and C) and highlights the calculated chosen urban layouts of each case. The mathematical expression of the FAR, GSI, L, and OSR demonstrate the compactness of the chosen areas. Therefore, these parameters are chosen as the basic criterion for the selection of the case study (Pont, 2012).

Selected case study areas and their parameters.

Type Of Layouts	FSI	GSI	L	OSR
Old Area (AlBalad)	3	0.85	3.1	0.05
Modern (AlSlamah)	2	0.48	4.5	0.25
Contemporary (Obhur AlShmalyah)	1.5	0.52	3	0.3



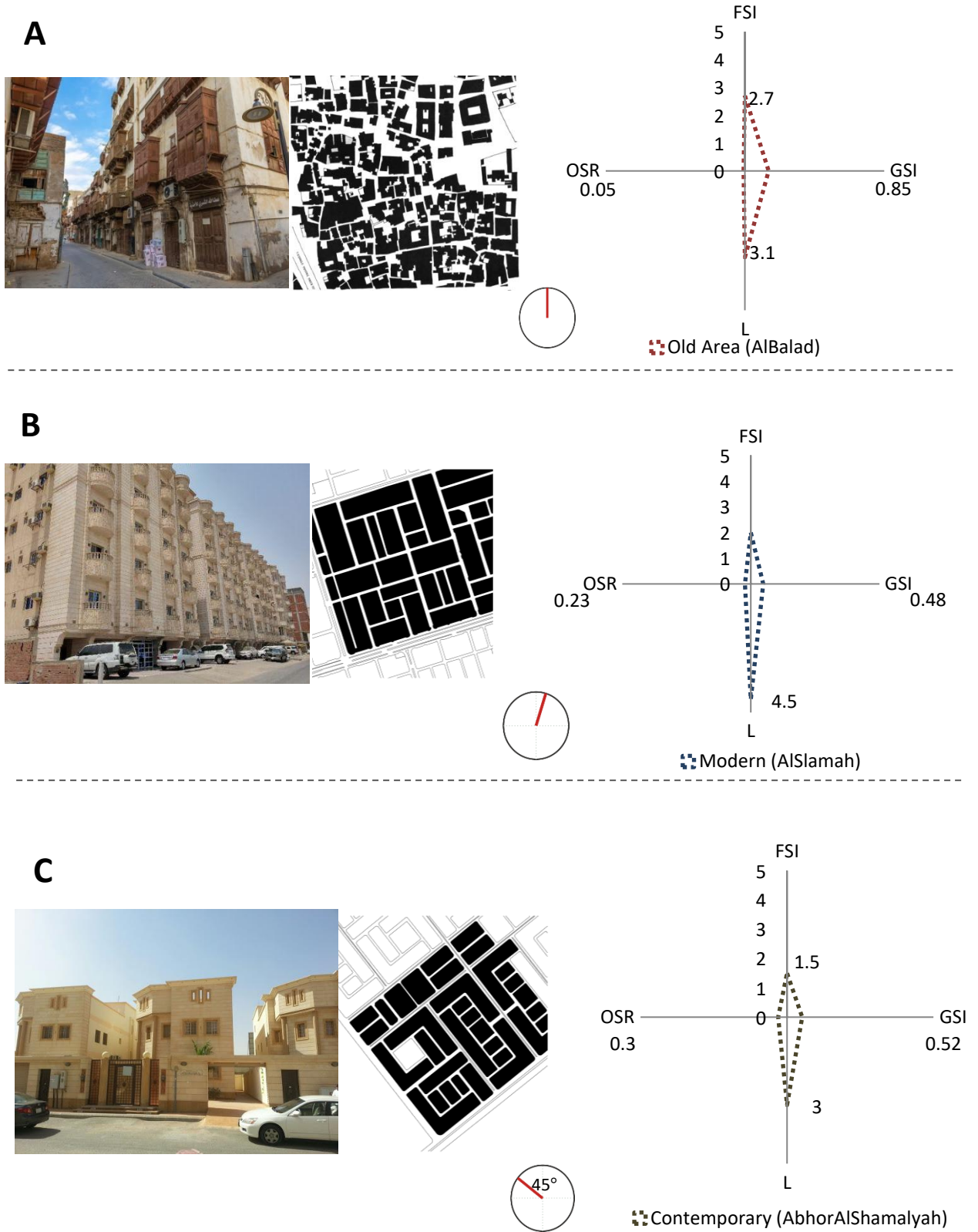


Figure 6 Built-up density descriptions of the choses case study areas.

2.3 OLD JEDDAH URBAN BUILDING HEIGHT REFERENCES

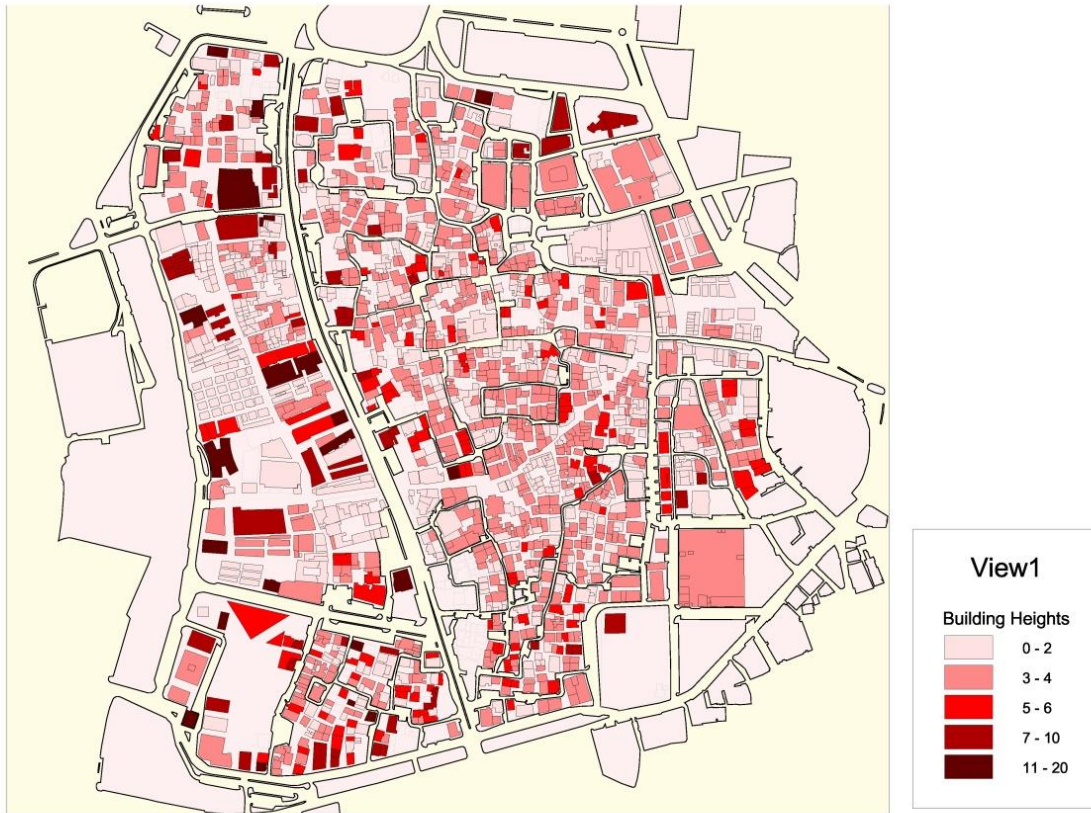
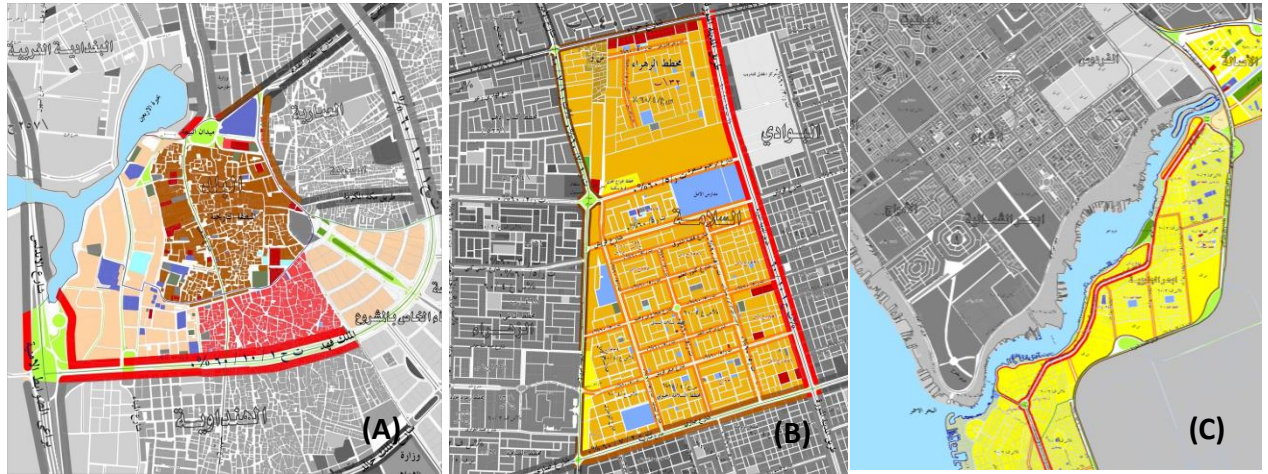


Figure 7 Jeddah old area (AlBalad) urban plan, showing the different building heights.



AlBalad (old area)

AlIslamah (Modern area)

Obhur AlShmalya (Contemporary area)

أطلس المخطط المحلي لمحافظة جدة



Figure 8 The cadastral plans of the three case studies with the key legend. A) AlBalad, B) Al Salamah, and C) Abhur AlShamaliah.

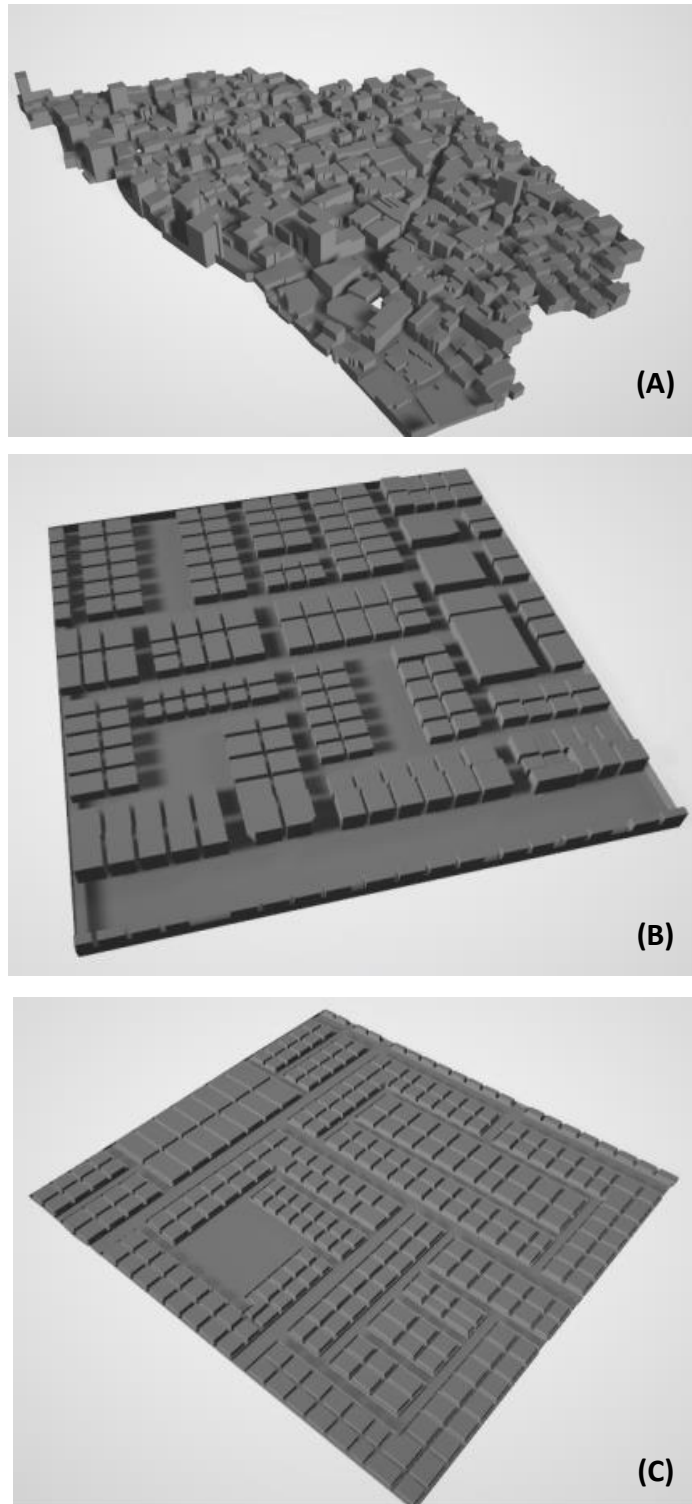


Figure 9 The three case studies 3D images. A) AlBalad, B) AISlamah, and C) Obhur AlShmalya.

Modern area, section
Jeddah Commercial streets

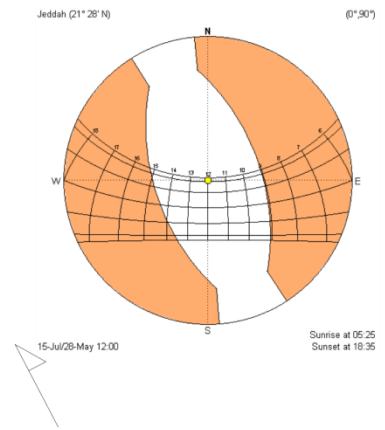
1



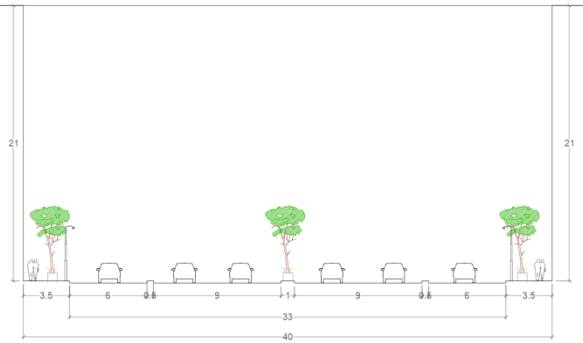
0 1 2 3

NS

H/W: 0.60



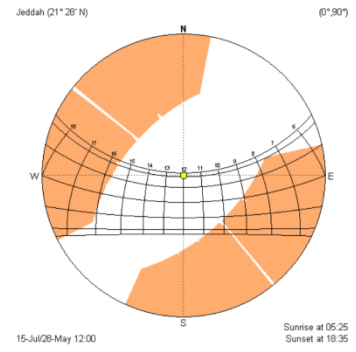
2



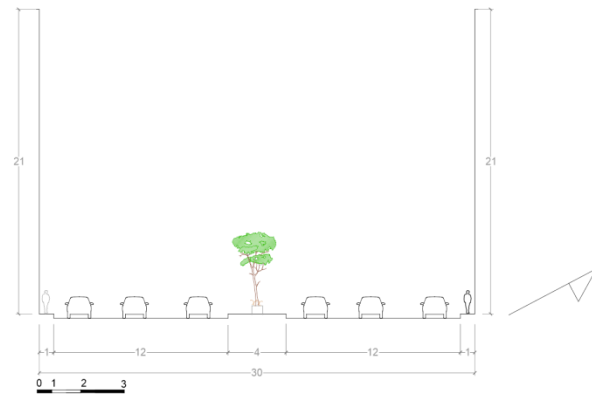
0 1 2 3

NESW

H/W: 0.52



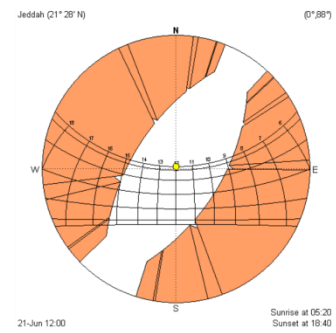
3



0 1 2 3

NESW

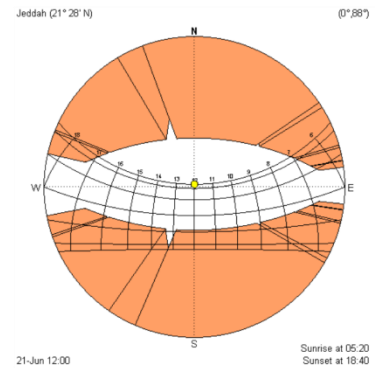
H/W: 0.70



4



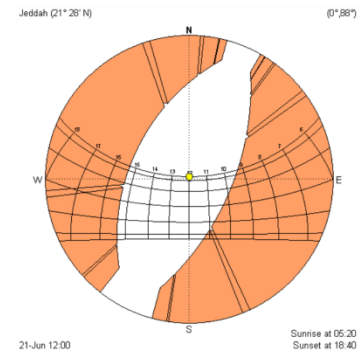
EW
H/W: 0.78



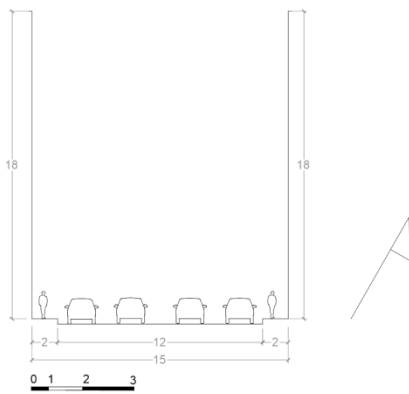
5



NS
H/W: 0.65



6



NS
H/W: 1.2

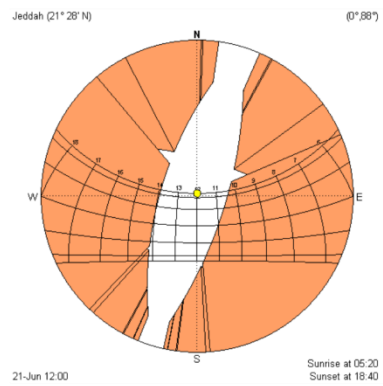


Figure 10 Modern area, commercial buildings sections.

Contemporary area, section
 Jeddah Residential (villas) streets (sections)

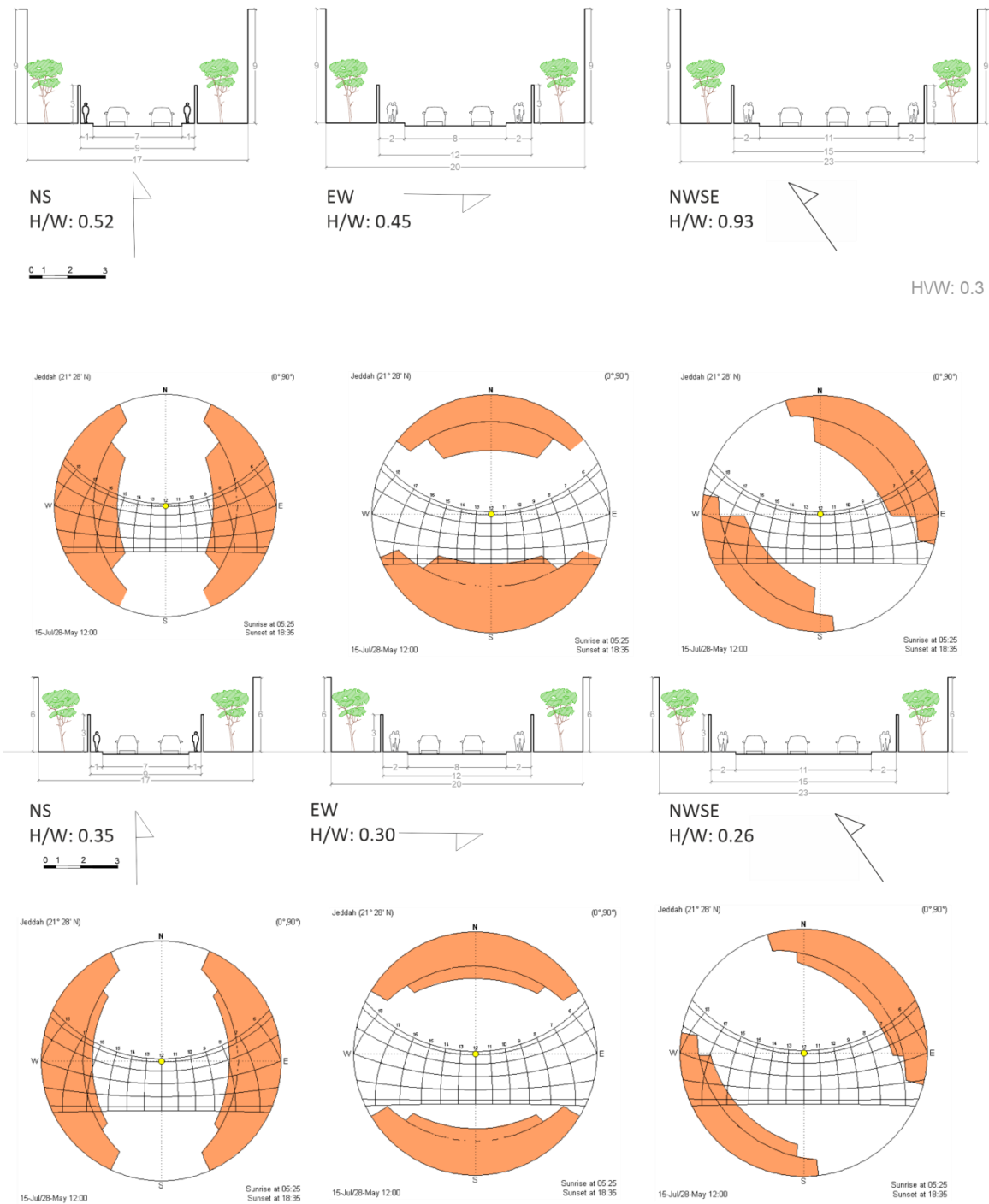


Figure 11 Contemporary area, residential buildings sections.

2.4 CANYONS AND STREETS SIMULATIONS TABLES

Case A, simulations

Table 12. Direct solar radiation simulation of case study A on the street level, on the 21st of June and the 21st of Dec.

Time	CASE A (21st Jun)	CASE A (21st Dec)
5:38	0.000491528	0
5:53	0.013762776	0
6:08	0.275419355	0
6:23	1.450662088	0
6:38	4.396551442	0
6:53	10.21558405	0
7:08	20.35825816	0.000163843
7:23	34.08318615	0.010322082
7:38	52.74829522	0.255102877
7:53	76.73025943	1.001078084
8:08	103.4662533	2.70438541
8:23	133.986519	5.789704788
8:38	168.6772334	10.63551255
8:53	206.033011	17.25229462
9:08	245.0417962	25.14246111
9:23	286.9473181	34.43380924
9:38	328.5244994	45.70650553
9:53	372.7693654	57.88770886
10:08	418.0326768	71.68702137
10:23	461.8261565	86.87965108
10:38	507.9573419	103.0822064
10:53	556.5872904	122.2417923
11:08	609.1751837	139.7763877
11:23	657.8577257	154.0739454
11:38	711.2119107	162.7480986
11:53	739.7293648	167.2888315
12:08	739.3397472	164.439937
12:23	714.9870073	153.7169325
12:38	662.4867697	140.0847394
12:53	607.789731	125.3888803
13:08	552.5269439	109.9111646
13:23	495.7600821	93.50691907
13:38	446.4908199	80.38804474
13:53	397.2030435	67.1425201
14:08	346.2745477	55.36256722
14:23	300.0135989	44.91170524
14:38	257.1045414	35.11310052
14:53	216.4240704	26.52414548
15:08	176.1817145	18.14802193
15:23	140.9300032	11.0002261
15:38	108.6657972	5.76234308
15:53	80.71343607	2.431423694
16:08	57.19498249	0.72828021
16:23	37.09821707	0.233147973
16:38	21.92410157	0.0727461
16:53	10.30733589	0.008847499
17:08	3.949261234	0
17:23	1.158694634	0
17:38	0.178752241	0
17:53	0.024412542	0
18:08	0	0
18:23	0	0
Average Solar flux	251.592764	45.06678223

Case B, simulations

Table 13. Direct solar radiation simulation of case study B on the street level, on the 21st of June and the 21st of Dec.

Time	CASE B (21st Jun)	CASE B (21st Dec)
5:38	0.018721761	0
5:53	2.207642362	0
6:08	13.74690398	0
6:23	36.28873671	0
6:38	69.47118652	0
6:53	106.0157873	0
7:08	145.6744411	0
7:23	185.3930044	0.255725392
7:38	226.0863475	2.986606313
7:53	268.3340129	7.064899332
8:08	314.796432	14.14879779
8:23	365.5834394	28.58369182
8:38	422.1980457	50.31632843
8:53	480.4697359	81.1391429
9:08	540.4857396	117.8608377
9:23	596.3460669	157.4156203
9:38	656.0504572	199.2579249
9:53	707.6365371	241.5311072
10:08	756.4113018	283.4527366
10:23	812.0977248	320.3562404
10:38	851.2349429	353.5454856
10:53	880.9190582	377.3741274
11:08	917.8765085	398.4992081
11:23	938.0674427	410.4048616
11:38	947.8819447	420.574245
11:53	953.1028199	417.0868662
12:08	953.4897363	413.1595954
12:23	948.7632543	400.1827799
12:38	938.9409862	377.2744166
12:53	922.9659153	357.2422707
13:08	893.679256	331.4184438
13:23	852.6358853	302.4751555
13:38	813.5644015	272.1744702
13:53	763.8590959	240.638842
14:08	700.1510222	209.927942
14:23	642.3629082	180.4175924
14:38	582.603462	154.460217
14:53	515.0621424	131.1710392
15:08	445.213331	108.4274275
15:23	376.0472399	86.04382834
15:38	308.4410181	64.57884358
15:53	244.0255393	44.41564529
16:08	185.7686878	26.12906089
16:23	135.3398901	11.62593643
16:38	92.77298408	3.532172307
16:53	59.26200204	0.338655861
17:08	34.47258718	0.00013868
17:23	15.79742222	0
17:38	4.342200514	0
17:53	0.533639538	0
18:08	0.020247238	0
18:23	0	0
Average Solar flux	463.2256831	199.9250035

Case C, simulations

Table 14. Direct solar radiation simulation of case study C on the street level, on the 21st of June and the 21st of Dec.

Time	CASE C (21st Jun)	CASE C (21st Dec)
5:38	0.000295814	0
5:53	0.45451789	0
6:08	4.42419106	0
6:23	14.78447747	0
6:38	31.11384246	0
6:53	55.37929984	0
7:08	90.61234934	0.102499479
7:23	129.5617075	1.70995162
7:38	181.0334551	10.31532271
7:53	242.0940067	30.22477411
8:08	305.6902741	58.54554275
8:23	368.8655985	92.45260693
8:38	431.8535248	131.9958113
8:53	496.8204455	168.9528636
9:08	549.9524479	204.449779
9:23	613.9773495	240.5912726
9:38	672.0151279	278.2636026
9:53	717.1742092	311.8625767
10:08	757.4464466	348.398686
10:23	789.6876354	380.6898673
10:38	816.7158457	406.568841
10:53	838.9104586	430.3575945
11:08	857.2960253	452.3538643
11:23	870.4737902	469.3939219
11:38	879.6145842	477.9686763
11:53	885.6601307	478.2187868
12:08	924.1986035	468.2350714
12:23	880.128117	452.6374018
12:38	871.0510708	446.7548488
12:53	857.5798586	436.9076514
13:08	839.7615149	409.002649
13:23	817.1926975	380.0827095
13:38	790.5568843	351.5158238
13:53	759.8750778	316.8352066
14:08	724.6264981	279.1486775
14:23	682.2740981	239.0488995
14:38	633.5983825	201.4150253
14:53	575.6398822	166.6610462
15:08	508.5882139	135.0030543
15:23	440.2845137	104.6433891
15:38	374.7301069	76.85005643
15:53	313.6549125	53.64731009
16:08	251.4451243	34.55474848
16:23	187.0285653	17.90871482
16:38	133.9752493	5.525209991
16:53	85.66974461	0.444608128
17:08	47.12920111	0.000147907
17:23	21.84052383	0
17:38	8.045691398	0
17:53	1.455403852	0
18:08	0.193314313	0
18:23	0.000443721	0
Average Solar flux	553.567215	232.9326608

2.5 FACADE SIMULATIONS

Case A Facade simulations (Old Jeddah – AlBalad):

Table 15 East facade, Summertime 21st of June.

Town:	Jeddah							
Latitude:	21° 31' N							
Altitude:	15 m (AMSL)							
Tau (transmissivity):	0.7							
AO (ref. altitude):	8200 m (AMSL)							
Day:	21-Jun							
Starting hour:	0:00							
Ending hour:	24:00:00							
Grid precision:	15 min							
Area (m²)	Total energy (kWh)	Solar Flux kWh/m²						
64104.6	87976.4	1.372388253						
Area (m²)	Mean daylight (h)	Min daylight (h)	Max daylight (h)	Total energy (kWh)	Min local flux (kWh/m²)	Max local flux (kWh/m²)	Variability factor	
104	6.8	6.8	6.8	246.1	2.4	2.4	1	
10.1	3.2	2.3	4.8	10.7	0.6	1.9	3.5	
44.4	2.4	2	3	28.6	0.4	0.9	2.12	
17.3	3.3	2	4.5	18.1	0.4	1.7	4.07	
5	3.6	0	4.8	6.5	0	1.8	1000	
455.9	6.7	6.8	6.8	983.4	2.2	2.2	1	
241.5	6.8	6.8	6.8	562.1	2.3	2.3	1	
699.9	5.3	1	6.8	1081	0.1	1.9	21.63	
267.8	0.8	0	6.8	35.5	0	1.9	1000	
709.3	5.8	0	6.8	1396	0	2.3	1000	
501	5.2	0.8	6.8	879.6	0.1	2.3	37.09	
53.1	3.3	0	6.8	58.2	0	2.4	1000	
452.1	4.8	0.8	6.8	621.8	0.1	2	39.56	
645.9	5.8	3	6.8	1318.7	0.9	2.2	2.51	
661.4	6.1	2.3	6.8	1313.9	0.5	2.1	4.26	
111.5	0.2	0	1.3	1	0	0.2	1000	
15.3	6.2	5.3	6.8	35	2.1	2.3	1.1	
29	0.6	0	2.5	3.4	0	0.7	1000	
25.5	3.7	3	5	35.2	0.9	2.1	2.21	
166.9	5.7	3	6.8	374.6	0.9	2.4	2.57	
21.6	5.8	3	6.8	48.4	1	2.4	2.56	
239.6	3.1	0.5	6.8	244.9	0	2.4	82.59	
292.2	2.8	1.3	6	238.9	0.2	2.2	13.4	
114.4	2.1	1.3	2.5	44.1	0.1	0.5	3.93	
24.9	4.4	3.3	5.5	43.2	1.1	2.3	2.11	
28.8	5.9	5.3	6.5	66.9	2.2	2.4	1.1	
94.2	5.7	3.5	6.5	215.1	1.2	2.4	1.96	
118.9	4.7	0	6.5	217.6	0	2.4	1000	
286.2	4.5	1.5	6.8	472	0.3	2.4	9.38	
29	1.7	0.5	3.5	12	0	1.2	45.02	
121	0.7	0.3	2.5	11.4	0	0.7	83.42	
72.3	6	4.5	6.5	172.5	1.9	2.4	1.25	
72.9	4.1	0	6.5	106.9	0	2.4	1000	
33.4	5.8	1	6.5	74.6	0.4	2.4	6.44	
148.9	4	0.8	6.5	217.8	0.1	2.4	36.83	
28.2	2.9	0	6.5	28.3	0	2.4	1000	
47.1	3.2	1.5	6.5	48.4	0.3	2.4	9.38	
89.6	3.4	1.5	6.5	101	0.3	2.4	9.38	
15.2	1.8	0	6.5	9.4	0	2.4	1000	
46.1	3.3	1.5	6.5	49.7	0.3	2.4	9.38	
12.1	2	0	6.5	9	0	2.4	1000	
36.4	3.7	1	6.5	52.5	0.1	2.4	20.41	
30.4	3.8	0	6.5	47.2	0	2.4	1000	
182.3	4.3	0	6.5	299.3	0	2.4	1000	
21.2	2.1	0	6.5	16.3	0	2.4	1000	
246.2	2.8	1	6.5	218.8	0.1	2.4	20.74	
170.2	2.1	0.5	6.5	106.8	0	2.4	79.85	
35.3	2.9	0	6	37.5	0	2.4	1000	
75.7	3.7	2	6.5	98.9	0.4	2.4	5.38	
188.7	4.9	0	6.8	351.8	0	2.4	1000	
185.4	4.4	0	6.8	297.4	0	2.4	1000	
185	4.6	1.3	6.8	321.6	0.2	2.4	13.41	
33	5.1	0	6.5	63.9	0	2.4	1000	
34.3	4.9	0	6.3	67.2	0	2.4	1000	
190	4.2	0.8	6	310.3	0.1	2.4	35.73	
76	5.1	3.8	6.5	150.9	1.4	2.4	1.74	
187.1	3.5	1.8	6.3	227.8	0.3	2.4	6.96	
31.8	4.6	0	5.8	58.7	0	2.3	1000	
18	3.8	0	6	25.8	0	2.3	1000	
17.8	4.9	4.3	5.5	33.8	1.6	2.1	1.35	
51.9	4.1	0	5	81.7	0	1.9	1000	
15.7	5.1	5	5.3	28.7	1.8	1.9	1.05	
94.7	4.4	0	6.8	156.2	0	2.3	1000	
33.1	1.5	0	5.3	18.3	0	2	1000	
67.7	4.2	2.8	4.8	103.8	0.8	1.8	2.4	
149.1	3.6	0.3	5	188.6	0	1.8	317.06	

Table 16 East facade, Wintertime 21st of December.

Town:	Jeddah							
Latitude:	21° 31' N							
Altitude:	15 m (AMSL)							
Tau (transmissivity):	0.7							
AO (ref. altitude):	8200 m (AMSL)							
Day:	21-Dec							
Starting hour:	0:00							
Ending hour:	24:00:00							
Grid precision:	15 min							
Area (m²)	Total energy (kWh)	Solar Flux kWh/m²						
64104.6	49182.6	0.767224193						
Area (m²)	Mean daylight (h)	Min daylight (h)	Max daylight (h)	Total energy (kWh)	Min local flux (kWh/m²)	Max local flux (kWh/m²)	Variability factor	
104	1	0	5.3	21.1	0	1.3	1000	
10.1	0.7	0.3	1.3	1.7	0.1	0.3	5.91	
44.4	1.5	0.3	3.8	22.9	0.1	1.1	12.93	
17.3	1.3	0	3.5	9.4	0	1.2	1000	
5	0.9	0	2.5	1.6	0	0.7	1000	
455.9	5.7	5.5	6	807.4	1.8	1.8	1.01	
241.5	5.5	5.5	5.5	342.5	1.4	1.4	1	
699.9	4.9	0	6.5	1089.2	0	2.1	1000	
267.8	2.6	0.8	6.5	182.2	0.1	2.2	33.18	
709.3	4.7	0	5.5	878.9	0	1.5	1000	
501	4.3	0	5.3	560	0	1.4	1000	
53.1	0.3	0	5.3	3.1	0	1.3	1000	
452.1	4.1	0.5	6.3	605.6	0	2	58.73	
645.9	5.6	0.8	6	1072.5	0.3	1.8	5.19	
661.4	5.2	0	6	1039.1	0	1.8	1000	
111.5	1.8	0	5.8	50.3	0	1.6	1000	
15.3	0	0	0	0	0	0	0	
29	1	0	3.3	4.3	0	0.7	1000	
25.5	0.3	0	2.3	1.1	0	0.3	1000	
166.9	0.2	0	2	2.5	0	0.2	1000	
21.6	0	0	0	0	0	0	0	
239.6	0.7	0	1.3	14.7	0	0.2	1000	
292.2	3.6	1.3	6	292.8	0.1	1.7	13.01	
114.4	2.7	0.8	6.3	96.2	0.1	2.2	16.13	
24.9	0.6	0	4.5	3.2	0	1	1000	
28.8	2.2	0.3	5	14.4	0	1.3	30.46	
94.2	1.9	0	4.5	44.2	0	1	1000	
118.9	1	0	3.5	19	0	0.7	1000	
286.2	2.3	0	5.3	166.8	0	1.3	1000	
29	0.2	0	5	1.8	0	1.5	1000	
121	1.9	0	5	53.4	0	1	1000	
72.3	2.6	0	3.5	42.3	0	0.8	1000	
72.9	3.3	0	5.3	64.2	0	1.3	1000	
33.4	3.7	3	4.3	28	0.7	0.9	1.29	
148.9	2.7	0	4.8	105.5	0	1.3	1000	
28.2	0.6	0	5.3	4.4	0	1.3	1000	
47.1	1.1	0	5.3	13.1	0	1.3	1000	
89.6	1.2	0	5	34.3	0	1.3	1000	
15.2	0.7	0	4.8	3.5	0	1.3	1000	
46.1	2.3	0.3	4.8	27.7	0.1	1.3	15.58	
12.1	0.2	0	4.8	0.6	0	1.3	1000	
36.4	0.3	0	4	1.8	0	0.8	1000	
30.4	3.1	0	4.8	21.3	0	1	1000	
182.3	3.2	0.5	5	143.8	0.1	1.2	13.76	
21.2	3.6	0	5	19.8	0	1.3	1000	
246.2	2.6	0	4.8	154.4	0	1.2	1000	
170.2	2	0	4.8	69.1	0	1.1	1000	
35.3	0.2	0	4.8	2.4	0	1.3	1000	
75.7	1.2	0	4.8	24.3	0	1.3	1000	
188.7	2.2	0	5	100.6	0	1.3	1000	
185.4	3.4	0.8	5.3	160.5	0.1	1.3	14.1	
185	3.6	0.5	5	176.4	0	1.3	26.24	
33	3.1	0	5.3	24.7	0	1.3	1000	
34.3	4.4	0.8	5.3	39.4	0.1	1.3	23.89	
190	2.6	0.5	4.8	105.3	0	1	34.11	
76	0.6	0	5.3	11.4	0	1.3	1000	
187.1	2.6	1.3	5	111.3	0.2	1.2	7.17	
31.8	0.5	0	3.5	5.3	0	1	1000	
18	0.5	0	3.8	3.3	0	1.1	1000	
17.8	2.4	1.8	3.5	15.4	0.7	1	1.46	
51.9	2.4	0	3.5	38	0	1	1000	
15.7	2.8	0	5	16	0	1.8	1000	
94.7	3.1	0	4.5	81.8	0	1.4	1000	
33.1	0.3	0	4.8	3.3	0	1.6	1000	
67.7	2.8	2	3.3	50.8	0.5	0.9	1.9	
149.1	2.2	0	4.8	93.8	0	1.2	1000	

Table 17 North facade, Summertime 21st of June.

Town:	Jeddah							
Latitude:	21° 31' N							
Altitude:	15 m (AMSL)							
Tau (transmissivity):	0.7							
A0 (ref. altitude):	8200 m (AMSL)							
Day:	21-Jun							
Starting hour:	0:00							
Ending hour:	24:00:00							
Grid precision:	15 min							
Area (m²)	Total energy (kWh)	Solar Flux kWh/m²						
65646.5	51971.8	0.791691865						
Area (m²)	Mean daylight (h)	Min daylight (h)	Max daylight (h)	Total energy (kWh)	Min local flux (kWh/m²)	Max local flux (kWh/m²)	Variability factor	
93.8	5	0	9.3	21.7	0	0.5	1000	
6.9	2.8	1.5	4.3	0.5	0	0.1	7.41	
74.8	12.7	10.8	13.5	85.6	1.1	1.2	1.09	
147.4	7.7	6.8	13.5	123.3	0.8	1.2	1.46	
48.1	7.2	4.3	7.8	27.3	0.3	0.6	2.33	
334.8	9	4.3	10.8	295.7	0.1	1.2	8.03	
286.9	12	3.3	13.5	311.4	0.3	1.2	4.01	
79.6	13.5	13.3	13.5	93.5	1.2	1.2	1	
1013.8	6.7	0.3	7.3	1471.4	0	1.5	340.94	
344.3	13.5	13.5	13.5	403.9	1.2	1.2	1	
19.6	13.5	13.5	13.5	23	1.2	1.2	1	
577.3	9.8	3.3	13.5	505.9	0.2	1.2	6.73	
40.9	9	9	9	53.5	1.3	1.3	1	
19.7	13.5	13.5	13.5	22.9	1.2	1.2	1	
71.4	8.5	6.8	13.5	30.4	0.3	1.2	4.63	
220.3	4.8	0.3	8.8	181.3	0	1.3	131.02	
735.2	8.6	0.8	10.5	787.7	0	1.2	58.23	
129.1	10.1	6.8	13.5	122.8	0.8	1.2	1.48	
598.4	8.4	4	10.3	667	0.7	1.2	1.79	
825.4	12.4	5.3	13.5	911.3	0.5	1.2	2.36	
27.4	4.5	0.3	13.5	6.9	0	1.2	152.11	
224.3	11.9	8.5	13.3	253.2	1	1.2	1.15	
60.1	1.9	0.5	6.3	3.5	0	0.3	13.36	
101.3	9.2	8	10.3	117.1	1.1	1.2	1.07	
87.9	3.2	0.5	6.3	101.1	0	2.4	75.02	
13.7	1.4	0.5	8.3	0.9	0	1	79.97	
57.8	4.5	3.5	5.5	14.7	0.2	0.4	2.06	
17.4	3.9	1.5	6	3.2	0.1	0.3	4.17	
22.8	7.4	4.3	8.3	13.9	0.4	0.7	1.57	
24.8	8.3	7.8	9	17.3	0.6	0.8	1.29	
5.9	1.3	0.8	2.5	0.3	0	0.2	16.17	
91.6	5.9	5.5	6.5	90.7	0.9	1.1	1.25	
57.3	6	4	9.8	50.1	0.6	1.1	1.96	
56.4	7.9	4.8	11.8	43.9	0.4	1.1	3.14	
51.9	10.8	8.8	12.8	52.4	0.8	1.2	1.54	
106.4	6.4	3.3	9	112.2	0.4	1.2	3.31	
70.1	7.2	3.3	12	42.4	0	1.1	24.63	
220.3	3.3	0.5	8.8	85.3	0	1.3	179.14	
209.7	7.4	3.3	12.5	121.9	0.1	1.1	7.69	
152.2	6.9	4.3	10	73.6	0.2	0.8	3.99	
28.5	1.7	0.5	10	2.7	0	1	76.66	
52.1	6.9	3.5	10.3	25.6	0.2	0.8	4.93	
254.3	8.5	3	10.8	228	0.1	1.2	13.85	
47.1	11.3	6.8	13.3	47.4	0.6	1.2	2	
90.4	11.3	2	13.3	90.7	0.1	1.2	16.01	
57.6	10.8	6.8	13.3	54.9	0.6	1.2	2	
73.7	8.4	6.8	10.5	81.3	1.1	1.2	1.1	
86.7	6.2	0.5	8.8	78	0	1.3	179.14	
42.5	5.7	2.8	10.5	32	0.3	1.2	3.64	
60.8	11.3	6.5	13.3	61.8	0.5	1.2	2.59	
947.6	11	4.8	13	978.9	0.4	1.2	3.05	
49.2	5.1	1.5	13.3	17.2	0.1	1.2	20.74	
100.3	5.2	2.3	12.8	36.4	0.1	1.2	13.74	
211.8	9.6	3	13.3	181	0.2	1.2	6.32	
40.2	9.3	6.8	12.8	31	0.6	1.2	1.99	
62.4	11.7	10.8	12.5	66.2	1	1.1	1.17	
24.2	7.7	5	12.5	16.5	0.5	1.2	2.48	
121.6	9.7	6.5	13.3	105.2	0.5	1.2	2.59	
158.9	7.6	4	13.3	90.7	0.2	1.2	6.19	
43.3	5.2	3.3	6.8	15.4	0.1	0.5	3.35	
25.8	6.1	3.5	12.5	15.7	0.3	1.2	3.89	
10.2	5.2	0	12.8	4.4	0	1.2	1000	
10.6	7.1	0	11.8	6.9	0	1.1	1000	
30.9	11.1	9.5	11.8	31.7	0.9	1.1	1.18	
23.9	1.5	0	11.8	2.1	0	1	1000	
23.8	7	6.3	7.5	26.4	1.1	1.1	1.07	

Table 18 Northwest facade, Summertime 21st of June.

Town:	Jeddah							
Latitude:	21° 31' N							
Altitude:	15 m (AMSL)							
Tau (transmissivity):	0.7							
A0 (ref. altitude):	8200 m (AMSL)							
Day:	21-Jun							
Starting hour:	0:00							
Ending hour:	24:00:00							
Grid precision:	15 min							
Area (m²)	Total energy (kWh)	Solar Flux kWh/m²						
6545.5	3532	0.539607364						
Area (m²)	Mean daylight (h)	Min daylight (h)	Max daylight (h)	Total energy (kWh)	Min local flux (kWh/m²)	Max local flux (kWh/m²)	Variability factor	
540.7	5.8	2.8	6.5	305	0.3	0.6	2.16	
56.4	0	0	0	0	0	0	0	
141.9	4.4	2.5	4.5	26.8	0.1	0.2	1.62	
227.6	3.4	0.8	4.3	29.6	0	0.2	11.63	
60.8	4.7	4.3	4.8	13.9	0.2	0.2	1.02	
112	1.7	0	6.3	13.8	0	0.5	1000	
117.7	0	0	0	0	0	0	0	
125.8	4.1	3	4.5	24.1	0.2	0.2	1.31	
98.8	4	2.8	5	81.6	0.5	1.1	2.19	
28.9	3.1	2	4.3	24.5	0.4	1.4	3.76	
54.8	3.6	1.8	4.8	39.2	0.2	1	4.51	
35	2	0	4.5	4.1	0	0.3	1000	
86.5	5.1	0	6.8	134.7	0	1.9	1000	
29.6	3.8	3	4.8	14.3	0.4	0.6	1.75	
95.8	2.5	2.5	2.5	2.3	0	0	1	
45.1	4.1	3.3	4.3	6.8	0.1	0.2	1.13	
35.6	0	0	0	0	0	0	0	
98.8	4.7	4	4.8	22.5	0.2	0.2	1.05	
68.4	3	0	6.8	53.1	0	1.8	1000	
132.1	3.4	1.3	6.8	113.3	0.1	1.8	13.64	
5.4	6.8	6.8	6.8	12.9	2.4	2.4	1	
57.7	3.8	0	6.8	66.2	0	2	1000	
77.5	3.1	1.3	6.8	62.2	0.1	1.9	13.58	
19.7	1.8	0	6.8	11.8	0	2.4	1000	
159.5	3	1.3	6.8	128.5	0.1	2	13.56	
22.8	1.2	0	6.8	6.1	0	1.9	1000	
136.8	0.8	0	1	0.1	0	0	1000	
54.7	4	1	6.8	79.6	0.4	2.2	6.26	
51.6	4.7	3.3	6.8	94	1.1	2.4	2.21	
643.3	5.8	4.8	6.3	294.5	0.4	0.5	1.07	
151.9	4.5	4.5	4.5	29.1	0.2	0.2	1	
370.8	5.6	4.5	6.3	174.4	0.4	0.5	1.08	
150.4	5	3.3	6.5	112	0.5	0.8	1.76	
45.3	0.8	0	3.8	0.8	0	0.1	1000	
62.3	5.1	2	6.3	46.3	0.2	0.8	3.88	
171.7	5.6	3.3	6.3	158.2	0.5	1	1.79	
100.3	5.7	4	6.3	46.7	0.4	0.5	1.25	
142.8	5	3	6.3	132.2	0.5	1	2.04	
120	5.4	4	6.3	96.4	0.6	0.8	1.33	
53.2	3.7	3	3.8	4.9	0.1	0.1	1.1	
249.2	4.4	3.5	4.5	47.5	0.2	0.2	1.12	
117	3.2	1.8	3.8	9.7	0	0.1	2.2	
39.7	0	0	0	0	0	0	0	
121.6	3.7	3.3	3.8	11.3	0.1	0.1	1.04	
117.7	0	0	0	0	0	0	0	
98.9	4.4	0	6.8	152.2	0	2.2	1000	
117	3	1	6.8	92	0.1	2	21.54	
24.3	2.9	1.3	6.8	22.3	0.2	2.4	13.41	
251.3	4.6	0	6.8	404.7	0	2.2	1000	
59.9	1.3	0	6	4.6	0	0.4	1000	
16.7	1	1	1	0	0	0	1	
18.1	1	1	1	0	0	0	1	
41.7	4.3	1.8	6.5	18.2	0.1	0.6	4.62	
62.7	4.6	2	6.8	95.5	0.4	2.1	5.33	
78.1	4.1	0	5.8	115.1	0	2.1	1000	
13.6	4.5	3.8	5.3	20.9	1.2	1.9	1.56	
11.6	4.8	4	5.5	18	1.2	1.8	1.46	
20.4	4.8	4	5.5	23	0.9	1.2	1.35	
13.7	2.6	1.5	4.5	2.1	0.1	0.3	3.83	
11.4	0	0	0	0	0	0	0	
70.6	0	0	0	0	0	0	0	
200.7	2.4	0	5	28.3	0	0.3	1000	

Table 19 Northwest facade, Wintertime 21st of December.

Town:	Jeddah						
Latitude:	21° 31' N						
Altitude:	15 m (AMSL)						
Tau (transmissivity):	0.7						
A0 (ref. altitude):	8200 m (AMSL)						
Day:	21-Dec						
Starting hour:	0:00						
Ending hour:	24:00:00						
Grid precision:	15 min						
Area (m²)	Total energy (kWh)	Solar Flux kWh/m²					
6545.5	12780.5	1.952562829					
Area (m²)	Mean daylight (h)	Min daylight (h)	Max daylight (h)	Total energy (kWh)	Min local flux (kWh/m²)	Max local flux (kWh/m²)	Variability factor
540.7	8.1	0	10.3	1538.9	0	3.5	1000
56.4	5.1	2	10.5	126.6	1.1	3.9	3.54
141.9	6.8	3.3	10.5	415.2	1.5	3.7	2.53
227.6	7.2	1.3	10.5	644.3	0.3	3.7	13.05
60.8	4.7	1.5	7.8	135.8	0.6	3.4	5.24
112	4	1	6.8	223.2	0.5	3	5.67
117.7	2.8	0.5	5.3	141.1	0.3	2	7.3
125.8	5.6	1.3	7.5	347.6	0.7	3.5	5.28
98.8	2.7	1.8	4.5	48.9	0.2	1.3	7.8
28.9	2.1	0.5	4.5	14.3	0	1.5	92.33
54.8	3.7	2.3	5.8	52.8	0.4	2	5.49
35	4.6	1.8	5.8	75.5	1	2.7	2.65
86.5	3.6	0.8	5.3	106.5	0.1	2	14.75
29.6	0.4	0	3.5	6.3	0	1.8	1000
95.8	6.3	0	9.3	269.4	0	3.7	1000
45.1	1.6	0.3	3.5	30.4	0.1	1.5	10.42
35.6	3.5	1.5	5.5	67.9	0.8	2.9	3.55
98.8	0.2	0	2.8	10.6	0	1.5	1000
68.4	6.3	1.5	7	154.9	0.5	2.3	4.95
132.1	3.2	1.5	6.8	115.8	0.2	2.3	13.39
5.4	1.1	0	5.3	1.6	0	1.3	1000
57.7	0.8	0	6	15.6	0	1.9	1000
77.5	1.7	0.8	5.5	25.3	0.1	1.6	27.73
19.7	0.8	0	2.5	1.6	0	0.3	1000
159.5	2	0.3	3.5	68.6	0	1	398.07
22.8	1.5	0	4	12.6	0	1.3	1000
136.8	1.6	0	7	83.6	0	1.9	1000
54.7	0.1	0	1.8	0.6	0	0.2	1000
51.6	0	0	0	0	0	0	0
643.3	7.6	1.8	10.5	1698.5	0.1	3.6	25.55
151.9	7.5	0.8	10.5	410.4	0.1	3.7	41.42
370.8	7.7	0.3	10.5	982	0	3.5	301.15
150.4	3.4	0.8	9.3	204.3	0.2	3.2	21.39
45.3	2.2	0.8	5.8	53.5	0.4	2.7	6.04
62.3	6.7	2.5	9.3	165.9	0.7	3.2	4.49
171.7	5.5	0	9	401.4	0	3.1	1000
100.3	6.7	4.5	10.5	241.4	1.2	3.5	2.9
142.8	5.9	4	8.3	320	1.2	3	2.39
120	5.2	0	8	288.9	0	3.1	1000
53.2	4.6	0	9.3	120.4	0	3.6	1000
249.2	6.4	0	10.5	681.7	0	3.7	1000
117	4.9	0.8	10	227.1	0.2	3.8	20.41
39.7	4.3	0.8	10	83.5	0.4	3.9	9.59
121.6	5.2	2.5	9	289.7	1	3.7	3.63
117.7	5.2	2.3	8.8	310.3	1.2	3.8	3.09
98.9	2.1	0.5	5.8	46.5	0	1.6	62.26
117	3.3	0.8	6.5	123	0.2	2.1	11.04
24.3	3.6	0.8	5.3	21.7	0.1	1.3	23.31
251.3	3.8	0	6	288	0	1.7	1000
59.9	6.3	2.5	10.3	156	1.1	3.6	3.31
16.7	1.9	0	10.5	15.4	0	3.8	1000
18.1	3	0.8	10.3	28	0.4	3.8	9.02
41.7	7.7	3.5	10.3	128.1	1.9	3.5	1.84
62.7	1.3	0.3	3.8	13.9	0	1.2	154.76
78.1	1.1	1	1.3	9.8	0.1	0.2	1.54
13.6	5.4	5	5.8	25.9	1.8	2	1.1
11.6	5.7	5.3	6	24.2	2	2.2	1.09
20.4	6.8	3.8	7.5	55.5	1.9	2.8	1.51
13.7	3.3	2.5	8	24.7	1.4	3.4	2.42
11.4	3.3	0	8	18.9	0	3.6	1000
70.6	2.7	0	7.8	99.6	0	3.5	1000
200.7	5.9	0	10	486.7	0	3.7	1000

Table 20 South facade, Summertime 21st of June.

Town:	Jeddah							
Latitude:	21° 31' N							
Altitude:	15 m (AMSL)							
Tau (transmissivity):	0.7							
A0 (ref. altitude):	8200 m (AMSL)							
Day:	21-Jun							
Starting hour:	0:00							
Ending hour:	24:00:00							
Grid precision:	15 min							
Total Area (m²)	Total energy (kWh)	Solar Flux kWh/m²						
60006.9	3374.9	0.056241866						
Area (m²)	Mean daylight (h)	Min daylight (h)	Max daylight (h)	Total energy (kWh)	Min local flux (kWh/m²)	Max local flux (kWh/m²)	Variability factor	
286.5	5.6	1.8	6.3	130.1	0.1	0.5	4.49	
132.3	5.3	2.3	6.5	78.1	0.2	0.7	3.07	
65.6	0.3	0	6.3	1.4	0	0.5	1000	
154.7	0.4	0	1.8	0.3	0	0	1000	
193.6	0	0	0	0	0	0	0	
680.1	0	0	0	0	0	0	0	
452.1	5	3.5	5.3	137	0.2	0.3	1.24	
255.5	6	6	6	99.6	0.4	0.4	1	
598.4	2.9	0	3.3	36.4	0	0.1	1000	
51	0.7	0	1	0	0	0	1000	
272.3	0	0	0	0	0	0	0	
409.3	0	0	0	0	0	0	0	
144.4	0	0	0	0	0	0	0	
62	0	0	0	0	0	0	0	
219.2	0	0	0	0	0	0	0	
18.1	0	0	0	0	0	0	0	
14.5	0	0	0	0	0	0	0	
45.1	0	0	0	0	0	0	0	
241	0	0	0	0	0	0	0	
284.3	3.6	0.8	3.8	25.7	0	0.1	11.41	
201.8	2.4	0.3	2.5	4.8	0	0	119.02	
209.7	0	0	0	0	0	0	0	
165.9	0	0	0	0	0	0	0	
125.6	0	0	0	0	0	0	0	
96.2	0	0	0	0	0	0	0	
68.6	0.9	0	1	0.1	0	0	1000	
24.6	1	1	1	0	0	0	1	
90.2	0	0	0	0	0	0	0	
22.8	0	0	0	0	0	0	0	
202.1	0	0	0	0	0	0	0	
295.5	0	0	0	0	0	0	0	
127.6	0	0	0	0	0	0	0	
101.8	1	1	1	0.1	0	0	1	
121.6	0	0	0	0	0	0	0	
151.9	0	0	0	0	0	0	0	
121.6	0	0	0	0	0	0	0	
174.7	0	0	0	0	0	0	0	
106.4	0	0	0	0	0	0	0	
56.2	0	0	0	0	0	0	0	
69.9	0	0	0	0	0	0	0	
203.5	0	0	0	0	0	0	0	
115.5	0	0	0	0	0	0	0	
212.7	0	0	0	0	0	0	0	
106.4	0	0	0	0	0	0	0	
23.4	0	0	0	0	0	0	0	
98.9	0	0	0	0	0	0	0	
121.6	0	0	0	0	0	0	0	
18.2	0	0	0	0	0	0	0	
31.9	0	0	0	0	0	0	0	
122	0	0	0	0	0	0	0	
12.3	0	0	0	0	0	0	0	
186.8	0	0	0	0	0	0	0	
129.6	0	0	0	0	0	0	0	
106.5	3.2	3.3	3.3	6.9	0.1	0.1	1	
201.1	0	0	0	0	0	0	0	
100.2	3.7	2.3	4	12.6	0.1	0.1	1.66	
104.1	4.2	3.3	4.5	17.9	0.1	0.2	1.52	
59.6	3.1	0	4.3	7.2	0	0.1	1000	
71	2.9	1.5	3.8	5.3	0	0.1	2.82	
113.2	1.7	1.5	1.8	1.1	0	0	1.04	
68.2	0	0	0	0	0	0	0	
32.3	0	0	0	0	0	0	0	
10.4	0	0	0	0	0	0	0	
103.8	0	0	0	0	0	0	0	
79.8	0	0	0	0	0	0	0	
39.5	0	0	0	0	0	0	0	

Table 21 South facade, Wintertime 21st of December.

Town:	Jeddah							
Latitude:	21° 31' N							
Altitude:	15 m (AMSL)							
Tau (transmissivity):	0.7							
A0 (ref. altitude):	8200 m (AMSL)							
Day:	21-Dec							
Starting hour:	0:00							
Ending hour:	24:00:00							
Grid precision:	15 min							
Total Area (m²)	Total energy (kWh)	Solar Flux kWh/m²						
60006.9	127667.1	2.127540333						
Area (m²)	Mean daylight (h)	Min daylight (h)	Max daylight (h)	Total energy (kWh)	Min local flux (kWh/m²)	Max local flux (kWh/m²)	Variability factor	
286.5	4.3	1.8	10.5	584.9	1	3.5	3.49	
132.3	8.3	3.8	9.8	423.4	2.1	3.4	1.62	
65.6	1.3	0.8	8.5	43.9	0.4	3.1	7.03	
154.7	10	7	10.5	588.4	3.4	3.8	1.12	
193.6	10.2	8.3	10.5	752.6	3.8	3.9	1.04	
680.1	8.6	0	10.5	2302.6	0	3.9	1000	
452.1	8.7	2.8	10.5	1549.6	1.6	3.7	2.29	
255.5	10.5	10.5	10.5	921	3.6	3.6	1	
598.4	9.1	0.3	10.5	2011	0	3.8	139.82	
51	4	0	10.5	82.6	0	3.9	1000	
272.3	8.8	1.8	10.5	928.1	0.9	3.9	4.26	
409.3	8.2	0	10.5	1256	0	3.9	1000	
144.4	7.1	0	10.5	425.5	0	3.9	1000	
62	0.6	0	6	19.8	0	2.5	1000	
219.2	7.1	0	10.5	625.1	0	3.9	1000	
18.1	2.5	1.5	3	26	0.9	1.7	1.92	
14.5	1.6	0.8	2.5	11.8	0.3	1.3	3.9	
45.1	5.2	3.5	7.8	109.5	1.6	3.4	2.03	
241	1.7	0	8.8	208.2	0	3.8	1000	
284.3	7.6	3	10.3	889.7	1.6	3.8	2.3	
201.8	2.3	0	10.5	217.8	0	3.8	1000	
209.7	4	0	10	386.1	0	3.9	1000	
165.9	1.7	0	8.5	117	0	3.6	1000	
125.6	0.1	0	1.8	2	0	0.3	1000	
96.2	6.7	0	10.5	255.2	0	3.9	1000	
68.6	6.3	1	10.5	197.5	0.6	3.8	6.57	
24.6	5.4	3.8	9.5	64.4	1.8	3.8	2.15	
90.2	5.8	0	10.5	224.7	0	3.9	1000	
22.8	3.3	0	7.8	33.1	0	3.3	1000	
202.1	6.5	0	10.5	548.1	0	3.9	1000	
295.5	5.3	0	10.3	648.7	0	3.9	1000	
127.6	2.2	0	10	140.7	0	3.9	1000	
101.8	1.1	0	10.3	48.7	0	3.8	1000	
121.6	8.7	0	10.5	422	0	3.9	1000	
151.9	8	0	10.5	488.5	0	3.9	1000	
121.6	6.8	0	10.5	372.9	0	3.9	1000	
174.7	6.2	1	10.3	494.3	0.6	3.9	6.79	
106.4	4.8	0	10.3	193.9	0	3.9	1000	
56.2	4.9	0	10.3	112.2	0	3.9	1000	
69.9	5.3	0	10	163.3	0	3.9	1000	
203.5	9.4	7.8	10.5	771.5	3.3	3.9	1.18	
115.5	8.7	5.8	10.3	411.1	2.4	3.9	1.63	
212.7	1	0	9.8	85.6	0	3.9	1000	
106.4	3.2	0	8.3	177.7	0	3.5	1000	
23.4	5.3	1.5	10.5	57.4	0.9	3.9	4.58	
98.9	7.5	4	10.5	335.8	2	3.9	1.93	
121.6	7.1	1.5	10	399.5	0.9	3.9	4.58	
18.2	7.8	4.5	10.3	64.9	2.4	3.9	1.65	
31.9	5.4	2.8	10.3	80.9	1.5	3.9	2.68	
122	7.9	5.8	10.3	428.2	3	3.9	1.31	
12.3	2.4	1.3	3.8	16.2	0.7	2.1	3.05	
186.8	6	0	10.5	494.4	0	3.9	1000	
129.6	6.3	0	10.3	363.2	0	3.9	1000	
106.5	2.5	0	10.5	91.9	0	3.8	1000	
201.1	4.3	0	10.3	371.3	0	3.9	1000	
100.2	0.5	0	2.5	19.3	0	1.4	1000	
104.1	3.1	0	9	152	0	3.5	1000	
59.6	9.6	2.3	10.5	218	1.2	3.7	3.06	
71	5.4	0	10.3	180.7	0	3.8	1000	
113.2	5.1	0	8.3	258.4	0	3.2	1000	
68.2	8.7	4.5	10.3	232	2	3.9	1.96	
32.3	3.6	1.5	8	60.3	0.8	3.4	4.08	
10.4	10.5	10.3	10.5	40.3	3.9	3.9	1	
103.8	3.9	0	10.5	169.5	0	3.9	1000	
79.8	2.8	0.8	6.8	107.2	0.4	2.9	6.76	
39.5	7	2.5	10.5	121.8	1.4	3.9	2.8	

Table 22 Southeast facade, Summertime 21st of June.

Town:	Jeddah							
Latitude:	21° 31' N							
Altitude:	15 m (AMSL)							
Tau (transmissivity):	0.7							
AO (ref. altitude):	8200 m (AMSL)							
Day:	21-Jun							
Starting hour:	0:00							
Ending hour:	24:00:00							
Grid precision:	15 min							
Area (m²)	Total energy (kWh)	Solar Flux kWh/m²						
3630.4	4135.7	1.139185765						
Area (m²)	Mean daylight (h)	Min daylight (h)	Max daylight (h)	Total energy (kWh)	Min local flux (kWh/m²)	Max local flux (kWh/m²)	Variability factor	
211.2	3.3	2	6.3	141	0.2	1.6	6.92	
53.2	4.4	2	5.8	58.2	0.2	1.6	6.64	
60.8	2.8	1.5	5.5	38.9	0.2	1.9	11.79	
37.2	4	2.8	6.3	37.3	0.5	1.8	3.67	
25.8	6.7	3.5	10.8	14	0.2	1	4.09	
244.7	5	2.3	7	322.5	0.3	1.8	5.56	
170.1	3.9	1.5	6.3	222.7	0.2	2.2	9.41	
149	1.9	0	6.8	80.5	0	2.4	1000	
110.9	4.7	0	6.5	195.3	0	2.4	1000	
97.2	5.3	3.8	7	136.6	0.8	1.7	2.05	
156.5	5.9	4	7	237.9	0.9	1.6	1.83	
76	5.6	0.5	6.8	161.4	0	2.4	76.01	
124.5	5	1	6.8	222.1	0.1	2.4	20.32	
56.1	2.5	1	6.8	41.4	0.1	2.4	20.22	
81.4	2.7	1	6.8	65	0.1	2.3	19.94	
106.4	2.8	1.3	6.3	91.3	0.2	2.4	13.27	
167.1	4.2	0	5.8	213.5	0	2	1000	
166.3	3.2	1	6.8	177.4	0.1	2.4	20.22	
246.9	6.4	4.3	7.5	342.8	0.9	1.5	1.65	
292.2	4.6	2.8	6.8	345.2	0.5	1.7	3.72	
395.1	5.3	3	6.8	598.3	0.6	1.9	3.12	
50.1	1.9	1.3	3.5	7.1	0.1	0.2	3.08	
106.4	1.3	1	2.3	11	0.1	0.3	5.2	
133.7	3.3	1.3	5.8	84.8	0.1	1.5	17	
93.8	3.3	0.3	6	111.5	0	2.4	239.62	
72.1	4.5	3.3	6	83.3	0.6	1.7	2.61	
145.9	3.1	1.3	5.8	94.6	0.1	1.7	17.52	

Table 23 Southeast facade, Wintertime 21st of December.

Town:	Jeddah							
Latitude:	21° 31' N							
Altitude:	15 m (AMSL)							
Tau (transmissivity):	0.7							
AO (ref. altitude):	8200 m (AMSL)							
Day:	21-Dec							
Starting hour:	0:00							
Ending hour:	24:00:00							
Grid precision:	15 min							
Total Area (m²)	Total energy (kWh)	Solar Flux kWh/m²						
3630.4	255.5	0.07037792						
Area (m²)	Mean daylight (h)	Min daylight (h)	Max daylight (h)	Total energy (kWh)	Min local flux (kWh/m²)	Max local flux (kWh/m²)	Variability factor	
211.2	0	0	0.3	0	0	0	160.08	
53.2	0	0	0	0	0	0	0	
60.8	1.3	1	1.5	3.6	0	0.1	1.94	
37.2	0	0	0	0	0	0	0	
25.8	0	0	0	0	0	0	0	
244.7	0.4	0	1	0.3	0	0	1000	
170.1	2	1	2.8	24.3	0.1	0.2	2.75	
149	0.5	0	4.3	10.6	0	0.6	1000	
110.9	3.6	0	4	54.4	0	0.5	1000	
97.2	0.2	0	0.5	0	0	0	1000	
156.5	0	0	0	0	0	0	0	
76	0.5	0	4.5	7	0	0.8	1000	
124.5	1.2	0	4.3	19.6	0	0.6	1000	
56.1	1.7	0.5	4	14.1	0.1	0.5	7.39	
81.4	1.2	0.5	3.3	7.4	0	0.3	17.01	
106.4	1.5	0.5	4	24.1	0.1	0.5	9.62	
167.1	0.7	0	2.5	4.4	0	0.1	1000	
166.3	3.2	0.5	4	78.8	0.1	0.5	4.98	
246.9	0	0	0	0	0	0	0	
292.2	0	0	0.3	0	0	0	564.57	
395.1	0.6	0	1.5	2.8	0	0	1000	
50.1	0	0	0	0	0	0	0	
106.4	0	0	0.5	0	0	0	518.09	
133.7	0	0	0.3	0	0	0	1.32	
93.8	0.2	0	2.8	3.9	0	0.4	1000	
72.1	0	0	0	0	0	0	0	
145.9	0.1	0	0.3	0.1	0	0	1000	

Table 24 West facade, Summertime 21st of June.

Town:	Jeddah							
Latitude:	21° 31' N							
Altitude:	15 m (AMSL)							
Tau (transmissivity):	0.7							
A0 (ref. altitude):	8200 m (AMSL)							
Day:	21-Jun							
Starting hour:	0:00							
Ending hour:	24:00:00							
Grid precision:	15 min							
Total Area (m²)	Total energy (kWh)	Solar Flux kWh/m²						
57828.7	84387.6	1.459268495						
Area (m²)	Mean daylight (h)	Min daylight (h)	Max daylight (h)	Total energy (kWh)	Min local flux (kWh/m²)	Max local flux (kWh/m²)	Variability factor	
80.9	4.6	2.8	6	150.5	0.8	2.4	2.96	
79.7	5.2	0	6.3	168.9	0	2.4	1000	
47.5	4.5	3	5.8	85.6	0.9	2.4	2.49	
362.2	4.4	0.8	6.8	544.7	0.1	2.3	37.11	
47.5	5.6	0	6.8	98.4	0	2.4	1000	
125.2	6.4	6	6.8	297.3	2.4	2.4	1.01	
424.9	5.9	2	6.8	917	0.4	2.4	5.47	
407.7	5.7	2.5	6.8	864.1	0.7	2.4	3.61	
252.1	1.3	0	6.8	91.9	0	2.4	1000	
686.7	6.3	0	6.8	1572.5	0	2.4	1000	
319.1	6.8	6.8	6.8	777.9	2.4	2.4	1	
57.7	6.7	6.8	6.8	136.9	2.4	2.4	1	
291.1	6.2	3.5	6.8	681.1	1.5	2.4	1.62	
143	6.8	6.8	6.8	349.4	2.4	2.4	1	
357.7	4.7	0	6.8	534.8	0	2.2	1000	
323.5	6.7	0	6.8	788.9	0	2.4	1000	
167.4	6.7	5.8	6.8	402.6	2.3	2.4	1.06	
119.4	2.8	0	6.8	121.8	0	2.4	1000	
146.6	3.9	0	6.8	203	0	2.4	1000	
137.8	4.3	0.3	6.8	208.9	0	2.4	307.78	
87.9	3	0.5	6.3	93.5	0	2.4	75.02	
37.4	0.6	0.3	1.3	2	0	0.2	19.57	
89.1	1.7	0.3	4.8	44	0	2	85.21	
161.7	4.6	0.3	6.3	290.3	0	2.4	313.99	
18.5	4.2	3.8	4.5	28.8	1.3	1.7	1.31	
14.6	4.5	4.3	5.5	24.7	1.6	2.1	1.35	
80.8	4.5	0	5.3	143.3	0	2.1	1000	
44.2	5.6	3.3	6.5	96	1.1	2.4	2.21	
151.4	4.9	0	6.5	296.4	0	2.4	1000	
182.3	5.4	0	6.8	365.8	0	2.4	1000	
57.7	5.2	0	6.8	100.2	0	2.1	1000	
101.8	3.2	0.8	6.8	99.5	0.1	2.2	37.97	
114	3.5	1.5	6.8	120.8	0.2	2.1	9.37	
161.1	1.7	1	3.5	58.4	0.1	1.2	10.7	
24.3	1.5	0.8	3.3	7.3	0.1	1.1	16.68	
91.2	3.8	0	6	134.9	0	2.4	1000	
24.6	2.4	0.5	6.5	17.9	0	2.4	81.22	
105.9	3.7	1	6.8	133.1	0.1	2.4	20.53	
116.9	2	0.8	6.8	58.2	0.1	2.4	35.94	
43.5	6.7	6.8	6.8	90.1	2.1	2.1	1	
16.9	2.8	0	6.8	14.5	0	2.1	1000	
31.9	6.7	5.8	6.8	67.3	2.1	2.1	1.02	
76	4.8	0	6.8	140	0	2.3	1000	
349.5	5.2	1.5	6.8	600.6	0.2	2.2	9.38	
92.8	6.2	3	6.8	201.2	0.9	2.3	2.52	
49.2	3.1	1.5	6.8	48	0.3	2.4	9.38	
25.4	2.6	0	6.8	22.1	0	2.4	1000	
15.6	6.8	6.8	6.8	36.9	2.4	2.4	1	
195.5	2.6	0	6.8	145.3	0	2.4	1000	
212.1	5.8	0	6.8	464.3	0	2.4	1000	
39.3	5.6	4.8	6.3	88.3	1.9	2.4	1.23	
179.1	5.3	2.3	6.8	369.9	0.5	2.4	4.31	
18.2	1.7	0	6.5	10.4	0	2.4	1000	
18.2	1.9	0	6.5	12.2	0	2.4	1000	
38.2	1.5	0	4.5	15.4	0	1.8	1000	
66.4	6.3	5	6.8	160.6	2.2	2.4	1.12	
115	4	1.3	6.3	172.3	0.2	2.4	13.31	
138.7	4.2	1	6.8	204.1	0.1	2.4	20.38	
120.4	2.8	0.5	6	111.3	0	2.4	79.42	
61.5	3.5	0	5.3	79.7	0	2.2	1000	
60.6	3.9	1.3	6	88.6	0.2	2.4	13.29	
197.4	3.6	1	6.8	247.4	0.1	2.4	20.54	
46.5	1.7	0.5	6.3	20.1	0	2.4	76.82	
122.4	2.5	0.5	6.3	98	0	2.4	74.96	
66.8	2.8	1.8	4.5	58.4	0.3	1.8	5.27	
124.6	4.2	2.5	5.3	206.8	0.7	2.2	3.25	

Table 25 West facade, Wintertime 21st of December.

Town:	Jeddah							
Latitude:	21° 31' N							
Altitude:	15 m (AMSL)							
Tau (transmissivity):	0.7							
AO (ref. altitude):	8200 m (AMSL)							
Day:	21-Dec							
Starting hour:	0:00							
Ending hour:	24:00:00							
Grid precision:	15 min							
Total Area (m²)	Total energy (kWh)	Solar Flux kWh/m²						
57828.7	29791.7	0.515171532						
Area (m²)	Mean daylight (h)	Min daylight (h)	Max daylight (h)	Total energy (kWh)	Min local flux (kWh/m²)	Max local flux (kWh/m²)	Variability factor	
80.9	1.7	0	3.3	46.3	0	0	1	1000
79.7	0.4	0	2.8	8.3	0	0	0.8	1000
47.5	0	0	0	0	0	0	0	0
362.2	3.3	0	5.5	282.8	0	0	1.4	1000
47.5	0.8	0	5	7.8	0	0	1.1	1000
125.2	4.2	0	5.3	125	0	0	1.3	1000
424.9	3	0.8	4	157.2	0	0	0.5	15.69
407.7	3	1.8	4	171.2	0.2	0	0.5	2.62
252.1	2.1	1	4	67.6	0.1	0	0.5	8.18
686.7	4.8	0	5.3	783.6	0	0	1.2	1000
319.1	4.7	3.8	4.8	305.9	0.9	0	1	1.09
57.7	0.6	0	5.3	7.8	0	0	1.3	1000
291.1	4	1.5	4.3	182.8	0.2	0	0.7	3.86
143	4.5	4.5	4.5	122.2	0.9	0	0.9	1
357.7	4	0	6	410.7	0	0	1.7	1000
323.5	4.5	2	4.5	269.1	0.5	0	0.8	1.64
167.4	5	5	5	193.9	1.2	0	1.2	1
119.4	3.2	0.3	5	81.6	0	0	1.1	83.88
146.6	2	0	5	71.9	0	0	1.1	1000
137.8	3.5	0.5	5	107.3	0	0	1.1	43.94
87.9	0.2	0	1	1.4	0	0	0.1	1000
37.4	0.9	0.8	1.3	3.1	0.1	0	0.1	2.48
89.1	3.4	2.3	4.3	56.8	0.4	0	0.7	1.79
161.7	3.8	0	5	153.7	0	0	1.2	1000
18.5	3.3	2.8	4	17.6	0.7	0	1.3	1.76
14.6	2.1	0	4.8	10.1	0	0	1.6	1000
80.8	0.9	0	5.5	21.9	0	0	1.5	1000
44.2	3.7	0	5.3	43.6	0	0	1.3	1000
151.4	3.2	0	4.8	112.4	0	0	1	1000
182.3	3.6	0	4.8	145.6	0	0	1	1000
57.7	1.2	0	6	20.8	0	0	1.8	1000
101.8	2.4	0	5.8	65.1	0	0	1.6	1000
114	2.3	0	6	76.5	0	0	1.8	1000
161.1	1.8	0	5.3	66	0	0	1.3	1000
24.3	3.9	1.8	5.3	24.9	0.3	0	1.3	4.47
91.2	3.3	0	5.3	80	0	0	1.3	1000
24.6	0.2	0	3.8	1.4	0	0	1	1000
105.9	1.4	0	3.3	18.9	0	0	0.7	1000
116.9	1.7	0	4.8	43	0	0	1	1000
43.5	2.6	0	6.3	33.5	0	0	1.9	1000
16.9	1.1	0	6	5.3	0	0	1.8	1000
31.9	1.8	0	6	17.4	0	0	1.8	1000
76	5.2	4	5.5	104.2	1.1	0	1.4	1.22
349.5	4.4	1.3	5.8	416.9	0.1	0	1.6	11.12
92.8	5.7	5.3	5.8	145.2	1.6	0	1.6	1.01
49.2	1.6	0	5.3	21.6	0	0	1.3	1000
25.4	0.4	0	5.3	1.9	0	0	1.3	1000
15.6	0.5	0	5.3	1.9	0	0	1.3	1000
195.5	1.1	0	2.5	28.5	0	0	0.6	1000
212.1	4	0	5.3	229.2	0	0	1.3	1000
39.3	1.9	0	5.3	21.8	0	0	1.3	1000
179.1	3.5	0	5.3	162.8	0	0	1.3	1000
18.2	3.7	1.3	4.8	17.9	0.2	0	1.3	8.47
18.2	4	2.8	5	20.2	0.7	0	1.3	1.97
38.2	1.3	0.5	2.5	6.2	0	0	0.5	12.64
66.4	3	0	4.3	35.1	0	0	0.7	1000
115	1.6	0.3	3.5	31.1	0	0	0.7	20.45
138.7	2	0	4	53.1	0	0	0.7	1000
120.4	1.9	0	4.3	46.1	0	0	1.1	1000
61.5	1.1	0.8	2	9.1	0.1	0	0.4	5.62
60.6	0.5	0	2.8	6.4	0	0	0.6	1000
197.4	1.6	0	3	49	0	0	0.6	1000
46.5	1.3	0.5	3.3	9.1	0.1	0	0.7	13.77
122.4	1.5	0	3.3	34.8	0	0	0.7	1000
66.8	3.3	0	4	40.3	0	0	0.7	1000
124.6	3.1	1.8	4.3	75.9	0.3	0	0.8	3.19

Case B Facades Simulations (AlSlamah):

Table 26 East façade, Summertime 21st of June.

Town:	Jeddah							
Latitude:	21° 31' N							
Altitude:	15 m (AMSL)							
Tau (transmissivity):	0.7							
A0 (ref. altitude):	8200 m (AMSL)							
Day:	21-Jun							
Starting hour:	0:00							
Ending hour:	24:00:00							
Grid precision:	15 min							
Total Area (m²)	Total energy (kWh)	Solar Flux kWh/m²						
20746	40345.5	1.944736335						
Area (m²)	Mean daylight (h)	Min daylight (h)	Max daylight (h)	Total energy (kWh)	Min local flux (kWh/m²)	Max local flux (kWh/m²)	Variability factor	
537.5	5.5	3	6.8	973.7	0.8	2.1	2.5	
538.7	5.4	3.5	6.8	975	1.1	2.1	1.92	
250.1	4.9	3.5	6.8	421.7	1.1	2.1	1.92	
145	6.2	5.8	6.8	299.2	2	2.1	1.02	
126.9	6.1	3.5	6.8	256.6	1	2.1	2.18	
136.2	6.2	5.8	6.8	284.5	2.1	2.1	1.02	
171.9	6.1	3.8	6.8	352.2	1	2.1	2.17	
186.5	6.1	5.5	6.8	387.5	2	2.1	1.05	
247.7	6.3	6	6.8	515.9	2.1	2.1	1.01	
247.7	6.3	6	6.8	515.5	2.1	2.1	1.01	
247.7	6.3	6	6.8	515.5	2.1	2.1	1.01	
205.8	6.3	6	6.8	428.4	2.1	2.1	1.01	
448	5	4	6	796.4	1.3	2.1	1.54	
247.8	5	4	6	443.6	1.3	2.1	1.54	
247.9	5.1	4	6.3	451.6	1.4	2.1	1.55	
271.5	5.4	4.3	6.3	520.6	1.5	2.1	1.42	
304.2	5.2	4.3	6.3	560.9	1.5	2.1	1.42	
353.9	5.5	4.3	6.5	692	1.5	2.1	1.42	
163.8	5.2	4.3	6.5	301.8	1.5	2.1	1.42	
271.3	6	5.3	6.5	556.5	1.9	2.1	1.09	
212.3	5.8	4.8	6.8	424.8	1.7	2.1	1.22	
231.4	5.8	4.8	6.8	463.2	1.7	2.1	1.22	
268.8	5.8	4.8	6.8	534.6	1.7	2.1	1.22	
212.4	5.8	4.8	6.8	423.5	1.7	2.1	1.22	
212.4	5.7	4.8	6.8	422	1.7	2.1	1.22	
235.9	5.2	1.8	6.8	423.6	0.3	2.1	6.9	
271.3	5.3	2	6.8	490.1	0.4	2.1	5.32	
247.7	5.5	4.5	6.8	475.7	1.6	2.1	1.31	
247.7	5.5	4.5	6.8	475.8	1.6	2.1	1.31	
247.7	5.6	4.5	6.8	478.8	1.6	2.1	1.31	
247.7	5.9	4.5	6.8	497.8	1.6	2.1	1.31	
251.3	5.5	4.5	6.8	482.6	1.6	2.1	1.31	
448.3	5.8	5	6.8	900.8	1.8	2.1	1.15	
359.7	6	5	6.8	735.8	1.8	2.1	1.15	
271.3	6.3	6	6.8	567.5	2.1	2.1	1.01	
247.7	6.3	6	6.8	518.2	2.1	2.1	1.01	
247.7	6.3	6	6.8	518.2	2.1	2.1	1.01	
247.7	6.3	6	6.8	518.2	2.1	2.1	1.01	
247.7	6.2	5.5	6.8	516.7	2	2.1	1.05	
242.8	5.4	2.3	6.8	454.4	0.5	2.1	4.25	
271.3	5.2	1.8	6.8	486.8	0.3	2.1	6.9	
247.7	5.5	4.5	6.8	478.2	1.6	2.1	1.31	
247.7	5.5	4.3	6.8	476.4	1.5	2.1	1.42	
247.7	5.5	4.3	6.8	475.5	1.5	2.1	1.42	
247.7	5.5	4.3	6.8	475.5	1.5	2.1	1.42	
391.9	5.6	4.3	6.8	752.9	1.5	2.1	1.42	
188.7	5.5	4.3	6.8	358.9	1.5	2.1	1.42	
212.3	5.5	4.3	6.8	402.2	1.5	2.1	1.42	
260.1	5.5	4.3	6.8	498.9	1.5	2.1	1.42	
108.9	5.6	4.3	6.8	211.5	1.5	2.1	1.42	
177	5.4	4.3	6.8	336	1.5	2.1	1.42	
188.7	5.7	4.8	6.8	374.1	1.7	2.1	1.22	
212.3	6	4.8	6.8	434.9	1.7	2.1	1.22	
188.7	5.7	4.8	6.8	376.2	1.7	2.1	1.22	
188.7	5.8	4.8	6.8	378.4	1.7	2.1	1.22	
188.7	5.7	4.8	6.8	373.6	1.7	2.1	1.22	
247.7	5.7	4.8	6.8	487.6	1.7	2.1	1.22	
169.2	5.7	4.8	6.8	335	1.7	2.1	1.22	
247.8	5.9	4.3	6.8	492.5	1.5	2.1	1.42	
247.8	6.4	6.3	6.8	515.6	2.1	2.1	1	
247.8	6.3	5.8	6.8	514.8	2	2.1	1.02	
236	6	4.8	6.8	481.5	1.7	2.1	1.22	
340.3	5.7	4.3	6.8	667.9	1.5	2.1	1.42	
443.9	5.6	4.5	6.8	863.1	1.6	2.1	1.31	
855.5	5.6	4.3	6.8	1649	1.5	2.1	1.42	
636.3	5.5	4.3	6.8	1218.1	1.5	2.1	1.42	
369.9	5.6	4.5	6.8	713.2	1.6	2.1	1.31	
393.6	5.3	0	6.8	694.5	0	2.1	1000	
295.9	6.2	5.3	6.8	610.9	1.9	2.1	1.09	
1232.2	5.6	4.3	6.8	2375.6	1.5	2.1	1.42	
243.9	5.5	4.5	6.8	467.9	1.6	2.1	1.31	
236.8	5.5	4.5	6.8	453	1.6	2.1	1.31	
182.6	5.4	4	6.8	343.7	1.3	2.1	1.57	

Table 27 East facade, Wintertime 21st of December.

Town:	Jeddah						
Latitude:	21° 31' N						
Altitude:	15 m (AMSL)						
Tau (transmissivity):	0.7						
AO (ref. altitude):	8200 m (AMSL)						
Day:	21-Dec						
Starting hour:	0:00						
Ending hour:	24:00:00						
Grid precision:	15 min						
Total Area (m²)	Total energy (kWh)	Solar Flux kWh/m²					
20746	33729.8	1.625845946					
Area (m²)	Mean daylight (h)	Min daylight (h)	Max daylight (h)	Total energy (kWh)	Min local flux (kWh/m²)	Max local flux (kWh/m²)	Variability factor
537.5	4.1	2.5	6.3	664.9	0.5	1.9	3.5
538.7	5.2	3	6.3	878.2	0.8	1.9	2.47
250.1	5.5	3.8	6.3	444.3	1.2	1.9	1.66
145	3.6	0	6.3	168.9	0	1.9	1000
126.9	3.1	0	6.3	126.1	0	1.9	1000
136.2	3.5	0	6.3	150.4	0	1.9	1000
171.9	3.1	0	6	172.3	0	1.8	1000
186.5	3.9	0	6.3	228.1	0	1.9	1000
247.7	5.9	5.3	6.3	464.3	1.8	1.9	1.06
247.7	5.9	5.3	6.3	464.1	1.8	1.9	1.06
247.7	5.9	5.3	6.3	464.2	1.8	1.9	1.06
205.8	6	5.3	6.3	388.3	1.8	1.9	1.06
448	4.6	3.3	6.3	671.8	0.9	1.9	2.13
247.8	4.3	3.3	5.5	346.8	0.9	1.9	2.09
247.9	4.1	3	5.5	343.2	0.9	1.8	2.15
271.5	4.3	3.3	5.5	392.2	1	1.8	1.88
304.2	4.8	3.5	6.3	479.6	1	1.9	1.88
353.9	4.5	3.5	5.8	520.1	1	1.9	1.87
163.8	5	3.5	6.3	271.9	1	1.9	1.87
271.3	4.5	3.5	6	403.5	1	1.9	1.87
212.3	5.3	4.3	6.3	366.7	1.4	1.9	1.36
231.4	5.5	4.3	6.3	410.8	1.4	1.9	1.36
268.8	5.2	4.3	6.3	465	1.4	1.9	1.36
212.4	5.2	4.3	6.3	365.9	1.4	1.9	1.36
212.4	5.2	4.3	6.3	367.7	1.4	1.9	1.36
235.9	5.2	4	6.3	407.3	1.3	1.9	1.49
271.3	5	3.8	6.3	439.3	1.1	1.9	1.66
247.7	5	3.8	6.3	409.1	1.1	1.9	1.66
247.7	5.1	3.8	6.3	411.5	1.1	1.9	1.66
247.7	5.6	3.8	6.3	444	1.1	1.9	1.66
247.7	5	3.8	6.3	411.2	1.1	1.9	1.66
251.3	5.2	3.8	6.3	429.9	1.1	1.9	1.66
448.3	5.4	4.3	6.3	787.8	1.4	1.9	1.36
359.7	5.3	4.3	6.3	622.5	1.4	1.9	1.36
271.3	6	5.3	6.3	505.7	1.8	1.9	1.06
247.7	5.9	5.3	6.3	459.5	1.8	1.9	1.06
247.7	5.9	5.3	6.3	459.5	1.8	1.9	1.06
247.7	5.9	5.3	6.3	459.5	1.8	1.9	1.06
242.8	5.9	5.3	6.3	450.6	1.8	1.9	1.06
271.3	5	3.8	6.3	434	1.1	1.9	1.67
247.7	5	3.8	6.3	398.3	1.1	1.9	1.67
247.7	5	3.8	6.3	398.1	1.1	1.9	1.67
247.7	4.9	3.5	6.3	392.6	1	1.9	1.88
247.7	4.9	3.5	6.3	392	1	1.9	1.88
391.9	4.8	3.5	6.3	623.2	1	1.9	1.86
188.7	4.8	3.5	6.3	302.2	1	1.9	1.86
212.3	5.2	3.8	6.3	361.2	1.2	1.9	1.65
260.1	5	3.5	6.3	422.3	1	1.9	1.88
108.9	4.9	3.5	6.3	173.1	1	1.9	1.88
177	4.8	3.5	6.3	274.6	1	1.9	1.88
188.7	5.6	4	6.3	336.8	1.3	1.9	1.5
212.3	5.2	4	6.3	357.3	1.3	1.9	1.5
188.7	5.2	4	6.3	317.3	1.3	1.9	1.5
188.7	5.2	4	6.3	317.6	1.3	1.9	1.5
188.7	5.2	4	6.3	318	1.3	1.9	1.5
247.7	3.8	2.8	6	287.6	0.7	1.9	2.91
169.2	5.1	4	6.3	281.6	1.3	1.9	1.5
247.8	4.4	2.5	6.3	348.9	0.5	1.9	3.5
247.8	5.6	3.8	6.3	440.5	1.1	1.9	1.66
247.8	6	5.8	6.3	469.9	1.9	1.9	1.01
236	6	5.8	6.3	447.4	1.9	1.9	1.01
340.3	4.4	2.8	6.3	473.4	0.6	1.9	2.92
443.9	5	3.5	6.3	726.8	1.1	1.9	1.67
855.5	5.2	3.5	6.3	1434.2	1	1.9	1.87
636.3	4.9	3.5	6.3	1018.4	1	1.9	1.87
369.9	5	3.8	6.3	605.7	1.2	1.9	1.66
393.6	5	3.8	6.3	655.5	1.2	1.9	1.66
295.9	5.9	5.3	6.3	555.5	1.8	1.9	1.06
1232.2	5	3.5	6.3	1963.8	1	1.9	1.88
243.9	5	3.8	6.3	403	1.2	1.9	1.65
236.8	5.3	3.8	6.3	410.9	1.2	1.9	1.65
182.6	3.8	2.8	5	211.9	0.6	1.7	2.64

Table 28 North facade, Summertime 21st of June.

Town:	Jeddah							
Latitude:	21° 31' N							
Altitude:	15 m (AMSL)							
Tau (transmissivity):	0.7							
A0 (ref. altitude):	8200 m (AMSL)							
Day:	21-Jun							
Starting hour:	0:00							
Ending hour:	24:00:00							
Grid precision:	15 min							
Total Area (m²)	Total energy (kWh)	Solar Flux kWh/m²						
23835.2	3877.2	0.16266698						
Area (m²)	Mean daylight (h)	Min daylight (h)	Max daylight (h)	Total energy (kWh)	Min local flux (kWh/m²)	Max local flux (kWh/m²)	Variability factor	
478.3	4.3	4.3	4.3	73.9	0.2	0.2	1	
436.7	4.2	4.3	4.3	67.5	0.2	0.2	1	
436.7	4.3	4.3	4.3	67.5	0.2	0.2	1	
436.7	4.3	4.3	4.3	67.5	0.2	0.2	1	
435.5	4.2	4.3	4.3	67.3	0.2	0.2	1	
472.5	4.5	4.5	4.5	78.7	0.2	0.2	1	
416.1	4.4	3.3	4.5	68.9	0.1	0.2	1.16	
436.7	4.3	4.3	4.3	69.2	0.2	0.2	1	
436.7	4.3	4.3	4.3	69.2	0.2	0.2	1	
436.7	4.3	4.3	4.3	69.2	0.2	0.2	1	
436.7	4.3	4.3	4.3	69.2	0.2	0.2	1	
415.9	4.3	4.3	4.3	65.9	0.2	0.2	1	
546.3	4.1	2.8	4.3	85.4	0.1	0.2	1.36	
332.8	4	4	4	43.6	0.1	0.1	1	
291.2	4	4	4	38.1	0.1	0.1	1	
485.8	3.7	0.3	4	59.7	0	0.1	128.23	
802.1	4.3	4.3	4.3	129.1	0.2	0.2	1	
259.5	4.5	4.5	4.5	43.9	0.2	0.2	1	
340.7	3.5	0	4.3	42.5	0	0.1	1000	
247.8	4.3	4.3	4.3	36.7	0.1	0.1	1	
247.8	4.2	4.3	4.3	36.7	0.1	0.1	1	
362	3.5	0	4.3	50.2	0	0.2	1000	
358.1	3.5	0	4.3	44.1	0	0.1	1000	
328.4	3.5	0	4.3	39	0	0.1	1000	
366.2	3.6	0	4.3	49.2	0	0.2	1000	
247.8	4.3	4.3	4.3	39.1	0.2	0.2	1	
247.8	4.2	4.3	4.3	39.1	0.2	0.2	1	
182.2	4.5	4.5	4.5	31	0.2	0.2	1	
225.4	4.5	4.5	4.5	41.2	0.2	0.2	1	
200.5	4.5	4.5	4.5	36.7	0.2	0.2	1	
224.1	4.5	4.3	4.5	40.9	0.2	0.2	1.01	
354.4	4.3	4.3	4.3	57.6	0.2	0.2	1	
330.3	4.2	3.8	4.3	53.7	0.2	0.2	1.04	
353.9	4.5	4.5	4.5	61	0.2	0.2	1	
306.7	4.2	4.3	4.3	49.5	0.2	0.2	1	
286.9	4.3	4.3	4.3	46.3	0.2	0.2	1	
306.7	4.2	4.3	4.3	49.5	0.2	0.2	1	
306.7	4.3	4.3	4.3	49.5	0.2	0.2	1	
294.9	4.2	4.3	4.3	48.7	0.2	0.2	1	
323.7	4.2	4	4.3	53.5	0.2	0.2	1.01	
319.5	4.5	4.5	4.5	56.3	0.2	0.2	1	
357.2	4.5	4.3	4.5	70.2	0.2	0.2	1.01	
247.7	4.5	4.5	4.5	48.7	0.2	0.2	1	
247.7	4.5	4.5	4.5	48.7	0.2	0.2	1	
271.3	4.5	4.5	4.5	53.3	0.2	0.2	1	
306.7	4.5	4.5	4.5	54	0.2	0.2	1	
212.3	4.3	4.3	4.3	34.4	0.2	0.2	1	
330.3	4.2	4.3	4.3	53.6	0.2	0.2	1	
236.1	4.2	4.3	4.3	38.3	0.2	0.2	1	
336.9	4.3	4.3	4.3	55.2	0.2	0.2	1	
294.9	4.3	4.3	4.3	48.3	0.2	0.2	1	
177	4.5	4.5	4.5	31.5	0.2	0.2	1	
188.8	4.5	4.5	4.5	33.6	0.2	0.2	1	
188.8	4.5	4.5	4.5	33.6	0.2	0.2	1	
188.8	4.5	4.5	4.5	33.6	0.2	0.2	1	
188.8	4.5	4.5	4.5	33.6	0.2	0.2	1	
305.1	4.5	4	4.5	54.3	0.2	0.2	1.02	
271.3	4.5	4.5	4.5	45.3	0.2	0.2	1	
256.6	4.5	4.5	4.5	42.8	0.2	0.2	1	
845.2	4	4	4	111.7	0.1	0.1	1	
200.4	5.6	4.3	6.5	135.1	0.6	0.7	1.22	
651.1	4.3	4.3	4.3	89.9	0.1	0.1	1	
340.4	4.2	4.3	4.3	53.8	0.2	0.2	1	
515.2	4.5	3.5	4.5	88.7	0.2	0.2	1.1	
414.3	4.2	3.5	4.3	66.8	0.1	0.2	1.08	
869.4	4.3	4.3	4.3	131.9	0.2	0.2	1	
340.4	4.2	4.3	4.3	50.4	0.1	0.1	1	
296.8	4.5	4.5	4.5	50.2	0.2	0.2	1	

Table 29 North facade, Wintertime 21st of December.

Town:	Jeddah					
Latitude:	21° 31' N					
Altitude:	15 m (AMSL)					
Tau (transmissivity):	0.7					
AO (ref. altitude):	8200 m (AMSL)					
Day:	21-Dec					
Starting hour:	0:00					
Ending hour:	24:00:00					
Grid precision:	15 min					
Area (m²)	Total energy (kWh)	Solar Flux kWh/m²				
23835.2	84365.5	3.539533967				
Mean daylight (h)	Min daylight (h)	Max daylight (h)	Total energy (kWh)	Min local flux (kWh/m²)	Max local flux (kWh/m²)	Variability factor
8.9	4	10.5	1711.6	2.1	3.7	1.78
10	7.8	10.5	1625.3	3.5	3.7	1.06
9.8	8.5	10.5	1621.6	3.6	3.7	1.04
9.8	8.8	10.5	1614.6	3.6	3.7	1.04
9.8	8.8	10.5	1610	3.6	3.7	1.04
10	9	10.5	1751.5	3.6	3.7	1.04
9.9	9	10.5	1538.9	3.6	3.7	1.04
9.9	9	10.5	1619.6	3.6	3.7	1.04
9.9	9.3	10.5	1617	3.6	3.7	1.04
10.1	9.3	10.5	1621.1	3.6	3.7	1.04
9.9	9.3	10.5	1613.6	3.6	3.7	1.04
9.9	9	10.5	1537.7	3.6	3.7	1.04
9.9	9	10.5	2024.1	3.6	3.7	1.04
10.2	9	10.5	1245	3.6	3.8	1.04
9	6.3	10.5	1061.2	3.2	3.8	1.19
9.7	6.5	10.5	1759.1	2.4	3.8	1.57
9.8	8.8	10.5	2966.8	3.5	3.7	1.06
8.5	6	10	869.9	2.2	3.7	1.69
8.7	5.5	10.5	1163.9	2.1	3.7	1.81
9.2	7	10.5	891.5	2.9	3.7	1.27
9	7	10	877.9	2.9	3.7	1.27
8.6	5.5	10.5	1214.3	2.1	3.7	1.82
8.2	5	10.5	1181	2	3.7	1.84
8.5	5.5	10.5	1093.4	2.1	3.7	1.8
8.7	5.5	10.5	1235.7	2.1	3.7	1.81
9.1	7	10.5	890	2.9	3.7	1.27
9.3	6	10.5	903.8	2.6	3.7	1.43
6.7	1.8	10.5	552.1	1	3.7	3.65
9.4	7.8	10.5	810.1	3.2	3.7	1.17
9.4	7.8	10.5	719	3.2	3.7	1.17
9.4	7.8	10.5	804.1	3.2	3.7	1.17
8.6	5.5	10.5	1231.6	2.6	3.7	1.42
9.2	6.8	10.5	1178.6	2.8	3.7	1.34
9.1	7.5	10.3	1246.1	2.9	3.7	1.27
8.6	6.8	10	1028.1	2.7	3.7	1.4
9.3	7.5	10.5	1026.7	3.1	3.7	1.22
10	7.5	10.5	1136.7	3.1	3.7	1.22
9.5	7.8	10.5	1119.2	3.2	3.7	1.17
9.3	7.5	10.5	1053.7	3.1	3.7	1.22
9.5	7.5	10.5	1173.9	3.1	3.7	1.22
9.3	7.5	10.5	1148.4	3.1	3.7	1.22
9.5	7.5	10.5	1287.8	3	3.7	1.22
9.3	7.5	10.5	881	3	3.7	1.22
9.3	7.3	10.5	875.1	2.9	3.7	1.28
9.2	7.3	10.5	953.1	2.9	3.7	1.28
8.8	6.3	10.5	1075.7	2.8	3.7	1.31
8.6	6	10.5	744.3	2.8	3.7	1.32
9.2	7	10.5	1189.9	2.9	3.7	1.27
6.9	1.8	10.5	732.8	1	3.7	3.66
7.5	2.3	10	1098.8	1.3	3.7	2.83
8.6	6	10	1018.6	2.6	3.7	1.43
9.2	7.3	10.5	648.9	3.4	3.7	1.11
9.5	8.3	10.3	699	3.6	3.7	1.03
9.3	7.5	10.3	685.8	3.2	3.7	1.17
8.9	6.8	10.3	650.5	2.6	3.7	1.41
9.1	7	10.3	659.9	2.8	3.7	1.34
9.4	7.3	10.3	1084.5	2.8	3.7	1.34
8.7	6.8	10	952.4	2.9	3.7	1.28
8.5	5.5	10	899.8	2.7	3.7	1.37
7.8	3.5	10.5	2597.3	1.3	3.7	2.94
9.2	6.8	9.8	664.9	2.3	3.4	1.46
8.4	4.8	10.5	2219.2	2.3	3.7	1.63
8.2	4.8	10.5	1156.7	2.4	3.7	1.58
9.3	6.8	10.5	1812.3	2.6	3.7	1.41
9.2	6.8	10.5	1455.5	2.7	3.7	1.41
8.7	4.3	10.5	3019.4	2	3.7	1.87
9.1	6.3	10.3	1199.8	2.4	3.7	1.58
8.9	6	10.3	1013.8	2.2	3.7	1.69

Table 30 West facade, Summertime 21st of June.

Town:	Jeddah						
Latitude:	21° 31' N						
Altitude:	15 m (AMSL)						
Tau (transmissivity):	0.7						
A0 (ref. altitude):	8200 m (AMSL)						
Day:	21-Jun						
Starting hour:	0:00						
Ending hour:	24:00:00						
Grid precision:	15 min						
Area (m²)	Total energy (kWh)	Solar Flux kWh/m²					
21441.8	47175.5	2.200165098					
Area (m²)	Mean daylight (h)	Min daylight (h)	Max daylight (h)	Total energy (kWh)	Min local flux (kWh/m²)	Max local flux (kWh/m²)	Variability factor
647.2	4.6	2.8	6.8	1154.2	0.8	2.4	3.01
560.2	5.2	3.3	6.8	1130.4	1.1	2.4	2.24
569.5	5.3	3.3	6.8	1182.4	1.1	2.4	2.24
136.9	4.6	0.5	6.8	238.4	0	2.4	75.12
166.9	4.8	0.5	6.8	287.4	0	2.4	74.95
171.1	4	0.5	6.8	242.8	0	2.4	75.34
149.1	5.2	0.5	6.8	305.1	0	2.4	75.08
247.7	5.9	4.5	6.8	572.3	1.8	2.4	1.33
247.7	5.7	4.3	6.5	562.6	1.7	2.4	1.44
247.7	5.6	4.3	6.5	556.4	1.7	2.4	1.44
235.9	5.6	4.3	6.5	529.8	1.7	2.4	1.44
271.3	5.3	4	6.8	580.8	1.5	2.4	1.58
247.7	5.3	4	6.8	530.8	1.5	2.4	1.58
247.7	5.3	4	6.5	530.8	1.5	2.4	1.58
247.7	5.3	4	6.5	530.5	1.5	2.4	1.58
247.7	5.3	4	6.5	530.8	1.5	2.4	1.58
254.4	5.3	4	6.5	544.4	1.5	2.4	1.58
228.6	5.3	4	6.5	488.4	1.5	2.4	1.58
186.7	5.3	4	6.5	401.6	1.5	2.4	1.58
265.6	5.4	4.3	6.5	579.6	1.7	2.4	1.44
212.3	5.4	4	6.5	465.5	1.5	2.4	1.58
212.3	5.4	4	6.5	463.4	1.5	2.4	1.58
235.9	5.3	4	6.8	506.5	1.5	2.4	1.58
271.3	5.6	4.5	6.5	616.5	1.8	2.4	1.33
247.7	5.9	4.5	6.5	574.7	1.8	2.4	1.33
247.7	5.7	4.5	6.5	566.6	1.8	2.4	1.33
250.1	5.6	4.5	6.8	562.4	1.8	2.4	1.33
247.7	5.6	4.5	6.5	563.2	1.8	2.4	1.33
247.7	5.6	4.5	6.5	564.1	1.8	2.4	1.33
271.3	6.2	5.8	6.8	655.5	2.4	2.4	1.03
247.7	6.1	5.8	6.8	598.5	2.4	2.4	1.03
247.7	6.1	5.8	6.5	598.5	2.4	2.4	1.03
247.7	6.1	5.8	6.5	598.5	2.4	2.4	1.03
247.7	6.1	5.8	6.5	598.5	2.4	2.4	1.03
253.1	6.1	5.8	6.5	611.3	2.4	2.4	1.03
379.3	5.6	4.8	6.5	861.6	2	2.4	1.24
448.4	5.7	4.8	6.5	1024.3	2	2.4	1.24
467.9	5.4	4	6.5	1012.1	1.5	2.4	1.58
401.1	5.3	4	6.5	845.4	1.5	2.4	1.58
200.5	5.3	3.8	6.5	422.8	1.4	2.4	1.76
212.3	5.2	3.8	6.5	446.8	1.4	2.4	1.76
212.3	6.4	6	6.5	516.7	2.4	2.4	1.01
212.3	6.3	6	6.5	516	2.4	2.4	1.01
235	6.3	6	6.5	571	2.4	2.4	1.01
194.5	5.5	4.3	6.5	431.3	1.7	2.4	1.44
177	5.6	4.5	6.5	398.1	1.8	2.4	1.33
212.3	6	5.5	6.5	508.9	2.3	2.4	1.06
188.7	6.1	5.5	6.5	455.8	2.3	2.4	1.06
167.1	6.1	5.8	6.5	403.8	2.4	2.4	1.03
188.7	6.1	5.8	6.5	456.1	2.4	2.4	1.03
188.7	6.2	5.8	6.5	456.5	2.4	2.4	1.03
188.7	6.2	5.8	6.5	456.4	2.4	2.4	1.03
330.3	5.4	4	6.5	708.8	1.3	2.4	1.8
444	5.8	4.3	6.8	998.4	1.7	2.4	1.44
857.3	5.7	4.3	6.8	1941.2	1.7	2.4	1.45
413.5	5.7	4.3	6.8	926.6	1.7	2.4	1.45
340.4	5.3	4.3	6.8	729.4	1.7	2.4	1.45
310.8	5.4	4	6.8	667.9	1.5	2.4	1.59
310.8	6.2	4.3	6.8	741.1	1.5	2.4	1.57
310.8	5.3	4	6.8	656.5	1.5	2.4	1.59
310.8	5.6	4	6.8	689.3	1.5	2.4	1.59
312.9	5.6	4	6.8	684.8	1.5	2.4	1.59
492.9	5.5	4	6.8	1085.3	1.5	2.4	1.58
236.7	5.4	4.3	6.8	513.6	1.7	2.4	1.44
266.3	5.5	4	6.8	586.1	1.5	2.4	1.58
295.9	5.1	4	6.8	614.2	1.5	2.4	1.59
310.7	5.1	4	6.8	644.9	1.5	2.4	1.59
1230.8	5.7	4.3	6.8	2753.4	1.7	2.4	1.44
310.7	5.5	4	6.8	689.2	1.5	2.4	1.59
310.7	5.6	4	6.8	683	1.5	2.4	1.59
193.6	5.3	4	6.8	410.9	1.5	2.4	1.59
310.7	5.2	3.8	6.8	643.8	1.4	2.4	1.76

Table 31 West facade, Wintertime 21st of December.

Town:	Jeddah							
Latitude:	21° 31' N							
Altitude:	15 m (AMSL)							
Tau (transmissivity):	0.7							
A0 (ref. altitude):	8200 m (AMSL)							
Day:	21-Dec							
Starting hour:	0:00							
Ending hour:	24:00:00							
Grid precision:	15 min							
Area (m²)	Total energy (kWh)	Solar Flux kWh/m²						
21441.8	14070.6	0.656222892						
Area (m²)	Mean daylight (h)	Min daylight (h)	Max daylight (h)	Total energy (kWh)	Min local flux (kWh/m²)	Max local flux (kWh/m²)	Variability factor	
647.2	3.7	2.8	4.3	441	0.5	0.7	1.34	
560.2	3.6	2.3	4.3	386.5	0.4	0.7	1.78	
569.5	3.8	2.5	4.3	399.4	0.5	0.7	1.52	
136.9	2.2	0	4.3	53.2	0	0.7	1000	
166.9	2.3	0	4.3	66	0	0.7	1000	
171.1	2.3	0	4.3	70.5	0	0.7	1000	
149.1	2.3	0	4.3	58.4	0	0.7	1000	
247.7	2.5	2	3.5	121.9	0.3	0.7	2.05	
247.7	3.2	2.3	3.8	160.6	0.4	0.7	1.76	
247.7	3.4	2.8	4	169.2	0.6	0.7	1.33	
235.9	3.5	2.8	4	161.7	0.6	0.7	1.33	
271.3	3.4	2.5	4.3	175.7	0.5	0.7	1.53	
247.7	3.4	2.5	4.3	160	0.5	0.7	1.53	
247.7	3.4	2.5	4.3	160	0.5	0.7	1.53	
247.7	3.3	2.5	4.3	157.9	0.5	0.7	1.53	
247.7	3.3	2.5	4.3	157.8	0.5	0.7	1.53	
254.4	3.5	1.8	4.3	169.1	0.3	0.7	2.69	
228.6	3.6	2	4.3	155.5	0.3	0.7	2.16	
186.7	3.4	2.5	4.3	119.5	0.5	0.7	1.53	
265.6	3.4	2.5	4.3	178.3	0.5	0.7	1.52	
212.3	3.4	2.5	4.3	140.3	0.5	0.7	1.52	
212.3	3.4	2.5	4.3	139.8	0.5	0.7	1.52	
235.9	3.4	2.5	4.3	155	0.5	0.7	1.52	
271.3	3.7	3	4.3	193	0.6	0.7	1.2	
247.7	3.5	2.8	4.3	168.4	0.6	0.7	1.33	
247.7	3.5	2.8	4.3	169	0.6	0.7	1.33	
250.1	3.5	2.8	4.3	170.3	0.6	0.7	1.33	
247.7	3.6	2.8	4.3	170.5	0.6	0.7	1.33	
247.7	3.6	2.8	4.3	172.9	0.6	0.7	1.33	
271.3	4	3.8	4.3	202.1	0.7	0.7	1.01	
247.7	4	3.8	4.3	184.6	0.7	0.7	1.01	
247.7	4	3.8	4.3	184.6	0.7	0.7	1.01	
247.7	4	3.8	4.3	184.6	0.7	0.7	1.01	
247.7	4	3.5	4.3	184.2	0.7	0.7	1.04	
253.1	3.6	1.8	4.3	177.4	0.3	0.7	2.65	
379.3	3.6	3	4.3	263.1	0.6	0.7	1.2	
448.4	3.6	2.8	4.3	313.6	0.5	0.7	1.33	
467.9	3.4	1.5	4.3	311.5	0.2	0.7	3.46	
401.1	3.3	2.5	4.3	259.4	0.5	0.7	1.52	
200.5	3.3	2.5	4.3	127.7	0.5	0.7	1.53	
212.3	3.9	3.8	4	152.9	0.7	0.7	1.01	
212.3	3.9	3.5	4	152.4	0.7	0.7	1.04	
212.3	3.7	3.3	4	150.9	0.7	0.7	1.11	
235	3.3	1	4	152.3	0.1	0.7	7.23	
194.5	3.5	2.8	4.3	134.5	0.6	0.7	1.33	
177	3.5	2.8	4.3	122.1	0.6	0.7	1.33	
212.3	3.9	3.8	4.3	154.4	0.7	0.7	1.01	
188.7	3.9	3.8	4.3	137.2	0.7	0.7	1.01	
167.1	3.2	1.5	3.8	107	0.2	0.7	3.46	
188.7	3.6	3.3	4	133.3	0.7	0.7	1.11	
188.7	3.8	3.5	4	136.1	0.7	0.7	1.04	
188.7	3.9	3.8	4.3	137.2	0.7	0.7	1.01	
330.3	2.3	1.8	3.3	132.6	0.3	0.6	2.48	
444	3.6	2.8	4.3	297.4	0.5	0.7	1.34	
857.3	3.6	2.5	4.3	570.1	0.5	0.7	1.36	
413.5	3.7	2.8	4.3	275.5	0.5	0.7	1.35	
340.4	3.4	2.8	4.3	209.4	0.5	0.7	1.35	
310.8	3.5	2.5	4.3	198.9	0.4	0.7	1.54	
310.8	3.4	2.5	4.3	189.2	0.4	0.7	1.54	
310.8	3.5	2.5	4.3	197.3	0.4	0.7	1.54	
310.8	3.3	2.5	4.3	188.9	0.4	0.7	1.54	
312.9	3.3	2.5	4.3	189.3	0.4	0.7	1.54	
492.9	3.5	2.5	4.3	326.2	0.5	0.7	1.53	
236.7	3.4	2.5	4.3	153.8	0.5	0.7	1.53	
266.3	3.4	2.5	4.3	172.4	0.5	0.7	1.53	
295.9	3.3	2.5	4.3	187.7	0.5	0.7	1.53	
310.7	3.4	2.5	4.3	203.8	0.5	0.7	1.53	
1230.8	3.5	1.5	4.3	813.7	0.2	0.7	3.53	
310.7	3.4	2.5	4.3	199.5	0.5	0.7	1.53	
310.7	3.4	2.5	4	205.3	0.5	0.7	1.53	
193.6	3.3	2.5	4	123.3	0.5	0.7	1.53	
310.7	2.8	2	3.8	172.1	0.3	0.7	2.13	

Table 32 South facade, Summertime 21st of June.

Town:	Jeddah					
Latitude:	21° 31' N					
Altitude:	15 m (AMSL)					
Tau (transmissivity):	0.7					
AO (ref. altitude):	8200 m (AMSL)					
Day:	21-Jun					
Starting hour:	0:00					
Ending hour:	24:00:00					
Grid precision:	15 min					
Area (m²)	Total energy (kWh)	Solar Flux kWh/m²				
23865.3	29242.1	1.225297817				
Area (m²)	Mean daylight (h)	Min daylight (h)	Max daylight (h)	Total energy (kWh)	Min local flux (kWh/m²)	Max local flux (kWh/m²)
478.4	8.1	6	9.3	602.6	1.2	1.3
439.9	7.6	2.5	9.3	548.3	0	1.3
401.3	8	6.8	9	517	1.2	1.3
374.4	8.1	6.3	9	482.8	1.2	1.3
391.2	8.4	7.3	9.3	495.4	1.2	1.3
436.7	8.4	6.8	9.3	553	1.2	1.3
436.8	8.5	7	9.3	554.4	1.2	1.3
436.8	8.5	7.3	9.3	554.4	1.2	1.3
420.9	8.5	7.5	9.3	532.8	1.2	1.3
478.4	8.5	7.3	9.3	608	1.2	1.3
429.7	8.5	7.8	9.3	543.1	1.2	1.3
436.7	8.5	6.8	9.3	548.8	1.2	1.3
436.7	8.5	6.8	9.3	548.8	1.2	1.3
436.7	8.4	6.8	9.3	548.8	1.2	1.3
374.3	8	7	9	478.7	1.2	1.3
436.8	8.6	6.8	9.5	532.8	0.9	1.2
436.7	8.5	7.3	9	563.7	1.3	1.3
270.4	7.6	2.8	9.5	258.1	0	1.2
294.9	7.3	5.5	9	350.4	1	1.3
247.9	7.6	6	9	279.6	1	1.2
247.7	7	5.5	8.5	290.6	1	1.3
345.6	6.6	5	8.8	418.3	1	1.3
353.8	6.4	4.8	8.5	437	1	1.3
353	6.8	5	9	422.3	1	1.3
374.8	6.8	5	9.3	448.7	1	1.3
223.7	7.8	6.3	8.8	281.2	1	1.3
200.8	7	5.5	8.8	246	1.1	1.3
200.5	7.4	6	8.8	246.4	1.1	1.3
306.8	7.3	6	8.5	393.3	1.2	1.3
306.8	7.4	6.5	8.5	390.2	1.2	1.3
306.8	7.5	6.5	8.5	390.3	1.2	1.3
280.6	7.7	6.8	8.5	362.2	1.2	1.3
271.3	7.8	6.8	8.8	335	1.1	1.3
247.7	8.1	7	8.8	316	1.2	1.3
247.7	8.3	7.8	8.8	319.8	1.3	1.3
370.3	7.8	6.8	8.8	458.7	1.1	1.3
330.3	7.8	6.8	8.8	407.6	1.1	1.3
212.3	7.7	6.8	8.8	260.9	1.1	1.3
242.4	6.5	2	8.8	217.1	0	1.3
333.9	7.2	3	8.8	357.4	0.1	1.3
294.9	7.7	6.3	8.8	360.5	1.1	1.3
88.5	7.9	7	9	105.9	1.1	1.3
188.7	8.1	7	9	231.9	1.1	1.3
188.7	8	7	9	228.1	1.1	1.3
188.7	8	7	9	228.2	1.1	1.3
188.7	8	7	9	228.5	1.1	1.3
307.5	8	7	9	375.8	1.1	1.3
252.7	8.2	7.3	9	316.9	1.1	1.3
271.3	8	7	9	336.8	1.1	1.3
235.9	7.9	6.5	8.8	296.9	1	1.3
271.3	7	3	8.8	283.4	0.1	1.3
247.7	7.6	6.3	8.8	300.7	1	1.3
247.7	7.5	6	8.8	300.2	1	1.3
247.7	7.6	6	8.8	309.4	1	1.3
237.2	7.5	6.3	8.8	303.8	1.2	1.3
353.5	7.7	6.3	9	421.1	1	1.3
247.7	7.8	6.8	8.8	304.4	1.1	1.3
247.7	7.8	6.8	9	304.3	1.1	1.3
247.7	8.1	6.8	9	315.7	1.1	1.3
247.7	8.3	7.5	9	320.2	1.3	1.3
212.4	6.9	4.3	8.8	268.9	0.7	1.3
188.8	7.6	6.5	9	221.9	1	1.3
188.8	7.5	6.3	8.8	221.2	1	1.3
148.7	7.5	6	9	180	1.1	1.3
45.5	6.5	5.5	8.8	57.9	1.2	1.3
266.3	8	6.5	9.3	320.7	0.9	1.3
850	7.7	5.8	9.3	986.9	0.9	1.3
837.3	7.8	5.3	9.3	987.4	0.8	1.3
600.4	8.2	6.5	9.5	717.3	0.9	1.3
414.4	7	5.3	8.8	518.8	1	1.3
724.7	7.6	5.3	9.3	898.1	1	1.3
340.6	8.3	6.8	9.5	404.5	0.9	1.2
392.8	7.8	5.8	9	485.1	1.1	1.3

Case C Facades Simulations (Obhur AISHmalya):

Table 33 Northeast facade, Summertime 21st of June.

Town:	Jeddah							
Latitude:	21° 31' N							
Altitude:	15 m (AMSL)							
Tau (transmissivity):	0.7							
AO (ref. altitude):	8200 m (AMSL)							
Day:	21-Jun							
Starting hour:	0:00							
Ending hour:	24:00:00							
Grid precision:	15 min							
Area (m²)	Total energy (kWh)	Solar Flux kWh/m²						
21956.9	30453.7	1.386976304						
Area (m²)	Mean daylight (h)	Min daylight (h)	Max daylight (h)	Total energy (kWh)	Min local flux (kWh/m²)	Max local flux (kWh/m²)	Variability factor	
118.7	5.6	2.5	6.8	155.7	0.4	1.5	3.38	
115.2	5.6	3.3	6.8	151.7	0.7	1.5	2.11	
198.3	6	5.8	6.3	290.1	1.4	1.5	1.02	
124.7	5.6	2.5	6.8	164.2	0.4	1.5	3.38	
124.7	5.5	2.5	6.8	163.9	0.4	1.5	3.38	
124.7	5.6	2.5	6.8	164.2	0.4	1.5	3.38	
124.7	5.5	2.5	6.8	163.9	0.4	1.5	3.38	
119.5	5.5	2.5	6.8	156.9	0.4	1.5	3.38	
94.7	5.5	2.5	6.8	125.8	0.4	1.5	3.38	
118.7	5.6	2.5	6.8	157.5	0.4	1.5	3.38	
122.4	5.6	3.3	6.8	163.1	0.7	1.5	2.11	
20	5.9	5.5	6.3	26.4	1.3	1.3	1.02	
574.3	5.9	0	6.5	823	0	1.5	1000	
189.2	6.3	5.8	6.5	282.5	1.5	1.5	1.02	
163.8	5.6	2.5	6.8	215.1	0.4	1.5	3.38	
124.7	5.5	2.5	6.8	163.5	0.4	1.5	3.38	
118.7	5.5	2.5	6.8	155.4	0.4	1.5	3.38	
311.3	6.1	5.8	6.5	456.8	1.5	1.5	1.02	
124.7	5.5	2.5	6.8	166.9	0.4	1.5	3.39	
118.7	5.5	2.5	6.8	158.9	0.4	1.5	3.39	
169.9	5.5	2.5	6.8	227.8	0.4	1.5	3.39	
15.5	5.8	5.5	6	21.2	1.3	1.4	1.02	
4	5.8	5.5	6.3	3.2	0.8	0.8	1.02	
309.1	6	5.3	6.5	462.1	1.4	1.5	1.09	
124.8	5.5	2.5	6.8	166.4	0.4	1.5	3.39	
166.1	5.5	2.5	6.8	221.9	0.4	1.5	3.39	
118.8	5.5	3	6.8	159.3	0.6	1.5	2.43	
329	6	5.5	6.5	496.6	1.5	1.5	1.05	
91.8	5.6	3	6.8	124.3	0.6	1.5	2.43	
100.7	5.6	2.5	6.8	135.4	0.4	1.5	3.38	
14.2	5.8	5.5	6.3	19	1.3	1.3	1.02	
155.1	6.2	5.8	6.5	231.7	1.5	1.5	1.02	
124.7	5.6	2.5	6.8	165.9	0.4	1.5	3.38	
124.7	5.6	2.5	6.8	165.9	0.4	1.5	3.38	
124.7	5.6	2.5	6.8	165.9	0.4	1.5	3.38	
124.7	5.6	2.5	6.8	165.9	0.4	1.5	3.38	
124.7	5.5	2.5	6.8	165.6	0.4	1.5	3.38	
124.7	5.5	2.5	6.8	165.6	0.4	1.5	3.38	
124.7	5.6	2.5	6.8	165.9	0.4	1.5	3.38	
124.7	5.5	2.5	6.8	165.6	0.4	1.5	3.38	
83.4	5.6	2.5	6.8	111.9	0.4	1.5	3.38	
124.7	5.5	2.5	6.8	165.6	0.4	1.5	3.38	
118.7	5.5	2.3	6.8	156.2	0.4	1.5	4.14	
1152.7	6.3	6	6.5	1725.2	1.5	1.5	1.01	
148.7	5.6	2.5	6.8	197.4	0.4	1.5	3.38	
154.8	5.5	2.5	6.8	206.1	0.4	1.5	3.39	
154.8	5.5	2.5	6.8	206.1	0.4	1.5	3.39	
117.8	5.5	2.5	6.8	156.9	0.4	1.5	3.39	
154.7	5.6	2.5	6.8	203.2	0.4	1.5	3.38	
154.7	5.6	2.5	6.8	203.2	0.4	1.5	3.38	
154.7	5.6	2.5	6.8	203.2	0.4	1.5	3.38	
154.7	5.6	2.5	6.8	203.2	0.4	1.5	3.38	
73.6	5.6	3.5	6.8	100.8	0.8	1.5	1.87	
81.1	5.6	2.5	6.8	107.6	0.4	1.5	3.38	
148.7	5.5	3	6.8	195.9	0.6	1.5	2.42	
1158.4	6	5.3	6.5	1713.5	1.4	1.5	1.09	
40.6	5.4	3.3	6.8	55.7	0.8	1.5	1.87	
36.6	3.1	0	5.5	7.7	0	0.3	1000	
124.7	5.5	2.5	6.8	164.4	0.4	1.5	3.39	
124.7	5.5	2.5	6.8	164.7	0.4	1.5	3.39	
124.7	5.5	2.5	6.8	164.4	0.4	1.5	3.39	
124.7	5.5	2.5	6.8	164.4	0.4	1.5	3.39	
198	5.4	2.5	6.8	259.3	0.4	1.5	3.39	
118.7	5.6	2.5	6.8	162.9	0.5	1.5	3.39	
114.8	5.6	2.5	6.8	156.8	0.5	1.5	3.39	
566.4	6.1	3.5	6.5	841	1	1.5	1.53	
177.3	6.1	5.8	6.5	269.6	1.5	1.5	1.02	
5.2	5.8	5.5	6.3	2.5	0.5	0.5	1.01	
304.6	5.6	2.8	6.8	400.6	0.5	1.5	2.83	
298.7	5.6	2.5	6.8	393.1	0.4	1.5	3.38	
124.7	5.5	2.5	6.8	163.7	0.4	1.5	3.38	
124.7	5.6	2.5	6.8	164	0.4	1.5	3.38	
124.7	5.5	2.5	6.8	163.7	0.4	1.5	3.38	
124.7	5.6	2.5	6.8	164	0.4	1.5	3.38	
118.7	5.5	3	6.8	156.4	0.6	1.5	2.42	

Table 34 Northeast facade, Wintertime 21st of December.

Town:	Jeddah							
Latitude:	21° 31' N							
Altitude:	15 m (AMSL)							
Tau (transmissivity):	0.7							
AO (ref. altitude):	8200 m (AMSL)							
Day:	21-Dec							
Starting hour:	0:00							
Ending hour:	24:00:00							
Grid precision:	15 min							
Area (m²)	Total energy (kWh)	Solar Flux kWh/m²						
21956.9	48108.7	2.19105156						
Area (m²)	Mean daylight (h)	Min daylight (h)	Max daylight (h)	Total energy (kWh)	Min local flux (kWh/m²)	Max local flux (kWh/m²)	Variability factor	
118.7	5.6	0.3	7.5	234.7	0.1	2.6	25.04	
115.2	5.5	0	7.5	227	0	2.6	1000	
198.3	6.4	5.8	7	483.5	2.2	2.6	1.17	
124.7	5.6	0	7.5	245.3	0	2.6	1000	
124.7	5.6	0	7.5	245.6	0	2.6	1000	
124.7	5.6	0	7.5	245.2	0	2.6	1000	
124.7	5.6	0	7.5	245.7	0	2.6	1000	
119.5	5.6	0	7.5	234.7	0	2.6	1000	
94.7	5.6	0	7.5	185	0	2.6	1000	
118.7	5.6	0	7.5	231.6	0	2.6	1000	
122.4	5.7	0	7.5	239.6	0	2.6	1000	
20	6.9	6.3	7.5	52.9	2.4	2.8	1.16	
574.3	6.5	5.8	7.5	1407.6	2.2	2.6	1.18	
189.2	7	6.5	7.5	488.3	2.5	2.6	1.04	
163.8	5.6	0	7.5	323.2	0	2.6	1000	
124.7	5.6	0	7.5	246	0	2.6	1000	
118.7	5.6	0	7.5	234.2	0	2.6	1000	
311.3	6.4	5.8	7.3	759.3	2.2	2.6	1.18	
124.7	5.6	0	7.5	242.3	0	2.6	1000	
118.7	5.6	0	7.5	229.3	0	2.6	1000	
169.9	5.6	0	7.5	329.8	0	2.6	1000	
15.5	6.7	6	7.3	40.5	2.4	2.7	1.17	
4	6.9	6	8.8	12	2.8	3.3	1.17	
309.1	6.4	5.8	7.5	746.8	2.2	2.6	1.18	
124.8	5.6	0	7.5	240.9	0	2.6	1000	
166.1	5.6	0	7.5	320.7	0	2.6	1000	
118.8	5.6	0	7.5	228.9	0	2.6	1000	
329	6.5	5.8	7.5	792.6	2.2	2.6	1.18	
91.8	5.5	0	7.5	177.7	0	2.6	1000	
100.7	5.6	0	7.5	195.9	0	2.6	1000	
14.2	6.7	6	7.3	37.3	2.4	2.8	1.16	
155.1	6.5	5.8	7.5	385	2.2	2.6	1.18	
124.7	5.6	0	7.5	243.7	0	2.6	1000	
124.7	5.6	0	7.5	243.7	0	2.6	1000	
124.7	5.7	0	7.5	243.7	0	2.6	1000	
124.7	5.6	0	7.5	243.7	0	2.6	1000	
124.7	5.7	0	7.5	244.1	0	2.6	1000	
124.7	5.7	0	7.5	244.1	0	2.6	1000	
124.7	5.7	0	7.5	244.1	0	2.6	1000	
124.7	5.6	0	7.5	243.7	0	2.6	1000	
124.7	5.7	0	7.5	244.1	0	2.6	1000	
83.4	5.5	0	7.5	160.9	0	2.6	1000	
124.7	5.7	0	7.5	244.1	0	2.6	1000	
118.7	5.7	0	7.5	232.4	0	2.6	1000	
1152.7	6.9	6.3	7.5	2963.1	2.4	2.6	1.08	
148.7	5.6	0	7.5	290.9	0	2.6	1000	
154.8	5.6	0.5	7.5	299.5	0.2	2.6	13.18	
154.8	5.6	0	7.5	299.2	0	2.6	1000	
117.8	5.6	0	7.5	227.6	0	2.6	1000	
154.7	5.6	0	7.5	305	0	2.6	1000	
154.7	5.6	0	7.5	305	0	2.6	1000	
154.7	5.6	0	7.5	305	0	2.6	1000	
73.6	5.6	0	7.5	142.8	0	2.6	1000	
81.1	5.7	2.8	7.5	161.9	0.6	2.6	4.31	
148.7	5.6	0	7.5	293.1	0	2.6	1000	
1158.4	6.5	5.8	7.5	2850.8	2.2	2.6	1.18	
40.6	5.5	0	7.5	76.6	0	2.6	1000	
36.6	6.9	1.5	10.5	104.6	0.4	3.6	10.19	
124.7	5.5	0	7.5	234.9	0	2.6	1000	
124.7	5.4	0	7.5	234.5	0	2.6	1000	
124.7	5.5	0	7.5	234.9	0	2.6	1000	
124.7	5.5	0	7.5	234.9	0	2.6	1000	
198	5.4	0	7.5	381.3	0	2.6	1000	
118.7	5.7	0	7.5	231.1	0	2.6	1000	
114.8	5.6	0	7.5	222.5	0	2.6	1000	
566.4	6.5	5.8	7.5	1376.6	2.2	2.6	1.18	
177.3	6.4	5.8	7.5	423.2	2.2	2.6	1.18	
5.2	9.4	8.8	10	17.6	3.2	3.5	1.11	
304.6	5.5	0	7.5	605.9	0	2.6	1000	
298.7	5.5	0	7.5	592.6	0	2.6	1000	
124.7	5.6	0	7.5	245.9	0	2.6	1000	
124.7	5.6	0	7.5	245.7	0	2.6	1000	
124.7	5.6	0	7.5	245.9	0	2.6	1000	
124.7	5.6	0	7.5	245.5	0	2.6	1000	
118.7	5.6	0	7.5	234.1	0	2.6	1000	

Table 35 Northwest facade, Summertime 21st of June.

Town:	Jeddah							
Latitude:	21° 31' N							
Altitude:	15 m (AMSL)							
Tau (transmissivity):	0.7							
A0 (ref. altitude):	8200 m (AMSL)							
Day:	21-Jun							
Starting hour:	0:00							
Ending hour:	24:00:00							
Grid precision:	15 min							
Area (m²)	Total energy (kWh)	Solar Flux kWh/m²						
14833.9	14402	0.970884258						
Area (m²)	Mean daylight (h)	Min daylight (h)	Max daylight (h)	Total energy (kWh)	Min local flux (kWh/m²)	Max local flux (kWh/m²)	Variability factor	
124.7	5.6	2	6.5	117.6	0.3	1	3.97	
124.7	5.7	2	6.5	118	0.3	1	3.97	
118.7	5.7	2.3	6.5	112.1	0.3	1	3.24	
109.5	5.6	2	6.5	103.4	0.3	1	3.97	
124.7	5.7	2	6.5	117.6	0.3	1	3.97	
487.1	6.2	6	6.5	487.4	1	1	1	
118.8	5.7	2	6.5	118.4	0.3	1.1	4	
119.6	5.6	2	6.5	118	0.3	1.1	4	
124.7	5.6	2	6.5	118.4	0.3	1	3.97	
124.7	5.6	2	6.5	118.4	0.3	1	3.97	
124.7	5.5	2	6.5	118.4	0.3	1	3.97	
118.7	5.6	2	6.5	113	0.3	1	3.97	
124.7	5.6	2	6.5	118.4	0.3	1	3.97	
10.4	6.4	6.3	6.8	16.8	1.6	1.6	1	
177.1	6.3	6	6.5	188.8	1.1	1.1	1	
12.6	4.8	2.5	6	15	0.6	1.4	2.2	
493.2	6	4.3	6.3	495.4	0.8	1	1.26	
100.8	5.6	2	6.5	91.4	0.2	1	3.95	
92.9	5.6	2.8	6.5	84.8	0.4	1	2.31	
12.7	6.1	6	6.3	15	1.2	1.2	1	
151	6.1	6	6.3	145.2	1	1	1	
100.3	5.6	2.8	6.5	96.5	0.4	1	2.33	
100.7	5.5	2	6.5	95.6	0.3	1	3.97	
7.5	5.7	5.8	5.8	2.7	0.4	0.4	1	
156.3	6.1	5.8	6.3	158.5	1	1	1	
81.5	5.5	2.8	6.5	80.7	0.4	1	2.34	
58.8	5.4	1.8	6.5	56.6	0.2	1	5.04	
123.8	5.8	4.8	6.3	128.5	0.9	1	1.12	
12.4	6.1	5.8	6.3	8	0.6	0.6	1	
145.8	5.7	2.8	6.5	139.9	0.4	1	2.33	
124.7	5.6	2	6.5	118	0.3	1	3.97	
124.7	5.6	2	6.5	117.9	0.3	1	3.97	
124.7	5.6	2	6.5	118.4	0.3	1	3.97	
124.7	5.6	2	6.5	118.4	0.3	1	3.97	
124.7	5.6	2	6.5	118.4	0.3	1	3.97	
124.7	5.6	2	6.5	118.4	0.3	1	3.97	
118.7	5.6	2	6.5	112.6	0.3	1	3.97	
811	6.1	5.3	6.3	813.1	1	1	1.04	
118.7	5.6	2	6.5	110.8	0.3	1	3.96	
109.2	5.6	2.5	6.5	102.9	0.4	1	2.71	
176.3	6.1	6	6.3	174.7	1	1	1	
168.2	5.6	2.8	6.5	164.6	0.4	1	2.33	
148.7	5.6	2	6.5	144.9	0.3	1	3.98	
236.9	6	5.3	6.3	244	1	1	1.04	
124.7	5.6	1.8	6.5	117.9	0.2	1	5.01	
124.7	5.6	1.8	6.5	118.4	0.2	1	5.01	
124.7	5.6	1.8	6.5	118.4	0.2	1	5.01	
124.7	5.6	1.8	6.5	118.4	0.2	1	5.01	
124.7	5.5	1.8	6.5	118.1	0.2	1	5.01	
120	5.6	2	6.5	114.7	0.3	1	3.98	
111.9	5.6	2.3	6.5	107.8	0.3	1	3.25	
118.7	5.6	1.8	6.5	112.2	0.2	1	5.01	
594.2	6	3	6.3	590.3	0.6	1	1.82	
171.7	6	5.5	6.3	175.2	1	1	1.02	
106.1	5.6	2	6.5	101	0.3	1	3.97	
154.7	5.6	2	6.5	146.7	0.3	1	3.97	
154.7	5.6	2	6.5	146.7	0.3	1	3.97	
154.7	5.6	2	6.5	146.7	0.3	1	3.97	
154.7	5.6	2	6.5	146.7	0.3	1	3.97	
194.4	5.6	2.3	6.5	183.2	0.3	1	3.24	
154.7	5.6	2	6.5	146.7	0.3	1	3.97	
148.7	5.6	2	6.5	141	0.3	1	3.97	
118.7	5.6	2.8	6.5	114.2	0.4	1	2.33	
124.7	5.6	2	6.5	119	0.3	1	3.97	
124.7	5.6	2	6.5	119	0.3	1	3.97	
130.9	5.6	2	6.5	124.5	0.3	1	3.97	
140.9	5.6	2	6.5	132.1	0.2	1	3.96	
124.8	5.6	2	6.5	116.4	0.2	1	3.96	
124.8	5.6	2	6.5	116.4	0.2	1	3.96	
118.8	5.6	2.3	6.5	110.6	0.3	1	3.24	
66.3	5.5	2	6.5	61.8	0.3	1	3.97	
94.7	5.6	2	6.5	90	0.3	1	3.97	
94.7	5.6	2	6.5	89.8	0.3	1	3.97	
94.7	5.6	2	6.5	90	0.3	1	3.97	
131	5.6	2	6.5	125	0.3	1	3.97	
92.2	5.8	4.5	6.5	90.3	0.9	1	1.18	

Table 36 Northwest facade, Wintertime 21st of December.

Town:	Jeddah							
Latitude:	21° 31' N							
Altitude:	15 m (AMSL)							
Tau (transmissivity):	0.7							
A0 (ref. altitude):	8200 m (AMSL)							
Day:	21-Dec							
Starting hour:	0:00							
Ending hour:	24:00:00							
Grid precision:	15 min							
Area (m ²)	Total energy (kWh)	Solar Flux kWh/m ²						
14833.9	38770.5	2.613641726						
Area (m ²)	Mean daylight (h)	Min daylight (h)	Max daylight (h)	Total energy (kWh)	Min local flux (kWh/m ²)	Max local flux (kWh/m ²)	Variability factor	
124.7	6.6	0	8.8	289.4	0	3.1	1000	
124.7	6.6	0	8.8	289	0	3.1	1000	
118.7	6.7	0	8.8	275.4	0	3.1	1000	
109.5	6.7	0.3	8.8	258.9	0.1	3.1	30.11	
124.7	6.6	0	8.8	289.4	0	3.1	1000	
487.1	8.1	7.5	8.8	1481.3	2.9	3.1	1.06	
118.8	6.5	0	8.5	271.2	0	3	1000	
119.6	6.5	0	8.5	271.9	0	3	1000	
124.7	6.5	0	8.8	287.5	0	3.1	1000	
124.7	6.6	0	8.8	287.7	0	3.1	1000	
124.7	6.6	0	8.8	287.7	0	3.1	1000	
118.7	6.5	0	8.8	272.7	0	3.1	1000	
124.7	6.6	0	8.8	287.6	0	3.1	1000	
10.4	7.1	7	7.3	25.8	2.5	2.5	1	
177.1	7.8	7.3	8.5	525.2	2.9	3	1.06	
12.6	7	6.5	7.5	33.4	2.5	2.7	1.07	
493.2	7.8	7	8.8	1439.9	2.7	3.1	1.14	
100.8	6.9	0	9	241.3	0	3.1	1000	
92.9	6.8	0	9	221.5	0	3.1	1000	
12.7	7.3	6.8	7.8	36	2.7	2.9	1.1	
151	7.9	7.3	8.8	450.1	2.8	3.1	1.14	
100.3	6.5	0	8.8	232.6	0	3.1	1000	
100.7	6.6	0	8.8	234	0	3.1	1000	
7.5	8	7	9.8	25.5	3.2	3.6	1.13	
156.3	7.6	7	8.5	456.9	2.7	3.1	1.14	
81.5	6.7	0	8.8	190.7	0	3.1	1000	
58.8	6.6	0	8.8	136.3	0	3.1	1000	
123.8	7.8	7	8.8	364.1	2.7	3.1	1.14	
12.4	8.7	7.3	9.8	40.8	3	3.4	1.12	
145.8	6.6	0	8.8	337.3	0	3.1	1000	
124.7	6.5	0	8.8	288.7	0	3.1	1000	
124.7	6.6	0	8.8	289	0	3.1	1000	
124.7	6.6	0	8.8	288.5	0	3.1	1000	
124.7	6.6	0	8.8	288.6	0	3.1	1000	
124.7	6.5	0	8.8	288.3	0	3.1	1000	
124.7	6.6	0	8.8	288.6	0	3.1	1000	
118.7	6.6	0	8.8	275.5	0	3.1	1000	
811	7.9	7	8.8	2409.2	2.7	3.1	1.14	
118.7	6.6	0	8.8	276.4	0	3.1	1000	
109.2	6.6	0	8.8	258.1	0	3.1	1000	
176.3	7.5	6.8	8.5	504.2	2.6	3.1	1.19	
168.2	6.7	0	8.8	385.8	0	3.1	1000	
148.7	6.6	0	8.8	340.9	0	3.1	1000	
236.9	7.7	7	8.5	684.6	2.7	3.1	1.14	
124.7	6.8	0	8.8	297.5	0	3.1	1000	
124.7	6.8	0	8.8	297	0	3.1	1000	
124.7	6.8	0	8.8	297	0	3.1	1000	
124.7	6.7	0	8.8	296.8	0	3.1	1000	
124.7	6.7	0	8.8	296.9	0	3.1	1000	
120	6.5	0	8.8	266.5	0	3.1	1000	
111.9	6.5	0	8.8	253.3	0	3.1	1000	
118.7	6.9	0	8.8	284.1	0	3.1	1000	
594.2	8.3	7	8.8	1804.1	2.7	3.1	1.14	
171.7	8	7.5	8.8	515.1	2.9	3.1	1.06	
106.1	6.6	0	8.8	247.1	0	3.1	1000	
154.7	6.6	0	8.8	359.2	0	3.1	1000	
154.7	6.7	0	8.8	359.2	0	3.1	1000	
154.7	6.6	0	8.8	359.2	0	3.1	1000	
154.7	6.6	0	8.8	359.2	0	3.1	1000	
194.4	6.7	0	8.8	465	0	3.1	1000	
154.7	6.6	0	8.8	359.2	0	3.1	1000	
148.7	6.7	0	8.8	346.2	0	3.1	1000	
118.7	6.6	0	8.8	274.2	0	3.1	1000	
124.7	6.6	0	8.8	288.1	0	3.1	1000	
124.7	6.6	0	8.8	288.1	0	3.1	1000	
130.9	6.7	0.3	8.8	303.9	0.1	3.1	30.15	
140.9	6.7	0	8.8	329.4	0	3.1	1000	
124.8	6.7	0	8.8	290.7	0	3.1	1000	
124.8	6.6	0	8.8	290.7	0	3.1	1000	
118.8	6.6	0	8.8	276.6	0	3.1	1000	
66.3	6.6	0	8.8	156.3	0	3.1	1000	
94.7	6.5	0	8.8	219.7	0	3.1	1000	
94.7	6.5	0	8.8	220	0	3.1	1000	
94.7	6.5	0	8.8	219.7	0	3.1	1000	
131	6.8	3.3	8.8	304.9	0.7	3.1	4.74	
92.2	6.6	0	8.8	213.8	0	3.1	1000	

Table 37 Southeast facade, Summertime 21st of June.

Location:	Jeddah						
Latitude:	21° 31' N						
Altitude:	15 m (AMSL)						
Tau (transmissivity):	0.7						
AO (ref. altitude):	8200 m (AMSL)						
Day:	21-Jun						
Starting hour:	0:00						
Ending hour:	24:00:00						
Grid precision:	15 min						
Area (m²)	Total energy (kWh)	Solar Flux kWh/m²					
15120.4	26656.2	1.762929552					
Area (m²)	Mean daylight (h)	Min daylight (h)	Max daylight (h)	Total energy (kWh)	Min local flux (kWh/m²)	Max local flux (kWh/m²)	Variability factor
124.7	5.5	3	7	196.4	0.6	1.9	3.11
124.7	5.5	3	7	196.4	0.6	1.9	3.11
118.7	5.5	3	7	187	0.6	1.9	3.11
124.7	5.5	3	7	196.4	0.6	1.9	3.11
108.1	5.5	3.5	7	170.7	0.8	1.9	2.31
493.4	5.9	5.5	6.5	903	1.7	1.9	1.11
173.9	5.5	3	7	273.4	0.6	1.9	3.11
124.7	5.5	3	7	196.1	0.6	1.9	3.11
124.7	5.5	3	7	196.1	0.6	1.9	3.11
124.7	5.5	3	7	196.1	0.6	1.9	3.11
124.7	5.5	3	7	196.1	0.6	1.9	3.11
122.9	5.5	3	7	193.2	0.6	1.9	3.11
118.7	5.5	3.5	7	187.2	0.8	1.9	2.31
725.9	6.2	5.8	6.8	1364.3	1.8	1.9	1.06
97.3	5.4	3	7	153.6	0.6	1.9	3.11
100.7	5.5	2.8	7	158.7	0.5	1.9	3.69
160.2	6.1	5.5	6.8	297.2	1.7	1.9	1.11
101.2	5.4	3	7	157.5	0.6	1.9	3.11
100.7	5.4	2.8	7	155.5	0.5	1.9	3.69
155.3	6	5.5	6.5	284.6	1.7	1.9	1.11
20.6	5.7	5.3	6.3	44.4	2	2.2	1.11
73.9	5.5	3	7	118.2	0.6	1.9	3.11
58.8	5.5	3.3	7	94.1	0.7	1.9	2.66
8.7	6	5.5	6.5	17.8	1.9	2.1	1.11
119.9	6	5.5	6.5	223.7	1.7	1.9	1.11
145.4	5.5	3	7	228.9	0.6	1.9	3.11
124.7	5.5	3	7	196.4	0.6	1.9	3.11
124.7	5.5	3	7	196.4	0.6	1.9	3.11
124.7	5.5	3	7	196.6	0.6	1.9	3.11
124.7	5.5	3	7	196.5	0.6	1.9	3.11
124.7	5.5	3	7	196.5	0.6	1.9	3.11
124.7	5.5	3	7	196.4	0.6	1.9	3.11
118.7	5.5	3.3	7	187.3	0.7	1.9	2.66
8.8	6.3	5.8	6.5	18.9	2	2.2	1.06
805.5	6.2	5.8	6.8	1516.1	1.8	1.9	1.06
203	10.9	9	13	1370	6.4	6.9	1.09
105.7	5.4	3	7	165.1	0.6	1.9	3.11
118.7	5.5	2.5	7	183.8	0.4	1.9	4.47
11.5	6.3	6.3	6.5	26.5	2.3	2.3	1
170.8	6	5.5	6.8	311.3	1.7	1.9	1.11
167.2	5.5	3	7	261.4	0.6	1.9	3.11
148.7	5.5	3.3	7	232.5	0.7	1.9	2.66
7	5.8	5.3	6.3	16.5	2.2	2.4	1.1
244.7	5.9	5.5	6.5	443.2	1.7	1.9	1.11
139.4	5.5	3	7	218	0.6	1.9	3.11
124.7	5.5	3	7	195	0.6	1.9	3.11
124.7	5.5	3	7	195	0.6	1.9	3.11
124.7	5.5	3	7	195	0.6	1.9	3.11
124.7	5.5	3	7	195	0.6	1.9	3.11
124.7	5.6	3	7	195	0.6	1.9	3.11
124.7	5.5	3	7	195.1	0.6	1.9	3.11
118.7	5.5	2.8	7	185.2	0.5	1.9	3.69
792.3	6.3	6	6.8	1498.7	1.9	1.9	1.03
11.9	6	5.8	6.3	27.3	2.3	2.3	1.03
106.8	5.1	2.8	7	149.2	0.5	1.9	3.69
124.8	5.5	3	7	195	0.6	1.9	3.11
124.8	5.5	3	7	194.8	0.6	1.9	3.11
118.8	5.5	3	7	185.5	0.6	1.9	3.11
139.8	5.6	3	7	217.9	0.6	1.9	3.11
117.5	5.5	3	7	183.9	0.6	1.9	3.11
118.7	5.5	3.3	7	185.9	0.7	1.9	2.66
100.7	5.5	3.5	7	158.2	0.8	1.9	2.31
104.2	5.5	3	7	163.2	0.6	1.9	3.11
124.7	5.6	3.5	7	196.5	0.8	1.9	2.31
124.7	5.5	3	7	196.1	0.6	1.9	3.11
124.7	5.5	3	7	195.9	0.6	1.9	3.11
124.7	5.5	3	7	196.1	0.6	1.9	3.11
124.7	5.5	3	7	195.9	0.6	1.9	3.11
118.7	5.5	3	7	186.6	0.6	1.9	3.11
18.1	5.7	3.5	7	30.9	0.8	1.9	2.31
65.7	5.5	3	7	104.4	0.6	1.9	3.11
94.7	5.5	3	7	149.4	0.6	1.9	3.11
94.7	5.5	3	7	149.5	0.6	1.9	3.11
94.7	5.5	3	7	149.4	0.6	1.9	3.11
112.3	5.1	2.8	7	157	0.5	1.9	3.69
84.2	5.6	3.5	7	123	0.8	1.7	2.05

Table 38 Southeast facade, Wintertime 21st of December.

Town:	Jeddah							
Latitude:	21° 31' N							
Altitude:	15 m (AMSL)							
Tau (transmissivity):	0.7							
A0 (ref. altitude):	8200 m (AMSL)							
Day:	21-Dec							
Starting hour:	0:00							
Ending hour:	24:00:00							
Grid precision:	15 min							
Area (m ²)	Total energy (kWh)	Solar Flux kWh/m ²						
15120.4	1016.1	0.067200603						
Area (m ²)	Mean daylight (h)	Min daylight (h)	Max daylight (h)	Total energy (kWh)	Min local flux (kWh/m ²)	Max local flux (kWh/m ²)	Variability factor	
124.7	1.2	0	1.8	2.7	0	0	1000	
124.7	1.2	0	1.8	2.7	0	0	1000	
118.7	1.2	0	1.8	2.6	0	0	1000	
124.7	1.2	0	1.8	2.7	0	0	1000	
108.1	1.2	0	1.8	2.4	0	0	1000	
493.4	1.5	0	1.8	13.5	0	0	1000	
173.9	1.3	0	1.8	4	0	0	1000	
124.7	1.2	0	1.8	2.7	0	0	1000	
124.7	1.2	0	1.8	2.7	0	0	1000	
124.7	1.2	0	1.8	2.7	0	0	1000	
124.7	1.2	0	1.8	2.7	0	0	1000	
122.9	1.2	0	1.8	2.6	0	0	1000	
118.7	1.3	0	1.8	2.6	0	0	1000	
725.9	1.6	1.5	1.8	20.6	0	0	1	
97.3	1.1	0	1.8	2.1	0	0	1000	
100.7	1.1	0	1.8	2.2	0	0	1000	
160.2	1.4	0.3	1.8	4.4	0	0	12.58	
101.2	1.2	0	1.8	1.6	0	0	1000	
100.7	1.2	0	1.8	1.7	0	0	1000	
155.3	1.6	1.5	1.8	3.6	0	0	1	
20.6	2.8	2.5	3	4.5	0.2	0.2	1.16	
73.9	1.1	0	1.8	1.6	0	0	1000	
58.8	1.1	0	1.8	1.2	0	0	1000	
8.7	2.3	2.3	2.5	1	0.1	0.1	1	
119.9	1.6	1.5	1.8	3.9	0	0	1	
145.4	1.3	0	1.8	3.3	0	0	1000	
124.7	1.2	0	1.8	2.7	0	0	1000	
124.7	1.2	0	1.8	2.7	0	0	1000	
124.7	1.2	0	1.8	2.8	0	0	1000	
124.7	1.2	0	1.8	2.8	0	0	1000	
124.7	1.2	0	1.8	2.7	0	0	1000	
118.7	1.2	0	1.8	2.7	0	0	1000	
8.8	2.7	2.5	2.8	1.3	0.1	0.1	1	
805.5	1.6	1.5	1.8	23.5	0	0	1	
203	8.8	5.8	10.5	646	2.3	3.4	1.49	
105.7	1.2	0	1.8	1.8	0	0	1000	
118.7	1.2	0	1.8	2.2	0	0	1000	
11.5	2.9	2.5	3.3	3.6	0.3	0.3	1.17	
170.8	1.5	0.8	1.8	3.9	0	0	2.12	
167.2	1.3	0	1.8	3.3	0	0	1000	
148.7	1.3	0	1.8	3	0	0	1000	
7	4.1	4	4.3	4.6	0.7	0.7	1	
244.7	1.6	1.5	1.8	6.1	0	0	1	
139.4	1.3	0	1.8	2.8	0	0	1000	
124.7	1.2	0	1.8	2.4	0	0	1000	
124.7	1.2	0	1.8	2.4	0	0	1000	
124.7	1.2	0	1.8	2.4	0	0	1000	
124.7	1.2	0	1.8	2.4	0	0	1000	
124.7	1.2	0	1.8	2.4	0	0	1000	
124.7	1.2	0	1.8	2.4	0	0	1000	
118.7	1.2	0	1.8	2.3	0	0	1000	
792.3	1.7	1.5	1.8	20.2	0	0	1	
11.9	3.4	3.3	3.5	3.9	0.3	0.3	1	
106.8	1.2	0	1.8	2	0	0	1000	
124.8	1.2	0	1.8	2.3	0	0	1000	
124.8	1.2	0	1.8	2.2	0	0	1000	
118.8	1.2	0	1.8	2.1	0	0	1000	
139.8	1.3	0	1.8	2.6	0	0	1000	
117.5	1.2	0	1.8	2.3	0	0	1000	
118.7	1.3	0	1.8	2.3	0	0	1000	
100.7	1.5	1	1.8	2.5	0	0	1.33	
104.2	1.2	0	1.8	2	0	0	1000	
124.7	1.1	0	1.8	2.6	0	0	1000	
124.7	1.2	0	1.8	2.6	0	0	1000	
124.7	1.2	0	1.8	2.6	0	0	1000	
124.7	1.2	0	1.8	2.6	0	0	1000	
124.7	1.2	0	1.8	2.6	0	0	1000	
118.7	1.2	0	1.8	2.5	0	0	1000	
18.1	0.1	0	1.8	0	0	0	1000	
65.7	1	0	1.8	1.2	0	0	1000	
94.7	1.1	0	1.8	2	0	0	1000	
94.7	1.1	0	1.8	2	0	0	1000	
94.7	1.1	0	1.8	2	0	0	1000	
112.3	1.2	0	1.8	2.1	0	0	1000	
84.2	0.3	0	1	0	0	0	1000	

Table 39 Southwest facade, Summertime 21st of June.

Town:	Jeddah							
Latitude:	21° 31' N							
Altitude:	15 m (AMSL)							
Tau (transmissivity):	0.7							
A0 (ref. altitude):	8200 m (AMSL)							
Day:	21-Jun							
Starting hour:	0:00							
Ending hour:	24:00:00							
Grid precision:	15 min							
Area (m²)	Total energy (kWh)	Solar Flux kWh/m²						
21805.9	41732.2	1.913803145						
Area (m²)	Mean daylight (h)	Min daylight (h)	Max daylight (h)	Total energy (kWh)	Min local flux (kWh/m²)	Max local flux (kWh/m²)	iability fa	
118.7	5.2	2.5	6.8	206.7	0.6	2.2	3.65	
118.4	5.1	3	6.8	206.7	0.8	2.2	2.63	
189	6.1	5.8	6.8	412	2.1	2.2	1.03	
124.7	5.2	3	6.8	219	0.8	2.2	2.62	
124.7	5.2	3	6.8	219	0.8	2.2	2.62	
124.7	5.2	3	6.8	219	0.8	2.2	2.62	
94.7	5.1	3	6.8	165.7	0.8	2.2	2.62	
154.7	5.1	3	6.8	271.6	0.8	2.2	2.62	
113.2	5.1	2.3	6.8	197.1	0.5	2.2	4.43	
118.6	5.2	3	6.8	208.3	0.8	2.2	2.62	
771.4	6.1	5.8	6.8	1688.7	2.2	2.2	1.03	
124.7	5.1	3	6.8	219.5	0.8	2.2	2.62	
169	5.1	3	6.8	297.3	0.8	2.2	2.62	
118.7	5.1	3	6.8	208.9	0.8	2.2	2.62	
323	5.5	5	6.5	665.3	1.9	2.2	1.17	
118.7	5.1	3	6.8	209.8	0.9	2.2	2.62	
124.7	5.1	3	6.8	220.4	0.9	2.2	2.62	
166.1	5.1	3	6.8	293.5	0.9	2.2	2.62	
320.8	5.6	5	6.5	668.4	1.9	2.2	1.17	
164.5	5.1	3	6.8	289	0.8	2.2	2.62	
124.7	5.1	3	6.8	219.2	0.8	2.2	2.62	
118.7	5.1	3	6.8	208.6	0.8	2.2	2.62	
12.1	5.8	5.3	6.3	22.8	1.7	2	1.16	
319.1	5.6	5	6.3	659.8	1.9	2.2	1.17	
95.7	5.1	3	6.8	167.6	0.8	2.2	2.62	
100.7	5.1	3	6.8	176.5	0.8	2.2	2.62	
2.5	6.1	5.8	6.5	4.3	1.7	1.8	1.06	
164.1	5.9	5.5	6.5	355.2	2.1	2.2	1.06	
124.7	5.1	3	6.8	219.3	0.8	2.2	2.62	
124.7	5.1	3	6.8	219.3	0.8	2.2	2.62	
124.7	5.1	3	6.8	219.3	0.8	2.2	2.62	
124.7	5.1	3	6.8	219.3	0.8	2.2	2.62	
124.7	5.1	3	6.8	219.3	0.8	2.2	2.62	
124.7	5.1	3	6.8	219.3	0.8	2.2	2.62	
124.7	5.1	3	6.8	219.3	0.8	2.2	2.62	
124.7	5.1	3	6.8	219.3	0.8	2.2	2.62	
124.7	5.1	3	6.8	219.3	0.8	2.2	2.62	
124.7	5.1	3	6.8	219.3	0.8	2.2	2.62	
124.7	5.1	3	6.8	219.3	0.8	2.2	2.62	
124.7	5.1	3	6.8	219.3	0.8	2.2	2.62	
82.6	5.1	2.8	6.8	144.6	0.7	2.2	3.07	
118.7	5.1	3	6.8	208.8	0.8	2.2	2.62	
1165	5.6	5	6.5	2411.9	1.9	2.2	1.17	
148.7	5.1	3	6.8	261.6	0.8	2.2	2.62	
154.7	5.1	3	6.8	272.2	0.8	2.2	2.62	
154.7	5.1	3	6.8	272.2	0.8	2.2	2.62	
110.8	5	3	6.8	194.1	0.8	2.2	2.62	
154.7	5.2	2.8	6.8	270.6	0.7	2.2	3.07	
154.7	5.1	3	6.8	271.6	0.8	2.2	2.62	
154.7	5.1	3	6.8	271.6	0.8	2.2	2.62	
148.7	5.1	3	6.8	261.1	0.8	2.2	2.62	
154.7	5.1	3	6.8	272.2	0.8	2.2	2.62	
1163.8	5.6	5	6.8	2432.3	1.9	2.2	1.17	
124.8	5.1	2.5	6.8	219	0.6	2.2	3.65	
125.3	5.1	3	6.8	220.3	0.8	2.2	2.62	
124.7	5.1	3	6.8	219.4	0.8	2.2	2.62	
124.7	5.1	3	6.8	219.4	0.8	2.2	2.62	
124.7	5.1	3	6.8	219.4	0.8	2.2	2.62	
124.7	5.1	3	6.8	219.4	0.8	2.2	2.62	
124.7	5.2	3	6.8	219.4	0.8	2.2	2.62	
107.9	5.1	3	6.8	189	0.8	2.2	2.62	
783.5	5.9	5.5	6.5	1696.4	2.1	2.2	1.06	
298.7	5.1	2.5	6.8	528.1	0.6	2.2	3.65	
316.1	5.1	2.8	6.8	558.8	0.7	2.2	3.07	
118.7	5.1	3	6.8	207	0.8	2.2	2.63	
109.5	5	3	6.8	190.2	0.8	2.2	2.63	
118.3	5.1	3	6.8	205.9	0.8	2.2	2.63	
118.8	5.1	2.5	6.8	206.1	0.6	2.2	3.65	
124.7	5.1	3	6.8	219.6	0.8	2.2	2.62	
124.7	5.2	3	6.8	219.7	0.8	2.2	2.62	
124.7	5.1	3	6.8	219.6	0.8	2.2	2.62	
124.7	5.1	3	6.8	219.6	0.8	2.2	2.62	
118.7	5.1	3	6.8	209.1	0.8	2.2	2.62	
81.2	5.1	2.3	6.8	143	0.5	2.2	4.43	
119.9	5.1	3	6.8	211.1	0.8	2.2	2.62	
124.7	5.2	3	6.8	219.5	0.8	2.2	2.62	

Table 40 Southwest facade, Wintertime 21st of December.

Town:	Jeddah							
Latitude:	21° 31' N							
Altitude:	15 m (AMSL)							
Tau (transmissivity):	0.7							
A0 (ref. altitude):	8200 m (AMSL)							
Day:	21-Dec							
Starting hour:	0:00							
Ending hour:	24:00:00							
Grid precision:	15 min							
Area (m²)	Total energy (kWh)							
21805.9	3894.7	0.178607625						
Area (m²)	Mean daylight (h)	Min daylight (h)	Max daylight (h)	Total energy (kWh)	Min local flux (kWh/m²)	Max local flux (kWh/m²)	Variability factor	
118.7	2.3	0	3	17.8	0	0.2	1000	
118.4	2.3	0	3	17.5	0	0.2	1000	
189	2.9	2.8	3	35.6	0.2	0.2	1	
124.7	2.3	0	3	20	0	0.2	1000	
124.7	2.3	0	3	20	0	0.2	1000	
124.7	2.3	0	3	20	0	0.2	1000	
124.7	2.3	0	3	20	0	0.2	1000	
124.7	2.3	0	3	20	0	0.2	1000	
94.7	2.2	0	3	15	0	0.2	1000	
154.7	2.3	0	3	25.2	0	0.2	1000	
113.2	2.2	0	3	18.1	0	0.2	1000	
118.6	2.3	0	3	18.8	0	0.2	1000	
771.4	2.9	2.5	3	154.9	0.2	0.2	1.02	
124.7	2.2	0	3	20.5	0	0.2	1000	
169	2.3	0	3	28.7	0	0.2	1000	
118.7	2.2	0	3	19.3	0	0.2	1000	
323	2.5	1.3	3	63.4	0.1	0.2	2.45	
118.7	2.2	0	3	20.9	0	0.2	1000	
124.7	2.2	0	3	21.5	0	0.2	1000	
166.1	2.2	0	3	29.2	0	0.2	1000	
320.8	2.5	1.3	3	65.3	0.1	0.2	2.39	
164.5	2.3	0	3	27.4	0	0.2	1000	
124.7	2.3	0	3	20.2	0	0.2	1000	
118.7	2.2	0	3	18.9	0	0.2	1000	
12.1	1.6	1.5	1.8	0.6	0.1	0.1	1.05	
319.1	2.6	2.5	2.8	64.1	0.2	0.2	1.02	
95.7	2.2	0	3	15.2	0	0.2	1000	
100.7	2.2	0	3	16.6	0	0.2	1000	
2.5	0.8	0.5	1	0	0	0	1.3	
164.1	2.8	2.5	3	33.3	0.2	0.2	1.02	
124.7	2.3	0	3	20.5	0	0.2	1000	
124.7	2.2	0	3	20.5	0	0.2	1000	
124.7	2.2	0	3	20.4	0	0.2	1000	
124.7	2.3	0	3	20.4	0	0.2	1000	
124.7	2.3	0	3	20.5	0	0.2	1000	
124.7	2.3	0	3	20.4	0	0.2	1000	
124.7	2.3	0	3	20.5	0	0.2	1000	
124.7	2.3	0	3	20.4	0	0.2	1000	
124.7	2.3	0	3	20.4	0	0.2	1000	
124.7	2.3	0	3	20.4	0	0.2	1000	
82.6	2.1	0	3	13.2	0	0.2	1000	
118.7	2.2	0	3	19.2	0	0.2	1000	
1165	2.6	1.5	3	232.8	0.1	0.2	1.82	
148.7	2.2	0	3	25.1	0	0.2	1000	
154.7	2.3	0	3	25.8	0	0.2	1000	
154.7	2.3	0	3	26	0	0.2	1000	
110.8	2.2	0	3	17.9	0	0.2	1000	
154.7	2.3	0	3	25.4	0	0.2	1000	
154.7	2.3	0	3	25.3	0	0.2	1000	
154.7	2.3	0	3	25.3	0	0.2	1000	
154.7	2.3	0	3	25.3	0	0.2	1000	
148.7	2.3	0	3	24.1	0	0.2	1000	
154.7	2.3	0	3	25.8	0	0.2	1000	
1163.8	2.6	1.5	3	232.3	0.1	0.2	1.83	
124.8	2.3	0	3	20.6	0	0.2	1000	
125.3	2.3	0	3	20.4	0	0.2	1000	
124.7	2.3	0	3	20.4	0	0.2	1000	
124.7	2.3	0	3	20.4	0	0.2	1000	
124.7	2.3	0	3	20.4	0	0.2	1000	
124.7	2.3	0	3	20.4	0	0.2	1000	
124.7	2.3	0	3	20.4	0	0.2	1000	
107.9	2.2	0	3	17.3	0	0.2	1000	
783.5	2.8	2.5	3	159.4	0.2	0.2	1.02	
298.7	2.3	0	3	51.7	0	0.2	1000	
316.1	2.3	0	3	54.2	0	0.2	1000	
118.7	2.3	0	3	17.5	0	0.2	1000	
109.5	2.2	0	3	16.1	0	0.2	1000	
118.3	2.2	0	3	16.7	0	0.2	1000	
118.8	2.2	0	3	16.8	0	0.2	1000	
124.7	2.3	0	3	20.7	0	0.2	1000	
124.7	2.3	0	3	20.8	0	0.2	1000	
124.7	2.3	0	3	20.7	0	0.2	1000	
124.7	2.3	0	3	20.7	0	0.2	1000	
118.7	2.2	0	3	19.5	0	0.2	1000	
81.2	2.1	0	3	13	0	0.2	1000	
119.9	2.4	1.5	3	21.4	0.1	0.2	1.82	
124.7	2.4	1.5	3	22.3	0.1	0.2	1.82	

Table 41 Results of the three case studies of the AV. Direct solar radiation received on the facades on the 21st of June and the 21st of December.

FACADES		CASE A		
ORIENTATION		21JUNE kWh/m ²	21 DEC kWh/m ²	AV.SVF %
N		0.8	0	20
S		0.05	2.1	20
E		1.37	0.76	20
W		1.4	0.5	19
NW		0.5	1.9	20.9
SE		1	0.07	19

FACADES		CASE B		
ORIENTATION		21JUNE kWh/m ²	21 DEC kWh/m ²	SVF %
N		0.16	3.5	36
S		1.2	0	37
E		1.9	1.6	36
W		2.2	0.65	37

FACADES		CASE C		
ORIENTATION		21JUNE kWh/m ²	21 DEC kWh/m ²	SVF %
NW		0.97	2.6	34
SE		1.76	0.067	34
NE		1.38	2.2	33
SW		1.9	0.17	33

Table 42. Results of the three case studies of the AV. Direct solar radiation received on the street level on the 21st of June and the 21st of December.

Canyons and Streets	Summer kWh/m ²	Winter kWh/m ²
CASE A	3.2	0.5
CASE B	5.9	1.9
CASEC	5.8	2.4

2.6 THREE LAYOUTS: AVERAGE SOLAR FLUX RECEIVED ON STREETS AND FACADES

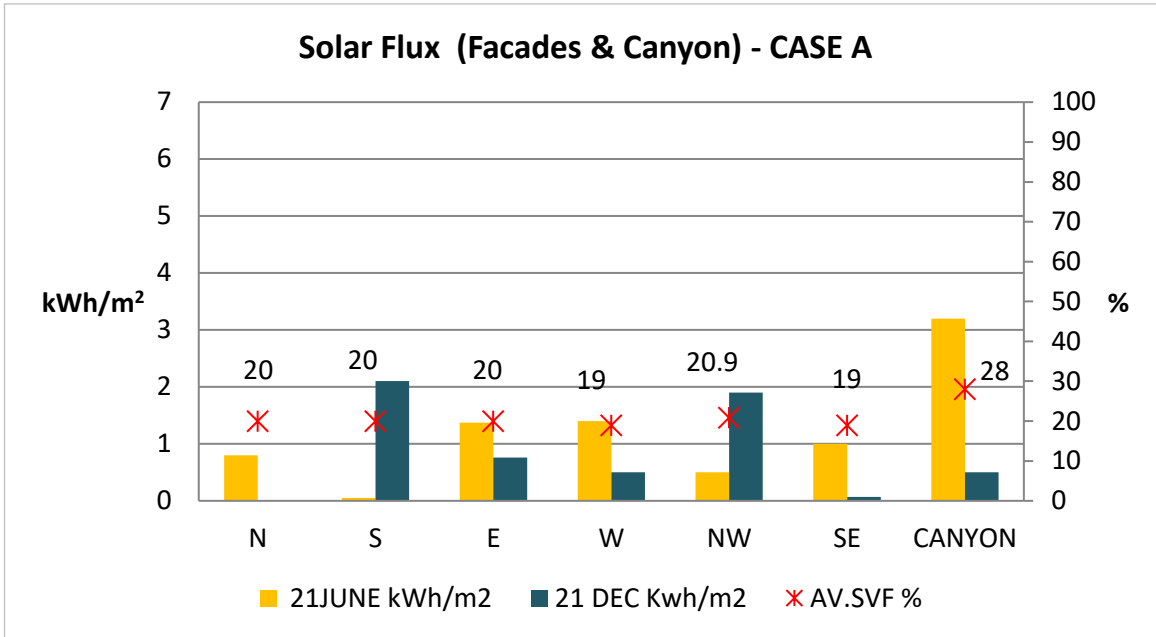


Figure 12 Average solar flux value on the horizontal surface (canyons) compared to the received solar flux on the facades for Case A in summer 21st June and winter 21st December.

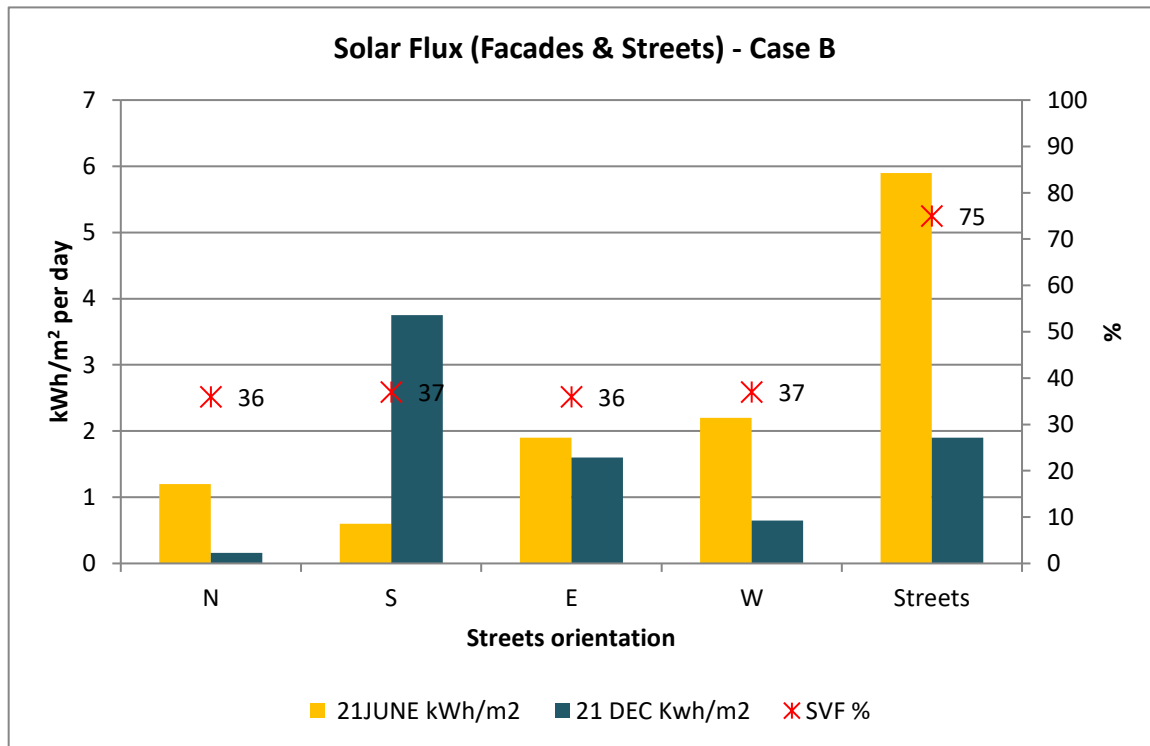


Figure 13 Average solar flux value on the horizontal surface (canyons) compared to the received solar flux on the facades for Case B in summer 21st June and winter 21st December.

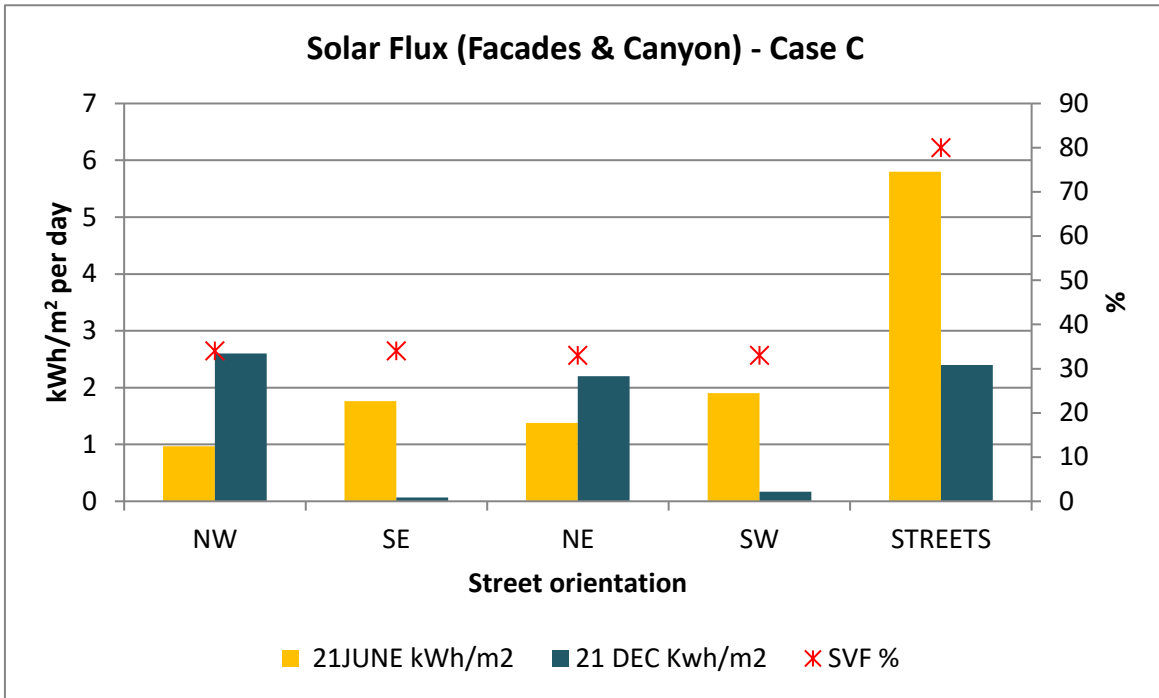


Figure 14 Average solar flux value on the horizontal surface (canyons) compared to the received solar flux on the facades for Case C in summer 21st June and winter 21st December.

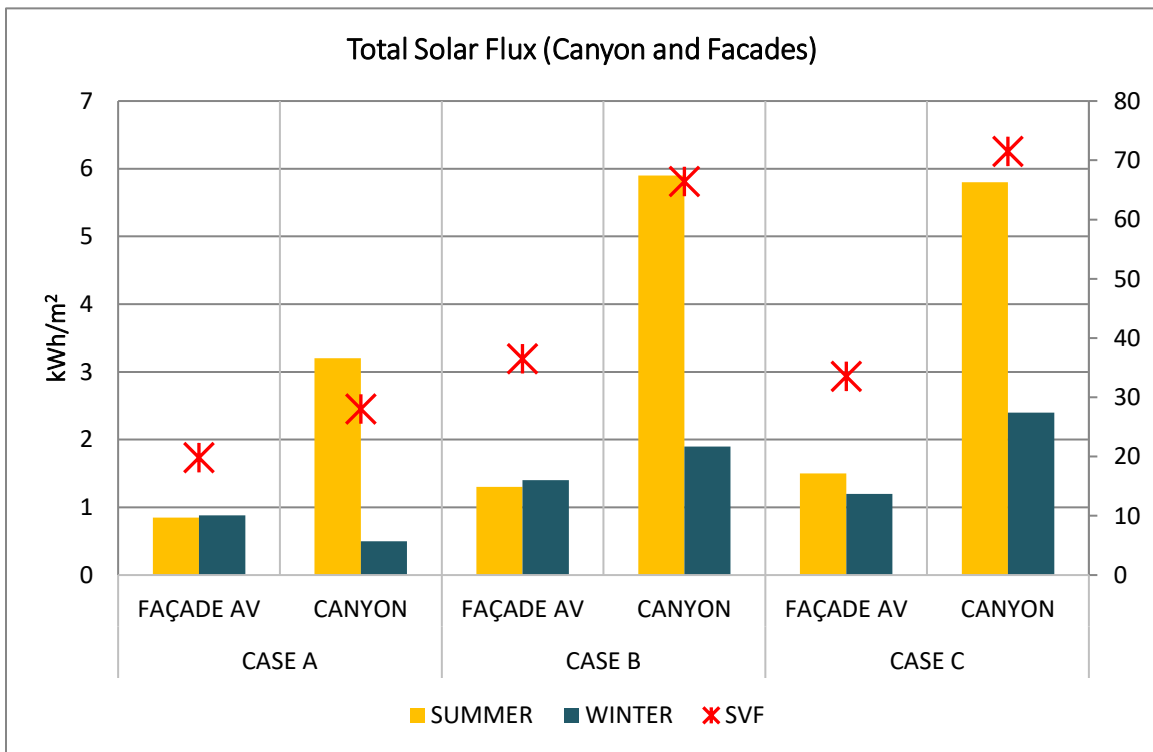


Figure 15 Average solar flux value on the horizontal surface (canyons) compared to the received solar flux on the average facades for the three case studies in summer 21st June and winter 21st December.

APPENDIX 3

3.1 HELIODON 2 SUMMARY SIMULATION OF THE CANYON ORIENTATIONS WITH AND WITHOUT RAWASHIN

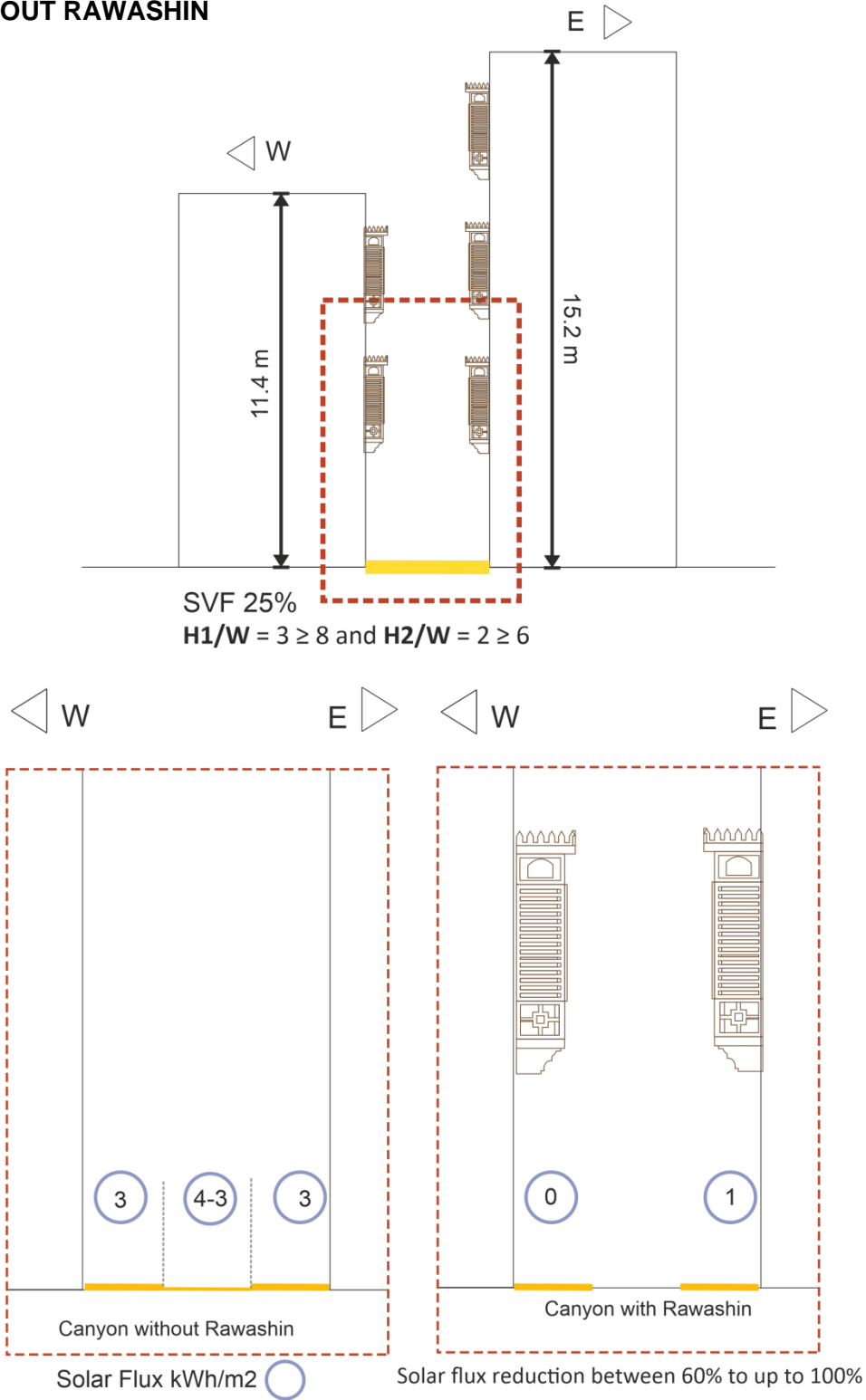


Figure 16 Received direct solar flux on the North-South canyon in the old area Jeddah demonstrating the results of the canyon before (left) and after (right) applying the Rawashin.

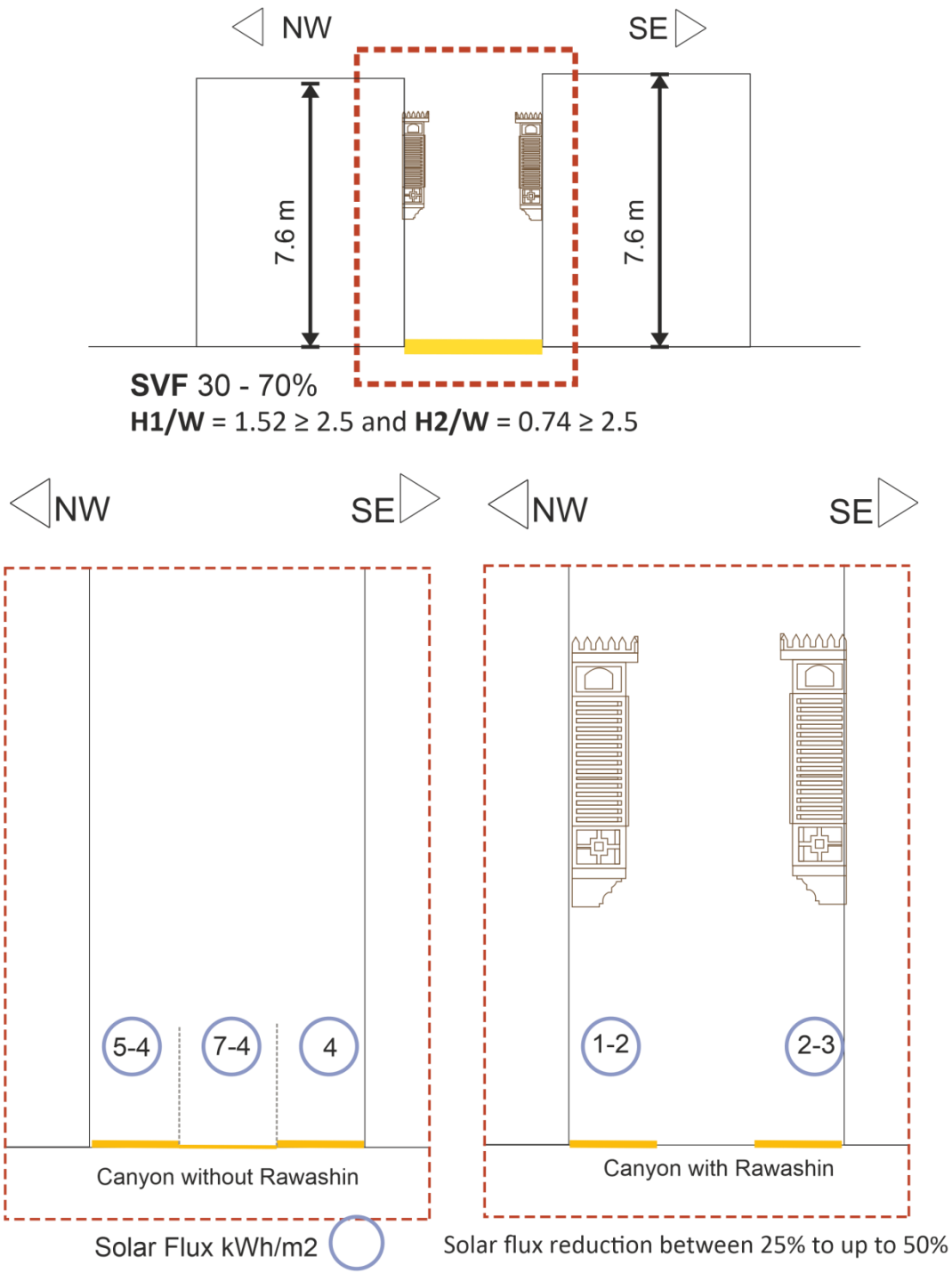


Figure 17 Received direct solar flux on the Northeast-Southwest canyon in the old area Jeddah demonstrating the results of the canyon before (left) and after (right) applying the Rawashin.

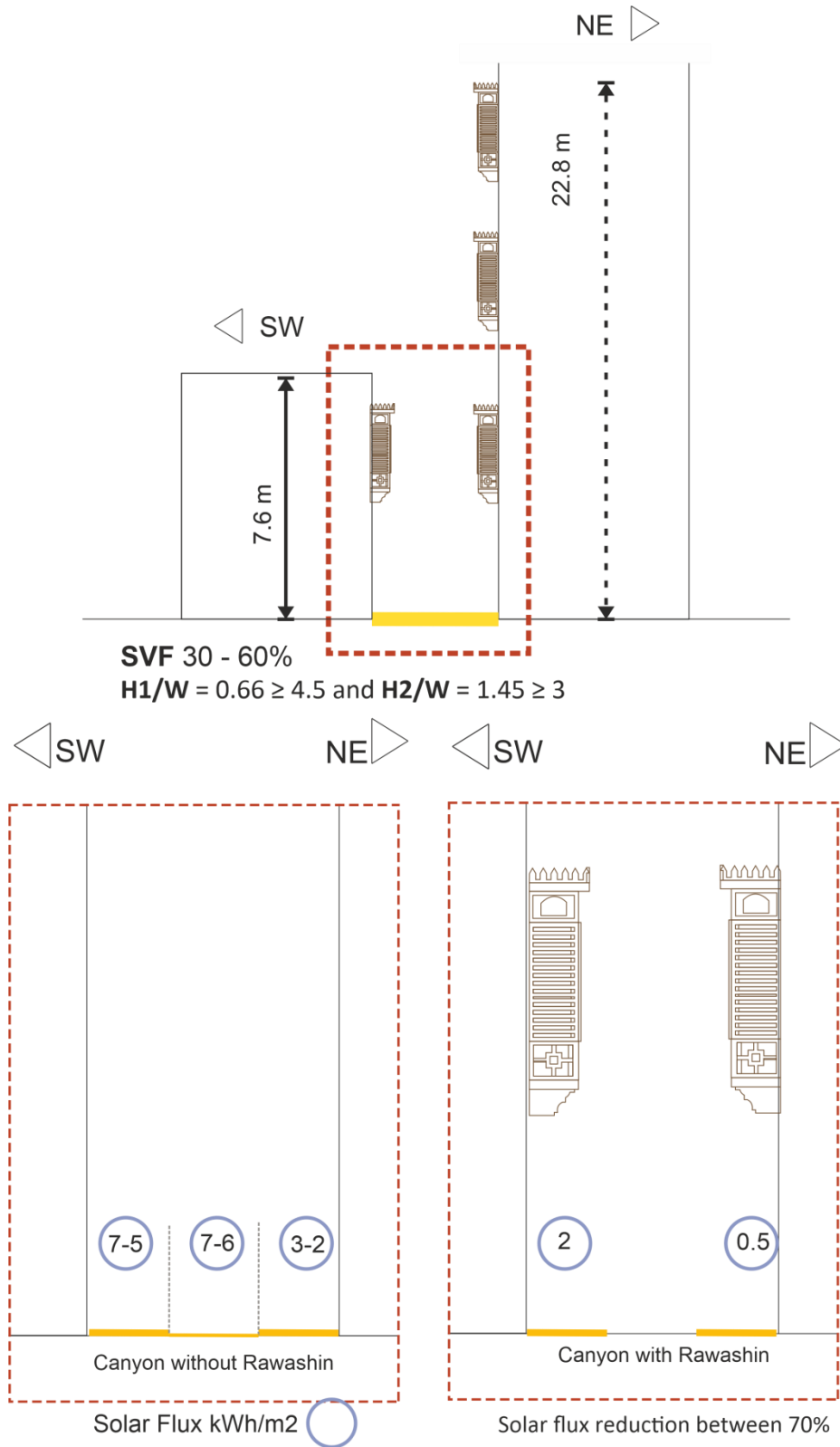


Figure 18 Received direct solar flux on the Northwest-Southeast canyon in the old area Jeddah demonstrating the results of the canyon before (left) and after (right) applying the Rawashin.

3.3 HELIODON PLUS SUMMARY SIMULATION OF THE CANYON ORIENTATIONS WITH AND WITHOUT RAWASHIN

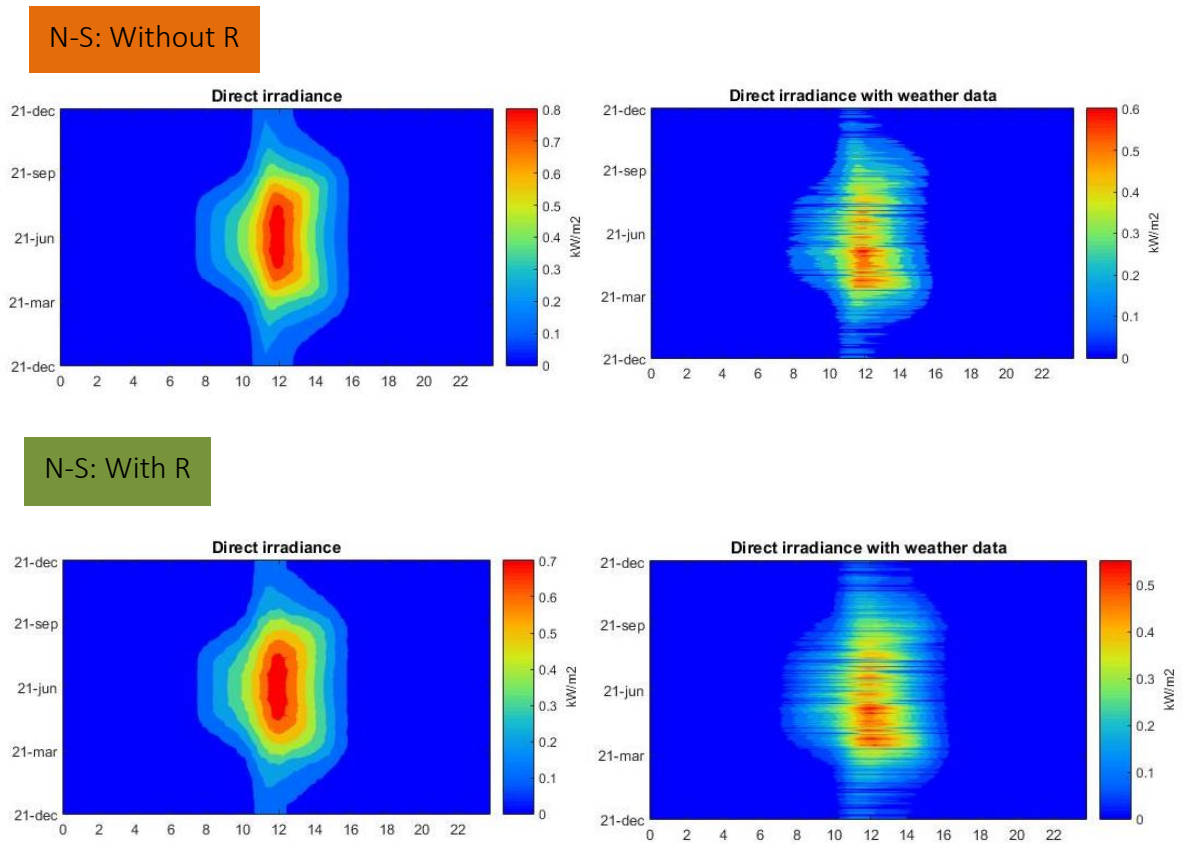
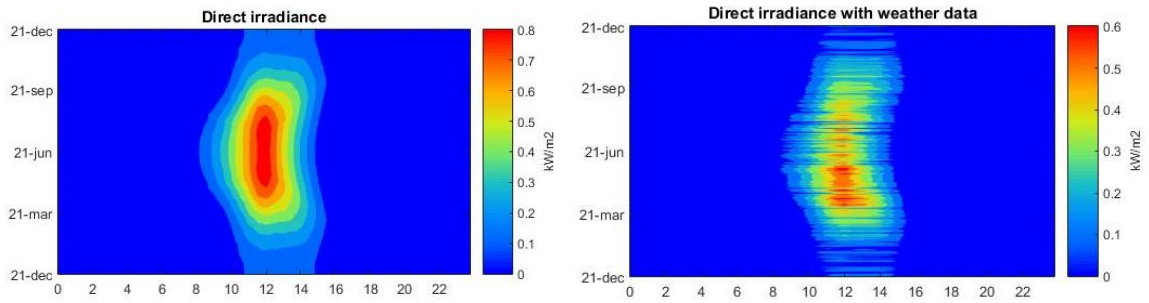


Figure 19 Heliodon Plus simulations on the North-South canyon with (bottom) and without (top) applying the Rawashin.

NE-SW: Without R



NE-SW: With R

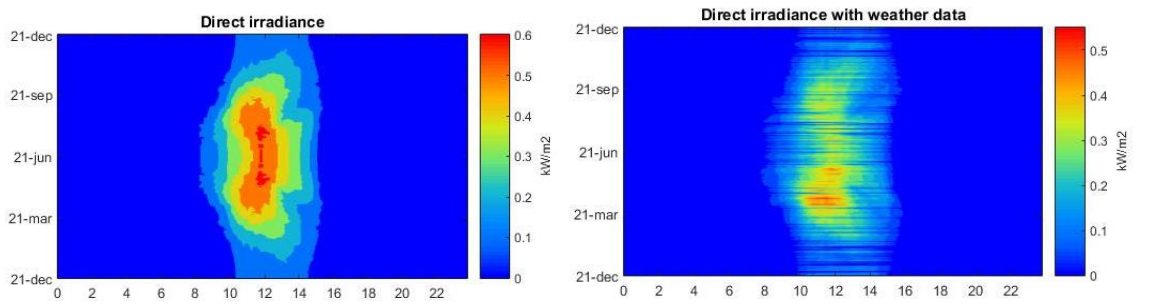
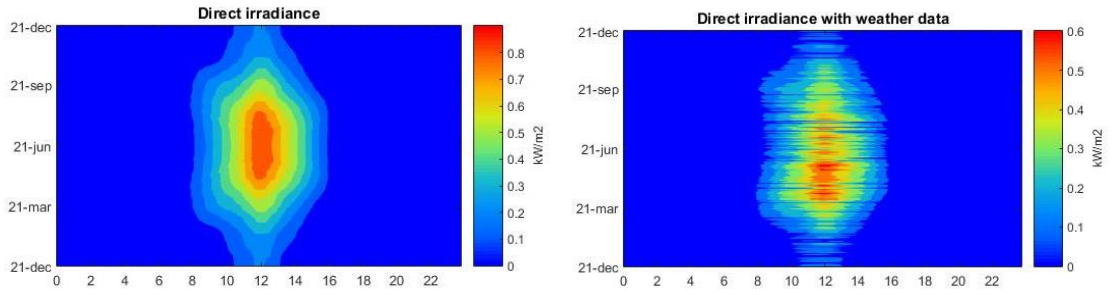


Figure 20 Heliodon Plus simulations on the Northeast-Southwest canyon with (bottom) and without (top) applying the Rawashin.

NW-SE: Without R



NW-SE: With R

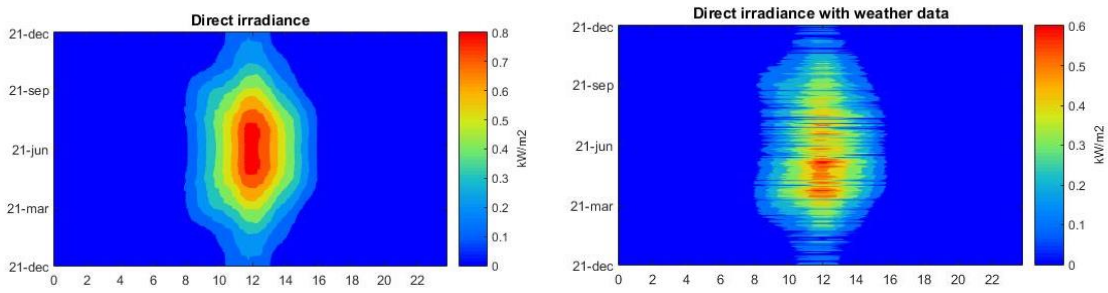


Figure 21 Heliodon Plus simulations on the Northwest-Southeast canyon with (bottom) and without (top) applying the Rawashin.

3.4 OVERHANGING FACADE SIMULATION SERIES 1

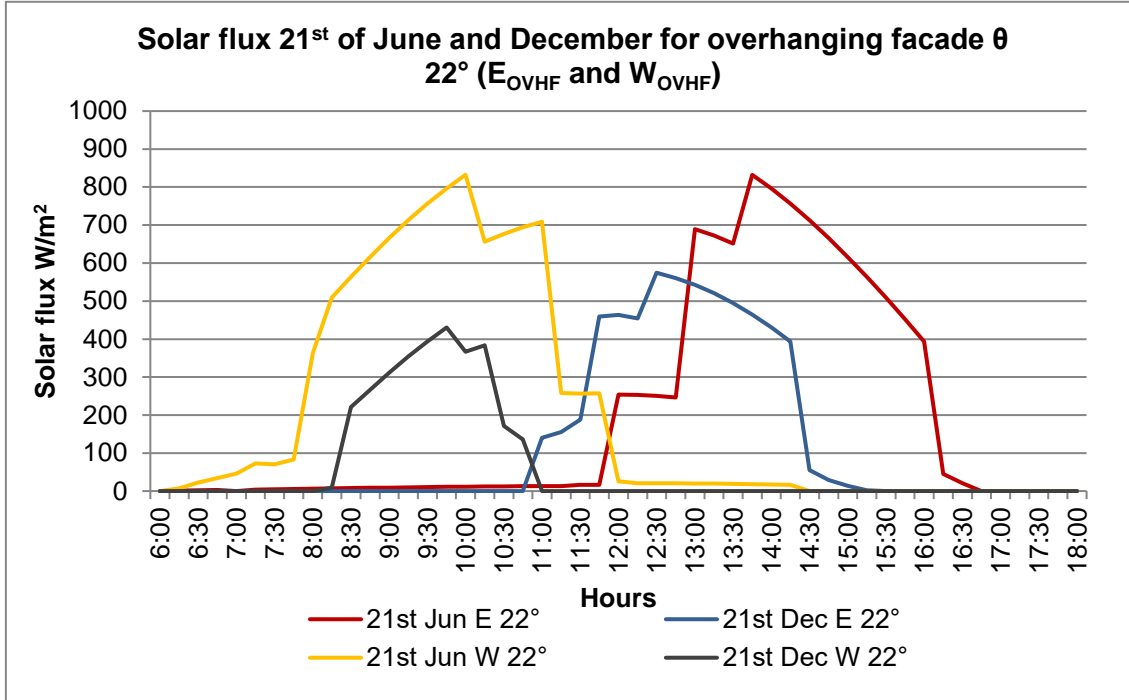


Figure 22 Received direct solar flux on the 21st of June and the 21st of December on the horizontal surface (pedestrian walkways) of θ 22° (W_{OVHF} (W) and E_{OVHF} (E)).

Figure 22 shows the solar flux of the OVHF on the horizontal surface of θ 22° of the W_{OVHF} and E_{OVHF} . This figure also shows clearly that the solar radiation time interval changes from the 21st of June to the 21st of December. Figure 22 also illustrates one of the OVHF geometries (θ 22°) to show the results of both orientations and their change in solar flux penetration in both seasons.

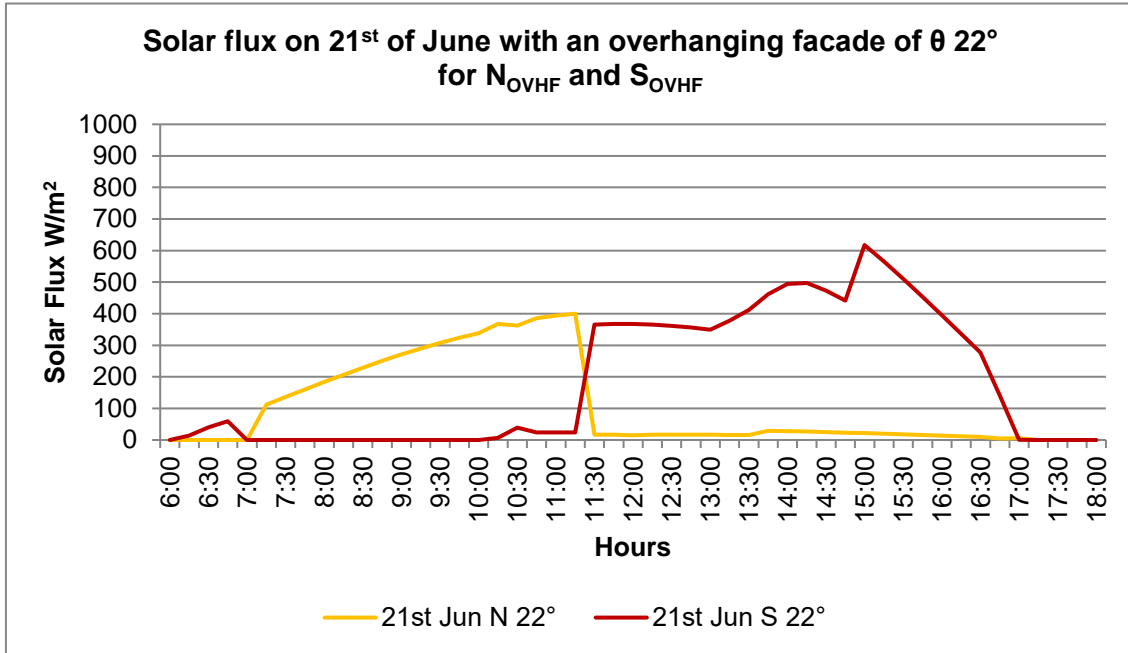


Figure 23 Received direct solar flux on the 21st of June of the θ 22° overhanging facades on the horizontal surface (pedestrian walkways) for N_{OVHF} (N) and S_{OVHF} (S).

The graph in Figure 23 illustrates the received direct solar flux at different times during the day in summer on the 21st of June for N_{OVHF} and the S_{OVHF} for an OVHF with θ 22°. It reveals opposite effects on solar flux during the day on the horizontal surface of both orientations due to the sun movement and orientation of the overhanging facades as was observed for the E_{OVHF} and the W_{OVHF} . Consequently, the N_{OVHF} receives a direct solar flux from sunrise until before noon and the S_{OVHF} from noon until sunset. Each orientation behaves differently during the day as well as in different seasons.

Moreover, the result shows that orientations appear to be reasonably asymmetrical. S_{OVHF} receives in some moments of the day a higher solar flux than N_{OVHF} (Figure 23).

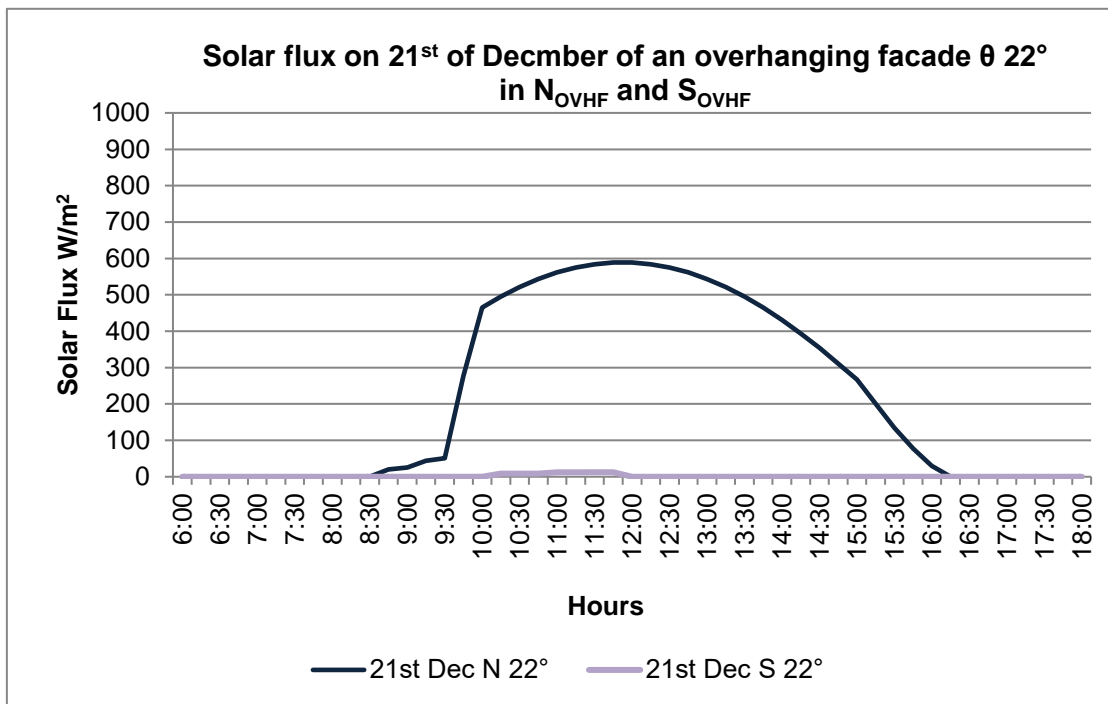


Figure 24 Received direct solar flux on the 21st of December on the θ 22° horizontal surface (pedestrian walkways) of the N_{OVHF} (N) and S_{OVHF} (S).

Moreover, to understand the performance of the horizontal surface under the overhanging facades, wintertime should be explained as well. Figure 45 reveals that θ 22° of N_{OVHF} receives a higher solar flux than S_{OVHF} and that there is no comparison between both orientations. The solar flux received on the horizontal surface of S_{OVHF} is very low in comparison to N_{OVHF} to a level that it is almost not detectable on the graph (Figure 24). This performance and result are similar in all studied geometrical angles, which might be due to the low solar angle in winter.

Figures 42 and 43 illustrate the performance of the direct solar flux on the horizontal surface on both orientations of the OVHFs in summer and winter. In summer, S_{OVHF} receives less solar flux than N_{OVHF} . Nevertheless, in wintertime, S_{OVHF} almost receives no solar flux throughout the entire day whereas N_{OVHF} receives a much higher direct solar flux during the day.

Besides, after analyzing separately the performance of the horizontal surface of all overhanging facade geometries in summer and winter for N_{OVHF} and the S_{OVHF} , the following two graphs in Figures 25 and 26 demonstrate the performance of the horizontal surface for both N_{OVHF} and the S_{OVHF} showing the reduction of direct solar flux in both seasons. Figure 25 illustrates the direct solar flux on the horizontal surface for N_{OVHF} for the OVHF θ 22° showing the different results of direct solar flux in their time intervals and the amount of solar flux in both seasons. In summertime, the horizontal surface receives less direct solar flux than in wintertime. In wintertime, the horizontal surface receives 30% more of solar flux than in summertime, especially in the peak hours around noon. Therefore, in summer, the OVHF protects the pedestrians from the direct solar radiation,

and in winter the pedestrians are exposed by it. On the one hand, pedestrians will be protected from the direct solar radiation under N_{OVHF} in summertime thirty minutes before noontime, which is the peak hour of the highest amount of solar flux and its solar time interval is in total 4.5 hrs. In wintertime, the horizontal surface starts receiving direct solar flux two hours before noontime until 16:30 hrs, not with a constant amount though, as it first increases then drops down with a total solar time interval of 6 hrs of solar flux.

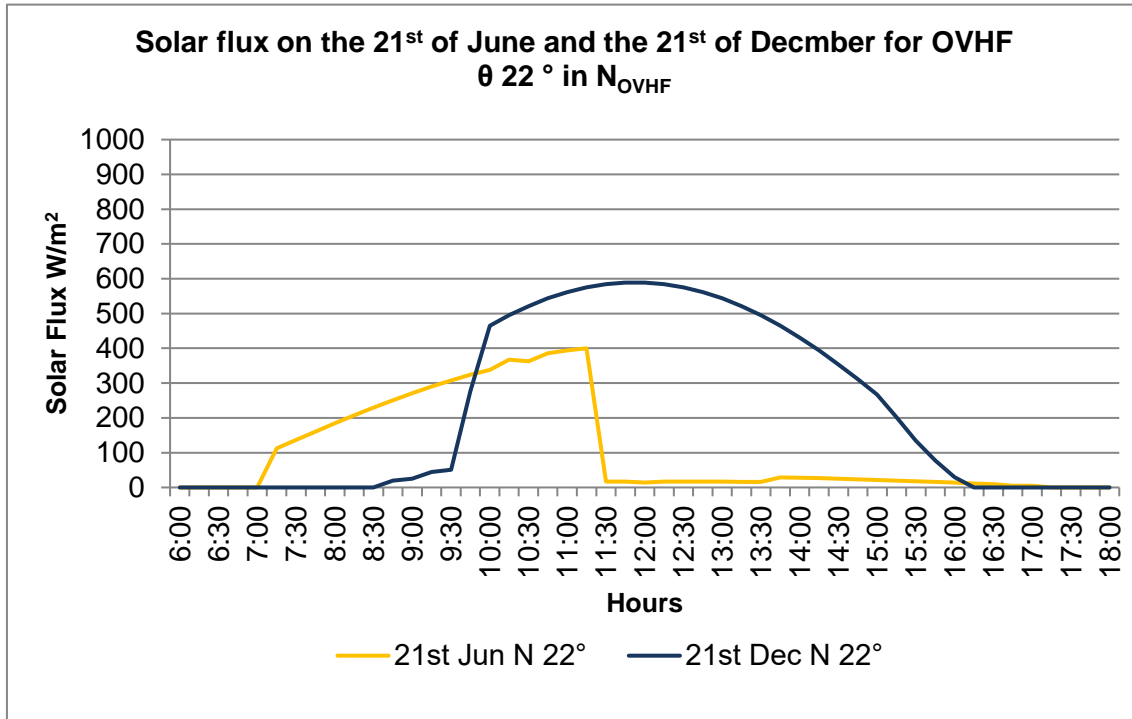


Figure 25 Received direct solar flux on the 21st of June and the 21st December of the $\theta 22^\circ$ overhanging facades on the horizontal surface (pedestrian walkways) of N_{OVHF} (N).

In Figure 26, the line graph shows horizontal surface performance concerning direct solar flux for S_{OVHF} of $\theta 22^\circ$ in summer and winter. The simulation reveals a dramatic difference in received direct solar flux between summertime and wintertime. In summer, the simulation exhibits fluctuating results, starting with an increase of solar flux in the morning, then it decreases and starts rising again half an hour before noontime and reaches its peak hour at 15:00h. Nevertheless, in winter, the S_{OVHF} horizontal surface almost receives no solar flux.

Consequently, on one hand, Pedestrians on this side of the streets will be protected from the direct solar radiation in wintertime as the direct solar radiation barely penetrates. On the other hand, in summertime, the direct solar radiation penetrates thirty minutes before noon, and from then on, it fluctuates until 17:00 h and receives 4.5 hrs of solar flux.

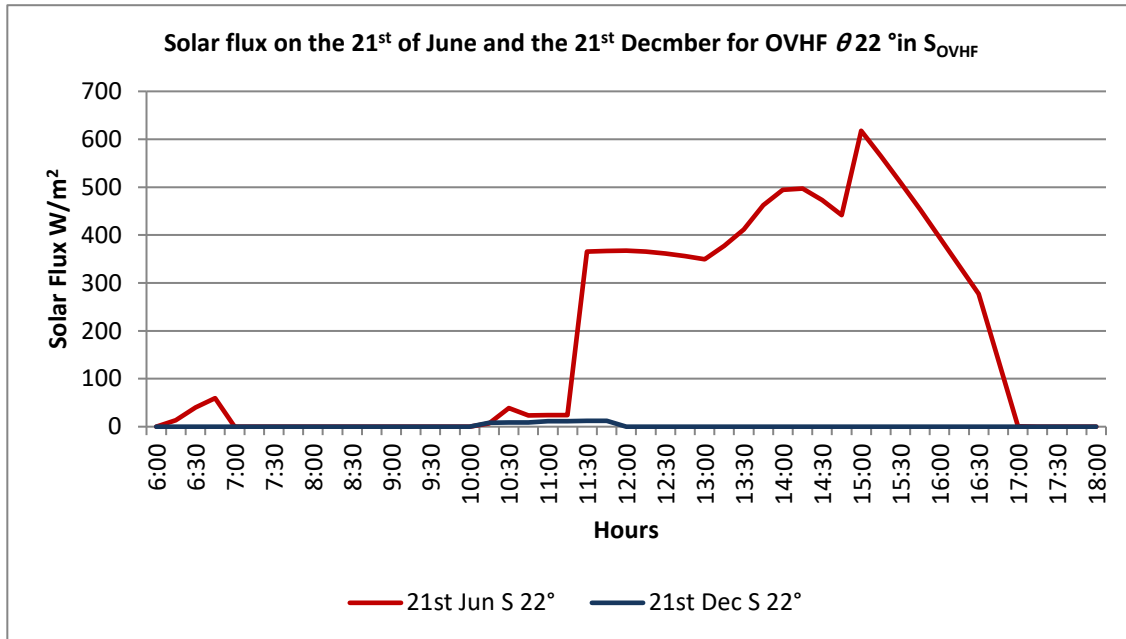


Figure 26 Received direct solar flux on the 21st of June and December of θ 22° overhanging facades on the horizontal surface (pedestrian walkways) of (S_{OVHF} (S)).

3.5 OVERHANGING FACADE STEREOGRAPH SERIES 2

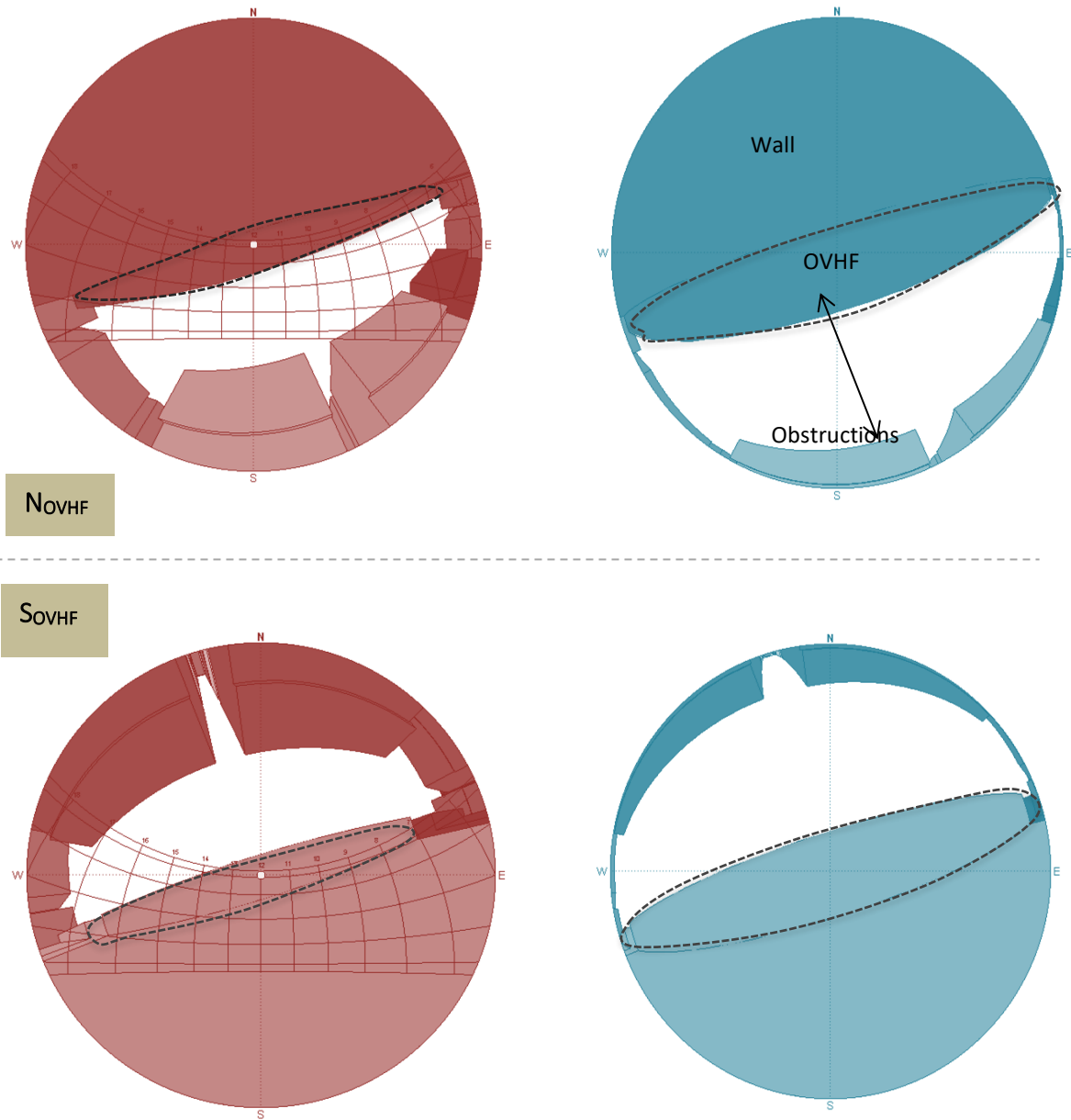


Figure 27 Overhanging facade series 2: $\theta 22^\circ$ N_{OVHF} (top) and S_{OVHF} (bottom). The orthographic projection is in blue (right) and the stereographic projection is in red (left).

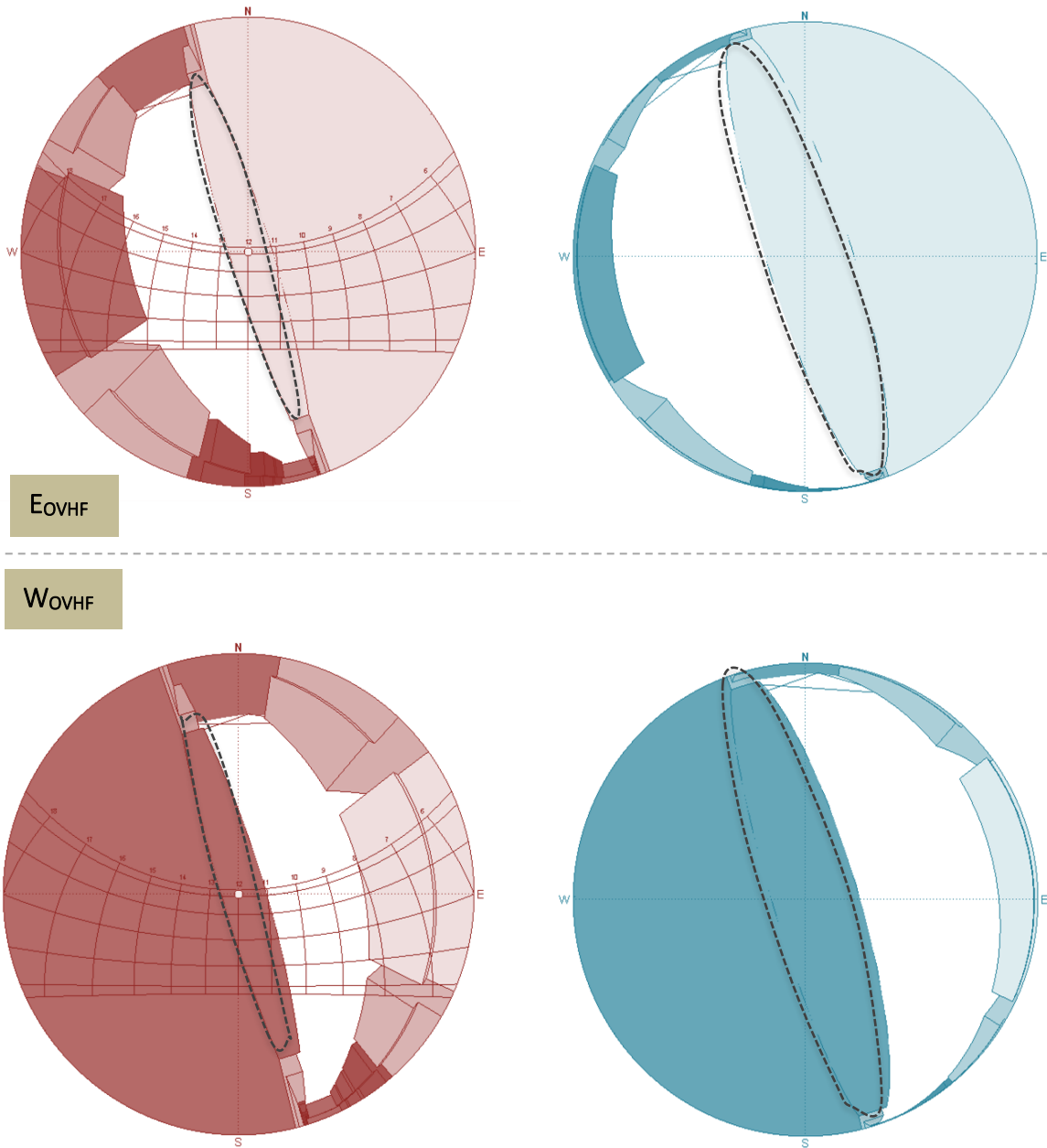


Figure 28 Overhanging facade series 2: $\theta 22^\circ$ E_{OVHF} (top) and W_{OVHF} (bottom). The orthographic projection is in blue (right) and the stereographic projection in red (left).

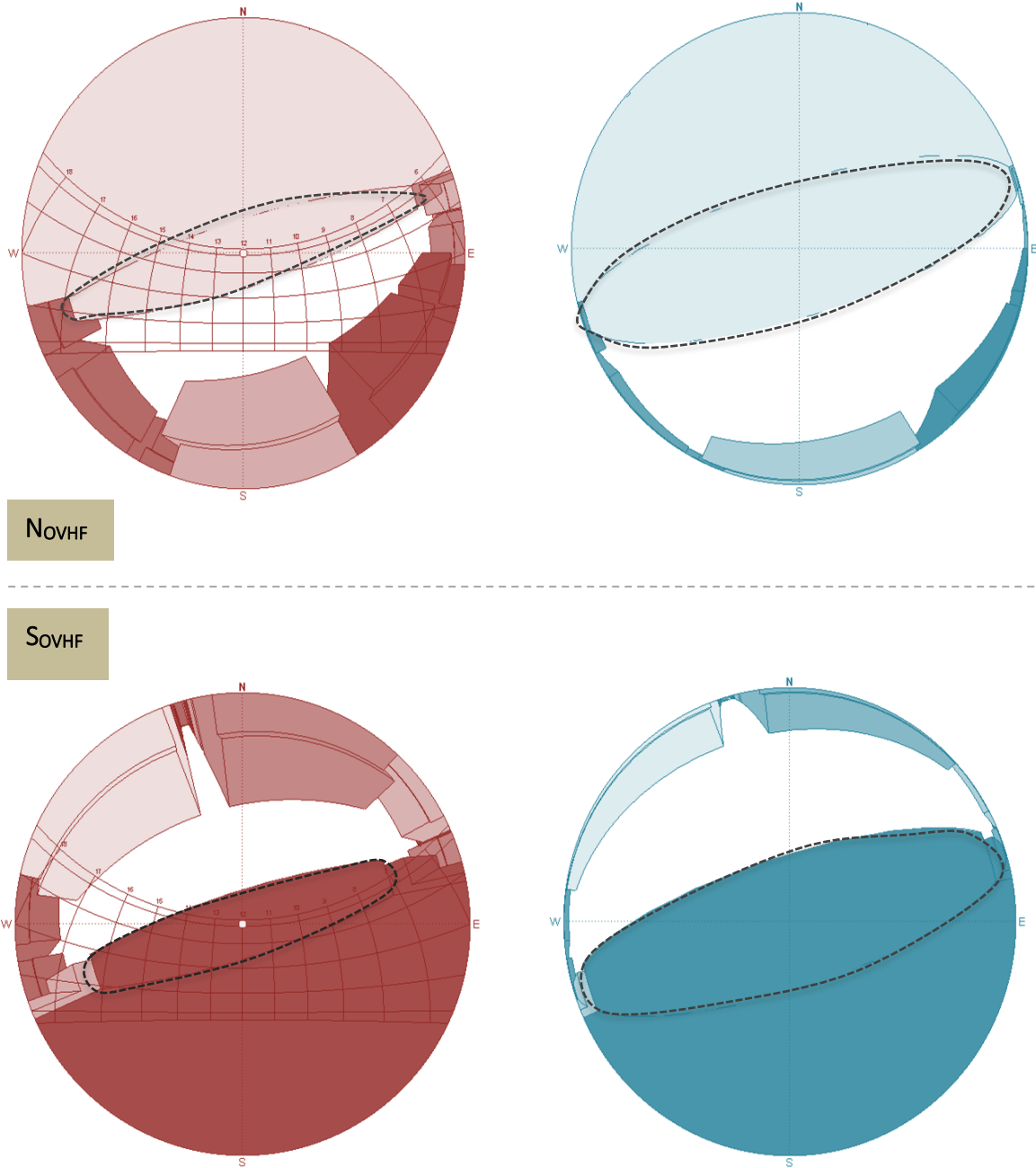


Figure 29 Overhanging facade series 2: θ 34° NOVHF (top) and SOVHF (bottom). The orthographic projection is in blue (right) and the stereographic projection in red (left).

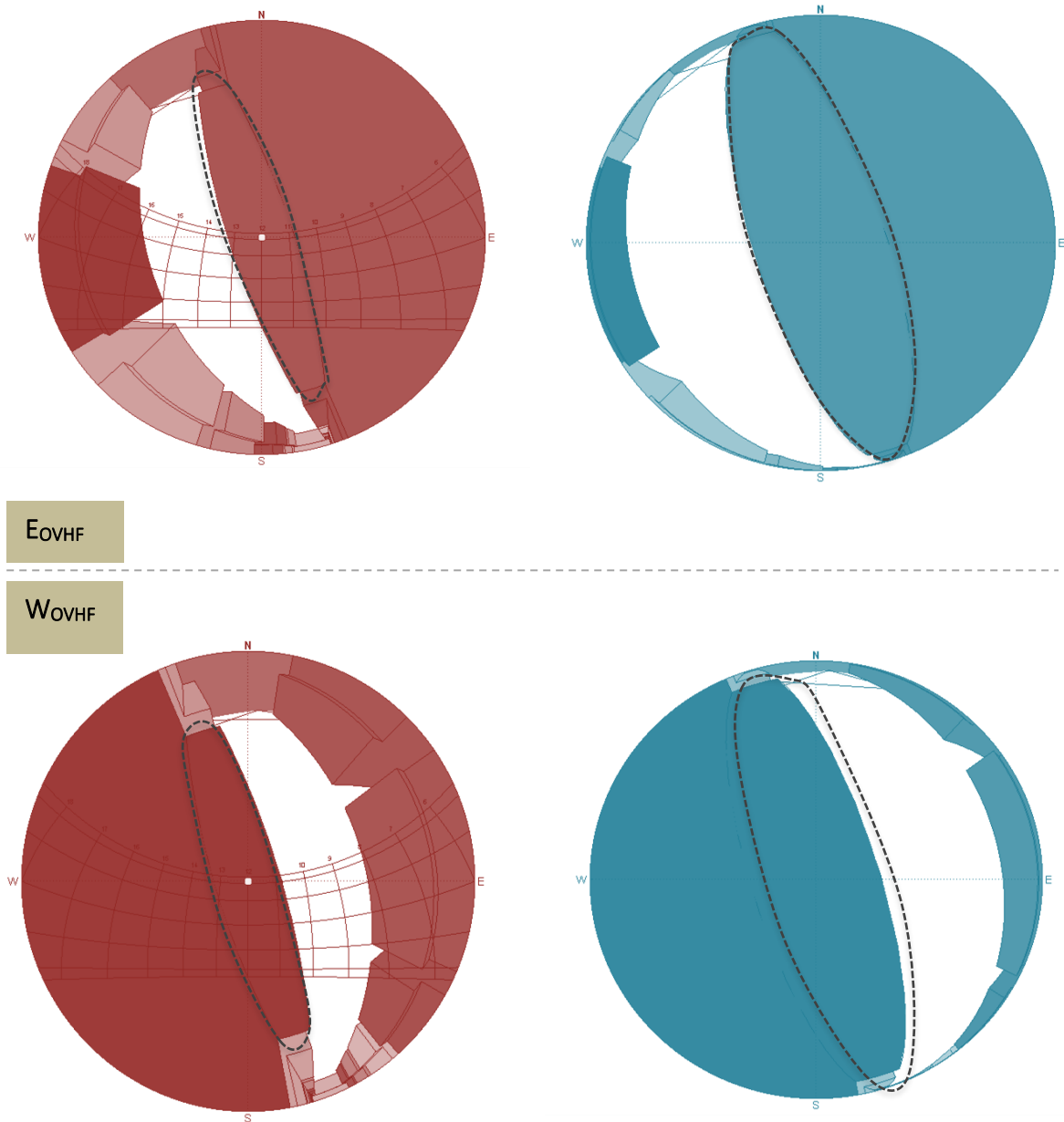


Figure 30 Overhanging facade series 2: θ 34° E_{ovHF} (top) and W_{ovHF} (bottom). The orthographic projection is in blue (right) and the stereographic projection in red (left).

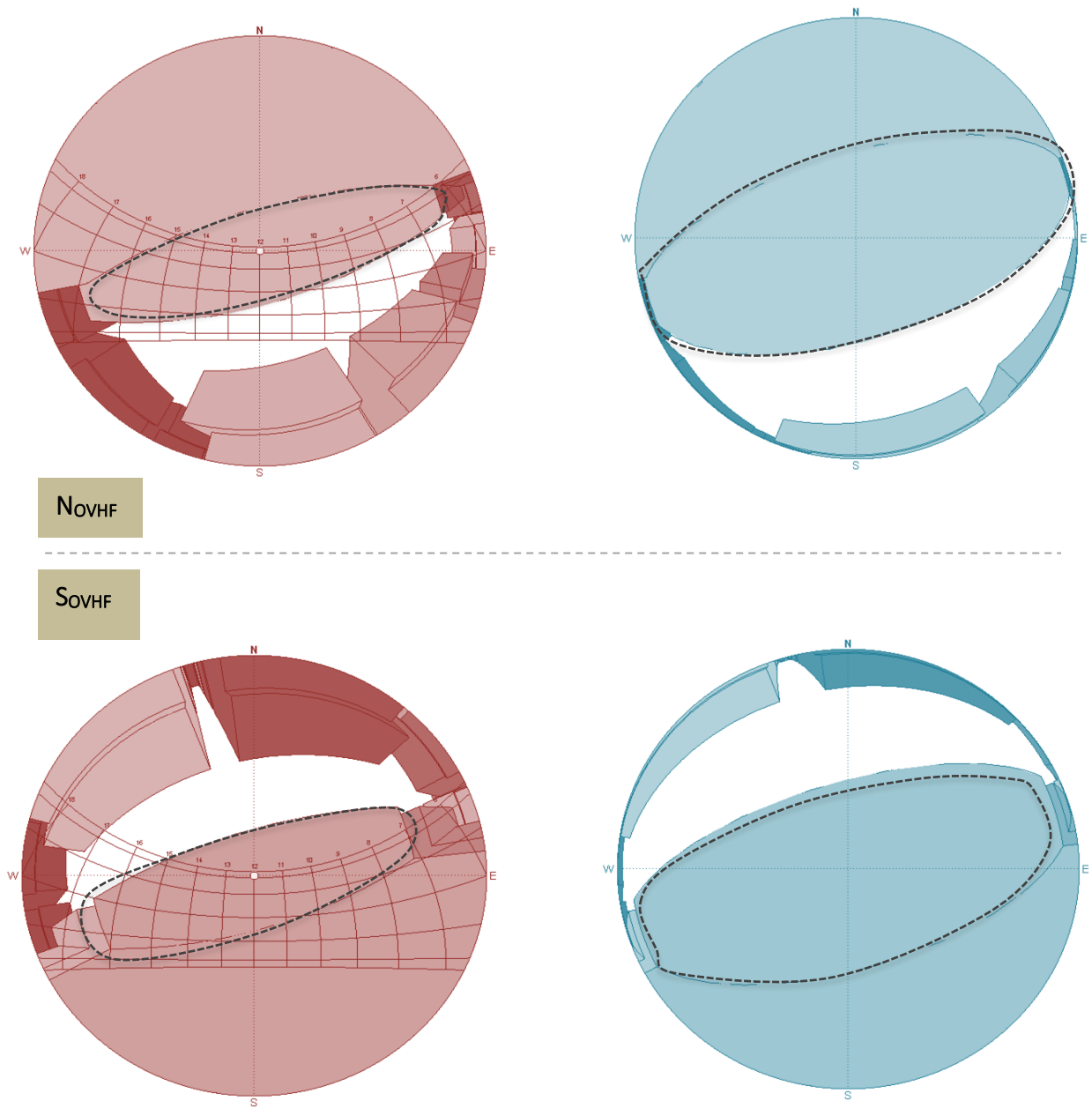


Figure 31 Overhanging facade series 2: θ 45° NOVHF (top) and SOVHF (bottom). The orthographic projection is in blue (right) and the stereographic projection in red (left).

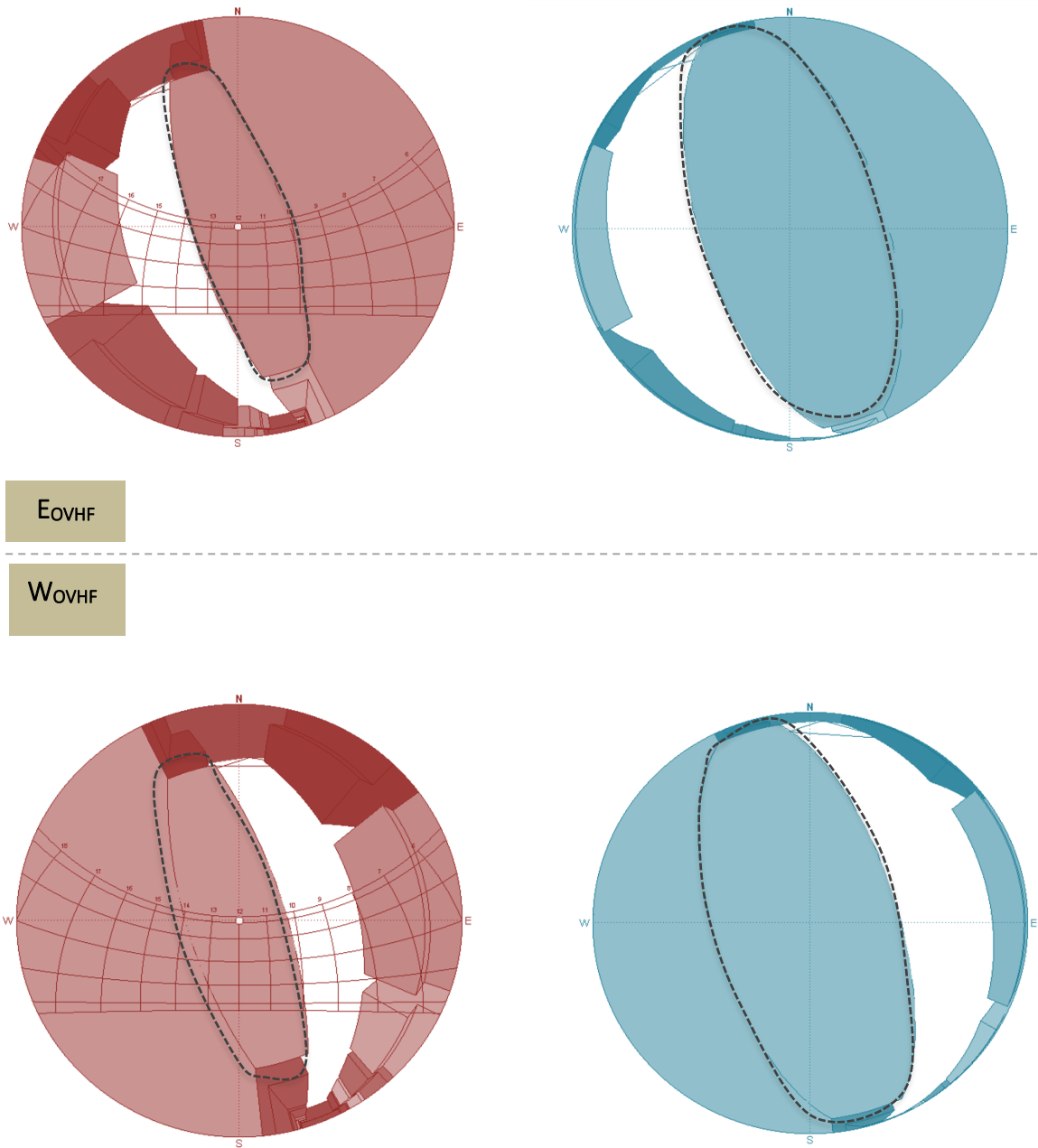


Figure 32 Overhanging facade series 2: θ 45° E_{ovHF} (top) and W_{ovHF} (bottom). The orthographic projection is in blue (right) and the stereographic projection in red (left).

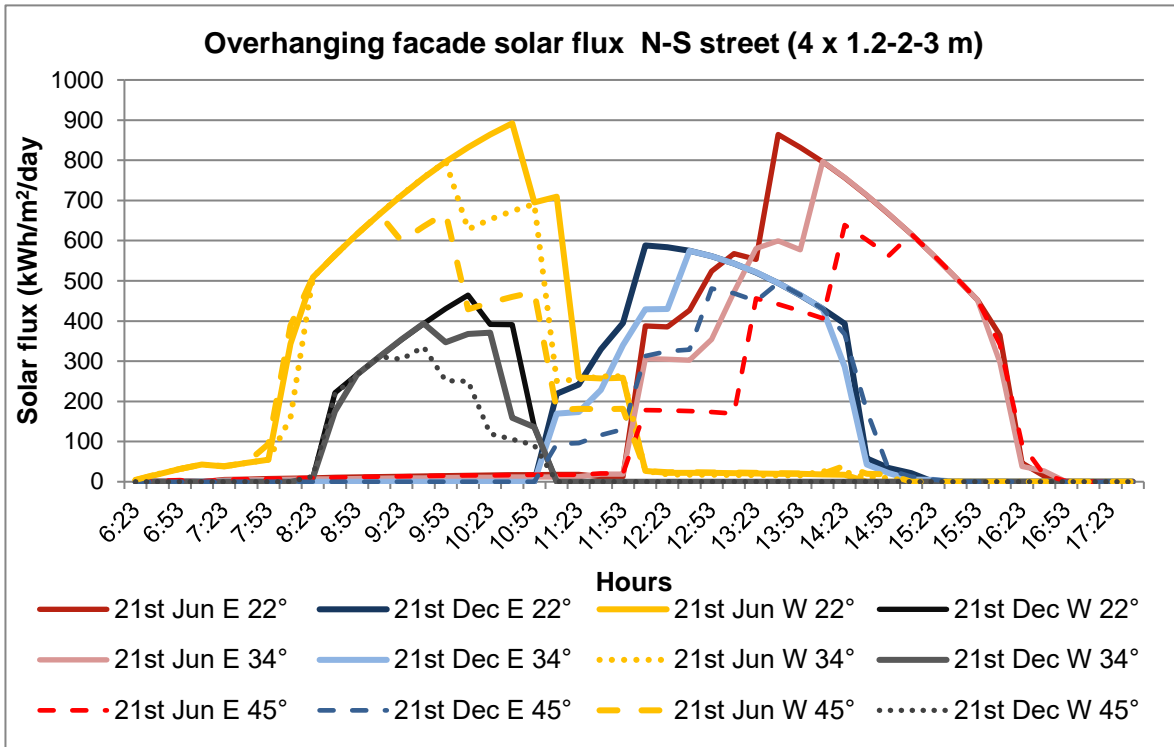


Figure 33 Received direct solar flux in E_{OVHF} (E) and W_{OVHF} (W) for θ 22°, θ 34°, and θ 45°, series 2.

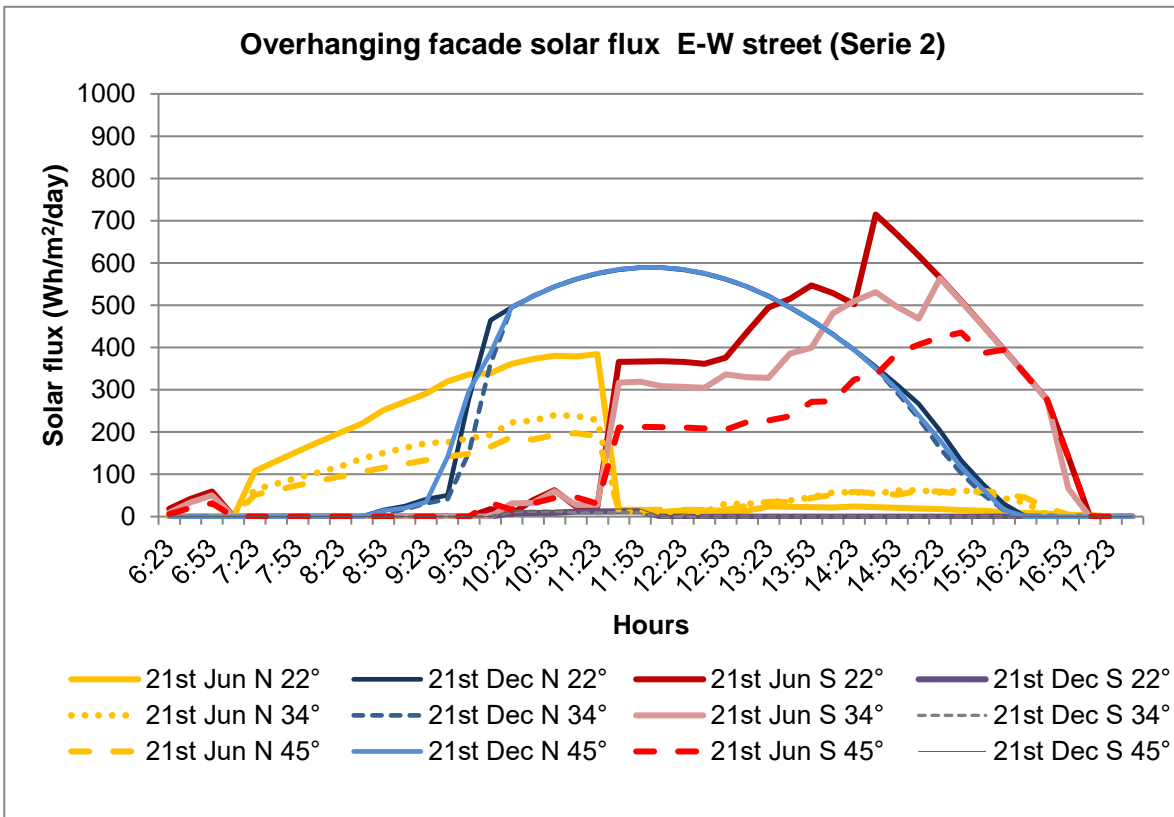


Figure 34 Received direct solar flux in N_{OVHF} (N) and S_{OVHF} (S) for θ 22°, θ 34°, and θ 45°, series 2.

